Development of Online Hybrid Testing

Theory and Applications to Structural Engineering

Development of Online Hybrid Testing

Theory and Applications to Structural Engineering

Peng Pan
Tsinghua University, China

Tao Wang
Institute of Engineering Mechanics, China Earthquake Administration, China

Masayoshi Nakashima
Kyoto University, Japan

ELSEVIER

AMSTERDAM • BOSTON • HEIDELBERG • LONDON
NEW YORK • OXFORD • PARIS • SAN DIEGO
SAN FRANCISCO • SINGAPORE • SYDNEY • TOKYO

Butterworth-Heinemann is an imprint of Elsevier

Butterworth Heinemann is an imprint of Elsevier
The Boulevard, Langford Lane, Kidlington, Oxford OX5 1GB, UK
225 Wyman Street, Waltham, MA 02451, USA

Notices
Knowledge and best practice in this field are constantly changing. As new research and experience broaden our understanding, changes in research methods, professional practices, or medical treatment may become necessary.

Practitioners and researchers must always rely on their own experience and knowledge in evaluating and using any information, methods, compounds, or experiments described herein. In using such information or methods they should be mindful of their own safety and the safety of others, including parties for whom they have a professional responsibility.

To the fullest extent of the law, neither the Publisher nor the authors, contributors, or editors, assume any liability for any injury and/or damage to persons or property as a matter of products liability, negligence or otherwise, or from any use or operation of any methods, products, instructions, or ideas contained in the material herein.

Library of Congress Cataloging-in-Publication Data
A catalog record for this book is available from the Library of Congress

British Library Cataloguing in Publication Data
A catalogue record for this book is available from the British Library

ISBN: 978-0-12-803378-4

Preface

Computer simulations play an important role in modern seismic design of structures, whereas experiments are commonly used to gain a better insight into structure behavior, and to validate or calibrate the analytical models used in the computer simulation. These are the traditional understandings of computer simulation and experiment. Recent years, however, have witnessed the birth and development of an entirely new method to reproduce seismic behavior of structures, which combines computer simulation with physical tests interactively. This method solves the dynamics of a structure in the computer domain using step-by-step time integration algorithms, while obtaining restoring forces from a physical specimen. The computer provides displacements to the specimen as the loading target, and the measured restoring forces are fed back to the computer to update the dynamic state. This interaction continues repeatedly until the end of the simulation. Because of the online communication and updating, this simulation technique is called the "online hybrid test." Several benefits can be expected from this method. First, the inertial effect is simulated numerically in a computer. There is no need to construct massive physical payload on a specimen, as it is loaded quasi-statically. Therefore, a large-scale specimen can be implemented. Second, because the loading rate is quite slow, one can closely observe the initiation and development of damages on the specimen, which is very important for better understanding of the seismic behavior. Finally, the online hybrid test can be realized by conventional load devices instead of sophisticated facilities such as shaking tables. It has been well developed over the past 30 years and has become one of the standard approaches to examine the seismic performance of structures.

The recent development of online hybrid tests has been classified into two categories: the real-time online hybrid test and the substructure online hybrid test. A real-time online hybrid test requires a very prompt response of loading devices. The dynamic interaction between the loading facility and the specimen must be considered explicitly because the response delay of the loading device may lead to divergence of the entire dynamic system. To compensate for this delay is the key problem of the real-time online hybrid test, and is essentially a hydro-mechanical control problem. A full discussion of the real-time online hybrid test is beyond the scope of this book and thus will not be discussed hereafter. The substructure online hybrid test takes the most critical part of a structure as the experimental substructure, while the rest with well-understood

performance, is numerically analyzed. The substructures are often distributed to different locations and connected through a network, thus being able to utilize resources from multiple laboratories. The substructure and network render the online hybrid test capable of investigating the seismic behavior of large-scale structures, so that, for example, the seismic responses of long-span bridges, braced frames, and concrete wall structures are reproduced.

In spite of the rapid growth of the online hybrid test, little has been published in book form to guide the practitioner. The purpose of this book is to provide comprehensive treatments of several topics pertinent to the substructure online hybrid test. Emphasis has been placed on three frameworks: host-station framework; separated model framework; and peer-to-peer framework. These frameworks have been developed within the Internet environment and are particularly suitable for distributed hybrid testing. In order to help the readers to understand the essence of the online hybrid test and further to build up their own system, an engineering practice has been introduced at the end of this book with the source code appended. We address ourselves primarily to readers who have some background in structural dynamics, finite elements, and computer science. Efforts have been made to consolidate and simplify material that has appeared only in journal articles, and to provide the reader with a perspective of the state-of-the-art.

Financial support from the "Twelfth Five-Year" plan major projects from the National Science and Technology under Grant Nos. 2011BAJ06B03, 2011BAJ08B05, and 2012BAJ07B02, and by the Natural Science Foundation of China under Grant Nos. 50808107, 51178250, and 51422809, are gratefully acknowledged. We also gratefully acknowledge the support and encouragement received from our colleagues at Kyoto University, Tsinghua University and the Institute of Engineering Mechanics, and the research contributions of graduate students and technicians. Our special thanks are extended to Mr Alexandre Lam and Mr Dongbin Zhang, who have spent many hours editing this book. We also thank our families for their support, patience, and above all their love, without which this book could not have been written.

Peng Pan, Tao Wang, and Masayoshi Nakashima
Beijing, China
May, 2015

Chapter 1

Introduction

Chapter Outline

1.1 BACKGROUND, OBJECTIVE, AND CHALLENGE

Two approaches are commonly used for simulating the earthquake responses of structures. One is the numerical simulation by which the equations of motion are formulated for a spatially discretized model and solved numerically by the time integration algorithms in the time domain. The other is the experimental simulation by imposing the ground motions directly on the tested specimens. In the numerical simulation, a sophisticated model with huge degrees of freedom can be implemented, which is able to supply accurate responses. The solution procedure for this huge model, however, may be time-consuming, and the convergence of this solution procedure is always a critical problem, especially when great material nonlinearity and geometric nonlinearity are considered simultaneously. Furthermore, the existing analytical tools, such as finite element method (FEM) programs, are often strong only for some types of structures. On the other hand, the experimental approach cannot handle full-scale structural models effectively either. It is very expensive and nearly impracticable to test a full-scale model of such a structural system, and a reduced-scale model is unable to duplicate the prototype behavior, particularly when it involves strong nonlinearities. Therefore, it is not necessarily easy to accurately simulate the seismic responses of a huge and complex structural system by using either a single analytical method or a single experimental method.

The online hybrid test [1–4] (also called the "pseudodynamic test") is appealing, since it can make use of the benefits of both the analysis and test. The online hybrid test has a history of more than 30 years, and many applications have demonstrated its effectiveness. The basic procedure of the first online tests can be described as follows. First, the test specimen representing the structural system whose earthquake response behavior is being studied is fabricated and installed

Development of Online Hybrid Testing. http://dx.doi.org/10.1016/B978-0-12-803378-4.00001-7

on the test bed. Assuming the specimen to be a discrete spring-mass system, a load-applying actuator is attached to the specimen at each mass position and in the direction in which the earthquake response of the specimen is to be examined. Then, the equations of motion are solved numerically in a computer by using time integration algorithms, while the restoring forces are obtained from a physical test. Therefore, the online test is a numerical technique utilizing the experimental information on the analyzed system's restoring force characteristics, which are difficult to model within a computer. Some of its major advantages are (1) less actuator capacity is required than in the shake table because the loading can be quasi-static; (2) since the loading can be a repeated process of loading and pausing, conventional measuring devices used in quasi-static tests are sufficient; and (3) the loading can be stopped because of the discrete loading, enabling us to make close observation of the local behavior.

Since accurate displacement control and measuring are keys to the success of the test, the results given by the online test are more and more accurate, due to the advancements in the technology of electronic devices, such as integration circuits and micro-processors. However, the online test is an approximate method including various assumptions and simplifications. The error sources are classified into two groups: intrinsic and experimental. Some of the major sources of intrinsic errors are (1) the analyzed system is represented by a spring-mass discrete system; (2) the equations of motion are discretized with respect to the time domain and solved as difference equations; and (3) the damping is characterized as velocity-proportional viscous damping. Some of the major sources of experimental errors are (1) the displacement value commanded to the servo controller differs from the computed displacement because of the finite resolution of the D/A converter; (2) the displacement reached after the actuator motion may be different from the command value because of the finite accuracy of the displacement sensor and the servo control limitation; (3) the force value measured may not be identical to the true force because of the finite accuracy of the load-measuring sensor; and (4) the measure force is changed to a digital value after the A/D conversion. Investigations on these error sources have been done by Nakashima and Kato to study and minimize them [5–8].

The online test has been improved over time by many researchers, using it with other techniques, hardware, and software. The test, when combined with substructuring techniques, is called a substructure online hybrid test, and is particularly appealing for the earthquake response simulation of large-scale structures [9–17]. In the substructure online test, part of the structure whose restoring force behavior is too complex to model is tested, while the rest of the structure is modeled in the computer, and the equations of motion that represents the entire structure are solved. Most previous applications of the substructure online hybrid test, however, have the following shortcomings: (1) the adopted numerical models used relatively crude assumptions and a limited number of degrees of freedom, a typical one of which was a stick model with lumped

masses; (2) most applications implemented the numerical and experimental substructures at a local structural laboratory, where the limitation of analytical tools and loading facilities limit the applicability of online hybrid test systems for the seismic simulations of large-scale structures.

The online hybrid test is in essence a test with displacement control. The displacements for the next time step are predicted and applied to the test structure; the reaction forces corresponding to the target displacements are measured and fed back to the equations of motion for the prediction of the next displacements. Displacement control, however, is not practicable when the test structure is too stiff to accurately control the loading actuator's displacement. However, we can find cases in which we wish to apply online tests to stiff structures, for example, an online test applied to a base-isolated building using the substructuring techniques in which only isolation devices, say, rubber bearings are tested. Therefore, a system which can combine control by displacement and force is appealing [18].

Subsequent improvements to numerical analyses have been very positive for earthquake response simulation, and many general-purpose FEM software applications have been made available. In such circumstances, it would seem very effective to use a FEM software application for the computation of the numerical substructures. Some important applications along this line are the online test system developed in European Laboratory for Structural Assessment (ELSA) [19]; the Network for Earthquake Engineering Simulation (NEES) of the National Science Foundation of USA [20]; and a portable online test system developed by Pan et al. [21]. The incorporation of the FEM source codes has been demonstrated to be capable of improving the accuracy of the numerical substructures and making the online hybrid test system more versatile. Two common features can be found from these applications: (1) only one numerical substructure was implemented in these proposed systems. The equations of motion of the entire structure were formulated based on the FEM model for the numerical substructure, and the restoring forces obtained from the experimental substructures were incorporated into the FEM model directly using the static condensation technique; and (2) the source codes of the FEM programs were modified to incorporate the experimental part into the entire analysis. This is, however, difficult, because the program is commonly so complex that modification of the source code involves huge efforts and needs special expertise. Furthermore, most commercial FEM programs are copyright-protected, and modifications to the source code have to resolve legal issues. Therefore, the developed online hybrid test systems are rather difficult to transfer from one laboratory to another, and the FEM programs employed in these systems are not easy to be replaced by the one most suitable for the concerned structures.

To geographically distribute the experimental substructures and analytical substructures to different locations and exchange the necessary data through the Internet is also desirable because this type of test environment will significantly increase the capacity of the substructure online hybrid test. The concept

of "Internet testing" or "distributed testing" has been addressed over recent years [22–24], and a few real applications have been reported: the distributed online tests conducted between Japan and Korea [25], in Taiwan [26], and in the United States as part of the George E. Brown, Jr. NEES [27]. All these applications demonstrate the advantage of distributing substructures to different locations. To fully take advantage of "Internet testing" or "distributed testing," it is important to standardize and simplify the interfaces of diverse subsystems so that they can be effectively incorporated into an integrated Internet test system. Such standardization and simplifications require the subsystems to be highly encapsulated. Therefore, in order to increase the flexibility and capacity of the substructure online hybrid test system, it would be feasible to treat all substructures equally and as independent as possible, and to develop a standard interface for the communication between all substructures.

One solution is to solve the equations of motion and obtain the hysteretic behavior of a structure by using separated models with different sophistication. The equations of motion are formulated for the entire structure and solved by using homemade source codes, while the hysteretic behavior is obtained from sophisticated FEM models or from physical tests. Disparity in the model sophistication would be reasonable in a situation, such as when a sophisticated static model is needed for accurate evaluation of member internal forces and deformations, while the dynamics of the structure are well represented by the first several vibration modes, which may be determined from a model with much fewer degrees of freedom. In this framework, the only responsibility of each substructure is to provide the static force-displacement relationship to the dynamic model. Therefore, all substructures can be treated equally. This implementation makes the system more versatile, since various FEM programs or experimental facilities can be selected for different substructures according to their individual characteristics [28].

As another solution, the equations of motion can be formulated for each substructure rather than for the entire structure. Each substructure is treated equally and as an independent dynamic subsystem, which can be selected for numerical simulation or physical test. Because of the independence and equal status of each substructure, this solution can be identified as a peer-to-peer (P2P) framework. The equilibrium and compatibility at the boundaries between the substructures can be satisfied by an equation-solution procedure. Each substructure only exchanges data with this equation-solution procedure, but does not with the other substructures. In this framework, each substructure is highly encapsulated, and only the standard input and output, i.e., the boundary displacements and corresponding reaction forces, are used as the data to exchange. Therefore, this substructure online hybrid test system is able to accommodate different simulation systems without much modification. Furthermore, the equations of motion are formulated independently for each substructure and solved in parallel. Indeed, parallel computing can increase the capacity and efficiency significantly for computation of large systems [29,30].

The objective of this book is to provide the basis of the online hybrid test, and an overview of recent developments with some applications is given. In this book, in addition to a summary of available algorithms and implementations of the online hybrid test, four online hybrid test systems based on the displacement-force mixed control, the host-station framework, the separated-model framework and the P2P framework, respectively, are presented. Each of them brings an improvement to the online hybrid test. Furthermore, some applications in engineering practice are given.

1.2 ORGANIZATION

This book consists of nine chapters. This chapter relates the background of this study, and Chapter 9 gives the summary and conclusions. Chapters 2–9 constitute the main part of the book: (1) basics of the online hybrid test; (2) time integration algorithms for the online hybrid test; (3) the online hybrid test using mixed control; (4) the Internet online hybrid test using the host-station framework; (5) the separated-model framework and its demonstration examples; (6) the P2P framework, its preliminary demonstration test and its convergence speed investigation; (7) its application in engineering practice. The contents of the seven chapters are summarized below.

In Chapter 2, the basics of the online hybrid test, which mainly include the components of the test system, the capacities of online hybrid test, and the procedures commonly adopted for the online hybrid test are introduced. This chapter is to provide users who are new to the online hybrid test, with a general introduction to this technique. After reading this chapter, the readers are expected to have the fundamentals to plan a simple online hybrid test, and understand how physical and computational components work together during the execution of an online hybrid test.

In Chapter 3, the time integration algorithms, which are important to solve the equations of motion of online hybrid tests, are introduced. The existing time integration algorithms are grouped into such families as (1) linear multistep methods; (2) Newmark's family; (3) collocation methods; (4) α-family; (5) ρ-family; and (6) mixed implicit-explicit methods. The superiority of one family over the others is summarized in terms of the following rules: (1) self-restart procedure; (2) second-order accuracy; (3) unconditional stability; and (4) optimal and controllable numerical dissipation. Also, the typical analysis methods for stability and accuracy are formulated, and numerical characteristics, such as stability, accuracy, numerical dissipation, and period distortion, are examined and compared for some notable time integration algorithms usable for the online hybrid test. Summarized also in this chapter are their algorithms and implementations, which include the implementations using the central difference algorithm, the hardware-dependent iterative scheme, the Newton-type iterative schemes, and the noniterative mixed schemes.

In Chapter 4, an online test technique that employs mixed control of displacement and force is presented. Indeed, displacement control is not practicable when the structure is too stiff to accurately control the loading actuator's displacement. Two types of mixed control "displacement-force combined control" and "displacement-force switching control" are proposed. In displacement-force combined control, one jack is operated by displacement control, and another is operated by force control. Validity of the combined control technique is demonstrated by a series of online tests applied to a base-isolated structure subjected to horizontal and vertical ground motions simultaneously. The substructuring technique is employed in the tests, and the base-isolation layer is tested, with the rest of the structure modeled in the computer. Displacement control and force control were adopted for simulating the horizontal and vertical response, respectively. In the displacement-force switching control, the jack was operated by displacement control when the test specimen was flexible but switched to force control once the specimen became stiff. Validity of the switching control technique was also checked by a series of online tests applied to the base-isolated structure subjected to vertical ground motions. Switching between displacement control and force control was achieved when the axial force applied to the base-isolation layer changed from tension to compression or from compression to tension.

In Chapter 5, an Internet online test system is developed in which a physical test is conducted in one location, the associated numerical analysis is performed in a remote location, and the two locations communicate over the Internet. To implement the system, a technique that links test and analysis domains located at different places is proposed, and an Internet data exchange interface is devised to allow data communication across Internet. A practical method that utilizes standard protocols implemented by operating systems for sharing files and folders is adopted to ensure stable and robust communication between remotely located servers that commonly protect themselves by strict firewalls. Therefore, the system consists of the host, stations, and data exchange interfaces. To combine the online test with a FEM program formulated in an incremental form and adopting an implicit integration scheme, a tangent stiffness prediction procedure is proposed. In this procedure, a tangent stiffness is estimated based on a few previous steps of experimental data. Using the system devised, tests on a base-isolated structure were carried out.

In Chapter 6, the development of the separated-model framework is introduced, and its validity is demonstrated. In this framework, two models are setup for the dynamics and the static behavior of one structure, respectively. The incorporation of general-purpose FEM programs into the static model is realized by repeatedly using its inherent restart capability. The general-purpose FEM program thus can be viewed as a black box with standard input and output interfaces, avoiding the modification of the source code. Furthermore, a high-speed scheme using a socket mechanism based on TCP/IP protocol is developed for data exchanged through Internet. A proxy program is setup to solve the data exchange difficulties when strict firewall exists. An encoding-decoding

procedure is also developed for various subsystems. The Internet online hybrid test environment based on this separated-model framework is developed, and three example structures are setup to demonstrate its effectiveness and validity. The one- and three-story braced frames are first examined by this system locally and numerically. Thereafter, an eight-story base-isolated structure is taken as the demonstration example for the Internet online hybrid test system.

In Chapter 7, the P2P framework is realized, and its validity is demonstrated by a preliminary study. In this framework, the simulated structure is divided into multiple substructures, all substructures are equally treated, and each substructure is analyzed or tested in a subsystem. The equations of motion are not formulated for the entire structure but for each substructure separately, and solved in parallel. Substructures are treated as highly encapsulated and independent subsystems, and only a standard I/O is used to exchange data on the displacements and forces at the boundaries. This enables the useful incorporation of existing FEM programs. The core of the framework, called "Coordinator," equipped with an iterative algorithm based on quasi-Newton iterations, is developed to achieve compatibility and equilibrium at the boundaries. A predictor-corrector test procedure featuring two rounds of quasi-Newton iterations is adopted to avoid iteration for the substructures being tested physically. In each round of quasi-Newton iteration, the tested substructures are assumed to be linear elastically without physical loading. The nonlinearity of the tested substructures is introduced only by the one-time physical loading between the two rounds of quasi-Newton iterations. One demonstration test is conducted for the seismic simulation of a base-isolated structure. The test environment developed for the separated-model framework is adopted. Three substructures are included: the base-isolation layer as the first substructure, the first to fourth stories as the second substructure, and the remaining part of the superstructure as the third substructure. The base-isolation layer is tested at the laboratory, while the second and third substructures are handled linearly using a homemade source code. The quasi-Newton procedure is essentially a trial and error procedure. The convergence speed of the P2P framework when considering nonlinearity of the numerical substructures is investigated by numerical examples. The P2P framework is applied for the seismic simulation of a base-isolated structure, where only the tested base-isolation layer involves great nonlinearity, while the numerical substructures are treated linearly. However, the convergence becomes more difficult and time-consuming when nonlinearity is considered for all substructures. In the P2P framework, the convergence is dominated by the quasi-Newton procedure, which is a typical equation-solution procedure. The convergence speed is the main concern to examine, because nonlinearity may result in a large number of iterations and thus the system becomes inefficient. Considering the procedure used for the P2P framework, the following factors are found to affect the convergence speed: (1) convergence criteria and tolerance; (2) type of divisions into substructures; (3) number of degrees of freedom on the boundaries; (4) initial stiffness prescribed for the first quasi-Newton procedure. The effects of the four factors are examined by

using a mass-spring model with nine degrees of freedom. The nonlinearity is mimicked by using the Ramburg-Osgood function. Moreover, the linear assumption adopted for the tested substructure during both predicting and correcting procedures would introduce extra energy into the dynamic system, which probably contaminates the dynamic responses, and even leads to instability. A spectral method is thus employed to examine numerical characteristics of the proposed predictor-corrector procedure.

In Chapter 8, two typical applications are presented, one of the conventional online hybrid test and one of the P2P Internet online hybrid test, in order to demonstrate the utility and efficiency of this method in engineering practice. First, the seismic performance of a retrofitted reinforced concrete shear wall building is evaluated through substructure online hybrid tests. Then, the collapse of a one-bay, four-story steel moment frame is simulated by the proposed P2P Internet online hybrid test system, using an improved test scheme.

REFERENCES

[1] Takanashi K, Udagawa K, Tanaka H. Earthquake response analysis of steel frames by computer-actuator online system, In: Proceedings of the 5th Japan earthquake engineering symposium, November; 1978. p. 1321–8.

[2] Mahin SA, Shing PB. Pseudodynamic method for seismic testing. J Struct Eng ASCE 1985;111(7):1482–501.

[3] Shing PB, Nakashima M, Bursi OS. Application of pseudodynamic test method to structural research. Earthq Spectra 1996;12(1):29–56.

[4] Takanashi K, Nakashima M. Japanese activities on online testing. J Eng Mech ASCE 1987;113:1014–32.

[5] Nakashima M. Part I: Relationship between integration time interval and response stability in pseudo dynamic testing. J Struct Constr Eng 1985;353:29–36.

[6] Nakashima M. Part II: Relationship between integration time interval and accuracy of displacement, velocity, and acceleration responses in pseudo dynamic testing. J Struct Constr Eng 1985;358:35–42.

[7] Nakashima M, Kato H. Part III: Experimental error growth in pseudo dynamic testing. J Struct Constr Eng 1988;386:36–48.

[8] Nakashima M, Kato H. Part IV: Control of experimental error growth in pseudodynamic testing. J Struct Constr Eng 1989;401:129–38.

[9] Nakashima M, Ishii K, Kamagata S, Tsutsumi H, Ando K. Feasibility of pseudo dynamic test using substructuring techniques. In: Proceedings of 9th world conference on earthquake engineering, vol. 4, Tokyo; 1988. p. 47–52.

[10] Nakashima M, Kaminosono T, Ishida M, Ando K. Integration techniques for substructure pseudodynamic test. In: Proceedings of 4th U.S. national conference on earthquake engineering, vol. 2, Palm Springs, CA; 1990. p. 515–24.

[11] Tsutsumi H, Sato K, Ando K. Substructure pseudo dynamic test with rotation control. In: Proceedings of 4th U.S. national conference on earthquake engineering, vol. 2, Palm Springs, CA; 1990. p. 525–34.

[12] Kanda M, Adachi J, Shirai N, Nakanishi M. Implicit integration scheme based on initial stress method for substructure online hybrid test. J Struct Constr Eng Archit Inst Jpn 1995;473:75–84 [in Japanese].

[13] Kusunoki K, Nakano Y, Okada T. Substructure online hybrid test of reinforce concrete column. J Struct Eng Archit Inst Jpn 1998;44B:141–8 [in Japanese].
[14] Ohi K, Lin X, Takanashi K. Sub-structure pseudo-dynamic test scheme suitable for bending-shear type flexible steel frames. J Struct Constr Eng Archit Inst Jpn 2001;540:49–55 [in Japanese].
[15] Maeda M, Kang D, Tanaka K, Inoue N. Evaluation of post-earthquake seismic capacity of reinforced concrete buildings by sub-structural pseudo-dynamic testing, part 1 and 2. In: Technical summary of annual convention. Japan: Architectural Institute of Japan; 2002. p. 213–6. Structure IV [in Japanese].
[16] Wu B, Xu G, Wang Q, Williams SM. Operator-splitting method for real-time substructure testing. Earthq Eng Struct Dyn 2006;35:293–314.
[17] Magonette G. Development and application of large-scale continuous pseudo-dynamic testing techniques. Philos Trans R Soc Lond A 2001;359:1771–99.
[18] Pan P, Nakashima M, Tomofuji H. Online test using displacement-force mixed control. Earthq Eng Struct Dyn 2005;34:869–88.
[19] Pinto AV, Pegon P, Magonette G, Tsionis G. Pseudo-dynamic testing of bridges using non-linear substructuring. Earthq Eng Struct Dyn 2004;33:1125–46.
[20] Multi-site, on-line simulation test, NEESgrid. http://www.neesgrid.org/most [13.11.03].
[21] Pan P, Tada M, Nakashima M. Online hybrid test by internet linkage of distributed test and analysis domains. Earthq Eng Struct Dyn 2005;34:1407–25.
[22] National Science Foundation. Network for earthquake engineering simulation (NEES): earthquake engineering research equipment, Program solicitation. Report NSC00-6, USA: National Science Foundation; 2000.
[23] National Science Foundation. Network for earthquake engineering simulation (NEES): system integration, program solicitation. Report NSC00-7, USA: National Science Foundation; 2000.
[24] Tsai K, Hsieh S, Yang Y, Wang K, Wang S, Yeh C, et al. Network platform for structural experiment and analysis (I). Report NCREE-03-021. Taiwan: National Center for Research on Earthquake Engineering; 2003.
[25] Watanabe E, Yun C, Sugiura K, Park D, Nagata K. Online interactive testing between KAIST and Kyoto University. In: Proceedings of the fourteenth KKNN symposium on civil engineering, Kyoto, Japan; 2001. p. 369–74.
[26] Wang K, Tsai K, Wang S, Cheng W, Yang Y. Networked hybrid test frameworks and examples. In: The fifth seminar on earthquake engineering for building structures (SEEBUS), Kyoto, Japan; 2003. p. 81–90.
[27] Takahashi Y, Fenves GL. Software framework for distributed experimental-computational simulation of structural systems. J Earthq Eng Struct Dyn 2006;35:267–91.
[28] Wang T, Nakashima M, Pan P. On-line hybrid test combining with general-purpose finite element software. Earthq Eng Struct Dyn 2006;35(12):1471–88.
[29] Pan P, Tomofuji H, Wang T, Nakashima M, Ohsaki M, Mosalam KM. Development of peer-to-peer (P2P) Internet online hybrid test system. Earthq Eng Struct Dyn 2006;35(7):867–90.
[30] Wang T, Yoshitake N, Pan P, Lee TH, Nakashima M. Numerical characteristics of peer-to-peer (P2P) internet online hybrid test system and its application to seismic simulation of SRC structure. Earthq Eng Struct Dyn 2008;37(2):265–82.

Chapter 2

Basics of the Online Hybrid Test

Chapter Outline

2.1 INTRODUCTION

The seismic performance of structural systems under earthquake loading is no doubt an area requiring extensive research. In fact, many research bodies all over the world have been engaged in investigating the seismic response of various types of structural systems. In general, research on the seismic performance of structural systems can be classified into two groups: analytical research and experimental research. Because of innovation in the fields of electronics and the mechanics, the progress of those two groups of research has been remarkable. It is now by no means difficult to simulate the static and dynamic earthquake response of complex structural systems using numerical techniques, such as the finite element method. The development of experimental hardware has also made it feasible to conduct large-scale static and dynamic tests with careful test control.

About 40 years ago, a new type of research techniques to study earthquake response behavior of structural systems was developed. This technique is unique because it combines the experiment and numerical analysis, and utilizes the benefits of both experimental and analytical research. With this technique,

Development of Online Hybrid Testing. http://dx.doi.org/10.1016/B978-0-12-803378-4.00002-9

one can directly simulate the earthquake response of structural systems with respect to the time domain, but without using a shake table device. This technique has been designated with various names: computer actuator online test, hybrid experiment, pseudodynamic test, or online computer test control method. Recently it is more often designated as hybrid simulation. In this book, this technique is designated as the online hybrid test control method, and simply referred to as the online hybrid test.

2.2 BASIC CONCEPTS AND APPLICATIONS

2.2.1 Test Methodology

The basic idea of the online hybrid test method is quite simple if one is familiar with the procedures involved in conventional quasi-static testing and numerical time integration techniques used in dynamic analysis of structures. First, the structure to be tested is idealized as a discrete-parameter system that has a limited number of degrees of freedom (DOF), each of which is controlled by an actuator in a quasi-static manner. This is why the online hybrid test is also referred as the pseudodynamic test. Consider, for example, the four-story frame shown in Fig. 2.1a. Since the axial stiffness of the floor beams is usually much higher than the flexural stiffness of the columns and the response of the frame under a horizontal base motion is expected to be dominated by the inertia forces developed at the floor levels, one can idealize the structure as a 4-DOF system, as shown in Fig. 2.1b. The equations of motion for this structure can thus be expressed as:

$$Ma + Cv + r = f \tag{2.1}$$

in which M and C are the mass and damping matrices of the structure, v and a are the vectors of nodal velocities and accelerations, r is the nodal restoring force vector, and f is the external excitation. For a linearly elastic system, $r = Kd$,

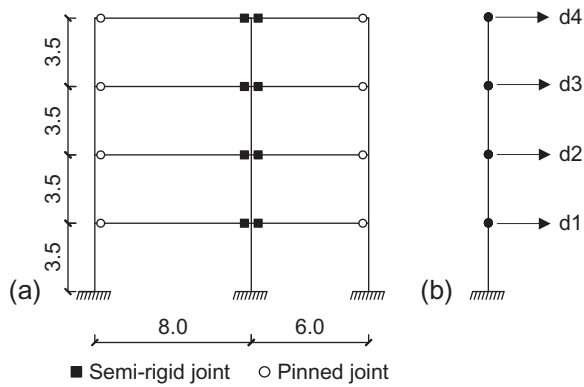

FIGURE 2.1 Online hybrid testing of a two-bay frame. (a) Two-bay frame, (b) discretized model.

where K is the stiffness matrix of the structure and d is the vector of nodal displacements. If the structure is subjected to a horizontal ground acceleration a_g, $f = -M\{1\}a_g$, where $\{1\}$ is a unit vector.

Once the structural model is discretized, its equations of motion are solved by means of a direct step-by-step integration scheme in an online hybrid test, with the mass and viscous damping properties of the structure modeled analytically. In every time step of a test, the displacement response computed for each DOF is imposed on the structure in a quasi-static fashion by means of actuators, and the restoring forces, r, developed by the structure are measured with load transducers and are used to compute the response in the next time step. Hence, one can see that the online hybrid test method is essentially similar in concept to dynamic structural analysis, except that the stiffness properties of the structure are directly measured from the structural specimen during a test. Since the inertia effects are modeled analytically, such a test can be conducted in a quasi-static fashion with conventional testing equipment. The details of this method have been summarized by Mahin and Shing [1].

2.2.2 Research Applications

A most desirable feature of the online hybrid test method is its versatility. It can be used to evaluate the earthquake performance of large full-scale structures [2–5], small-scale structures [6], and structural subassemblies and components [7–10]. Both the planar and three-dimensional response of a structure can be investigated with this method [11,12]. Even though the shaking table test method has been known as the most direct experimental technique to simulate the earthquake response of structures, it has some limitations, such as the size and weight of a structure that can be tested. Furthermore, the cost of a table goes up rapidly with its size, capacity, and number of DOF. On the other hand, an online hybrid test can be carried out with a large-scale structure because of the relatively slow rate of load application. For a given hydraulic power capacity, a slow-moving actuator can have a larger-diameter piston and, thereby, produce a larger force than a fast-moving actuator.

The physical limitations of an online hybrid test system are, however, the number and capacities of actuators that are available, and the dimensions and load capacities of reaction systems that are used to support the structural specimen and the actuators. However, the capacity of such a system can be expanded gradually to meet any changing needs. When compared with conventional quasi-static tests, the online hybrid test method can be considered as a major enhancement that requires only a small incremental investment. The online hybrid test method is especially attractive for evaluating the earthquake performance of multi-DOF structures and structural subassemblies. While conventional quasi-static testing is useful for comparing the performance of different structural designs under a standardized load history, it does not account for the ductility demand of an earthquake ground motion on a structural specimen

or the proper distribution of earthquake-induced forces. Such problems can be resolved with the online hybrid test method, in which the displacement history and pattern applied to a structure are determined from the equations of motion.

With an analytical substructuring procedure, the online hybrid test method can be applied to structural subassemblies. Very often, the damage inflicted upon a structure by seismic excitation is localized in a few critical regions or subassemblies. In such a case, there is no compelling reason to test the entire structural system. One can take advantage of such a situation in an online hybrid test by testing only the critical subassembly and modeling the rest of the structure in a computer. The equilibrium and displacement compatibility conditions between the experimental and analytical substructures can be enforced with a standard substructuring approach. For example, let us consider the four-story frame shown in Fig. 2.1a, and we are only interested in testing the critical beam-column subassembly located at the bottom of the frame, which is shown in Fig. 2.2. To derive the proper displacement or load boundary conditions that are to be imposed on the experimental substructure, the rest of the frame is modeled in a computer. The equations of motion for the entire structure and the total restoring forces developed can then be assembled for direct step-by-step analysis. The displacement responses computed are imposed on the analytical and experimental substructures accordingly. The displacements are imposed on the experimental substructure with actuators, as shown in Fig. 2.2. This method was first developed and implemented by Dermitzakis and Mahin [13], and has had a number of promising developments in recent years [9,14–16].

One useful application of the substructuring test method is to evaluate the performance of base-isolation devices, as shown by the example in Fig. 2.3. The main intention of a base-isolation device is to dissipate energy and prevent the transmission of large seismic forces to the superstructure. In such a case, the major source of nonlinearity in the system is in the isolation devices, and the superstructure can be modeled with a reasonable level of accuracy in a

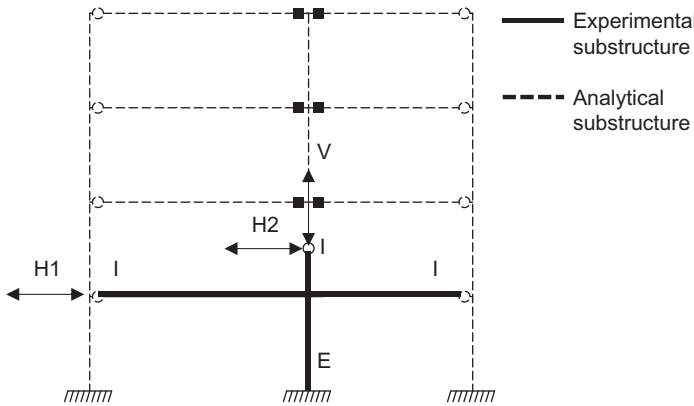

FIGURE 2.2 Substructure test of a two-bay frame.

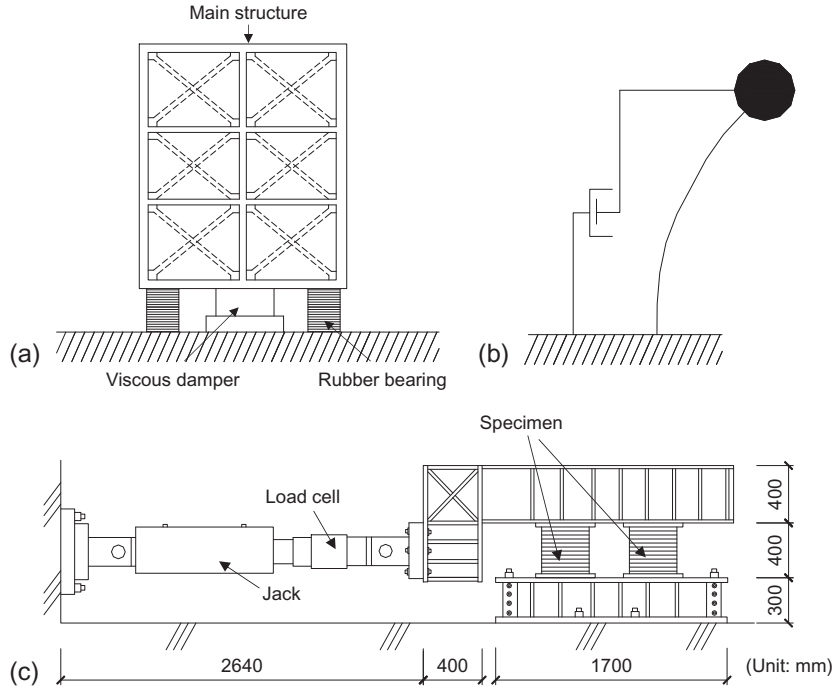

FIGURE 2.3 Substructure test of base-isolation devices. (a) Structural model, (b) spring-mass representation, and (c) test setup used in pseudo-dynamic test.

computer. Hence, one can treat the superstructure as an analytical substructure, and test only the isolation device as shown in Fig. 2.3. The interaction of the superstructure with the isolation device can be handled analytically with a standard substructuring scheme. Since the damping characteristics of many isolation devices are sensitive to the rate of loading, a fast online hybrid testing technique has been developed by Nakashima [7] for such applications. Fast online hybrid testing, which is also known as real-time online hybrid testing, has been developed rapidly within the last 10 years. In this book, real-time online hybrid testing is not included.

2.2.3 Advantages and Constraints

The online hybrid test is a numerical technique utilizing the experimental information on the analyzed system's restoring force characteristics, which often are the most difficult properties to model within the computer domain. Application of this technique was made possible for the first time after the advancement of experimental hardware and their control systems, with the use of computers. The online hybrid test has some advantages over both pure numerical analysis and quasi-static tests. Different from the pure numerical analysis, it obtains the

restoring force directly from the test, thus it can simulate the complex behavior of structures or structural members without having their numerical model. Different to the quasi-static test, which can only be used to investigate the capacity of structures or structural members, it can simulate the seismic responses of structures or structural members and can be used to investigate both the seismic demands and structural capacity.

The online hybrid test possesses a variety of advantages over the shaking table test, the most direct test method for simulating the earthquake response behavior of structural systems. Some of the major advantages of the online hybrid test are as follows: (1) as the loading can be quasi-static, less actuator capacity is required than in the shaking table test if the same specimen is tested; (2) since the loading can be repeated, the process of loading and pausing, conventional measuring devices used in quasi-static test are sufficient, whereas in the shaking table test measurements should be simultaneously and continuous; and (3) because of the discrete loading, the loading can be stopped at any time upon request, and this enables us to closely observe the local behavior of individual structural elements.

As stated above, the online hybrid test has been found to be a very attractive technique for simulating the earthquake response behavior of a structural system, and many researchers in Japan, the United States, and more recently in Europe and China, have employed this technique for their individual research and studies on the seismic characteristics of various structural systems.

While the online hybrid test method provides an efficient means for experimental research, it is not without limitations. The method is not practical for testing a structure which requires a fairly refined spatial discretization to capture its dynamic behavior in a realistic manner. This includes structures, such as concrete dams, which have a fairly uniform mass distribution. The testing of this type of structure with the online hybrid method may require a large number of actuators, which reduces the attractiveness of the method. Furthermore, it is important to emphasize that in an online hybrid test, the viscous damping properties of a structure are assigned rather arbitrarily in accordance with conventional wisdom. This is based on the notion that the energy dissipation in a structure is usually dominated by hysteretic damping, which can be accurately accounted for in an online hybrid test. Hence, the online hybrid test method would not be appropriate if the response of a structure is highly sensitive to its viscous damping properties and if one has difficulties in identifying them precisely.

Online hybrid test results should be carefully interpreted with consideration of the rate-of-loading effects. Usually, the strength of a material is lower with a lower rate of loading. Therefore, a quasi-static rate of loading may yield a lower structural resistance and may, therefore, lead to a higher ductility demand on a structure than a dynamic load [17]. Furthermore, there are cases that the failure mechanism of a structure, such as the localization of damage, may depend on the rate of loading. Such possibilities should be considered when test results are

interpreted. However, it should also be noted that when a small-scale model is tested on a shaking table, it is not possible to satisfy the dynamic similitude and yet maintain the same strain rate as the prototype structure at the same time. As a consequence, a small-scale model is often subjected to a higher rate of loading when compared with the prototype.

It is evident that the online hybrid test method is not suitable for problems where real-time dynamic response is a key consideration. Even though this problem has been partially resolved by Nakashima [7] by introducing a real-time online hybrid testing technique, it cannot be used, for example, for the performance evaluation of active control systems, where time delay is an important consideration. In summary, the online hybrid test method can be considered as a good alternative to conventional static and dynamic test methods for a specific class of problems that are commonly encountered in structural research, but it is certainly not a replacement for these methods.

2.3 IMPLEMENTATION AND MAJOR COMPONENTS

2.3.1 Implementation

The basic equipment requirement for an online hybrid test is essentially the same as that for a conventional quasi-static test [1,15]. In such a test, the deformation of the structural specimen is controlled by hydraulic actuators or mechanical jacks. To control the motions of different actuators in a steady and synchronized manner, a function generator is needed. A function generator is a digital device with which incremental displacement signals can be programmed and modulated as functions of time. The output from this device commands the motions of the actuators through electronic controllers. The controllers provide a closed-loop displacement control based on the feedback from displacement transducers attached to the structure or actuators. Nowadays, one can easily find a digital controller which has a built-in function generator. Furthermore, a data-acquisition system and a computer are needed. The latter is used for the numerical computation.

Figure 2.4 shows a conceptual flow of an online hybrid test. In each step of a test, the equations of motion are solved and displacement increments are computed. The computer can also be used to determine the velocities with which the displacement increments are to be imposed on the structure. The velocities should be set in such a way that the target displacements will be reached more or less at the same instant of time. This information is sent to a function generator, which commands the actuator controllers. Once the displacements are imposed on the structure, the computer is signified to collect data. The restoring forces developed by the structure are acquired and used to compute the displacement increments in the next step.

The control of structural displacements in an online hybrid test usually requires a much higher precision than conventional quasi-static tests. Any errors

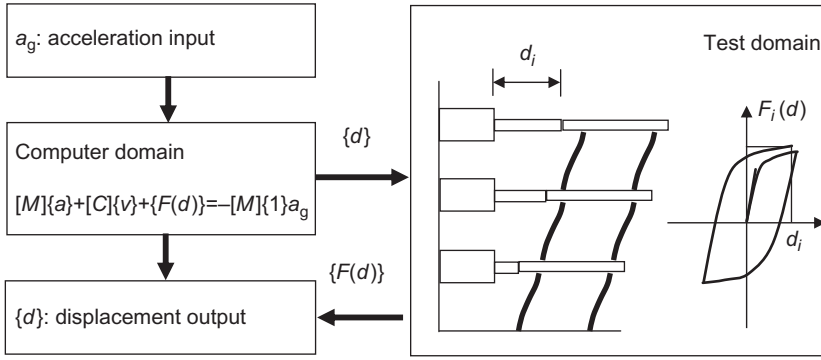

FIGURE 2.4 Conceptual flow of online hybrid test.

in displacement control are reflected in the restoring forces measured, which are used in the step-by-step computation. These errors can thus accumulate rapidly as time marches on [18–21]. The tolerance for these errors depends on the specific numerical algorithm used. A number of time integration schemes have been adopted and modified for online hybrid tests. They can be divided into two types. One is explicit [22] and the other is implicit [11,14,23–25]. Explicit schemes are conditionally stable, whereas a number of implicit schemes are unconditionally stable. The latter are, therefore, more suitable for testing multi-DOF structures. In the following sections, three different time integration schemes are presented. They are the central difference method, the α-method [24–26], and the operator-splitting (OS) method [14]. The first is an explicit method, while the last two are implicit and unconditionally stable. The implementation of these schemes for online hybrid tests is illustrated with test examples.

2.3.2 Major Components [27]

In its most basic application, an online hybrid test requires a numerical model of the structure with at least one physical tested component. Starting with a complete numerical model of the structure being analyzed represented by the dynamic equilibrium equation of motion, the component to be tested in the lab is removed numerically and replaced through a specialized link to the laboratory that allows data interchange at each integration step. For the purposes of this primer, it is assumed that there is only one computational and one physical component.

Figure 2.5 shows a configuration of basic components in such an online hybrid test. In a typical online hybrid test, the computational component sends target displacement to the physical component and the physical component returns measured force.

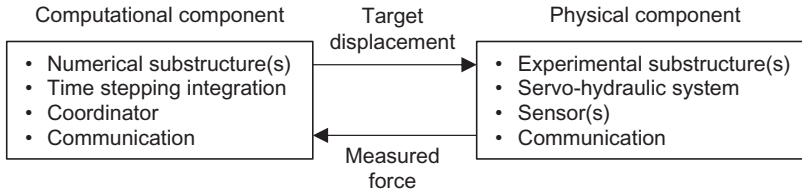

FIGURE 2.5 Basic components in online hybrid test.

The equipment used for quasi-static testing in most structural testing facilities can be utilized to conduct an online hybrid test. As shown in Fig. 2.5, the required laboratory setup includes: (1) a servo-hydraulic system, consisting of an actuator, controller, and pressurized hydraulic oil supply; (2) a physical specimen with the actuators attached at the DOF, where the displacements are to be imposed; and (3) sensors to measure the responses of the physical specimen. The major addition to standard equipment typically available in structural testing laboratories is a computer that can be programed to solve the equation of motion for the whole structure. This computer can be linked to hydraulic controllers and data acquisition, either by digital means or via analog/digital converters to send and receive analog signals to the equipment. In an online hybrid test, an experimental substructure can have one or more DOF and thus, the experimental setup will have one or more actuators. Additionally, an online hybrid test can have multiple experimental substructures.

The laboratory equipment above should be linked to a computer hosting the numerical simulation that is capable of computing a target displacement based on feedback from the laboratory transducers and then sending this displacement as a new command to the actuators. This may require custom coding to program the simulation and communication protocols with the laboratory; however, there are now some standard packages (e.g., UI-SIMCOR [12]; OpenFresco [16]) to accomplish these tasks to link to the experimental setup.

A hybrid simulation requires a controlling simulation component, often called the "master simulation" or "simulation coordinator," which encapsulates the whole structural model including all substructures. This master simulation/simulation coordinator controls a time-stepping integration algorithm and coordinates the communication between substructures.

2.4 SINGLE DOF STRUCTURE WITH EXPLICIT SCHEME

2.4.1 Test Structure

A 9-mm (0.35-in.)-thick steel panel was tested as a single DOF structure [13]. The panel was confined by top and bottom plates and a flange on each side. The test setup is shown in Fig. 2.6. A horizontal actuator was attached to the specimen via an L-shaped crosshead. The centerline of the applied load passed

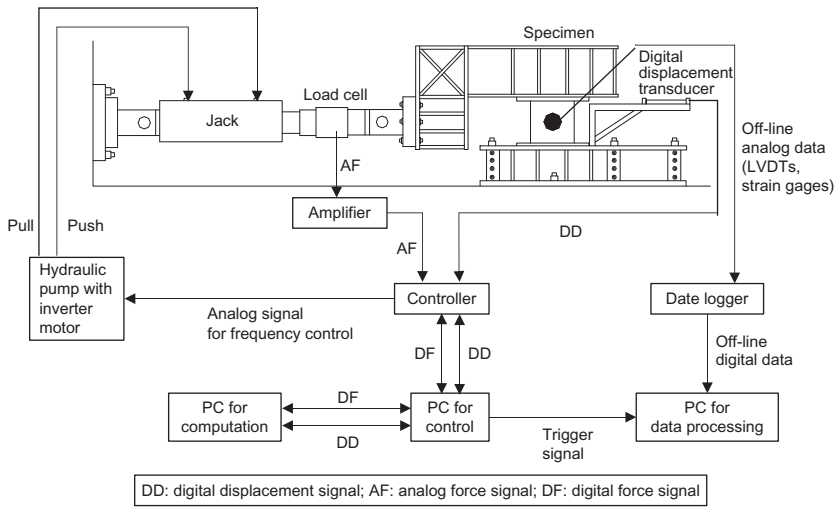

FIGURE 2.6 Online hybrid test of a shear panel.

through the mid-height of the panel to prevent the rotation at the top. The horizontal displacement at the top of the panel was measured by a digital transducer as shown in the figure. The initial elastic stiffness of the specimen was measured to be 500 MN/m (2855 kip/in.). It was assumed that the structure had a mass of 12.9 Mkg (73.7 kip s^2/in.) and a viscous damping of 2% of the critical. The ground acceleration record obtained at the Tohoku University in the 1978 Miyagiken-oki earthquake was used as the input excitation.

2.4.2 Test Method

The test was conducted with typical testing apparatus that were used for conventional quasi-static tests. As shown in Fig. 2.6, a hydraulic jack was used to control the displacement of the specimen. The stroke and velocity of the jack were regulated by a digital controller based on the feedback of the digital displacement transducer. The restoring force developed by the specimen was measured by a load cell. The unique feature of this setup is that three personal computers were employed. One was used for data processing. One was used to determine the ram speed and send the information to the digital controller, which also had a function generator. The third computer was used to solve the equation of motion and calculate the displacement response in each time step.

The central different method was employed to solve the equation of motion. This method is explicit and conditionally stable, which is certainly not a problem for a single DOF structure. By applying the central difference

approximations to the velocity and acceleration quantities and substituting them into Equation (2.1), the computation procedure can be expressed as follows:

$$d_{i+1} = \left(\frac{M}{\Delta t^2} + \frac{C}{2\Delta t}\right)^{-1} \left[\frac{2M}{\Delta t^2} d_i - \left(\frac{M}{\Delta t^2} - \frac{C}{2\Delta}\right) d_{i-1} - r_i - M a_{gi}\right] \tag{2.2}$$

in which Δt is the integration time interval and the subscript i represents the respective quantities at $t = i\Delta t$. The scheme is stable provided $\omega\Delta t$ is ≤ 2, where ω is the angular frequency of the structure. The central different method is a two-step method, which needs the displacement quantities at the two previous time steps to compute the response in the current step. To evaluate d_i at time equal to zero, one can introduce a fictitious displacement d_{-1} that is consistent with the central difference approximation as follows [19]:

$$d_{-1} = d_0 - \Delta t v_0 + \frac{\Delta t^2}{2} a_0 \tag{2.3}$$

in which a_0 can be computed from the equation of motion knowing the initial velocity and displacement.

The test procedure can be summarized as follows. In each step i, the displacement d_i was imposed on the specimen by the jack. The restoring force r_i developed by the structure was measured by the load cell and substituted into Equation (2.2) to compute d_{i+1}. This procedure was repeated by setting $i = i + 1$ until the entire response history was obtained. The integration time interval Δt was chosen to be 0.02 s. This resulted in a $\omega\Delta t$ of 0.128, which is considered to be sufficiently small to ensure an accurate solution.

Additional remarks. Experimental errors are often inevitable in an online hybrid test. For example, the target displacement computed may not be precisely imposed on a structural specimen. As a result, the structural restoring force developed and measured will have an error. The propagation of these errors in a test depends on the integration scheme used. With the central difference method, one should be aware of the following conditions to assure good test results [19,20].

1. It is better to use computed displacement values in Equation (2.2) for finding d_{i+1}. Using experimentally measured displacements will severely amplify the cumulative errors in the numerical results.
2. Systematic errors are often introduced in the control of structural displacements. Undershoot errors are introduced when the stroke of a jack tends to lag behind the target displacement consistently. With the central difference method, this type of error introduces spurious energy into the system. Overshoot errors occur when a jack tends to overshoot the target displacement. This introduces an energy dissipation effect. For a single DOF structure, the impacts of these two types of errors are similar. While the former will excite the structural response, the latter will attenuate the response. However, for a multi-DOF structure, the former is very undesirable as they can excite the

higher-mode response of a structure in a very severe manner. Hence, this type of error should be avoided by all means.

3. One way to detect overshoot and undershoot errors is to construct the Fourier amplitude spectrum of the displacement errors, which can be obtained by calculating the difference between the computed and measured displacements. Overshoot and undershoot errors are represented by long spikes in the Fourier spectrum occurring near the natural frequencies of the structure [19]. For a multi-DOF structure, overshoot errors are reflected by a spike at the fundamental frequency, while undershoot errors are reflected by a spike at the highest natural frequency. The latter is due to the excitation of the highest mode.
4. Before any destructive test, one should always conduct a small-amplitude trial test to detect the presence of the aforementioned errors and tune the loading apparatus if necessary. For a single DOF structure, these errors are usually not very crucial as long as they are relatively small, depending on the number of time steps in a test. It is recommended that they be smaller than 0.2% of the peak displacement of the structure for a typical test with 1000 steps. For multi-DOF structures, while overshoot errors can follow the same guideline as above, undershoot errors are not acceptable under any circumstances.

2.4.3 Test Results

The online hybrid test results obtained with the steel panel subjected to a high level of ground acceleration are shown in Fig. 2.7. The experimental results are compared with the numerical results obtained by modeling the hysteretic behavior of the specimen with modified Ramberg-Osgood functions [28]. An excellent correlation was obtained. It should be mentioned that the undershoot errors detected in this test were around 0.01 mm, which was about 0.05% of the peak displacement response. In general, the energy effects introduced by systematic errors are diminished by the hysteretic damping of a structure.

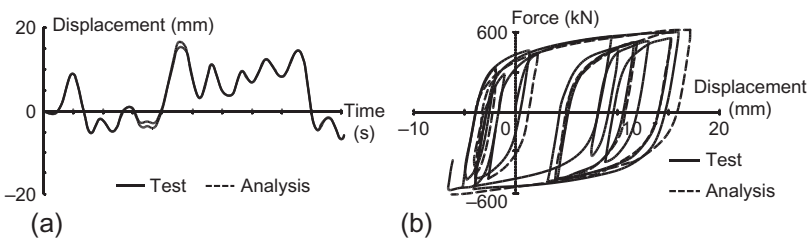

FIGURE 2.7 Results of an online hybrid test conducted on a shear panel. (a) Displacement response, (b) force-displacement response.

2.5 SUBSTRUCTURE TEST WITH OS SCHEME

2.5.1 Test Structure

A substructure test was conducted on a 10-story building model, which had a hysteretic damper in each story, as shown in Fig. 2.8. Each damper was a panel made of low-yield steel. It dissipated energy through shear deformation. The yield stress of the steel was about one-third of that of mild steel. The building was modeled as a 10-DOF spring-mass system, as shown in the Fig. 2.8. The inherent viscous damping of the structure was assumed to be proportional to the initial stiffness and the damping for the first mode was set to 2% of the critical. The ground motion record obtained at the Tohoku University during the 1987 Miyagiken-oki earthquake was used as the input excitation.

2.5.2 Test Method

Substructuring techniques were used to treat the hysteretic damper in the first story as an experimental substructure, while the rest of the frame was modeled in a computer. In the computer model, the frame was assumed to respond elastically and the dampers were modeled with modified Ramberg-Osgood functions [28]. The test setup shown in Fig. 2.6 was used again.

The time integration scheme used in this test is unconditionally unstable and is termed the OS method [14]. Unlike the implicit scheme presented above, the

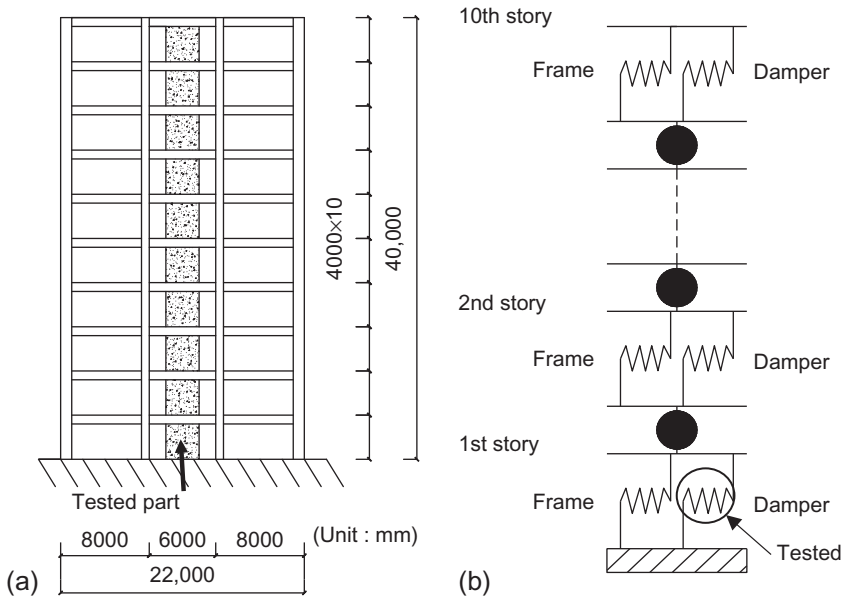

FIGURE 2.8 Ten-story building model with hysteretic damper. (a) 10 story building model with hysteretic damper, (b) 10-DOF system representing 10 story building model.

OS method does not require any iteration for the nonlinear analysis. In this method, the equations of motion are formulated as follows.

$$Ma_{i+1} + Cv_{i+1} + Kd_{i+1} + \left(\widetilde{r}_{i+1} - K\widetilde{d}_{i+1}\right) = f_{i+1} \tag{2.4}$$

in which K is the predictor stiffness matrix of the structure and $\widetilde{r}_{i+1}$ is the restoring force vector based on predictor displacements $\widetilde{d}_{i+1}$. The displacement and velocity quantities are approximated in the same way as in the constant-average-acceleration method, i.e.,

$$d_{i+1} = \widetilde{d}_{i+1} + \frac{\Delta t^2}{4} a_{i+1} \tag{2.5}$$

$$v_{i+1} = v_i + \frac{\Delta t}{2}(a_i + a_{i+1}) \tag{2.6}$$

where

$$\widetilde{d}_{i+1} = d_i + \Delta t v_i + \frac{\Delta t^2}{4} a_i \tag{2.7}$$

With this scheme, a test can be conducted as follows. Assuming that the response in step i has been computed, calculate the predictor displacements $\widetilde{d}_{i+1}$ with Equation (2.7) and impose them on the analytical and experimental substructures, respectively. Measure the restoring forces developed by the specimen and assemble $\widetilde{r}_{i+1}$ for the entire structure. Substitute $\underline{\widetilde{r}}_{i+1}$ and $\widetilde{d}_{i+1}$ into Equation (2.4) and solve for d_{i+1} with Equations (2.4)–(2.7). Repeat the above procedure by setting $i = i+1$ until the entire response history is obtained.

The OS method is unconditionally stable as long as predictor stiffness K adopted in Equation (2.4) is greater than or equal to the actual secant stiffness of the structure. This method has a major advantage, in that it requires no iteration for a nonlinear structure by introducing an approximate correction, i.e., $\left(\widetilde{r}_{i+1} - K\widetilde{d}_{i+1}\right)$, to the restoring forces. However, because of this, the method also introduces a more severe frequency distortion than the constant-average-acceleration method [14]. Furthermore, since the accuracy of the force correction term is also affected by the quality of the restoring forces measured, an accurate control of structural displacements is important for this scheme.

The OS method has been combined with substructuring techniques by Pan [29] to investigate the performance of base-isolation pads in a nine-story steel frame, Tsutsumi [30] to study the behavior of a steel column, and Tsai [9] to study the performance of energy-dissipating devices in an eight-story steel frame.

2.5.3 Test Results

The integration time interval chosen for this test was 0.2 s, leading to a $\omega_{\max}\Delta t$ of 2.29, where $\omega_{\max}$ represents the highest angular frequency of the structure.

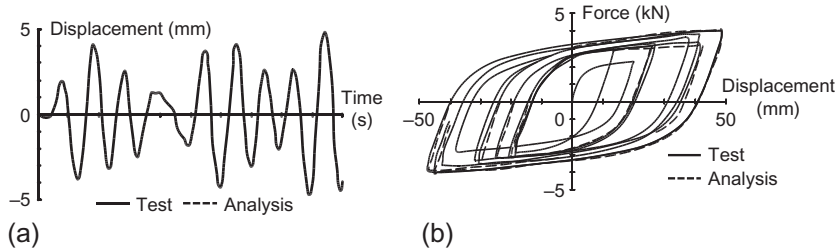

FIGURE 2.9 Results of a substructure test conducted on a 10-story building. (a) Story shear force response, (b) force-displacement relationship.

This would not be possible for the conditionally stable central different method. The test results are shown in Fig. 2.9. A close correlation was obtained between the experimental and numerical results. The latter was obtained with the full structural model whose dampers were simulated with modified Ramberg-Osgood functions.

2.6 CONCLUSIONS

This document presents a brief introduction of the online hybrid test including basic ideas, procedures, and components with a few simple examples. It is intended to help new users get a better understanding of online hybrid testing, identify the applicability of the online hybrid test to their research, and conduct online hybrid tests for their research needs.

REFERENCES

[1] Mahin SA, Shing PB. Pseudodynamic method for seismic testing. J Struct Eng 1985;111 (7):1482–503.

[2] Takanashi K, Nakashima M. Japanese activities on on-line testing. J Eng Mech 1987;113 (7):1014–32.

[3] Seible F, Hegemier GA, Igarashi A, Kingsley GR. Simulated seismic-load tests on full-scale five-story masonry building. J Struct Eng 1994;120(3):903–24.

[4] Negro P. Tests on a four-storey full-scale R/C frame designed according to Eurocodes 8 and 2: preliminary report. 15879 EN. Ispra, Italy: Joint Research Centre; 1994. Report EUR, 80 p. (517.5 T48 1994), http://nisee.berkeley.edu/documents/elib/www/documents/201010/negro-rc-frame.pdf.

[5] Ozcelik R, Binici B, Kurc O. Pseudo dynamic test of a deficient reinforced concrete frame upgraded with internal steel frames. Earthq Eng Struct Dyn 2013;42:763–78.

[6] Takanashi K, Nakashima M. On-line computer test control method and its application to earthquake response simulation of steel structural models. J Constr Steel Res 1988;11(1):27–40.

[7] Nakashima M, Kato H, Takaoka E. Development of real-time pseudo dynamic testing. Earthq Eng Struct Dyn 1992;21(1):79–92.

[8] Benson Shing P, Bursi OS, Vannan MT. Pseudodynamic tests of a concentrically braced frame using substructuring techniques. J Constr Steel Res 1994;29(1):121–48.

[9] Tsai KC, Li JW, Wang TF. Pseudodynamic performance of steel plate energy-dissipating substructures. In: Proceedings of the 5th US national conference on earthquake engineering, vol. 1, Chicago, IL; 1994. p. 735–44.

[10] Eatherton RM, Hajjar FJ. Hybrid simulation testing of a self-centering rocking steel braced frame system. Earthq Eng Struct Dyn 2014;43:1725–42.
[11] Thewalt CR, Mahin SA. Hybrid solution techniques for generalized pseudodynamic testing. Springfield, VA: Earthquake Engineering Research Center, College of Engineering, University of California; 1987. Available from the National Technical Information Service.
[12] Thewalt CR, Mahin SA. Non-planar pseudodynamic testing. Earthq Eng Struct Dyn 1995;24 (5):733–46.
[13] Dermitzakis SN, Mahin SA. Development of substructuring techniques for on-line computer controlled seismic performance testing. Diss Abstr Int B Sci Eng 1986;46(9).
[14] Nakashima M, Kaminosono T, Ishida M, Ando K. Integration techniques for substructure pseudodynamic test. In: Proceedings of 4th US national conference on earthquake engineering, vol. 2, Palm Springs, CA; 1990. p. 515–24.
[15] Nakashima M, Akazawa T, Igarashi H. Pseudo-dynamic testing using conventional testing devices. Earthq Eng Struct Dyn 1995;24(10):1409–22.
[16] Terzic V, Stojadinovic B. Hybrid simulation of bridge response to three-dimensional earthquake excitation followed by truck load. J Struct Eng ASCE 2014;140(8):657–70.
[17] Shing PSB, Mahin SA. Rate-of-loading effects on pseudodynamic tests. J Struct Eng 1988;114 (11):2403–20.
[18] Shing PB, Mahin SA. Experimental error propagation in pseudodynamic testing. Earthquake engineering research report UCB/EERC-83/12. Berkeley: University of California; 1983. p. 168.
[19] Shing PSB, Mahin SA. Cumulative experimental errors in pseudodynamic tests. Earthq Eng Struct Dyn 1987;15(4):409–24.
[20] Shing PB, Mahin SA. Experimental error effects in pseudodynamic testing. J Eng Mech 1990;116(4):805–21.
[21] Nakashima M, Kato H. Experimental error growth behavior and error growth control in on-line computer test control method. Japan: Building Research Institute; 1987.
[22] Shing PSB, Mahin SA. Computational aspects of a seismic performance test method using on-line computer control. Earthq Eng Struct Dyn 1985;13(4):507–26.
[23] Thewalt CR, Mahin SA. An unconditionally stable hybrid pseudodynamic algorithm. Earthq Eng Struct Dyn 1995;24(5):723–31.
[24] Shing PSB, Vannan MT, Cater E. Implicit time integration for pseudodynamic tests. Earthq Eng Struct Dyn 1991;20(6):551–76.
[25] Shing PSB, Vannan MT. Implicit time integration for pseudodynamic tests: convergence and energy dissipation. Earthq Eng Struct Dyn 1991;20(9):809–19.
[26] Hilber HM, Hughes TJR, Taylor RL. Improved numerical dissipation for time integration algorithms in structural dynamics. Earthq Eng Struct Dyn 1977;5(3):283–92.
[27] Nakata N, Dyke S, Zhang J, Mosqueda G, Shao X, Mahmoud H, et al. Hybrid simulation primer and dictionary; 2014. https://nees.org/resources/7702.
[28] Nakashima M, Akazawa T, Tsuji B. Strain-hardening behavior of shear panels made of low-yield steel. II: model. J Struct Eng 1995;121(12):1750–7.
[29] Pan P, Tada M, Nakashima M. Online hybrid test by internet linkage of distributed test and analysis domains. Earthq Eng Struct Dyn 2005;34:1407–25.
[30] Tsutsumi H, Ando K, Sato K. Substructure pseudo dynamic test with rotation control. In: Proceedings of 4th US national conference on earthquake engineering, vol. II; 1990. p. 525–34.

Chapter 3

Time Integration Algorithms for the Online Hybrid Test

Chapter Outline

3.1 INTRODUCTION

In order to solve the equations of motion in an online hybrid test, time integration algorithms are used. Therefore, the study of these algorithms and their characteristics is of great importance. This chapter gives the basics to help the reader

Development of Online Hybrid Testing. http://dx.doi.org/10.1016/B978-0-12-803378-4.00003-0

to have a better understanding of them. First introduced in this chapter are the principles of time integration algorithms and definitions of important properties. Second, the development of time integration algorithms, which are categorized into families, and the improvements in each family are presented. They are also summarized in Appendix A. Third, the typical analysis methods for stability and accuracy of integration algorithms are introduced. Fourth, several frequently used time integration algorithms are presented and their stability and accuracy are analyzed. Finally, important applications of time integration algorithms for online hybrid tests are summarized.

3.2 PRINCIPLE OF TIME INTEGRATION ALGORITHMS AND PROPERTIES

The equations of motion for structural dynamics are second-order ordinary differential equations [1], which are based on a spatially discretized structure model, as shown in Equation (3.1) where $\mathbf{M}$, $\mathbf{C}$, and $\mathbf{K}$ represent the mass, damping, and stiffness matrices, respectively, $\ddot{\mathbf{d}}(t)$, $\dot{\mathbf{d}}(t)$, and $\mathbf{d}(t)$ are the acceleration, velocity, and displacement vectors, respectively, and $\mathbf{f}(t)$ is the external force vector. These vectors are continuous functions of time. Therefore, Equation (3.1) is also called semi-discretized equation.

$$\mathbf{M}\ddot{\mathbf{d}}(t) + \mathbf{C}\dot{\mathbf{d}}(t) + \mathbf{K}\mathbf{d}(t) = \mathbf{f}(t) \tag{3.1}$$

The essence to solve Equation (3.1) by a time integration algorithm is to discretize Equation (3.1) further in the time domain and integrate it step by step. To this end, researchers have already developed many time integration algorithms which can be basically categorized into two groups: explicit algorithms and implicit algorithms. In the following part, each algorithm is grouped as families according to their developing basis.

Before the introduction of algorithms, some definitions of numerical properties of the algorithms should be clarified first. The most important numerical properties are stability and accuracy [2].

Stability is defined as the ability to suppress the initial error in the step-by-step integration. If the initial error is always kept under a certain level, the algorithm is called stable, otherwise instable. If stability is related to the size of time step (time interval), it is called conditionally stable, otherwise unconditionally stable.

Accuracy is defined as the similarity between the analytical solution of Equation (3.1) and the time integration result. If the time interval gets closer to zero and the time integration result also gains upon the analytical solution, this method is called "accurate" or "consistent." To explore accuracy of a time integration algorithm, a truncation error τ is introduced to reflect the difference between the analytical solution and the time integration result. If Equation (3.2) is satisfied, the algorithm is called accurate and k is called the "order of accuracy."

$$\tau = O\left(\Delta t^k\right) \tag{3.2}$$

where Δt is the time interval, k is a constant which is independent of Δt, and $k > 0$.

Other important numerical properties are numerical dissipation (damping) and period distortion. Numerical damping is helpful to suppress the spurious high-frequency excitation introduced by the spatially discretized approximation or the experimental measuring errors. It is always expected to be small for low-frequency responses but relatively big for high-frequency responses. The period distortion is always expected to be small for all frequencies.

3.3 DEVELOPMENT OF TIME INTEGRATION ALGORITHMS

Based on the genetic development of existing time integration algorithms, they are grouped as (1) linear multi-step methods; (2) Newmark's family; (3) collocation methods; (4) α-family; (5) ρ-family, and (6) mixed implicit-explicit methods.

3.3.1 Linear Multi-Step Methods

Linear multi-step methods [3], namely the central difference method (CDM), the trapezoidal rule, Gear's two-step method [4], Houbolt's method [5], and Park's method [6], are based on the second- or first-order difference of displacement. The numerical characteristics of these methods have been previously investigated [4,6–10], and the following conclusions can be drawn: (1) the CDM is the only explicit one among these methods; (2) the trapezoidal rule, Gear's two-step method, Houbolt's method, and Park's method are unconditionally stable, while the CDM is conditionally stable; (3) all these methods are second-order accurate; (4) the CDM and the trapezoidal rule have no numerical damping; (5) Houbolt's method and Gear's two-step method have similar numerical damping which, however, affects the low-frequency modes greatly; (6) Park's method has a more desirable numerical damping (also referred to as the optimal numerical damping in the following text), which affect the low-frequency modes very little but suppress the high-frequency modes greatly; (7) based on (4)–(6), the accuracy of these methods, when applied for linear undamped systems dominated by low-frequency modes, ranks from higher to lower as: the trapezoidal rule, the CDM, Houbolt's method, Gear's method, and Park's method; (8) the CDM shortens the period, while the other methods enlarge the period; (9) a common shortcoming of the linear multi-step methods is that they are not self-starting. A starting procedure has to be inserted before the time integration procedure to get the initial values of several previous steps.

3.3.2 Newmark's Family Methods

Newmark's family [11] is a group of one-step methods, which was developed by introducing two parameters, i.e., β and γ. The most notable members of this family include: the average acceleration algorithm (identical to the trapezoidal rule), the linear acceleration algorithm, Fox-Goodwin algorithm, and an explicit method, the numerical properties of which are identical to the central difference algorithm. The average acceleration algorithm is unconditionally stable, while the other three are conditionally stable. The common feature of these methods is that they are at least second-order accurate and they do not include numerical dissipation. If the numerical dissipation is included for the Newmark's family, they become first-order accurate. This numerical dissipation, called γ-dissipation, however, not only affects the high-frequency modes greatly, but also the low-frequency modes. Several algorithms were proposed to improve the numerical dissipation of the explicit Newmark method, without degrading its accuracy. Shing and Mahin [12] proposed an explicit method with two parameters, i.e., α and ρ. The numerical dissipation is controlled by selecting the values satisfying $\alpha \geq 0$ and $\rho < 0$. The numerical dissipation for low-frequency modes, however, is not small. A better control of the numerical dissipation was proposed by Chang [13], which is also called the γ-function method. By carefully selecting the values for γ, a desirable numerical dissipation for lower or higher modes is provided. The selection of γ, however, is rather complex because initial stiffness and mass are involved. A similar method with easier control of numerical dissipation was developed by Chung and Lee [14]. If the controllable parameter β is chosen in a range of $1 \leq \beta \leq 28/27$, the desirable numerical dissipation can be obtained. These explicit algorithms of Newmark's family are conditionally stable. Chang [15] proposed an explicit time integration algorithm with unconditional stability, but without any numerical dissipation.

3.3.3 Collocation Methods

The idea of collocation was first proposed by Wilson when developing the so-called Wilson-θ method [16]. The key is that the equations of motion are satisfied at the time $(n+\theta)\Delta t$ $(\theta \geq 1)$, but not at the time $(n+1)\Delta t$. The Wilson-θ method is an unconditionally stable and second-order accurate method if $\theta \geq 1.37$. The period is elongated by this method. The desirable numerical dissipation is realized by adjusting θ. This numerical dissipation, however, cannot be reduced continuously to zero, and the effect on low-frequency modes is small but still not negligible. The collocation method [17] combines aspects of the Newmark-β algorithm and the Wilson-θ algorithm, and includes the Wilson-θ algorithm as one special case. If the parameters are properly selected, this method is unconditionally stable and second-order accurate. Optimal θ values for given β are derived to achieve a desirable numerical dissipation, the magnitude of which is controlled continuously by the value of β.

3.3.4 α-Family Methods

The numerical dissipation property of the Newmark's methods can be improved significantly by introducing a parameter α into the equations of motion. Improved methods are classified as a new group, the α-family methods [18–22]. The numerical dissipation property of the α-family methods basically is better than the optimal collocation method [17]. When the parameter α is employed for the damping and the stiffness terms of the equations of motion, it is formulated as the Hilber-Hughes-Taylor (HHT)-α method [18,19]. If the α parameter is associated with the mass term only, the Wood-Bossak-Zienkiewicz (WBZ)-α method [20] is formed. Both the HHT-α method and the WBZ-α method are second-order accurate and unconditionally stable methods with optimal numerical dissipation. The numerical dissipation properties of the WBZ-α method can be adjusted similarly to the HHT-α method. But for some special cases, the WBZ-α method is more accurate than the HHT-α method [20]. Chung and Hulbert [21] combined the HHT-α method and the WBZ-α method to construct the generalized-α method. Parameters are optimized to achieve unconditional stability, second-order accuracy, and optimal numerical dissipation. It permits high-frequency dissipation to vary from the no dissipation case to the so-called asymptotic annihilation case. It is advantageous, from the user's viewpoint, to be able to specify the algorithmic parameters in terms of the high-frequency dissipation, since the desired degree of high-frequency dissipation is usually a known quantity. An explicit form of the generalized-α algorithm was also developed by Hulbert and Chung [22]. The optimal numerical dissipation is also available. It is second-order accurate, but conditionally stable.

3.3.5 ρ-Family Methods

A family of time integration method with desirable numerical properties, such as second-order accuracy, unconditional stability, and optimal numerical dissipation, was proposed by Bazzi and Anderheggen [23,24]. They employed shape functions to approximate the nonlinear restoring forces and displacement, and set the nonweighted integral of the residuals of the equations of motion to be zero. The parameter ρ is used to control the magnitude of the optimal numerical dissipation, which is quite similar to the HHT-α method. The notable advantage of this family is that the average value of the external force is used and thus can capture the high-frequency components in the external force [24]. An explicit form of this algorithm was also developed [23], which was found to be identical to the central difference algorithm in terms of numerical properties.

3.3.6 Mixed Implicit-Explicit Methods

The mixed implicit-explicit methods are developed by combining the merits of the explicit methods and the implicit methods. The most famous one was proposed by Hughes and Liu [25,26]. In this method, a structure is divided into two

parts. One is handled implicitly, while the other is done explicitly. The stability and accuracy analyses should be carried out for the two domains separately. In the implicit domain, the unconditional stability may be achieved. In the explicit domain, however, it is conditionally stable. This method was further generalized by Hughes et al. [27], where the stiffness matrix is divided into linear and nonlinear parts. The explicit method is employed for the integration associated with the nonlinear part, while the implicit method for the integration associated with the linear part. These methods become the theoretical basis of many sequel online hybrid tests, which are introduced in Section 3.6.

Some special techniques are often employed to improve stability and accuracy of a time integration algorithm, such as the modal truncation technique [28] to improve the stability of explicit time integration algorithms, the integral formulation [29,30], and the state space procedure (SSP) [31] to improve the simulation accuracy. These techniques are summarized in detail in Section 3.5.

3.4 NUMERICAL CHARACTERISTICS OF TIME INTEGRATION ALGORITHMS

A time integration method is said to be convergent if the result obtained from this method gains upon the analytical result of Equation (3.1) when time interval gets closer to zero. Based on the Lax equivalence theorem [32], which may be stated as "consistency (accuracy) plus stability is necessary and sufficient for convergence," stability and accuracy properties of time integration methods should be explored to demonstrate their effectiveness.

3.4.1 Spectral Stability

The time-discretized Equation (3.1) for a single degree-of-freedom (SDOF) system is formulated as Equation (3.3) where m, c, and k represent the mass, viscous damping, and stiffness of the SDOF system, respectively. a_{n+1}, v_{n+1}, d_{n+1}, and f_{n+1} are discretized values of acceleration, velocity, displacement, and external excitation, respectively, at the time $(n+1)\Delta t$.

$$ma_{n+1} + cv_{n+1} + kd_{n+1} = f_{n+1} \tag{3.3}$$

Equation (3.3), when combined with the finite difference formulae provided by individual time integration algorithm, can be reformulated into a recursive matrix form as shown in Equation (3.4), where $\mathbf{A}$ is called amplification matrix, $\mathbf{L}$ is the load operator, and $\mathbf{X}_{n+1}$ and $\mathbf{X}_n$ represent the state at the time $(n+1)\Delta t$ and $n\Delta t$, respectively.

$$\mathbf{X}_{n+1} = \mathbf{A}\mathbf{X}_n + \mathbf{L}f_{n+1} \tag{3.4}$$

The essence of stability condition is that the error introduced into the approximate solution by a particular difference method remains uniformly bounded as $n \to \infty$ with n as the solution time step. The stability presented here is concerned

with the rate of growth or decay of powers of the amplification matrix. To investigate the stability of a time integration method, the Jordan form of the amplification matrix is employed as formulated in Equation (3.5) where **P** is the matrix of eigenvectors of **A** and **J** is the Jordan form of **A** with the eigenvalues λ_i of **A** on its diagonal. Then Equation (3.4) can be further written as Equation (3.6) by introducing Equation (3.5) where $\mathbf{X}_0$ is the initial state. Let $\rho(\mathbf{A})$ be the spectral radius of **A**, defined as Equation (3.7). Then $\mathbf{J}^n$ is bounded for $n \to \infty$ if and only if $\rho(\mathbf{A}) \leq 1$. And it should be supplemented that eigenvalues of **A** of multiplicity greater than one should be strictly less than one in modulus [4].

$$\mathbf{A} = \mathbf{P}^{-1}\mathbf{J}\mathbf{P} \tag{3.5}$$

$$\mathbf{X}_n = \mathbf{A}^n\mathbf{X}_0 + \sum_{i=1}^{n} \mathbf{A}^{n-i}\mathbf{L}f_i, \quad \mathbf{A}^n = \mathbf{P}^{-1}\mathbf{J}^n\mathbf{P} \tag{3.6}$$

$$\rho(\mathbf{A}) = \max|\lambda_i|, \quad i = 1,2,3 \tag{3.7}$$

Several applications on the spectral stability analysis for existing time integration algorithms have been carried out [2,33]. Amplification matrices for most of the existing time integration algorithms are 3×3. Therefore, eigenvalues can be obtained according to a standard procedure for solving the following algebraic equation, as shown in Equation (3.8). If the order of the amplification matrix is larger than three, the implementation of spectral stability analysis can be found [4]:

$$\det(\mathbf{A} - \lambda\mathbf{I}) = \lambda^3 - 2A_1\lambda^2 + A_2\lambda - A_3 = 0 \tag{3.8}$$

where $A_1 = \frac{1}{2}$ of the trace of **A**, A_2 = sum of the principal minors of **A**, and A_3 = determinant of **A**.

3.4.2 Accuracy Analysis

Velocities and accelerations may be eliminated by repeated use of Equation (3.4) to obtain a difference equation in terms of displacements, as shown in Equation (3.9). Suppose d(t) is a function that satisfies Equation (3.1) without external force, then the truncation error τ can be defined as Equation (3.10). The truncation error is a measure of the error occurring when the difference Equation (3.9) is used instead of the differential Equation (3.1). The definition of the order of accuracy or rate of convergence has already formulated in Equation (3.2). By expanding $d(t)$ about t using the Taylor series in Equation (3.10), yields Equation (3.11).

$$d_{n+1} - 2A_1 d_n + A_2 d_{n-1} - A_3 d_{n-2} = 0 \tag{3.9}$$

$$\tau = \frac{d(t+\Delta t) - 2A_1 d(t) + A_2 d(t-\Delta t) - A_3 d(t-2\Delta t)}{\Delta t^2} \tag{3.10}$$

$$\tau = \sum_{i=1}^{m} T_i \Delta t^{i-2} \frac{d^i d(t)}{d\, t^i} + O\left(\Delta t^{m-1}\right) \tag{3.11}$$

where $T_0 = 1 - 2A_1 + A_2 - A_3$, $T_i = \frac{1 + (-1)^i A_2 - (-2)^i A_3}{i!}$, $i > 0$.

Numerical dissipation and period distortion are often employed to specify the accuracy of a time integration method. They can be formulated as the following text. Comparison of Equations (3.8) and (3.9) indicates that the discrete solution has the representation as Equation (3.12), where, c_1, c_2, and c_3 are determined by the initial value. Note that Equation (3.12) is the general solution of Equation (3.9) only if the eigenvalues are distinct. The cases with eigenvalues of multiplicity of two and three are formulated as Equations (3.13) and (3.14), respectively.

$$d_n = \sum_{i=1}^{3} c_i \lambda_i^n \tag{3.12}$$

$$d_n = (c_1 + nc_2)\lambda_{1,2}^n + c_3 \lambda_3^n \tag{3.13}$$

$$d_n = \left(c_1 + nc_2 + n^2 c_3\right)\lambda_{1,2,3}^n \tag{3.14}$$

What we care about here is the case that has two complex conjugate eigenvalues, $\lambda_{1,2}$, called "principal roots," and a so-called "spurious root," λ_3, which satisfy Equation (3.15). The solution of Equation (3.9) then can be expressed as Equation (3.16). The accuracy of a time integration method is defined by two measures: numerical damping ratio $\bar{\xi}$ and the period distortion, $(\bar{T} - T)/T$, where $T = 2\pi/\omega$ and $\bar{T} = 2\pi/\bar{\omega}$.

$$|\lambda_3| < 1 \text{ and } \left|\lambda_{1,2}\right| \le 1 \tag{3.15}$$

$$d_n = \exp\left(-\bar{\xi}\bar{\omega}t_n\right)\left(c_1 \cos\bar{\omega}t_n + c_2 \sin\bar{\omega}t_n\right) + c_3\lambda_3^n \tag{3.16}$$

where $\lambda_{1,2} = A \pm Bi = \exp\left[\bar{\Omega}\left(-\bar{\xi} \pm i\right)\right]$, $\bar{\omega} = \bar{\Omega}/\Delta t$, $\bar{\xi} = -\ln\left(A^2 + B^2\right)/\left(2\bar{\Omega}\right)$, $\bar{\Omega} = \arctan\left(B/A\right)$.

Note that the stability and accuracy analysis methods are given only for a linear SDOF system since response of a multi-degree-of-freedom (MDOF) system can be treated as an assembly of SDOF systems if the concept of modal analysis is employed. The above stability and accuracy analyses can be carried out for each individual mode and select the most critical conditions for the MDOF system.

3.5 ANALYSIS OF TYPICAL TIME INTEGRATION ALGORITHMS

Because of their good properties in terms of stability, accuracy, or implementation, several time integration algorithms are frequently used. Typical time

integration algorithms are presented in detail in this section, while the others are only given in Appendix A.

3.5.1 Central Difference Method

The CDM is widely used because of its simplicity. It is called the "central difference method" because the velocity and acceleration are formulated as the classical first- and second-order central difference approximations, as shown in Equations (3.18) and (3.19), respectively. Numerical properties have already been studied completely [7–9]. It is found to be a conditionally stable method with the second-order accuracy. It has no numerical damping. The equation of motion is formulated below, based on a SDOF system.

Algorithm

$$ma_n + cv_n + kd_n = f_n \tag{3.17}$$

$$v_n = \frac{d_{n+1} - d_{n-1}}{2\Delta t} \tag{3.18}$$

$$a_n = \frac{d_{n+1} - 2d_n + d_{n-1}}{\Delta t^2} \tag{3.19}$$

Stability

The stability analysis follows the procedure described in the preceding section. Equations (3.17)–(3.19) at first are reformulated as the recursive matrix form based on a linear SDOF system.

$$\begin{Bmatrix} d_{n+1} \\ d_n \end{Bmatrix} = \begin{bmatrix} \frac{2-\omega^2\Delta t^2}{1+\xi\omega\Delta t} & \frac{\xi\omega\Delta t - 1}{1+\xi\omega\Delta t} \\ 1 & 0 \end{bmatrix} \begin{Bmatrix} d_n \\ d_{n-1} \end{Bmatrix} + \begin{Bmatrix} \frac{\Delta t f_n}{(1+\xi\omega\Delta t)m} \\ 0 \end{Bmatrix} \tag{3.20}$$

where $\xi = \frac{c}{2m\omega}$ and $\omega = \sqrt{\frac{k}{m}}$.

The eigenvalues of the amplification matrix are:

$$\lambda_{1,2} = \frac{\{(2-\omega^2\Delta t^2) \pm \mathrm{i}\omega\Delta t\sqrt{4(1-\xi^2) - \omega^2\Delta t^2}}{2(1+\xi\omega\Delta t)} \tag{3.21}$$

The stability condition of the CDM is summarized as follows:

$$\begin{aligned} &\text{Condition 1}: \quad \omega\Delta t > 2 && \text{Unstable} \\ &\text{Condition 2}: \quad \omega\Delta t < 2\sqrt{1-\xi^2} && \text{Stable with two complex eigenvalues} \\ &\text{Condition 3}: \quad 2\sqrt{1-\xi^2} \le \omega\Delta t \le 2 && \text{Stable with two real eigenvalues} \end{aligned} \tag{3.22}$$

Accuracy

Using Equations (3.16) and (3.21), both numerical damping ratio and period distortion can be obtained. The following conclusions are drawn for the CDM:

(1) The numerical damping ratio and the distorted period gain upon the real damping ratio and the real period, respectively, when the time interval becomes smaller.
(2) If real damping ratio is <0.7, the distorted period is always smaller than the real period; if real damping ratio is >0.7, the distorted period will increase to infinite when time interval becomes larger.
(3) This method is second-order accurate.

3.5.2 Newmark's Method

The Newmark-β method [11] is the most widely used family of time integration methods. It adopts two parameters, namely β and γ, to indicate how much of the acceleration at the end of the time interval enters into the relations for velocity and displacement at the end of the time interval, as shown in Equations (3.24) and (3.25). The Newmark's family contains some special cases which may be well-known and widely used, such as average acceleration method when $\beta = 0.25$ and $\gamma = 0.5$, which is also called the "trapezoidal rule"; linear acceleration method when $\beta = 1/6$ and $\gamma = 0.5$; Fox-Goodwin method [34] when $\beta = 1/12$ and $\gamma = 0.5$, and an explicit Newmark-β method when $\beta = 0$ and $\gamma = 0.5$, which actually is the same as the CDM. By carefully selecting the parameters, the Newmark-β method can be an implicit unconditionally stable algorithm with second order accurate. The numerical dissipation property of the Newmark-β method, however, is not so desirable, since it damps the low-frequency modes also and degrades the accuracy to first-order. The equation of motion is formulated based on a SDOF system as Equation (3.23).

Algorithm

$$ma_{n+1} + cv_{n+1} + kd_{n+1} = f_{n+1} \tag{3.23}$$

$$d_{n+1} = d_n + \Delta t v_n + (0.5 - \beta)\Delta t^2 a_n + \beta \Delta t^2 a_{n+1} \tag{3.24}$$

$$v_{n+1} = v_n + \Delta t(1 - \gamma)a_n + \Delta t \gamma a_{n+1} \tag{3.25}$$

Stability

Equations (3.23)–(3.25) are reformulated as the recursive matrix form based on a linear SDOF system:

$$\begin{Bmatrix} a_{n+1} \\ v_{n+1} \\ d_{n+1} \end{Bmatrix} = \mathbf{A} \begin{Bmatrix} a_n \\ v_n \\ d_n \end{Bmatrix} + \mathbf{L}\frac{f_{n+1}}{m} \tag{3.26}$$

$$A=\begin{bmatrix} -\left(\frac{1}{2}-\beta\right)C-2(1-\gamma)D & \frac{-C-2D}{\Delta t} & \frac{-C}{\Delta t^2} \\ \Delta t\left[(1-\gamma)(1-2\gamma D)-\left(\frac{1}{2}-\beta\right)\gamma C\right] & 1-C\gamma-2\gamma D & \frac{-C\gamma}{\Delta t} \\ \Delta t^2\left[\left(\frac{1}{2}-\beta\right)(1-\beta C)-2(1-\gamma)\beta D\right] & \Delta t(1-\beta C-2\beta D) & 1-\beta C \end{bmatrix}, \text{ and } L=\begin{bmatrix} \frac{C}{\omega^2\Delta t^2} \\ \frac{C\gamma}{\omega^2\Delta t} \\ \frac{C\beta}{\omega^2} \end{bmatrix} \tag{3.27}$$

where $C=\dfrac{1}{\dfrac{1}{\omega^2\Delta t^2}+\dfrac{2\xi\gamma}{\omega\Delta t}+\beta}$, $D=\dfrac{\xi\beta}{\omega\Delta t}$.

The stability condition of the Newmark-β method is summarized as follows:

$$\begin{array}{ll} \text{Unconditional stability condition}: & 2\beta\geq\gamma\geq 0.5 \\ \text{Conditional stability condition}: & \gamma\geq 0.5,\ \beta<0.5\gamma,\ \Omega\leq\Omega_{\text{crit}} \end{array} \tag{3.28}$$

where

$$\Omega_{\text{crit}}=\left\{\xi(\gamma-0.5)+\left[0.5\gamma-\beta+\xi^2(\gamma-0.5)^2\right]^{1/2}\right\}/(0.5\gamma-\beta).$$

More strict condition for two complex conjugate eigenvalues:

$$\begin{array}{ll} \text{Unconditional stability condition}: & 0\leq\xi<1,\ \gamma\geq 0.5,\ \beta\geq(\gamma+0.5)^2/4 \\ \text{Conditional stability condition}: & 0\leq\xi<1,\ \gamma\geq 0.5,\ \Omega\leq\Omega_{\text{crit}} \end{array} \tag{3.29}$$

where

$$\Omega_{\text{crit}}=\left\{0.5\xi(\gamma-0.5)+\left[0.25(\gamma+0.5)^2-\beta+\xi^2(\beta-0.5\gamma)\right]^{1/2}\right\}/\left[0.25(\gamma+0.5)^2-\beta)\right].$$

Accuracy

The numerical damping and period distortion can be formulated as follows:

$$\text{Numerical damping ratio}: \quad \bar{\xi}=\xi+\Omega(\gamma-0.5)/2+O\left(\Omega^2\right) \tag{3.30}$$

$$\text{Period distortion}: \quad \frac{\bar{T}-T}{T}=O\left(\Omega^2\right) \tag{3.31}$$

where Ω is called the "sampling frequency."

The following conclusions are drawn for the Newmark-β method:

(1) If $\gamma=0.5$, there is no numerical damping, and this method has a second-order accuracy.

(2) If $\gamma>0.5$, the numerical damping (γ-dissipation) is larger than real damping and increases with the sampling frequency. But the method only has the first-order accuracy. Both higher modes and lower modes are affected significantly.

(3) If $\gamma = 0.5$ and the unconditional stability condition is satisfied, the period is elongated.

(4) If $\gamma = 0.5$ and the conditional stability condition is satisfied, the period may be elongated or shortened, which depends on the selection of parameter β. If a special β is selected as 1/12, the method has the fourth-order accuracy.

Summary of well-known members of Newmark family

The numerical properties of some members of the Newmark's family are summarized in Table 3.1.

3.5.3 HHT-α Method

The HHT-α method [18,19] is an improvement over the Newmark-β method [11] to realize a controllable numerical dissipation without degrading accuracy by introducing a single parameter α into the equilibrium equation. The dissipation introduced by α is called the α-dissipation, which is similar to linear viscous damping and is ineffective in the higher modes. The numerical dissipation of this algorithm has an improved performance by combining the positive Newmark γ-dissipation with the negative α-dissipation. In order to determine the three parameters, namely α, β, and γ, the procedures used for spectral stability and accuracy analysis formulated in the preceding section are used and intentionally the algorithm is made to be unconditionally stable, second-order accurate, and, more importantly, to have an optimal numerical dissipation. Based on these conditions, the HHT-α method becomes a one-parameter algorithm with β and γ definitely decided by α. The numerical dissipation is only related to the parameter α. The equation of motion is formulated based on a SDOF system as Equation (3.32).

TABLE 3.1 Numerical Properties of Well-known Members of the Newmark Family

Method	β	γ	Stability condition	Accuracy
Average acceleration method (trapezoidal rule)	$\frac{1}{4}$	$\frac{1}{2}$	Unconditional	Second order
Linear acceleration method	$\frac{1}{6}$	$\frac{1}{2}$	$\Omega_{\text{crit}} = 2\sqrt{3} \approx 3.5$	Second order
Fox-Goodwin method	$\frac{1}{12}$	$\frac{1}{2}$	$\Omega_{\text{crit}} = \sqrt{6} \approx 2.4$	Fourth order
Central difference method	0	$\frac{1}{2}$	$\Omega_{\text{crit}} = 2$	Second order

Algorithm

$$ma_{n+1}+(1+\alpha)cv_{n+1}-\alpha cv_n+(1+\alpha)kd_{n+1}-\alpha kd_n=(1+\alpha)f_{n+1}-\alpha f_n \quad (3.32)$$

$$d_{n+1}=d_n+\Delta tv_n+(0.5-\beta)\Delta t^2a_n+\beta\Delta t^2a_{n+1} \quad (3.33)$$

$$v_{n+1}=v_n+\Delta t(1-\gamma)a_n+\Delta t\gamma a_{n+1} \quad (3.34)$$

where $\beta=\frac{1}{4}(1-\alpha)^2$, $\gamma=\frac{1}{2}-\alpha$.

Stability

The recursive matrix form of Equations (3.32)–(3.34) is formulated as follows based on an undamped SDOF system:

$$\begin{Bmatrix} d_{n+1} \\ \Delta tv_{n+1} \\ \Delta t^2a_{n+1} \end{Bmatrix}=\mathbf{A}\begin{Bmatrix} d_n \\ \Delta tv_n \\ \Delta t^2a_n \end{Bmatrix}+(1+\alpha)\mathbf{L}\frac{f_{n+1}}{m}-\alpha\mathbf{L}\frac{f_n}{m} \quad (3.35)$$

$$\mathbf{A}=\frac{1}{D}\begin{bmatrix} 1+\alpha\beta\Omega^2 & 1 & 0.5-\beta \\ -\gamma\Omega^2 & 1-(1+\alpha)(\gamma-\beta)\Omega^2 & 1-\gamma-(1+\alpha)(0.5\gamma-\beta)\Omega^2 \\ -\Omega^2 & -(1+\alpha)\Omega^2 & -(1+\alpha)(0.5-\beta)\Omega^2 \end{bmatrix},\ \text{and}\ \mathbf{L}=\frac{1}{D}\begin{bmatrix} \beta\Delta t^2 \\ \gamma\Delta t^2 \\ \Delta t^2 \end{bmatrix} \quad (3.36)$$

where $D=1+(1+\alpha)\beta\Omega^2$.

The stability condition of the HHT-α method is summarized as follows:

$$\text{Unconditional stability condition}: \quad -\frac{1}{3}\le\alpha\le 0 \quad (3.37)$$

Accuracy

The following conclusions are drawn for the HHT-α method:

(1) When time interval is getting closer to zero, the spurious root also gain to zero.
(2) The higher modes are effectively damped, while the lower modes are kept unchanged.
(3) The period is also elongated.
(4) The accuracy is second order.

3.5.4 Generalized-α Method

The generalized-α method [21] combines the HHT-α algorithm [18] and WBZ-α algorithm [20] to achieve the unconditional stability, second-order accuracy, and optimal numerical dissipation. Four parameters, namely α_f, α_m, β, and γ, are included in this method, as shown in Equations (3.38)–(3.43). The parameters are determined using the procedures described in Section 3.4. A parameter ρ_∞ is introduced to indicate the user-specified value of the spectral radius in the high-frequency limit ($\Omega\to\infty$), in another words, it represents the user-defined

high-frequency dissipation. The parameters α_f and α_m can be defined in terms of ρ_∞ if the optimal numerical dissipation is achieved. Therefore, it permits high-frequency dissipation to vary from the no dissipation case $(\rho_\infty = 1)$ to the so-called asymptotic annihilation case $(\rho_\infty = 0)$. It is advantageous to be able to specify the algorithmic parameters in terms of the high-frequency dissipation, since the desired degree of high-frequency dissipation is usually a known quantity. The equation of motion is formulated based on an SDOF system.

Algorithm

$$ma_{n+1-\alpha_m} + cv_{n+1-\alpha_f} + kd_{n+1-\alpha_f} = f_{n+1-\alpha_f} \tag{3.38}$$

$$d_{n+1} = d_n + \Delta t v_n + (0.5-\beta)\Delta t^2 a_n + \beta \Delta t^2 a_{n+1} \tag{3.39}$$

$$v_{n+1} = v_n + \Delta t(1-\gamma)a_n + \Delta t \gamma a_{n+1} \tag{3.40}$$

$$d_{n+1-\alpha_f} = (1-\alpha_f)d_{n+1} + \alpha_f d_n \tag{3.41}$$

$$v_{n+1-\alpha_f} = (1-\alpha_f)v_{n+1} + \alpha_f v_n \tag{3.42}$$

$$a_{n+1-\alpha_m} = (1-\alpha_m)a_{n+1} + \alpha_m a_n \tag{3.43}$$

$$f_{n+1-\alpha_f} = (1-\alpha_f)f_{n+1} + \alpha_f f_n \tag{3.44}$$

Stability

The recursive matrix form of Equations (3.38)–(3.44) is formulated as follows based on an undamped SDOF system:

$$\begin{Bmatrix} d_{n+1} \\ \Delta t v_{n+1} \\ \Delta t^2 a_{n+1} \end{Bmatrix} = \mathbf{A} \begin{Bmatrix} d_n \\ \Delta t v_n \\ \Delta t^2 a_n \end{Bmatrix} + (1-\alpha_f)\mathbf{L}\frac{f_{n+1}}{m} + \alpha_f \mathbf{L}\frac{f_n}{m} \tag{3.45}$$

$$\mathbf{A} = \frac{1}{D}\begin{bmatrix} 1-\alpha_f\beta\Omega^2-\alpha_m & 1-\alpha_m & 0.5-\beta-0.5\alpha_m \\ -\gamma\Omega^2 & 1-\alpha_m+(1-\alpha_f)(\beta-\gamma)\Omega^2 & 1-\gamma-\alpha_m+(1-\alpha_f)(\beta-0.5\gamma)\Omega^2 \\ -\Omega^2 & -(1-\alpha_f)\Omega^2 & -(1-\alpha_f)(0.5-\beta)\Omega^2-\alpha_m \end{bmatrix}, \tag{3.46}$$

$$\text{and } \mathbf{L} = \frac{1}{D}\begin{bmatrix} \beta\Delta t^2 \\ \gamma\Delta t^2 \\ \Delta t^2 \end{bmatrix}$$

where $D = 1 + (1-\alpha_f)\beta\Omega^2 - \alpha_m$.

The stability condition of the generalized-α method is summarized as follows:

$$\text{Unconditional stability condition}: \quad \alpha_m \le \alpha_f \le \frac{1}{2},\ \beta \ge \frac{1}{4} + \frac{1}{2}(\alpha_f - \alpha_m) \tag{3.47}$$

Accuracy

The following conclusions are given for the generalized-α method:

(1) If $\gamma = \frac{1}{2} - \alpha_m + \alpha_f$, it is second-order accurate.

(2) If $\beta = \frac{1}{4}\left(1-\alpha_m+\alpha_f\right)^2$, highest damping is obtained for high-frequency modes.
(3) If $\alpha_m = \frac{2\rho_\infty - 1}{\rho_\infty + 1}$, $\alpha_f = \frac{\rho_\infty}{\rho_\infty + 1}$, and $\rho_\infty \in [0,1]$, the low-frequency modes are affected little.
(4) This method has the best numerical damping attributes and is the closest one to the trapezoidal rule.
(5) For the optimal case, the spurious root value in the low frequency limit is nonzero. But the impact on the algorithmic accuracy is negligible.

3.5.5 Implicit-Explicit Method

The implicit-explicit method [25,26] is a partitioned analysis procedure, in which a structure is divided into two parts geometrically. One is handled using an implicit algorithm, while the other using an explicit algorithm. The geometrical partition also divides the mass matrix, damping matrix, and stiffness matrix into two parts. The separation of these matrices is viewed as the general definition of "operator splitting." To explore the stability of this method, the spectral stability analysis method is not applicable. An energy-based method [11] is attempted to derive bounds on energy-like norms of the discrete solution. The stability and accuracy analyses should be examined for the two domains separately. In the implicit domain, the unconditional stability may be achieved. In the explicit domain, however, it is conditionally stable. The numerical characteristics of the two domains significantly depend on the algorithm adopted for each domain. In the following formulation, the Newmark-β method is adopted for the implicit domain, while the predictor-corrector method is adopted for the explicit domain.

Algorithm

$$\mathbf{M}\mathbf{a}_{n+1} + \mathbf{C}^{\mathrm{I}}\mathbf{v}_{n+1} + \mathbf{C}^{\mathrm{E}}\widetilde{\mathbf{v}}_{n+1} + \mathbf{K}^{\mathrm{I}}\mathbf{d}_{n+1} + \mathbf{K}^{\mathrm{E}}\widetilde{\mathbf{d}}_{n+1} = \mathbf{F}_{n+1} \tag{3.48}$$

$$\widetilde{\mathbf{d}}_{n+1} = \mathbf{d}_n + \Delta t\mathbf{v}_n + (0.5-\beta)\Delta t^2\mathbf{a}_n \tag{3.49}$$

$$\widetilde{\mathbf{v}}_{n+1} = \mathbf{v}_n + \Delta t(1-\gamma)\mathbf{a}_n \tag{3.50}$$

$$\mathbf{d}_{n+1} = \widetilde{\mathbf{d}}_{n+1} + \beta\Delta t^2\mathbf{a}_{n+1} \tag{3.51}$$

$$\mathbf{v}_{n+1} = \widetilde{\mathbf{v}}_{n+1} + \Delta t\gamma\mathbf{a}_{n+1} \tag{3.52}$$

where $\mathbf{M} = \mathbf{M}^{\mathrm{I}} + \mathbf{M}^{\mathrm{E}}$, $\mathbf{C} = \mathbf{C}^{\mathrm{I}} + \mathbf{C}^{\mathrm{E}}$, $\mathbf{K} = \mathbf{K}^{\mathrm{I}} + \mathbf{K}^{\mathrm{E}}$, $\mathbf{F} = \mathbf{F}^{\mathrm{I}} + \mathbf{F}^{\mathrm{E}}$, superscripts I and E refer to the implicit and explicit groups, respectively.

Stability and accuracy

The details about the stability and accuracy using the energy method can be found in other publications [11] and [25], and therefore are not formulated here. The stability and accuracy of the method are summarized as follows:

(1) If $\gamma \geq 0.5$, and $\mathbf{B}^{\mathrm{I}} + \bar{\mathbf{B}}^{\mathrm{E}}$ is positive definite, then $\mathbf{a}_n$ and $\mathbf{v}_n$ are bounded.
where $\mathbf{B}^{\mathrm{I}} = \mathbf{M}^{\mathrm{I}} + \Delta t(\gamma - 0.5)\mathbf{C}^{\mathrm{I}} + \Delta t^2(\beta - 0.5\gamma)\mathbf{K}^{\mathrm{I}}$,
$\bar{\mathbf{B}}^{\mathrm{E}} = \mathbf{M}^{\mathrm{E}} + \Delta t(\gamma - 0.5)\mathbf{C}^{\mathrm{E}} + \Delta t^2(\beta - 0.5\gamma)\mathbf{K}^{\mathrm{E}} - \Delta t\gamma\mathbf{C} - \Delta t^2\beta\mathbf{K}$.

(2) If $\mathbf{K}^{-1}$ exists, then $\mathbf{d}_n$ is also bounded.

(3) For a given value of $\gamma \geq 0.5$, selection of $\beta \geq (\gamma + 0.5)^2/4$ makes the implicit domain unconditionally stable. And $\Omega < \Omega_{\mathrm{crit}} = \left(\left(2\gamma + \xi^2\right)^{1/2} - \xi\right)/\gamma$ should be satisfied for the explicit domain, or a stricter condition $\Omega < \Omega_{\mathrm{bif}} = 2(1 - \xi)/(\gamma + 0.5)$ should be satisfied for two complex conjugate eigenvalues for the explicit domain.

(4) If $\gamma = 0.5$ and no damping for explicit part, this method has a second-order accuracy, otherwise, this method is first-order accurate.

3.5.6 Modal Truncation Technique

Modal truncation technique [28] is a procedure to improve the stability characteristic of explicit time integration algorithms in terms of time interval. Explicit time integration algorithms, such as the CDM, when applied for large-scale structures, require a very small time interval because of the involvement of higher vibration modes. The contribution of higher vibration modes to the entire response, however, is not the dominant part, even in the inelastic domain. It is always possible to discard higher vibration modes to improve the stability but without significantly attenuating the accuracy.

Formulation

The equations of motion are formulated in the modal coordinates with mass orthonormality, as shown in Equation (3.54), and uncoupled into individual equations with SDOF, as shown in Equation (3.56).

$$\mathbf{Ma} + \mathbf{Kd} = \mathbf{0} \tag{3.53}$$

$$\mathbf{\Psi}^{\mathrm{T}}\mathbf{M}\mathbf{\Psi} = \mathbf{I},\ \mathbf{\Psi}^{\mathrm{T}}\mathbf{K}\mathbf{\Psi} = \mathbf{\Lambda} \tag{3.54}$$

$$\mathbf{d} = \sum_{m=1}^{n_{\mathrm{eq}}} x_m \mathbf{\Psi}_m \tag{3.55}$$

$$\ddot{x}_i + \lambda_i x_i = 0,\ \lambda_i = \omega_i^2 \tag{3.56}$$

where $\mathbf{M}$ and $\mathbf{K}$ are mass and stiffness matrices, respectively; $\mathbf{a}$ and $\mathbf{d}$ are acceleration and displacement vectors, respectively; note here damping is neglected; $\mathbf{\Psi}$ includes the normalized eigenvectors corresponding to eigenvalue matrix $\mathbf{\Lambda}$, which is a diagonal matrix with diagonal terms of λ_i; x_i is the modal coordinates, and ω_i is the circular frequency of ith vibration mode. Equation (3.56) can be solved by any time integration algorithm. Here, central difference algorithm is used as an example. The central difference formulation for each individual equation is:

$$x_i^{n+1} = \left[2 - (\omega_i \Delta t)^2\right] x_i^n - x_i^{n-1} \tag{3.57}$$

A parameter γ is introduced into Equation (3.42) to control the partition of modes as:

$$x_i^{n+1} = \left[2 - (\gamma_i \omega_i \Delta t)^2\right] x_i^n - x_i^{n-1}, \quad 0 \le \gamma_i \le 1 \tag{3.58}$$

Next, it is transferred into the Cartesian basis as:

$$\mathbf{d}^{n+1} = \Delta t^2 \boldsymbol{\Psi}\boldsymbol{\Gamma}\boldsymbol{\Psi}^{\mathrm{T}}\mathbf{M}\ddot{\mathbf{d}}^n + 2\mathbf{d}^n - \mathbf{d}^{n-1} \tag{3.59}$$

The direct integration of the global dynamics is processed based on Equation (3.59) implemented with a weighted parameter $\boldsymbol{\Gamma}$, which is a diagonal matrix with unit of the diagonal term related to the retaining modes, while zero for the discarded modes.

Stability and accuracy

The stability of the time integration algorithm, here the CDM, is controlled by the highest vibration mode of the structure. Using the mode truncation technique, higher vibration modes which contribute little to global response are trimmed, thus stability may be achieved using a larger time interval.

The accuracy of the time integration method can be maintained by carefully selecting the weighted parameter. In this particular case, if $\gamma_i = 1$ is selected, the retaining modes will be treated up to second-order accuracy.

3.5.7 Integral Form of Existing Algorithms

By this technique [29,30], the second-order differential equation is converted to a first-order equation by integrating it with respect to time step. This integral form is taken as the governing equation of motion. The main advantage of this technique is its capability of capturing the rapid changes of structural properties and dynamic loading, and in eliminating the adverse linearization errors. The explicit Newmark method is taken as the example.

Algorithm

$$mv_{n+1} + cd_{n+1} + \bar{r}_{n+1} = \bar{f}_{n+1} \tag{3.60}$$

$$s_{n+1} = s_n + \Delta t d_n + 0.5\Delta t^2 v_n \tag{3.61}$$

$$d_{n+1} = d_n + 0.5\Delta t(v_n + v_{n+1}) \tag{3.62}$$

where s_{n+1}, $\bar{r}_{n+1}$, and $\bar{f}_{n+1}$ are the integral forms of d_{n+1}, r_{n+1}, and f_{n+1}, respectively.

3.5.8 State Space Procedure

This algorithm formulates the equations of motion in state space and uses their analytical solution to derive a recursive discrete-time equation. The SSP [31]

can be considered as a generalization for MDOF systems of the Duhamel's integral used for SDOF systems. The analytical solution in state space leads to a more accurate discrete-time model. It is noted that the proposed SSP algorithm does not need a previous modal uncoupling of the equations of motion and, consequently, it does not require any hypothesis about damping and the hypothesis about the variation of acceleration between two time increments. SSP is known to be stable and to give accurate results with a reasonable computation time. Several applications [35,36] were proposed recently.

Formulation

The state space formulation of the equations of motion is shown by the following equations:

$$\dot{\mathbf{x}}(t) = \mathbf{F}\mathbf{x}(t) + \mathbf{v}(t) \tag{3.63}$$

where

$$\mathbf{x}(t) = \begin{Bmatrix} \mathbf{d}(t) \\ \dot{\mathbf{d}}(t) \end{Bmatrix},\ \mathbf{F} = \begin{bmatrix} \mathbf{0} & \mathbf{I} \\ -\mathbf{M}^{-1}\mathbf{K} & -\mathbf{M}^{-1}\mathbf{C} \end{bmatrix},\ \mathbf{v}(t) = \begin{Bmatrix} 0 \\ \mathbf{M}^{-1}\mathbf{f}(t) \end{Bmatrix} \tag{3.64}$$

With $\mathbf{x}(t_0) = \mathbf{x}_0$, the analytical solution is:

$$\mathbf{x}(t) = \exp[(t-t_0)\mathbf{F}]\mathbf{x}_0 + \int_{t_0}^{t} \exp[(t-\tau)\mathbf{F}]\mathbf{v}(\tau)\mathrm{d}\tau \tag{3.65}$$

The following discrete-time equation is obtained:

$$\mathbf{x}(k\Delta t + \Delta t) = \exp[\Delta t\mathbf{F}]\mathbf{x}(k\Delta t) + \int_{k\Delta t}^{(k+1)\Delta t} \exp[((k+1)\Delta t - \tau)\mathbf{F}]\mathbf{v}(\tau)\mathrm{d}\tau \tag{3.66}$$

Using linear interpolation for continuous form of external force based on discretized values:

$$\mathbf{v}(\tau) = \mathbf{v}(k\Delta t) + (\tau - k\Delta t)\frac{\mathbf{v}(k\Delta t + \Delta t) - \mathbf{v}(k\Delta t)}{\Delta t},\quad k\Delta t \le \tau \le k\Delta t + \Delta t \tag{3.67}$$

Then the discrete-time equation is obtained:

$$\mathbf{x}(k\Delta t + \Delta t) = \mathbf{A}\mathbf{x}(k\Delta t) + \mathbf{P}_1\mathbf{v}(k\Delta t + \Delta t) + \mathbf{P}_2[\mathbf{v}(k\Delta t + \Delta t) - \mathbf{v}(k\Delta t)] \tag{3.68}$$

where

$$\begin{gathered} \mathbf{A} = \exp(\Delta t\mathbf{F}),\ \mathbf{P}_1 = \mathbf{F}^{-1}(\mathbf{A} - \mathbf{I}),\ \mathbf{P}_2 = \mathbf{F}^{-1}\left(\frac{1}{\Delta t}\mathbf{P}_1 - \mathbf{A}\right), \\ \mathbf{F}^{-1} = \begin{bmatrix} -\mathbf{K}^{-1}\mathbf{C} & -\mathbf{K}^{-1}\mathbf{M} \\ \mathbf{I} & \mathbf{0} \end{bmatrix} \end{gathered} \tag{3.69}$$

Stability and accuracy

The stability of the method is controlled by the eigenvalues of $\mathbf{A}$, which should be smaller than 1. The expression of $\mathbf{A}$ can be expanded using an odd number p as

$$\mathbf{A} = \exp(\Delta t\mathbf{F}) \approx \left\{ \mathbf{I} + \frac{1}{1!}\frac{\Delta t\mathbf{F}}{2^q} + \frac{1}{2!}\left(\frac{\Delta t\mathbf{F}}{2^q}\right)^2 + \cdots + \frac{1}{p!}\left(\frac{\Delta t\mathbf{F}}{2^q}\right)^p \right\}^{2^q} \tag{3.70}$$

For each value of p, there exist suitable values for Δt and q such that the spectral radius of $\mathbf{A}$ equals to 1 for undamped systems or <1 for damped systems.

The error is introduced by the algorithm in two points: the interpolation of the excitation, Equation (3.67), and the computation of matrix $\mathbf{A}$, Equation (3.70). The following conclusions can be drawn for the accuracy:

(1) The error of SSP is appreciably smaller than the error corresponding to the other algorithms, such as CDM, trapezoidal rule, and Wilson method.
(2) The period may be elongated or reduced. The error decreases with the increase of p and q.

3.6 APPLICATIONS FOR AN ONLINE HYBRID TEST

Although most of the time integration algorithms can be implemented for an online hybrid test, only a few of them have been employed because of their simplicity or inherent excellent numerical properties.

One of the earliest applications was developed by Takanashi et al. [37]. The equations of motion are solved by using the linear acceleration method. The tangential stiffness of the specimen is measured and the equation of motion is formulated in an incremental form. When applied for complex and stiff systems, it is found difficult to estimate the instantaneous stiffness because of the accuracy limit of the measuring devices. The first online hybrid test system with great universality and applicability was developed by Tanaka [38] using the CDM. The incremental form and measuring tangential stiffness are not required. However, the explicit algorithms are not suitable for stiff MDOF systems, including high-frequency vibration modes because their conditional stability requires a limited time interval, which results in inefficiency.

Implicit algorithms are always appealing in terms of unconditional stability and numerical dissipation. But difficulties are encountered when applied to online hybrid tests. The main concern is that the iterative procedure in implicit algorithms may introduce undesirable loading and unloading hysteretic behavior in tested structures, which is history-dependent. Recently, some applications of implicit algorithms were proposed successfully to overcome the difficulty mentioned above. These applications could be categorized into three approaches: (1) hardware-dependent iterative schemes; (2) Newton iterative schemes; and (3) noniterative mixed schemes.

Thewalt and Mahin [39] developed an online hybrid test system based on the HHT-α method and iterations carried out at a hybrid digital-analog level. This method belongs to the first approach of applications of implicit algorithms that depends greatly on the special hardware. Shing et al. [40] proposed an iterative procedure also based on the HHT-α method. This procedure uses modified Newton iterations with a displacement reduction factor and dual displacement control to avoid overshooting the load path of the specimen. The noniterative mixed schemes are based on implicit-explicit algorithms. These schemes allow a larger time interval for MDOF systems to reduce both the computational and experimental effort. On the other hand, they preserve the simplicity of the implementation for online hybrid test. Dermitzarkis et al. [41] proposed a testing scheme based on the implicit-explicit algorithm of Hughes and Liu [25,26]. The structure is divided into two substructures: one containing experimental DOF and the other containing analytical DOF. The experimental part is solved explicitly by using a predicting-correcting procedure. The analytical part is solved by an implicit Newmark's method. Another implementation, called operator-splitting (OS) scheme, was developed by Nakashima et al. [42], based on the modified implicit-explicit algorithm [27]. This OS scheme is based on Newmark's method. Later Nakashima et al. [43] proposed the α-OS scheme based on the HHT-α method for the dissipative properties to control experimental error growth. This method was further formulated in state space to increase the accuracy by Wang et al. [35]. In 2004, a predictor-corrector scheme was developed by Bonelli and Bursi [44]. It is based on the implicit generalized-α method, the so-called IPC-ρ_∞ method. This method provides a user-controlled dissipation property. Recently, Ghaboussi et al. [45] developed a predictor-corrector scheme, which has an important advantage, as it does not require the determination of the initial stiffness values of experimental components and is thus suitable for elastic and inelastic systems. The applications to online hybrid tests are summarized as follows.

3.6.1 Applications of Central Difference Method

Tanaka [38] devised a system to overcome the difficulties in earlier online hybrid test implementation [37]. The CDM was adopted to solve the dynamics of the system. With this method, neither the tangential stiffness nor the incremental formulation is needed. Instead, the reactional force r measured from the load cell is used directly to solve the equation of motion. The test procedure is implemented for an SDOF system as follows:

(1) Calculate the target displacement d_{n+1} of the $(n+1)$th step by Equation (3.71) which is derived from Equations (3.17)–(3.19). r_n is the reactional force measured from the load cell at the previous step.

$$d_{n+1} = \frac{2md_n + (\Delta tc/2 - m)d_{n-1} - \Delta t^2(r_n - f_n)}{m + \Delta tc/2} \tag{3.71}$$

(2) Use the loading facility to push/pull the specimen to the target displacement.
(3) Measure the reactional force r_{n+1} from the load cell for the next step analysis.
(4) Let $n = n + 1$ and go to step (1).

Note that the target displacement is completely determined by known quantities. In this system, the equations of motion need not be formulated in an incremental form, thus the iteration procedure is avoided. Because of the simplicity and applicability of the CDM, it is adopted for most of the early online hybrid tests.

3.6.2 Hardware-Dependent Iterative Scheme

Thewalt and Mahin [39] constructed the first online hybrid test application using implicit algorithms. While any implicit algorithms can be employed for this system, the HHT-α method [18] was employed in their study. The iteration was not employed in the numerical integration level, but processed by an analog electronic device in the displacement control. The Equations (3.32)–(3.34) are reformulated as Equation (3.72), with the only unknowns of r_{n+1}. The displacement can be viewed as the sum of an explicit part, the first four terms of the right side of Equation (3.72), and an implicit part, the last term of the right side. The explicit part can be solved readily because all the variables are known at the beginning of the time step. The implicit part, however, requires the iteration procedure. The test procedure is given based on an undamped SDOF system.

$$d_{n+1} = d_n + \Delta t v_n + \Delta t^2 \left(\frac{1}{2} - \beta\right) a_n + \Delta t^2 \beta (f_{n+1} + \alpha r_i)/m - \Delta t^2 \beta (1+\alpha) r_{i+1}/m \tag{3.72}$$

(1) Solve the explicit part of Equation (3.57), and take it as the initial value of the target displacement.
(2) Impose the target displacement on the specimen.
(3) Measure the reactional force from the load cell.
(4) Use Equation (3.72) to update the target displacement.
(5) If the target displacement does not change too much, this loading step is finished. Otherwise, go to Step (2).

Note that the displacement feedback control loop from Step (2) to Step (5) is achieved through an analog electronic device. The servo-controller displacement command for each step is taken as the analog sum of the explicit part and an analog function of the measured reactional force (implicit part), and is continuously updated until the reactional force and target displacement satisfied Equation (3.72).

This application has proved to be reliable and far superior to existing explicit applications. However, it is more difficult to implement because of the additional hardware required. Moreover, even though displacement convergence is constantly enforced by the analog device, convergence errors could still be introduced by the positioning of loading facilities, depending on the performance of the servo-hydraulic control system. These errors could excite the spurious higher-mode response of a structure and impair the accuracy of test results.

3.6.3 Newton Iterative Scheme Based on HHT-α Method

The implicit HHT-α method is implemented in an iterative form and applied for the online hybrid test [40]. However, this implementation is more general for most of the implicit algorithms. This is also an iterative procedure. But unlike the hardware-dependent iterative schemes, the iteration is employed on the numerical scheme which is based on the modified Newton-Raphson procedure. In each iteration, the target displacement is reduced by a factor and imposed on the specimen to overcome undesirable loading and unloading overshooting. The displacement is achieved by a dual displacement control and an error-correction procedure is added after one step of loading. This testing scheme supplies a favorable numerical dissipation that eliminates the spurious higher-mode response, which can often be excited by experimental errors. This method maintains the advantages of the HHT-α method as much as possible and does not require special hardware for the hybrid testing. Equations (3.32)–(3.34) are reformulated into an effective static form as shown in Equations (3.73) and (3.74) in order to specify the implementation.

$$\bar{m}d_{n+1} = \bar{m}\widehat{d}_{n+1} - \Delta t^2\beta(1+\alpha)r_{n+1} \tag{3.73}$$

where r is the reactional force measured from tested structure;

$$\begin{aligned}
&\bar{m} = m + \Delta t\gamma(1+\alpha)c; \text{ and}\\
&\bar{m}\widehat{d}_{n+1} = \bar{m}\left[d_n + \Delta t v_n + \Delta t^2(0.5-\beta)a_n\right]\\
&\quad + \Delta t^2\beta[(1+\alpha)f_{n+1} - \alpha f_n - cv_n - (1+\alpha)(1-\gamma)\Delta t c a_n + \alpha r_n]
\end{aligned} \tag{3.74}$$

The testing procedure is summarized as follows:

(1) Use Equation (3.58) to calculate $\bar{m}\widehat{d}_{n+1}$
(2) Set $k=0$, $r_{n+1}^{(k)} = r_n$, $d_{n+1}^{c(k)} = d_n^c$, $d_{n+1}^{\mathrm{ex}(k)} = d_n^{\mathrm{ex}}$
(3) Evaluate $\bar{m}e_{n+1}^{(k)} = \bar{m}d_{n+1}^{\mathrm{ex}(k)} - \bar{m}\widehat{d}_{n+1} + \Delta t^2\beta(1+\alpha)r_{n+1}^{(k)}$
(4) Solve $k^*\Delta d_{n+1}^{(k)} = -\bar{m}e_{n+1}^{(k)}$ for $\Delta d_{n+1}^{(k)}$
(5) If $\left|\Delta d_{n+1}^{(k)}\right| < \varepsilon$ then go to step 10
(6) Evaluate the displacement $d_{n+1}^{c(k+1)} = d_{n+1}^{c(k)} + \theta\Delta d_{n+1}^{(k)}$
(7) Impose $d_{n+1}^{c(k+1)}$ on the tested specimen
(8) Measure $r_{n+1}^{(k+1)}$ and $d_{n+1}^{\mathrm{ex}(k+1)}$

(9) Set $k = k+1$, go to Step (3)

(10) Calculate $d_{n+1} = d_{n+1}^{\mathrm{ex}(k)} + \Delta d_{n+1}^{(k)}$, $r_{n+1} = r_{n+1}^{(k)} + k^{\mathrm{I}} \Delta d_{n+1}^{(k)}$, $d_n^c = d_{n+1}^{c(k)}$, $d_n^{\mathrm{ex}} = d_{n+1}^{\mathrm{ex}(k)}$

(11) Calculate $a_{n+1} = [d_{n+1} - d_n - \Delta t v_n - \Delta t^2 (0.5-\beta) a_n] / (\Delta t^2 \beta)$, $v_{n+1} = v_n + \Delta t[(1-\gamma)a_n + \gamma a_{n+1}]$

(12) Set $n = n+1$, go to Step (1).

In the above formulation, n is the step number; k is the iteration number; ε is the convergence tolerance; θ is the displacement reduction factor which satisfies $0 \le \theta \le 1$; k^{I} is the initial stiffness of the tested specimen; and $k^* = \bar{m} + \Delta t^2 \beta (1+\alpha) k^{\mathrm{I}}$.

It has already been demonstrated that if $F = \bar{m} / (\Delta t^2 \beta (1+\alpha)) + k^{\mathrm{a}}$ is positive definite, the above iteration procedure is convergent where k^{a} is the real stiffness of the tested specimen [46].

3.6.4 α-OS Method

Nakashima et al. [43] developed the α-OS testing scheme based on Hughes's work [27]. The stiffness of the tested structure is divided into a linear part and a nonlinear part. The explicit predictor-corrector method is employed for the integration associated with the nonlinear stiffness and the HHT-α method is used for the integration associated with the linear stiffness. The solution algorithm is given in Equations (3.75)–(3.78). In this study, initial stiffness of the tested structure is needed, which is not necessarily the same as the real initial stiffness. The effect on the stability and accuracy of the HHT-α method by the initial stiffness was explored by Nakashima [43] and Combescure [47]. It is found that if the tested structure is a softening type, the numerical properties of the HHT-α method, such as unconditional stability and optimal numerical dissipation, are always kept. Because of the predictor-corrector procedure, it needs no iterations in this implementation, which makes it very favorable for online hybrid tests.

$$\text{Predictors}: \ \widetilde{d}_{n+1} = d_n + \Delta t v_n + (0.5-\beta)\Delta t^2 a_n \tag{3.75}$$

$$\text{Balanced equation}: \ m a_{n+1} + (1+\alpha) c v_{n+1} - \alpha c v_n + (1+\alpha) r_{n+1} - \alpha r_n = (1+\alpha) f_{n+1} - \alpha f_n \tag{3.76}$$

$$\text{where } r_{n+1}(d_{n+1}) \approx k^{\mathrm{I}} d_{n+1} + \widetilde{r}_{n+1}\left(\widetilde{d}_{n+1}\right) - k^{\mathrm{I}} \widetilde{d}_{n+1}$$

$$\text{Correctors}: \ d_{n+1} = \widetilde{d}_{n+1} + \beta \Delta t^2 a_{n+1}, \ v_{n+1} = v_n + \Delta t (1-\gamma) a_n + \Delta t \gamma a_{n+1} \tag{3.77}$$

where

$$\alpha \in [-1/3, 0], \ \beta = (1-\alpha)^2/4, \ \gamma = (1-2\alpha)/2 \tag{3.78}$$

The testing procedure is summarized as follows:

(1) Calculate the displacement predictor $\widetilde{d}_{n+1}$ using Equation (3.75).
(2) Apply the predictor $\widetilde{d}_{n+1}$ to the specimen.
(3) Measure the reactional force $\widetilde{r}_{n+1}$.
(4) Solve the corrector d_{n+1}, and corresponding v_{n+1} and a_{n+1} by Equations (3.76)–(3.78).

Set $n = n+1$, go to Step (1).

3.6.5 Predictor-Corrector Implementation of Generalized-α Method (IPC-ρ_∞)

The generalized-α method was implemented in a predictor-corrector form giving rise to the implicit IPC-ρ_∞ method [44]. It entails a single movement of the loading facility per time step, thus is viewed as a noniterative procedure. The implicit IPC-ρ_∞ method maintains the computational efficiency of the α-OS method [43], but enhances the accuracy by using an implicit predictor such as the iterative method [40] mentioned in Section 3.3.3. A quasi-Newton procedure is employed to closely approximate the actual tangential stiffness, rather than a prescribed initial stiffness employed in previous studies [40,43]. It was demonstrated that this method enhances the performance of the online hybrid test even in an environment characterized by considerable experimental error. The testing procedure is summarized as follows:

(1) Solve Equations (3.38)–(3.43) of the standard generalized-α method to obtain the displacement predictor $\bar{d}_{n+1}$. Note that this predictor displacement is calculated by the equilibrium based on the secant stiffness k_n derived from the quasi-Newton procedure of previous step, which is different from the conventional predictor as Equation (3.75).
(2) Impose the displacement predictor $\bar{d}_{n+1}$ on the specimen.
(3) Measure the reactional force $\bar{r}_{n+1}$ of the tested structure.
(4) Update the secant stiffness k_{n+1} by a quasi-Newton method, the Davidson procedure for example.
(5) Solve Equations (3.38)–(3.43) again, but the updated stiffness is used to update the reactional force: $r_{n+1} = \bar{r}_{n+1} + k_{n+1}(d_{n+1} - d_n)$.
(6) Set $n = n+1$, go to Step (1).

The numerical properties of the generalized-α method are maintained if $0 < k^a/k < 2$, where k^a is the actual stiffness of the tested structure, and k is the stiffness updated by quasi-Newton procedure.

3.6.6 Ghaboussi Predictor-Corrector Method

Ghaboussi et al. [45] developed a novel predictor-corrector scheme for online hybrid test. A structure is divided into experimental parts and analytical parts.

The experimental parts are performed quasi-statically based on explicit prediction of displacement, while the analytical parts are solved by implicit time integration algorithms. Implicit Newark's method was taken as an example. The unique advantage of the new predictor-corrector scheme is that it does not require iteration for the initial stiffness values as well as nonlinear experimental component. This scheme treats interaction effect between analytical model and experimental parts effectively by regarding it as a nonlinear external loading. First the Newmark-β method is modified by the predictor-corrector procedure and formulated in an incremental form, as follows:

$$\mathbf{M}\Delta\ddot{\mathbf{X}}_n + \mathbf{C}^{\mathrm{L}}\Delta\dot{\mathbf{X}}_n + \mathbf{K}^{\mathrm{L}}\Delta\mathbf{X}_n + \Delta\widetilde{\mathbf{r}}_n\left(\widetilde{\mathbf{X}}^{\mathrm{b}}_{n+1}\right) = \Delta\mathbf{F}_n \tag{3.79}$$

$$\Delta\mathbf{X}_n = \Delta t\dot{\mathbf{X}}_n + (0.5-\beta)\Delta t^2\ddot{\mathbf{X}}_n + \beta\Delta t^2\ddot{\mathbf{X}}_{n+1} \tag{3.80}$$

$$\Delta\dot{\mathbf{X}}_n = \Delta t(1-\gamma)\ddot{\mathbf{X}}_n + \gamma\Delta t\ddot{\mathbf{X}}_{n+1} \tag{3.81}$$

$$\widetilde{\mathbf{X}}^{\mathrm{b}}_{n+1} = \mathbf{X}^{\mathrm{b}}_n + \Delta t\dot{\mathbf{X}}^{\mathrm{b}}_n + (0.5-\beta)\Delta t^2\ddot{\mathbf{X}}^{\mathrm{b}}_n \tag{3.82}$$

$$\mathbf{X}_{n+1} = \begin{Bmatrix} \mathbf{x}^{\mathrm{c}}_{n+1} \\ \mathbf{x}^{\mathrm{b}}_{n+1} \end{Bmatrix},\ \widetilde{\mathbf{X}}^{\mathrm{b}}_{n+1} = \begin{Bmatrix} \mathbf{0} \\ \widetilde{\mathbf{x}}^{\mathrm{b}}_{n+1} \end{Bmatrix} \tag{3.83}$$

$$\begin{aligned} &\Delta\mathbf{X}_n = \mathbf{X}_{n+1} - \mathbf{X}_n,\ \Delta\dot{\mathbf{X}}_n = \dot{\mathbf{X}}_{n+1} - \dot{\mathbf{X}}_n,\ \Delta\ddot{\mathbf{X}}_n = \ddot{\mathbf{X}}_{n+1} - \ddot{\mathbf{X}}_n, \\ &\Delta\mathbf{F}_n = \mathbf{F}_{n+1} - \mathbf{F}_n,\ \Delta\widetilde{\mathbf{r}}_n = \widetilde{\mathbf{r}}_{n+1} - \widetilde{\mathbf{r}}_n \end{aligned} \tag{3.84}$$

where $\mathbf{C}^{\mathrm{L}}$ and $\mathbf{K}^{\mathrm{L}}$ are viscous damping and stiffness matrices of analytical parts; $\mathbf{X}$, $\dot{\mathbf{X}}$, and $\ddot{\mathbf{X}}$ are vectors of displacement, velocity, and acceleration, respectively; $\mathbf{X}^{\mathrm{b}}$, $\dot{\mathbf{X}}^{\mathrm{b}}$, and $\ddot{\mathbf{X}}^{\mathrm{b}}$ are vectors of displacement, velocity, and acceleration at the boundary connecting to the experimental parts, respectively; $\widetilde{\mathbf{r}}$ and $\mathbf{F}$ are reactional force and external load vectors; $\widetilde{\mathbf{X}}^{\mathrm{b}}_{n+1}$ is the predicted displacement vector; $\mathbf{x}^{\mathrm{c}}_{n+1}$ is the displacement vector with analytical model; $\mathbf{x}^{\mathrm{b}}_{n+1}$ is the displacement vector at the boundary; $\widetilde{\mathbf{x}}^{\mathrm{b}}_{n+1}$ is the predicted displacement vector at the boundary.

The testing procedure is summarized as follows:

(1) Predict the displacement for the experimental part using Equation (3.82).
(2) Impose the displacement on the experimental parts.
(3) Measure the reactional forces of the experimental parts.
(4) Solve Equations (3.79)–(3.81) to get the corrected values for both analytical parts and experimental parts.
(5) Set $n = n+1$. Go to Step (1).

The predictor-corrector implementation impairs the stability of the implicit Newmark-β method. It becomes conditionally stable, and the sampling

frequency is defined as Equation (3.85) where χ is defined as the stiffness contribution of analytical model to the boundary over the total stiffness of the boundary.

$$\text{Conditional stability condition}: \quad \Omega < 2\sqrt{\frac{1}{1-\chi}} \tag{3.85}$$

3.7 CONCLUSIONS

In this chapter, the basics of time integration algorithms, which are important to solve the equations of motion of online hybrid tests, have been introduced. The existing time integration algorithms are grouped into such families as: (1) linear multi-step methods; (2) Newmark's family; (3) collocation methods; (4) α-family; (5) ρ-family; and (6) mixed implicit-explicit methods. The superiority of one family over the others is summarized in terms of the following rules: (1) self-restart procedure; (2) second-order accuracy; (3) unconditional stability; and (4) optimal and controllable numerical dissipation. Formulations and implementations of some notable time integration algorithms for the online hybrid test are also introduced. They are categorized into: (1) application of explicit algorithms; and (2) applications of implicit algorithms. Major conclusions obtained from this chapter are as follows:

(1) Most linear multi-step methods require information of several previous steps and thus are not self-started. By carefully selecting the difference equations for the acceleration and velocity terms, the other three rules can be satisfied.

(2) Newmarks' family methods are self-started. If the parameters are carefully selected, the second-order accuracy and unconditional stability can be achieved. The numerical dissipation, however, exist only when the method is first-order accurate. Furthermore, numerical dissipation of the methods is not necessarily desirable, since it may affect the lower modes significantly.

(3) Collocation methods, α-family methods, and ρ-family methods can satisfy all of four rules.

(4) The numerical properties of mixed implicit-explicit methods are different for the implicit and explicit domains. They are quite dependent on the algorithm adopted for each domain.

(5) Explicit algorithms are most convenient and easiest to be incorporated into the online hybrid test system, but most of them have time interval limitations.

(6) Implicit algorithms are always appealing in terms of unconditional stability and numerical dissipation. Difficulties are encountered, however, when applied to online hybrid tests. The main concern is that the iterative procedures required in implicit algorithms may introduce undesirable loading and unloading in tested structures whose hystereses are path-dependent.

REFERENCES

[1] Chopra AK. Dynamics of structures, theory and applications to earthquake engineering. 2nd ed. Englewood Cliffs, NJ: Prentice-Hall; 2001.

[2] Bathe KJ, Wilson EL. Stability and accuracy analysis of direct integration methods. J Earthq Eng Struct Dyn 1973;1:283–91.

[3] Belytschko T, Hughes TJR. Computational methods for transient analysis. Computational methods in mechanics. 1. Amsterdam, The Netherlands: Elsevier Science B.V.; 2001.

[4] Gear CW. Numerical initial value problems in ordinary differential equations. Englewood Cliffs, NJ: Prentice-Hall; 1971.

[5] Houbolt JC. A recurrence matrix solution for the dynamic response of elastic aircraft. J Aeronaut Sci 1950;17:540–50.

[6] Park KC. An improved stiffly stable method for direct integration of nonlinear structural dynamic equations. J Appl Mech ASME 1975;42:464–70.

[7] Leech JW, Hsu PT, Mack EW. Stability of a finite difference method for solving matrix equations. AIAA J 1965;3(11):2172–3.

[8] Nakashima M. Part I: Relationship between integration time interval and response stability in pseudo dynamic testing. J Struct Constr Eng 1985;353:29–36.

[9] Nakashima M. Part II: Relationship between integration time interval and accuracy of displacement, velocity, and acceleration responses in pseudo dynamic testing. J Struct Constr Eng 1985;358:35–42.

[10] Johnson DE. A proof of the stability of the Houbolt method. AIAA J 1966;4:1450–1.

[11] Newmark NM. A method of computation for structural dynamics. ASCE Proc 1959;85 (EM3):67–94.

[12] Shing BP, Mahin SA. Experimental error propagation in pseudo dynamic testing. Report No. UCB/EERC-83/12, Berkeley, CA: Earthquake Engineering Research Center, The University of California; 1983.

[13] Chang SY. Improved numerical dissipation for explicit methods in pseudo dynamic tests. J Earthq Eng Struct Dyn 1997;26:917–29.

[14] Chung JT, Lee JM. A new family of explicit time integration methods of linear and nonlinear structural dynamics. Int J Numer Methods Eng 1994;37:3961–76.

[15] Chang SY. Explicit pseudo dynamic algorithm with unconditional stability. J Eng Mech ASCE 2002;128(9):935–47.

[16] Wilson EL. A computer program for the dynamic stress analysis of underground structures. SESM Report 68-1, Berkeley, CA: Department of Civil Engineering, University of California; 1968.

[17] Hilber HM, Hughes TJR. Collocation, dissipation and 'Overshoot' for time integration schemes in structural dynamics. J Earthq Eng Struct Dyn 1978;6:99–118.

[18] Hilber HM, Hughes TJR, Taylor RL. Improved numerical dissipation for time integration algorithms in structural dynamics. J Earthq Eng Struct Dyn 1977;5:283–92.

[19] Hilber HM. Analysis and design of numerical integration algorithms in structural dynamics. Report No. UCB/EERC-76/29, Berkeley, CA: Earthquake Engineering Research Center, The University of California; 1976.

[20] Wood WL, Bossak M, Zienkiewicz OC. An alpha modification of Newmark's method. Int J Numer Methods Eng 1981;15:1562–6.

[21] Chung J, Hulbert GM. A time integration algorithm for structural dynamics with improved numerical dissipation: the generalized alpha-method. J Appl Mech ASME 1993;60:371–5.

[22] Hulbert GM, Chung J. Explicit time integration algorithms for structural dynamics with optimal numerical dissipation. Comput Methods Appl Mech Eng 1996;137:175–88.
[23] Bazzi G, Anderheggen E. The thou-family of algorithms for time-step integration with improved numerical dissipation. J Earthq Eng Struct Dyn 1982;10:537–50.
[24] Anderheggen E, Bazzi G. On a new algorithm for time-step integration of nonlinear structures. In: Symposium of future trends in computational structural analysis synthesis, Washington, DC; 1978.
[25] Hughes TJR, Liu WK. Implicit-explicit finite elements in transient analysis: stability theory. J Appl Mech ASME 1978;45:371–4.
[26] Hughes TJR, Liu WK. Implicit-explicit finite elements in transient analysis: implementation and numerical examples. J Appl Mech ASME 1978;45:375–8.
[27] Hughes TJR, Pister KS, Taylor RL. Implicit-explicit finite elements in nonlinear transient analysis. Comput Methods Appl Mech Eng 1979;17(18):159–82.
[28] Gutierrez E, Cela JJL. Improved explicit time integration by modal truncation techniques. J Earthq Eng Struct Dyn 1998;27:1541–57.
[29] Chen CC, Robinson AR. Improved time history analysis for structural dynamics. I: treatment of rapid variation of excitation and material nonlinearity. J Eng Mech ASCE 1992;119:2496–513.
[30] Chang SY, Tsai KC, Chen KC. Improved time integration for pseudo dynamic tests. J Earthq Eng Struct Dyn 1998;27:711–30.
[31] Lopez-Almansa F, Harbat AH, Rodellar J. SSP algorithm for linear and nonlinear dynamic response simulation. Int J Numer Methods Eng 1988;26:2687–706.
[32] Lax PD, Richtmyer RD. Survey of the stability of finite difference equations. Commun Pure Appl Math 1956;9:267–93.
[33] Nickell RE. On the stability of approximation operators in problems of structural dynamics. Int J Solids Struct 1971;7:301–19.
[34] Fox L, Goodwin ET. Some new methods for the numerical integration of ordinary differential equations. Proc Camb Philos Soc 1949;45:373–88.
[35] Wang YP, Lee CL, Yo TH. Modified state-space procedures for pseudo dynamic testing. J Earthq Eng Struct Dyn 2001;30:59–80.
[36] Zhang YF, Sause R, Ricles MJ, Naito JC. Modified predictor-corrector numerical scheme for real-time pseudo dynamic tests using state-space formulation. J Earthq Eng Struct Dyn 2005;34:271–88.
[37] Takanashi K, Udagawa K, Seki M, Okada T, Tanaka H. Seismic failure analysis of structures by computer pulsator on-line system. J Inst Ind Sci Univ Tokyo 1974;26(11):13–25.
[38] Tanaka H. A computer-actuator on-line system for non-linear earthquake response analysis of structures. J Inst Ind Sci Univ Tokyo 1975;27(12):15–9.
[39] Thewalt CR, Mahin SA. Hybrid solution techniques for generalized pseudo dynamic testing. Report No. UCB/EERC-87/09, Berkeley, CA: Earthquake Engineering Research Center, University of California; 1987.
[40] Shing PB, Vannan MT, Cater E. Implicit time integration for pseudo dynamic tests. J Earthq Eng Struct Dyn 1991;20:551–76.
[41] Dermitzarkis SN, Mahin SA. Development of substructuring techniques for online computer controlled seismic performance testing. Report No. UCB/EERC-85/04, Berkeley, CA: Earthquake Engineering Research Center; 1985.
[42] Nakashima M, Kaminosomo T, Ishida M, Ando K, Nakashima M, Kaminosomo T, et al. Integration techniques for substructuring pseudo dynamic test. In: Fourth U.S. national conference on earthquake engineering, vol. 2, Palm Springs, CA; 1990.

[43] Nakashima M, Akazawa T, Sakaguchi O. Integration method capable of controlling experimental error growth in substructure pseudo dynamic test. J Struct Constr Eng AIJ 1993;454:61–71.
[44] Bonelli A, Bursi OS. Generalized-alpha methods for seismic structural testing. J Earthq Eng Struct Dyn 2004;33:1067–102.
[45] Ghaboussi J, Yun GJ, Hashash YMA. A novel predictor-corrector algorithm for substructure pseudo dynamic testing. J Earthq Eng Struct Dyn 2006;35:453–76.
[46] Shing PB, Vannan MT. Implicit time integration for pseudo dynamic tests: convergence and energy dissipation. J Earthq Eng Struct Dyn 1991;20:809–19.
[47] Combescure D, Pegon P. Alpha operator splitting time integration technique for PSD testing error propagation analysis. Soil Dyn Earthq Eng 1997;16:427–44.

Chapter 4

The Online Hybrid Test Using Mixed Control

Chapter Outline

4.1 INTRODUCTION

The online test is in essence a test with displacement control. The displacements for the next time step are predicted and applied to the test structure; the reaction forces corresponding to the target displacements are measured and fed back to the equations of motion for the prediction of the next displacements. Displacement control, however, is not practicable when the test structure is too stiff to accurately control the loading actuator's displacement. We find, however, cases in which we wish to apply online tests to stiff structures. Suppose an online test

Development of Online Hybrid Testing. http://dx.doi.org/10.1016/B978-0-12-803378-4.00004-2

applied to a base-isolated building using the substructuring techniques in which only isolation devices, e.g., rubber bearings are tested. Because the axial forces exerted on rubber bearings (due to the combination of gravity, overturning moment caused by horizontal ground motion, and vertical vibration caused by vertical ground motion) significantly affect the horizontal restoring forces of the bearings, we obtain accurate horizontal restoring forces only by imposing the axial forces on the tested rubber bearings. Displacement-control for the vertical direction is not feasible because of very high stiffness in this direction, while conventional displacement-control can still apply flexible horizontal deformations. In such a case, combined control by displacement (for the flexible horizontal direction) and force (for the stiff vertical direction) is appealing. Another example is an online test to simulate the responses of a base-isolated structure subjected to vertical ground motions. Rubber bearings are very stiff as long as they sustain compression but become suddenly very flexible once they sustain tension. During the responses when the rubber bearings sustain compression, force-control is more practical, whereas displacement-control is a natural choice once they sustain tension. A similar situation occurs when we deal with an reinforced concrete column in which the horizontal restoring force behavior depends much on the axial force exerted, and the axial stiffness is very large as long as it sustains compression.

For these situations in which force-control is more feasible in the online test, this chapter introduces an online test that employs mixed control of displacement and force. Two types of mixed control are considered in the chapter. One, named "displacement-force combined control," is a control in which one jack is operated in displacement-control, while the other jack is operated in force-control. The other, named "displacement-force switching control," is a control in which one actuator is controlled by displacement sometimes and by force otherwise. In order to investigate their accuracy, a base-isolated building structure subjected to ground motions is analyzed by those two tests. The chapter consists of three sections. In the first section, the loading, measuring, and computation system developed for this study are presented. The second section describes the procedure of displacement-force combined control and demonstration tests applied to a base-isolated building structure. Finally, the third section describes the procedure of displacement-force switching control and demonstration tests applied to the same base-isolated building structure.

4.2 PRESENTATION OF THE ONLINE TEST SYSTEM

4.2.1 Loading System

The loading system shown in Fig. 4.1 was developed for the mixed control online test presented in the study. Primary hardware devices include: (1) two quasi-static loading jacks; (2) two hydraulic pump systems activated by an inverter motor, each of which supplies oil to one jack; (3) two load cells, each

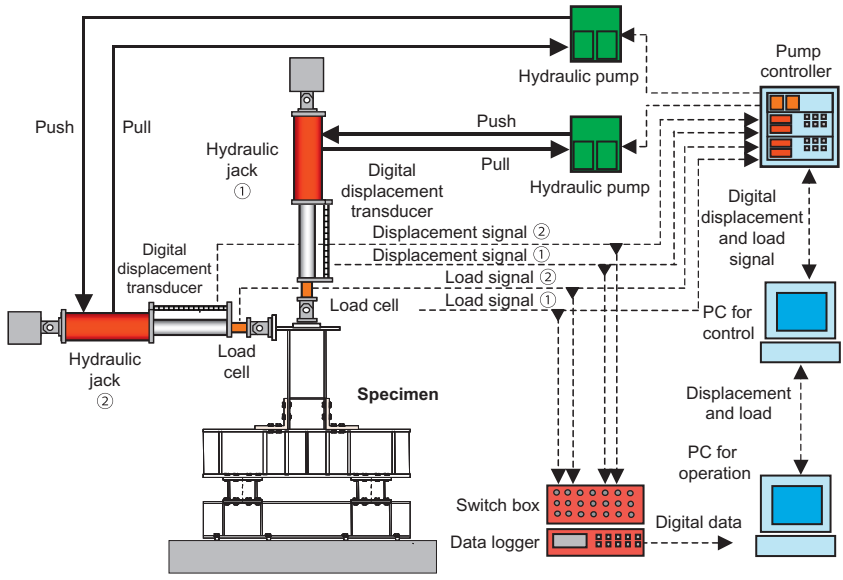

FIGURE 4.1 Outline of online test system.

of which measures the reactional force of one jack; (4) two digital displacement transducers, each of which measures the displacement of one jack; (5) two pump controllers that control the frequency of the inverter motor to adjust the jack's ram speed; (6) a switch box and data logger that collects strain gauge, linear variable differential transformer (LVDT), and other data; (7) a PC that controls the controllers, called "PC for Control"; and (8) a PC, called "PC for Operation," that supervises "PC for Control" and stores the data collected by the data logger. Specifications and major functions of the individual devices, as well as data transfers between those devices are detailed below.

Quasi-Static Jacks and Hydraulic Pump Systems

One of the two quasi-static jacks incorporated into the system has a stroke capacity of ±250 mm with a force capacity of ±1500 kN, and the other has a stroke capacity of ±200 mm with a force capacity of ±2000 kN. For the tests described later, the first and second jacks were used for horizontal and vertical loading, respectively. In order to measure the movement of the jack's cylinder, a digital displacement transducer is attached to the jack. Unlike conventional LVDTs in which the resolution decreases for a larger stroke, this digital displacement transducer maintains a resolution of 0.01 mm regardless of the total stroke. A load cell is inserted between the jack's cylinder and the swivel head to measure the force applied by the jack. The pump system provides oil to the jack. Unlike conventional hydraulic pumps, an inverter motor that can adjust its frequency (from 1 to 60 Hz) has been used, thereby making it possible to

control the rate of oil flow (0.01–0.48 l/min) and accordingly the jack's ram speed. For loading, the pump unit selects the chamber into which oil is to flow ("push" or "pull"). The chamber is selected using a solenoid valve, and the frequency of the motor is set in proportion to a voltage signal. Unloading is accomplished by releasing oil through a high-speed on/off valve (20 Hz). The frequency of this valve, i.e., the rate of oil release, is set also in proportion to a voltage signal to adjust the jack's ram speed during unloading. The jack's ram speed that can be adjusted in the system ranges from 0.02 to 2 mm/s.

Controllers

The controller, whose main tasks are accomplished with a 16-bit microprocessor, selects the direction of jack motion ("push" or "pull"), the frequency of the inverter motor during loading, the frequency of the valve during unloading, and changes between the loading and unloading modes. The controller can adopt either force- or displacement-control. Suppose that displacement control is chosen and the test structure is at rest. When a controller is given a new target displacement, together with the time set to reach this displacement, it computes the necessary displacement signals at every 10 ms time interval and starts the jack motion. After every 10 ms, the controller receives a displacement feedback signal from the digital transducer attached to the jack, computes the difference between the displacement assigned for 10 ms later and the current displacement, converts the difference to an analog voltage signal, and sends the signal to the pump system. This operation continues until the measured displacement reaches the target displacement within an allowable displacement error. When the operation is completed, the jack is held to maintain the current displacement. For the force-control mode, the operation remains the same except that the force (measured by the load cell) is taken as the feedback signal, and this signal is converted from analog to digital using a 12-bit A/D converter.

Combination of PC for Control and PC for Operation

"PC for Control" is connected to the two jack controllers via RS485 serial cables. It sends the target displacements or forces assigned for the two jacks and the time set for loading, both in digital form, to the controllers. During the loading, it receives the displacement and force values from the two controllers continuously (with a frequency of 5 Hz) and adjusts the loading by monitoring the deviation of the measured signals from the commanded signals. "PC for Operation" has two major functions: to trigger a data logger for data collection and store the data, and to create and send the displacement or force signals to "PC for Control." When the system is used for the online test, the associated equations of motion are solved in this PC. The data logger is a conventional one used for quasi-static loading tests, having a scanning speed of 1000 channels per second, connected to "PC for Operation" via a general-purpose interface bus cable. "PC for Operation" is also connected to "PC for Control" by an

RS232C serial cable for data exchange. As soon as one step of loading is completed, the controllers send a set of displacement and force values to "PC for Control," and "PC for Control" passes the values to "PC for Operation." Then "PC for Operation" sends a trigger signal to the data logger, asking for data collection. Upon receiving this signal, the data logger starts collecting and sending the data to "PC for Operation." Note that during this process, the jacks hold the structure at rest. "PC for Operation" creates and sends displacement or force signals to "PC for Control." A prototype system, developed for one jack operation, was used successfully in a series of online tests [1].

Characteristics of Mixed Control

The online test using mixed control needs both hardware and software support. The following three characteristics are the keys for realistic implementation of mixed control. First is the high-speed feedback mechanism of the controllers. In the displacement-force combined control, two jacks are operated simultaneously, one with displacement-control and the other with force-control. The movement of one jack interferes with the movement of the other jack. The high-speed feedback mechanism of the controllers, with a feedback frequency of 100 Hz, accomplishes tuned, proportional loading of the two jacks. The second characteristic is the use of quasi-static jacks. The maximum ram speed is at most 2 mm/s, which avoids uncontrollable flow of oil and eventual jack movement that may endanger the test operation. This slowness is particularly beneficial when the control mode is switched from displacement to force or from displacement to force in the displacement-force switching control. The third characteristic is the encapsulated framework adopted in the test system, which enables the programmer to focus on the mixed control algorithm without knowing all the hardware details. An ActiveX control [2], which is programmed in the C++ language by experts in hydraulics and control, is installed on "PC for Operation." It provides all the programming interfaces for hardware control. The programmers, who are not necessarily seasoned in hardware control, only need to work on "PC for Operation." Thanks to intensive encapsulation, communication between "PC for Operation" and "PC for Control" is minimized. The programmers working on mixed control algorithms in "PC for Operation" need to be concerned only with four commands that have been provided as four methods in the ActiveX control: "send displacement (or force) and time to PC for Control," "receive displacement and force from PC for Control," "switch displacement-control to force-control," and "switch force-control to displacement-control."

4.2.2 Base-Isolated Structure Model

The proposed loading system was used to simulate earthquake responses of a base-isolated structure subjected to horizontal and vertical ground motions.

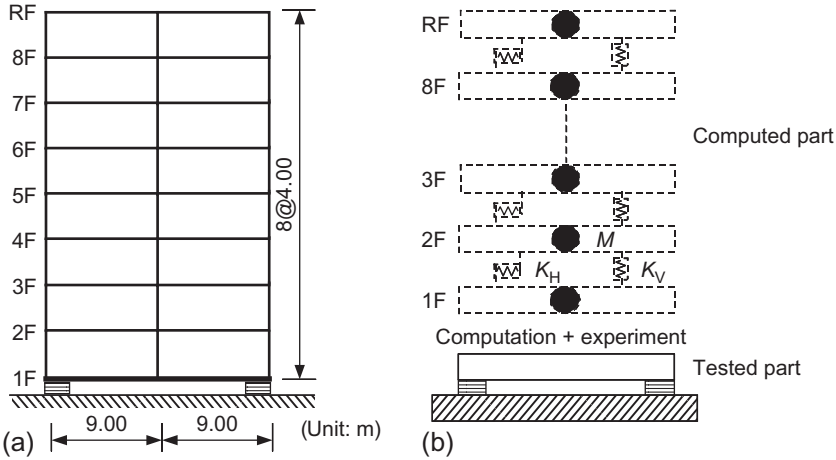

FIGURE 4.2 Base-isolated structure: (a) basic dimensions, (b) division into substructures.

The structure considered is shown in Fig. 4.2a, which resembles a base-isolated structure constructed recently in downtown Tokyo. It is an eight-story and two-span steel moment frame isolated by high damping rubber bearing (HDRB). This structure is also used to test the frameworks presented in the next chapters. In the analysis, it was treated as a planar structure as shown in Fig. 4.2a. The substructuring technique was employed, and the superstructure (the steel moment frame) and base-isolation layer (consisting of two HDRBs) were assigned as the computed part and the tested part, respectively. As shown in Fig. 4.2b, the superstructure was modeled as a linear spring-mass system, with one mass per floor and one horizontal spring and one vertical spring per story. The equations of motion were formulated for the entire base-isolated structure, represented as an 18 degrees of freedom (DOFs) system, with one horizontal and one vertical DOF added for the base-isolation layer. Table 4.1 shows the mass and stiffness properties assigned for the structure. The horizontal and vertical stiffnesses of the base-isolation layer were those corresponding to the yield horizontal stiffness and compressive stiffness of the HDRBs, respectively. The natural periods of the base-isolated structure are listed in Table 4.2.

4.2.3 Test Setup

The test setup, shown in Fig. 4.3a and b, includes the loading frame, two jacks (one for horizontal loading and the other for vertical loading), and the test specimen. The test specimen featured two identical HDRBs securely fastened by high-tension bolts to the base steel beam at the bottom and to an inverted T-shaped loading frame at the top. The base steel beam was tied down to the loading frame, and the inverted T-shaped loading frame was attached by the

TABLE 4.1 Mass and Stiffness Properties of Base-isolated Structure

	Mass ($\times 10^3$ kg)	Horizontal stiffness (kN/mm)	Vertical stiffness (kN/mm)
R	180	–	–
8	108	65.4	2170
7	108	72.0	2170
6	108	75.6	2310
5	108	77.8	2310
4	108	80.7	2310
3	108	86.8	2448
2	108	102	2971
1	108	148	2971
B	-	3.00	6702

TABLE 4.2 Natural Period of Base-isolated Structure(s)

	Horizontal		Vertical	
Model	*Base-fixed*	*Base-isolated*	*Superstructure*	*Entire structure*
Period(s)	1.26	3.76	0.24	0.25

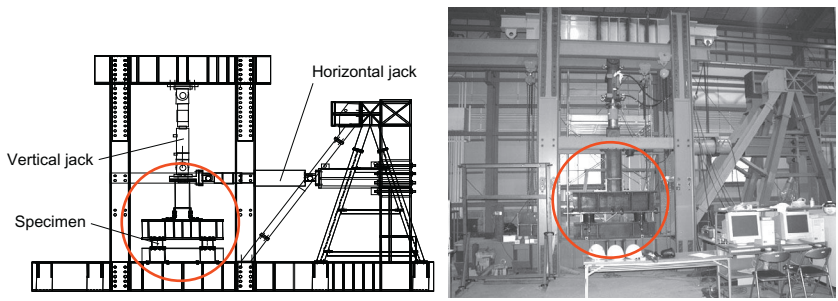

FIGURE 4.3 Test setup: (a) test specimen and loading frame, (b) view of test setup.

two jacks. The out-of-plane movement of the specimen was restricted at the top of the T-shaped loading frame where the two jacks were attached: hence the rubber bearings sustained horizontal and vertical deformations only in one plane. The two rubber bearings were placed 1.0 m apart in the center-to-center length, and the jacks were attached at a height of 1.5 m, measured from the bottom of the HDRBs to the top of the T-shaped loading frame (Fig. 4.4a). Figure 4.4a shows the measurement details. The digital displacement transducers and load cells of the two jacks, both attached at Point A, measures the horizontal displacement U_T, the horizontal reaction force F_H, the vertical displacement V_T, and the vertical reaction force F_V. The displacement transducers attached at Points B and C measure the vertical displacements of the rubber bearings V_L and V_R, and the displacement transducer attached at Point D measures the horizontal displacement of the base-isolation layer U_B. Figure 4.4b shows measurement details of the vertical displacement V_R at point C.

In reference to the vibration of the base-isolated structure shown in Fig. 4.2a, three independent loads should be controlled for the test specimen. They are the horizontal load, the vertical load, and the overturning moment, all applied to the base-isolation layer. Because the test system of Fig. 4.3 featured only two jacks, it was assumed that the overturning moment applied to the base-isolation layer was always proportional to the horizontal force applied to the layer. This assumption was commensurate with the assumption that the location of the center of horizontal forces applied to the superstructure would remain unchanged. This justified the loading system used in the test, in which both the horizontal force and overturning moment were applied by the horizontal jack through the inverted T-shaped loading frame. The T-shaped loading frame was designed to be sufficiently rigid with respect to the rubber bearings. Therefore, the vertical jack's displacement was taken to be the vertical displacement of the test

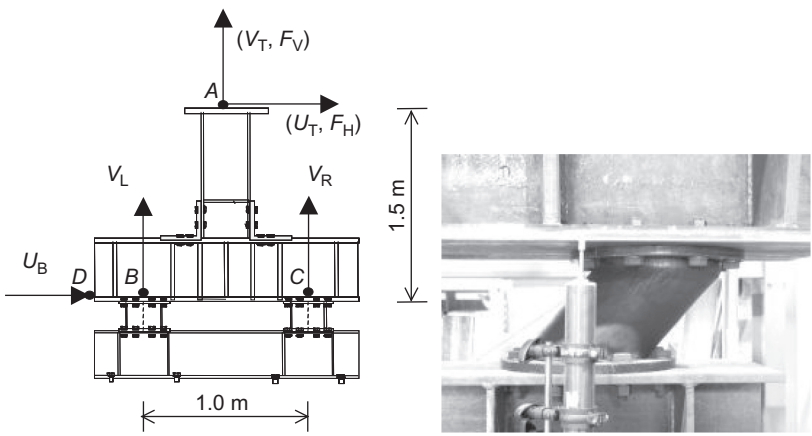

FIGURE 4.4 Measurement: (a) measured points, (b) example measurement.

specimen. The horizontal jack's displacement was taken to be the horizontal displacement of the test specimen. This was justified because the test specimen did not rotate due to the very large compressive stiffness of the tested HDRBs, as shown later.

The tested HDRBs had a diameter of 200 mm and a total rubber thickness of 85 mm. From comparison in the cross-sectional area, the total rubber thickness, the shape factors, rubber shear modulus between the prototype HDRBs and the tested HDRBs, scale ratios of 1:4 and 1:20 were adopted for the horizontal displacement and horizontal force, respectively. In other words, one-fourth of the base-isolation layer's displacement, predicted by solving the equations of motion of the base-isolated structure, was applied to the test specimen, and the horizontal force measured by the test specimen was increased by 20 times when inserted into the solution of the equations of motion.

4.3 DISPLACEMENT-FORCE COMBINED CONTROL

4.3.1 Static Test for Combined Control

Preliminary static tests were carried out to examine the horizontal restoring force characteristics of the tested HDRBs, in particular their dependency on vertical forces. Three types of loading (Types PA, PB, and PC shown in Fig. 4.5) were adopted. In Type PA, cyclic horizontal displacements with increasing amplitudes were applied in a triangular pattern by displacement-control (Fig. 4.5a), with a constant vertical load applied by force-control (Fig. 4.5b). The maximum amplitude was set at 150 mm, which corresponded to a 175% shear strain in the rubber, and the constant vertical load was set at 250 kN, which corresponded to a compressive stress of 4 MPa in each rubber bearing (to maintain the exact similitude between the prototype and test specimen, a compressive force of 500 kN was to be applied to the test HDRBs; however, because of the capacity of the loading frame, the compressive force applied

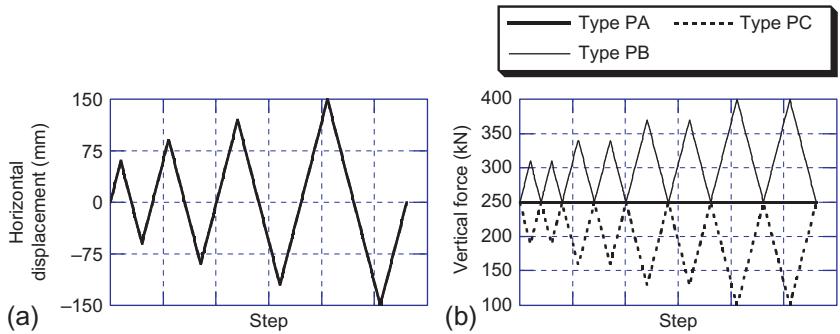

FIGURE 4.5 Types of loading in preliminary static test: (a) horizontal loading pattern, (b) vertical loading pattern.

in the test was reduced to half that required in the test). The loading patterns adopted for Types PB and PC were the same as that for Type PA for horizontal loading, but for vertical loading varying forces between 100 and 400 kN were employed. The varying forces were in-phase with the horizontal displacements in Type PB, but out-of-phase in Type PC. The horizontal force-displacement relationships are plotted in Fig. 4.6. The figure indicates the dependency of the horizontal hysteretic characteristics of the base-isolation layer on the magnitude of vertical load.

4.3.2 Algorithm of Online Test Using Displacement-Force Combined Control

In the proposed displacement-force combined control, displacement-control and force-control were adopted for the loading of the horizontal and vertical jacks, respectively. The integration method using the operator-splitting (OS) scheme [3,4] was employed for displacement-control. The concept of the method is to split the stiffness into a linear and a nonlinear stiffness. The explicit predictor-corrector method is employed for the integration associated with the nonlinear stiffness, whereas the unconditionally stable Newmark method is employed for the integration associated with the linear stiffness. The basic formulations are described as follows:

$$Ma_{n+1} + Cv_{n+1} + K^{\mathrm{I}} d_{n+1} + K^{\mathrm{E}}_{n+1} \widetilde{d}_{n+1} = P_{n+1} \tag{4.1}$$

$$\widetilde{d}_{n+1} = d_n + \Delta t v_n + \left(\Delta t^2/4\right) a_n \tag{4.2}$$

$$d_{n+1} = \widetilde{d}_{n+1} + \left(\Delta t^2/4\right) a_{n+1} \tag{4.3}$$

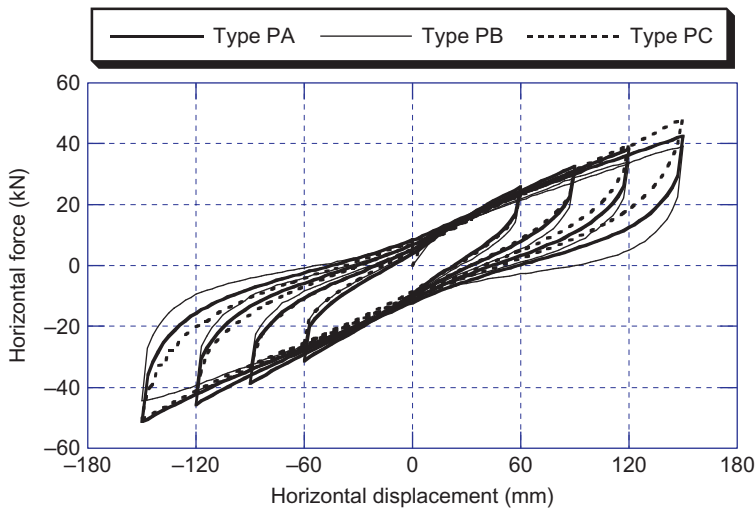

FIGURE 4.6 Horizontal force-displacement relationships for loading of Types PA, PB, and PC.

$$v_{n+1} = v_n + (\Delta t/2)(a_n + a_{n+1}) \tag{4.4}$$

In which, K^{I} and K^{E}_{n+1} are the linear and nonlinear stiffness matrices, M and C are the mass and viscous damping matrices, $\tilde{d}$ and d are the predictor and corrector displacement vectors, v and a are the velocity and acceleration vectors, and Δt is the integration time interval. The online test using the OS scheme ensures unconditional stability if the initial stiffness is taken as the linear stiffness and the nonlinearity is of softening type [4]. The procedure of implementation is as follows:

(1) Setup the equations of motion as shown in Equation (4.1).
(2) Set the initial stiffness matrix of the structure at K^{I} based on the preliminary static test.
(3) Apply the predictor displacement $\tilde{d}_{n+1}$ to the structure and measure the corresponding reaction force f_{n+1} (see Fig. 4.7a).
(4) Calculate $f_{n+1} - K^{\mathrm{I}}\tilde{d}_{n+1}$, substitute it into the term $K^{\mathrm{E}}_{n+1}\tilde{d}_{n+1}$, and calculate the corrector displacement d_{n+1}.

The algorithm when applied to force-control is also based on the OS scheme. In implementations of this algorithm, Steps (1) and (2) are identical with the procedure above, but in Step (3), the predictor-force $\tilde{f}_{n+1}$, which is taken to equal $K^{\mathrm{I}}\tilde{d}_{n+1}$, is applied to the structure (see Fig. 4.7b). Here, K^{I} is the elastic stiffness, and the structure is assumed to behave only elastically. Then the term $f_{n+1} - K^{\mathrm{I}}\tilde{d}_{n+1}$ in Step (4) becomes zero, and the procedure becomes identical to the unconditionally stable implicit Newmark method.

4.3.3 The Online Test Using Displacement-Force Combined Control

The responses of the base-isolated structure as shown in Fig. 4.2 were simulated by the online test using the displacement-force combined control. It was assumed that both the superstructure and base-isolation layer would respond

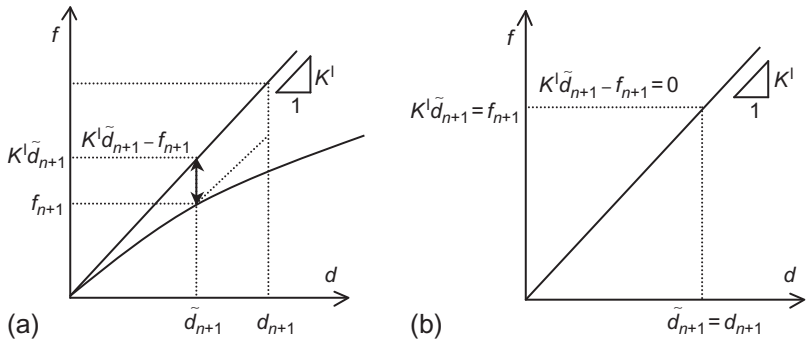

FIGURE 4.7 Outline of displacement-force combined control algorithm: (a) inelastic behavior for horizontal response, (b) elastic behavior for vertical response.

linearly in the vertical motion. Because of this assumption, the 9° in the horizontal direction and the other 9° in the vertical direction are uncoupled in the equations of motion. Nevertheless, interaction did exist between the horizontal and vertical responses. Effects of the vertical forces on the horizontal restoring force of the test specimen (i.e., the base-isolation layer) were automatically taken into account in the physical test. A ground motion recorded at the Japan Meteorological Agency (JMA) in the 1995 Hyogoken-Nanbu (Kobe) earthquake was chosen as the input ground motion [5]. The fault-normal and vertical components were adopted as the horizontal and vertical excitations, respectively. Their pseudovelocity spectra corresponding to 5% critical damping are shown in Fig. 4.8. In the online tests described below, 15 s of the primary ground motion were chosen. The vertical ground motion did not cause tension in the bearings in the test.

For the purpose of comparison, two tests (Tests CA and CB) were carried out. In Test CA, the response when subjected to the horizontal ground motion only was simulated. In Test CB, the response when subjected to the horizontal and vertical ground motions simultaneously was simulated. In both tests, vertical load corresponding to gravity (250 kN) was imposed at the beginning of the test. In both tests, the displacement-force combined-control was implemented successfully. Figure 4.9a and b shows target (by a short thin line) and measured (by a thick line) horizontal displacements and vertical forces, respectively. Note that only the first 5 s are presented in order to show the differences clearly. The two curves are nearly identical, indicating that, although the horizontal and vertical jacks interacted with each other, both displacement and force were controlled accurately. The time history of the horizontal displacement of the test specimen, measured by the horizontal digital transducer at Point D (Fig. 4.4a), is also plotted by the dashed line (designated as "Bottom") in Fig. 4.9a. The time history is very close to the time history of the horizontal displacement at the loading point (designated as "Top"), indicating that the vertical (compressive) stiffness of the test specimen was large enough so that the rotation of the test specimen was negligible.

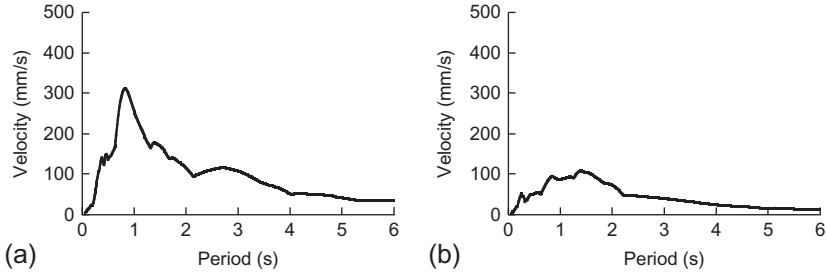

FIGURE 4.8 Pseudo velocity spectra of JMA ground motion: (a) fault-normal component, (b) vertical component.

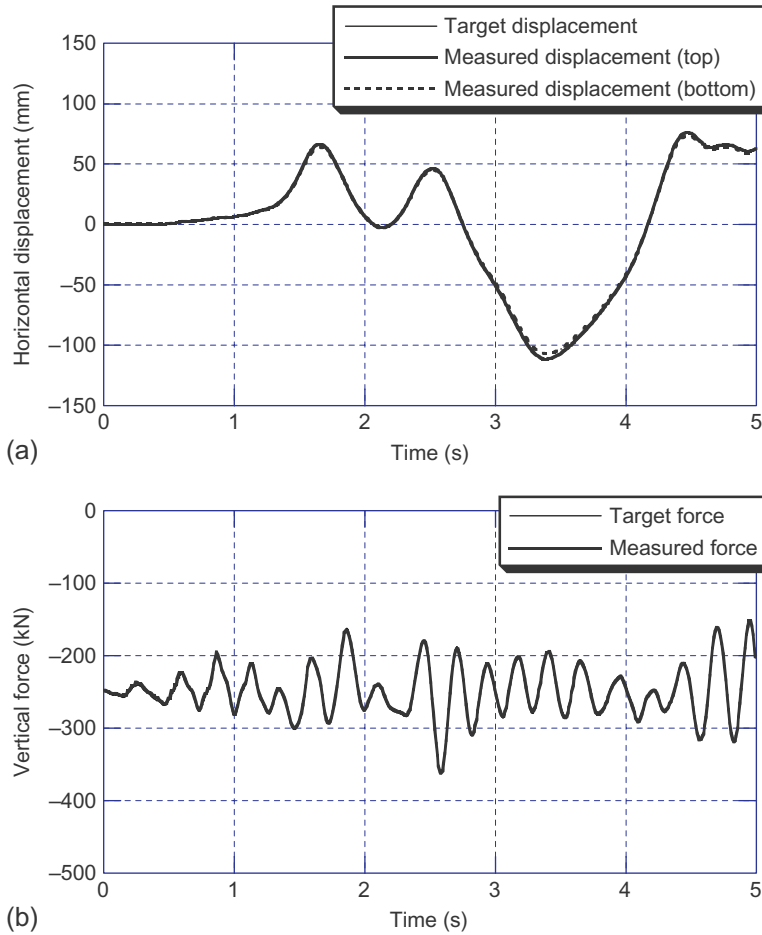

FIGURE 4.9 Comparison between target and measured values for Test CB: (a) displacement, (b) force.

The force-displacement relationships and displacement time histories are shown in Fig. 4.10a and b, respectively. In the figures, the thin and thick solid lines represent Tests CA and CB. Behavior of the test specimen for Test CB, in which both the horizontal and vertical ground motions were applied simultaneously, is significantly more complicated than the behavior for Test A. In Fig. 4.10a, the horizontal stiffness of the test specimen fluctuates in tune with the variation of the axial force. As a result, the displacement time history of the base-isolation layer is somewhat different, with a difference of the maximum displacement of about 15% between Tests CA and CB. The responses of the base-isolated structure were also analyzed numerically and are shown by a dashed line in Fig. 4.10. A modified bilinear model [6] was used to represent

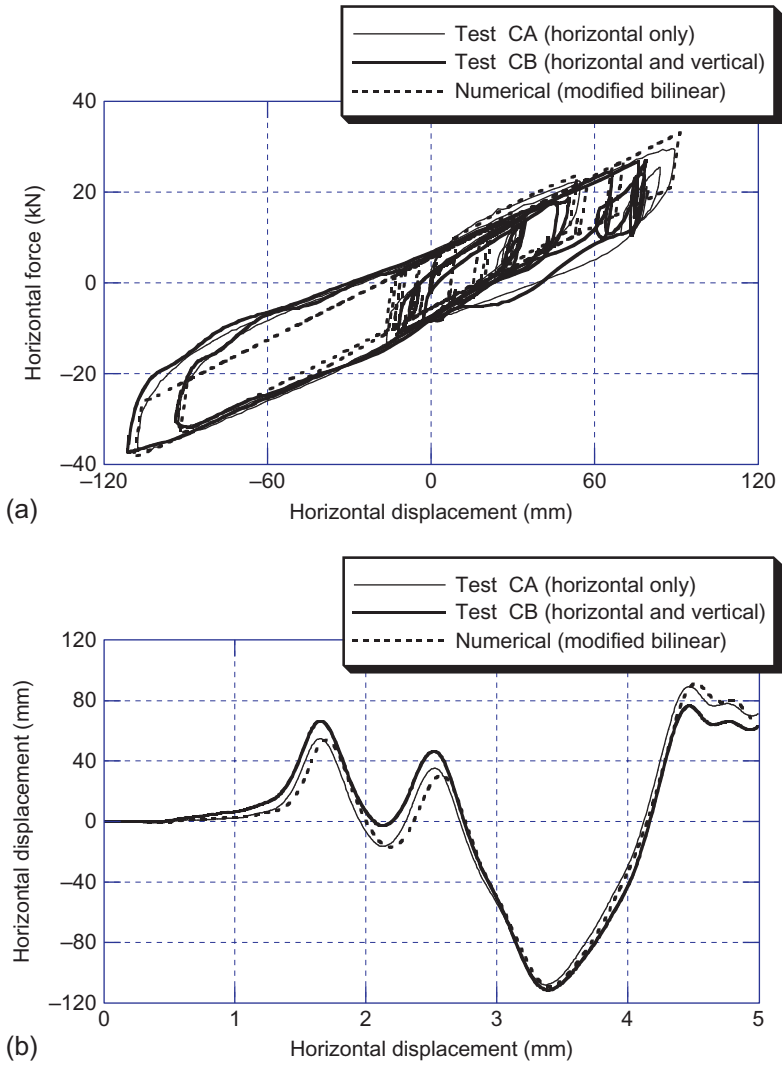

FIGURE 4.10 Responses obtained by online tests and numerical simulation: (a) hysteresis curves, (b) displacement time histories.

the hysteretic behavior of the HDRBs. The modified bilinear model is widely used in Japanese design to represent the nonlinearity and strain-hardening behavior of the horizontal hysteresis behavior of high-damping and lead rubber bearings. The difference with respect to the common bilinear model is that the main parameters, i.e., initial stiffness, post-elastic stiffness, and yield force, are not constant, but depend primarily on the maximum shear strain experienced in the loading history. The response obtained from the numerical analysis is close

TABLE 4.3 Comparison Between Models NA, NB, and NC

Model		NA	NB	NC
Natural period (s)	1st	0.25000	0.25330	0.24810
	2nd	0.08566	0.08695	0.08489
Maximum force (MN)		12.2860	12.2920	12.0350

to that of Test CA, in which the constant vertical load (corresponding to gravity) was applied, but the numerical analysis failed to trace the fluctuation of horizontal hysteresis due to varying axial load.

The vertical force-displacement relationship of the base-isolation layer was assumed to be linear-elastic. This would create errors, because (1) the assumed vertical stiffness may be different from the true stiffness; and (2) the vertical stiffness varies with the horizontal displacement. Three numerical models (Models NA, NB, and NC) were compared, to investigate the errors possibly caused by the difference between the assumed and true vertical stiffness. Model NA was the same as the base-isolated structure used in the test (Fig. 4.2 and Table 4.1). Models NB and NC were identical with Model NA for the superstructures but different in the rubber bearings. As compared with Model NA, the vertical stiffness of the base-isolation was reduced to 50% for Model NB, whereas it was increased to 200% for Model NC. Modal analysis and time history analysis (using the vertical component of JMA) were carried out for the three models, and the obtained natural periods in the vertical direction and maximum vertical axial forces exerted on the base-isolation layer are shown in Table 4.3. The natural period is almost the same for all three models, with a difference not greater than 2%. The maximum axial forces are also similar among the three models, with a maximum difference of about 2%. This observation suggests that vertical forces would change little with respect to the deviation of the base-isolation layer's vertical stiffness. This is understandable in the analogy of "rigid element" used for obtaining the reactional forces in finite element programs. As long as the rigid element is significantly stiffer than the rest of the structure, the force applied to the rigid element, given as the product of the stiffness and displacement, remains unchanged even if the stiffness values are different.

4.4 FORCE-DISPLACEMENT SWITCHING CONTROL

4.4.1 Static Test for Displacement-Force Switching Control

This section presents another form of mixed control, in which displacement-control is adopted when the stiffness is low and there is a switch to force-control

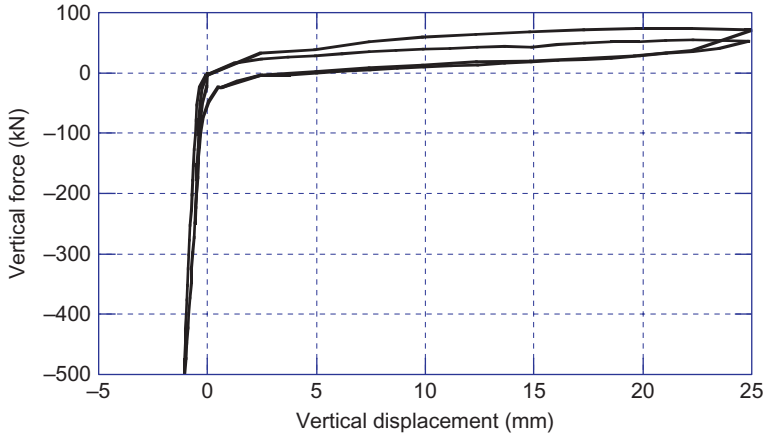

FIGURE 4.11 Vertical force-displacement relationship.

when the stiffness becomes higher. To demonstrate this control, online tests were carried out for the simulation of responses of the base-isolated structure (Fig. 4.2a) when subjected to vertical ground motion. Preliminary static tests were carried out to examine the test specimen's behavior under vertical loads. The loading program adopted was as follows. A compressive vertical load was applied monotonically to a force of 500 kN, and then it was unloaded to zero. Next, tensile vertical load was applied to a vertical elongation of 25 mm (corresponding to about a 30% tensile strain in the rubber), and unloaded again. This loading was repeated twice. The vertical forced-displacement relationships obtained are plotted in Fig. 4.11. As shown in Fig. 4.11, the vertical stiffness differs notably between compression and tension, with a compressive stiffness about 60 times larger than the tensile stiffness. The strength in tension was very small, exhibiting a small yield force and a large plastic deformation afterward. This significant difference in stiffness was the reason that switching control was developed.

4.4.2 Algorithm of Displacement-Force Switching Control

In the displacement-force switching control devised in this study, one jack was force-controlled when the test specimen (HDRBs) sustained compression, and displacement-controlled when it sustained tension. As in the displacement-force combined control, the OS scheme was used for direct integration. During the force-control segment, the force equal to the product of the predicted displacement and the assumed vertical stiffness was applied to the tested structure, while the conventional displacement-control was employed during the displacement-control. The control mode was switched when the sign of the force changed from compression to tension or from tension to compression. The integration algorithm for computation is as follows:

(1) Set the initial stiffness based on preliminary compression test, and set control-mode at force-control.
(2) Apply a compressive force corresponding to gravity to the test specimen and measure the corresponding displacement, which is set to be the initial displacement.
(3) Compute the predictor displacement $\widetilde{d}_{n+1}$.
(4) Compute the predictor force $\widetilde{f}_{n+1}$ by $K^1\widetilde{d}_{n+1}$.
(5) Select a control mode. If $\widetilde{f}_{n+1}$ is negative, the test specimen is taken to sustain compression, and force-control is adopted. If $\widetilde{f}_{n+1}$ is positive, the test specimen is taken to sustain tension, and displacement-control is adopted.
(6) Load the specimen. In force-control, apply the computed load to the structure, substitute zero into the term $K^{\mathrm{E}}_{n+1}\widetilde{d}_{n+1}$ (Equation 4.1). In displacement-control, apply the predicted displacement, measure the reactional force f_{n+1}, compute $f_{n+1}-K^1\widetilde{d}_{n+1}$, substitute it into the term $K^{\mathrm{E}}_{n+1}\widetilde{d}_{n+1}$ (Equation 4.1), and compute the corrector displacement d_{n+1}.

Figure 4.12a shows the details of switching the control mode from force to displacement. In Step n, the test specimen, sustaining compression, is led to Point A by force-control. The predictor displacement computed for Step $n+1$ is positive. Then control mode is switched from force to displacement, and the test specimen is led to Point B. The corresponding force is measured and used for computation in the following step. Figure 4.12b shows the details of switching the control mode from displacement to force. In Step n, the test specimen, sustaining tension, is led to Point A by displacement-control. The predictor displacement computed for Step $n+1$ is negative, and the control mode is switched to force-control. The test specimen is led to Point B whose force equals $K^1\widetilde{d}_{n+1}$. As shown in Fig. 4.12b, direct loading from Points A to B may create a large imbalanced energy in the computation. To avoid this, varying time integration was adopted for the step when the control-mode is switched from displacement to force as shown (Fig. 4.12c). If the (negative) predictor displacement is larger than a tolerance displacement d_c, the integration time interval is reduced to 0.9 Δt, and the corresponding predictor displacement is estimated again. This procedure is repeated by reducing the integration time interval to $0.9^2\ \Delta t$, $0.9^3\ \Delta t$,

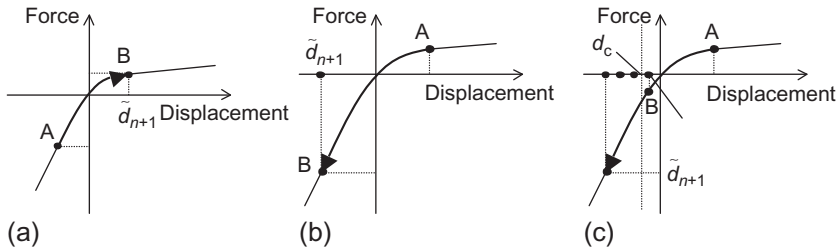

FIGURE 4.12 Implementation of displacement-force switching control: (a) switching from force to displacement, (b) switching from displacement to force, (c) varying time integration.

etc., until the predictor displacement becomes smaller than the tolerance displacement. Then, the control-mode is switched to force at point A (Fig. 4.12c), and the specimen is led to the predictor force, which is estimated as the product of the assumed stiffness and predictor displacement. The force-control mode is adopted for the succeeding steps.

4.4.3 Online Test Using Displacement-Force Switching Control

Using the proposed switching control, two online tests (Tests SA and SB) were applied for the simulation of the base-isolated structure (Fig. 4.2), when subjected to vertical motion. The vertical component of the JMA record (Fig. 4.8) was adopted, and 10 s of the time history including large accelerations were chosen for simulation. In Test SA, an initial compressive force of 250 kN was applied on the specimen to simulate gravity of the superstructure, and the online test was performed. In Test SB, an initial compressive force of 50 kN (instead of 250 kN) was imposed, and the online test was performed. Because of the smaller initial compressive force, the tested HDRBs sustained significant tensile deformations in Test SB, while no tension occurred in Test SA.

Figure 4.13a and b shows the vertical displacement and force time histories obtained from Test SB. To demonstrate the control accuracy, 1 s of time histories involving large responses is presented. The difference between the predicted and measured values is very small, with the maximum difference, at most, 0.5% of the largest displacement for displacement-control and 2% of the largest force for force-control. This demonstrates that the proposed system ensured accurate control even when many rounds of switching between displacement- and force-control took place during the test.

Figure 4.14a compares the hysteresis curves obtained from Tests SA and SB. The dashed line represents the results of Test SA where no tension occurred, and the solid line the results of Test B where tension occurred. For purposes of comparison, force values obtained for Test SA are shifted by 200 kN. Since no tension occurred in Test SA, the corresponding displacement-force relationship is linear, while significant plastic deformations occur a few times in Test SB. Figure 4.14b shows the time histories (between 5 and 6 s) of the vertical force. In Test SA without tension, it vibrates smoothly with a response period of about 0.25 s, which corresponds to the first natural period of the base-isolated structure in the vertical direction. In Test SB, the tensile force does not grow because of yielding in tension. Rather high-frequency vibration is also notable during the response in compression. This is attributed to bumping that occurred at the instant when the test specimen (base-isolation layer) started taking compression. It is analogous to the situation in which the superstructure leaps upward (because the tensile stiffness of the base-isolation layer is very small), falls down and bumps into the ground (because the compressive stiffness of the base-isolation layer is very large). This bumping effect caused large vertical accelerations in the first floor, located immediately above the base-isolators.

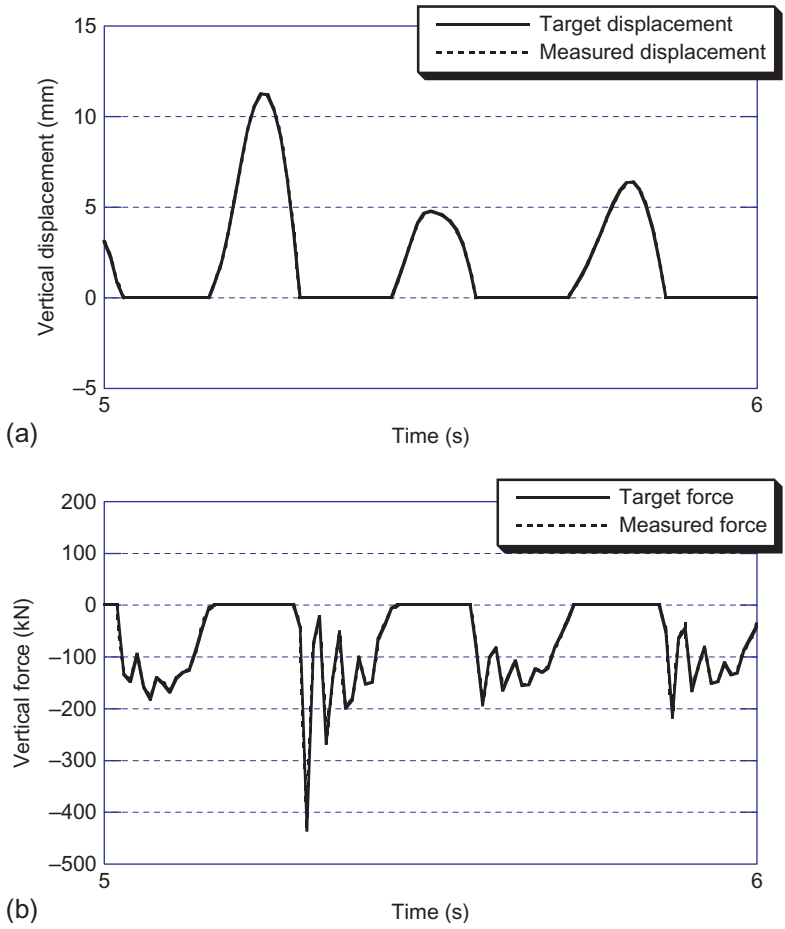

FIGURE 4.13 Comparison between target and measured values for Test SB: (a) displacement, (b) force.

4.5 CONCLUSIONS

The online test is in essence a test with displacement-control. The displacement control for stiff members, however, is not an easy task. To expand the capacity of the online test, a displacement-force mixed control technique is devised. The test system consisted of quasi-static jacks, digital-displacement transducers, hydraulic pumps, controllers, PCs for control, signal generation, and data storage, and a data acquisition unit. Two types of mixed control are considered. One is called "combined control," in which one jack is force-controlled and the other is displacement-controlled, with fine tuning of motion of the two jacks; and the other is called "switching control," in which one jack is operated by displacement-control but switched to force-control upon request. The proposed

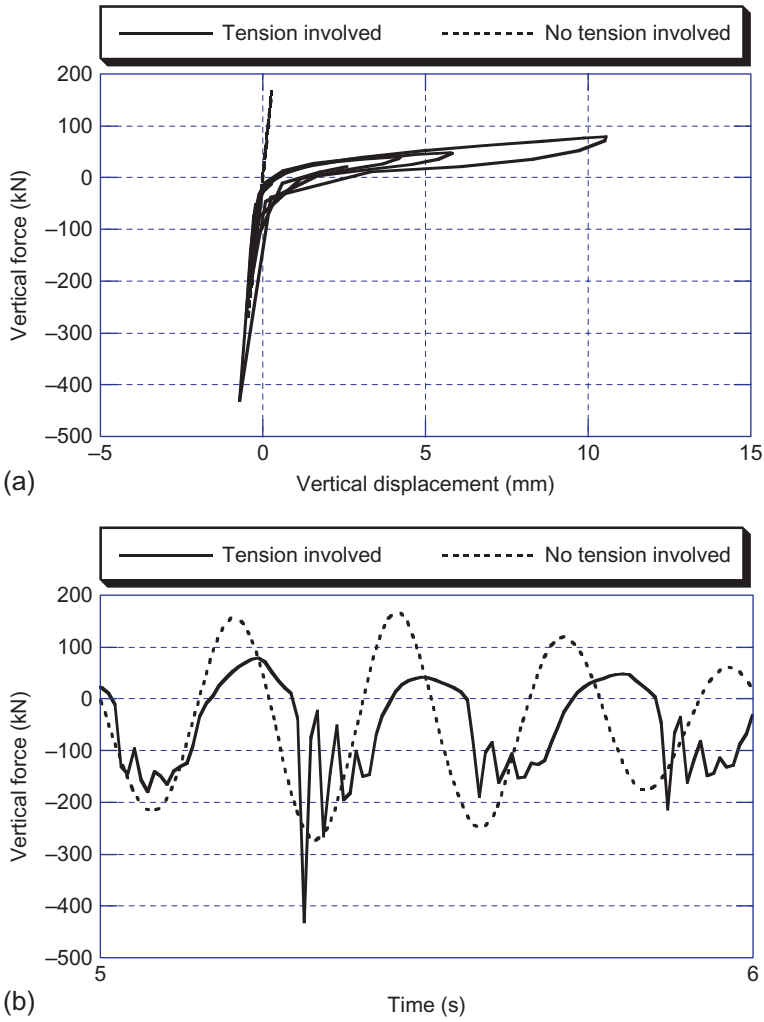

FIGURE 4.14 Responses obtained by online tests with switching control: (a) hysteresis curves, (b) force time histories.

mixed control technique was used to simulate earthquake responses of an eight-story base-isolated structure. The superstructure and base-isolation layer were assigned as the computed part and tested part, respectively. The superstructure was treated as a mass-spring system, with one mass per floor and one horizontal and one vertical spring per story.

"Combined control" was applied to simulate the earthquake responses of the base-isolated structure when subjected to both horizontal and vertical ground motions. A horizontal jack was used to impose lateral displacement of the

base-isolation layer (displacement-controlled), and a vertical jack was used to impose axial forces on the layer (force-controlled). The force applied was given as the product of the assumed stiffness and the vertical displacement (estimated by the direct integration of the associated equations of motion). In consideration of rather strong dependency of the horizontal stiffness of the base-isolation layer on the vertical stresses imposed on the layer, application of varying axial forces in tune with the horizontal deformations is justified. The online test with the proposed mixed control was successful, with accurate displacement and force control achieved for both jacks.

"Switching control" was applied to simulate the earthquake responses of the base-isolated structure when subjected to large vertical motions and hence involving tension in base-isolation layer. To consider significant differences in stiffness when the layer takes compression and tension, force-control (similar to the one used in combined mixed control) was adopted when taking compression and switched to displacement-control once taking tension. Switching from force to displacement or vice versa was satisfactory particularly when adopting time-varying integration to specify the precise switching point.

REFERENCES

[1] Nakashima M, Akazawa T, Igarashi H. Pseudo dynamic testing using conventional testing devices. J Earthq Eng Struct Dyn 1995;24(10):1409–22.

[2] Kruglinski D, Wingo S, Shepherd G. Programming visual C++. 5th ed. Microsoft Press, US; 1998.

[3] Hughes TJR, Pister KS, Taylor RL. Implicit-explicit finite elements in nonlinear transient analysis. Comput Methods Appl Mech Eng 1979;17/18:159–82.

[4] Nakashima M, Kaminosono T, Ishida M, Ando K. Integration techniques for substructure pseudo dynamic test. In: 4th US national conference on earthquake engineering, Palm Springs, CA, May; 1990.

[5] Nakashima M, Matsumiya T, Asano K. Comparison in earthquake responses of steel moment frames subjected to near-fault strong motions recorded in Japan, Taiwan, and the U.S. In: International workshop on annual commemoration of Chi-Chi earthquake, Taipei, Taiwan, September 18-20; 2000. p. 112–23.

[6] Miyazaki M. Current of isolated buildings in Japan after 1995 Kobe earthquake. In: International post-SMiRT conference seminar on seismic isolation, passive energy dissipation and active control of seismic vibration of structures, Taormina, Italy, August; 1997.

Chapter 5

An Internet Online Hybrid Test Using Host-Station Framework

Chapter Outline

5.1 INTRODUCTION

Among various advantages of the online test over the shaking table test, known to be the most direct experimental technique for the simulation of earthquake responses, the online test's capacity to combine itself with substructuring techniques is very appealing [1,2]. In the substructure online test, part of the structure whose restoring force behavior is too complex to model is tested, while the rest of the structure is modeled in the computer, and the equations of motion that represent the entire structure are solved. The substructure online test naturally leads to a path of tests on a larger scale.

The substructure online test has already been applied by many researchers, with notable applications in the early development stage [3–5] (see also, Chapter 4). In all previous substructure online tests, the analytical part was modeled into rather small degrees-of-freedom (DOF), and the equations of motion

Development of Online Hybrid Testing. http://dx.doi.org/10.1016/B978-0-12-803378-4.00005-4

of the entire structure (including the tested and computed parts) were developed by the researchers themselves and solved in the computers that ran the test. To increase the accuracy for the behavior of the computed part, it is always appealing to use a finite element method (FEM) type of program that has been developed for numerical analysis. Difficulties do exist, however, because such a program is commonly formulated in an incremental form (to allow for various nonlinearities) and adopts implicit integration algorithms (to ensure unconditional stability). On the other hand, an explicit method is used, and the equations of motion are solved for the overall quantities, instead of incremental quantities in the online test, because iterative solutions are not acceptable in the online test that involves physical testing. These dilemmas, i.e., implicit versus explicit and incremental versus overall, should be resolved if a FEM type of program is used in the substructure online test.

Considering the online communication between the test and computation in the online test, it is not necessary to conduct the test and computation at the same location. Because of the very fast data communication over the Internet, it is practicable to conduct tests and analyses in multiple locations, exchange necessary data among them, and simulate the earthquake response of a very large structural system. The concept of "Internet testing" or "distributed testing" has been addressed over the past few years [6–9], and a few real applications have been reported [10–12]. The concept is very promising, in that it will increase the capacity of the substructure online test significantly, but there is a problem to be resolved for the versatile application of this concept. That is, the data exchange over the Internet should be handy, stable, secure, and robust. Some troubles may be tolerable if only numerical analyses are carried out, because the analyses can be restarted in the worst case; but in the online test that involves physical testing, the test structure would not be able to recover the intact properties once loaded. Security across the Internet is becoming very strict, which makes it very difficult to exchange data securely without delay. Some special procedures for data exchange may be developed for Internet testing, but esoteric procedures are difficult to share with the majority of researchers engaged in earthquake engineering.

This chapter presents challenges to the two issues addressed above, i.e., the substructure online test combined with a FEM type of program, and the Internet testing. This chapter consists of three sections. First, a data exchange interface with host and stations is devised for the Internet test system with the tests conducted in geographically distributed locations. A practical method that utilizes standard protocols implemented by operating systems for sharing files and folders, a generic data format to standardize the communication, and a data exchange algorithm fit for physical tests are adopted. Second, a procedure is developed in which the tangent stiffness of the tested part is estimated based on a few steps of previously obtained data. Errors associated with the prediction are suppressed by compensation in the following step. Third, the proposed system is applied to a base-isolated structure, in which the base-isolation layer is

tested and the superstructure is modeled by a FEM program, and the applicability and effectiveness of the proposed system is calibrated.

5.2 PRESENTATION OF THE INTERNET ONLINE TEST SYSTEM

5.2.1 System Framework

The framework of the proposed Internet online test system is illustrated in Fig. 5.1. The system consists of the host, stations, and data exchange interfaces. The simulated structure is divided into computed parts and tested parts, by the use of substructuring techniques. The host analyzes the computed parts, collects information from the stations, and simulates the response of the entire structure. Each station performs a physical test in accordance with the (displacement) command transferred from the host, and creates information on the behavior of each substructure. The data exchange interfaces are in charge of communication between the host and the stations. A base-isolated structure equipped with isolators and a damper is used as a specific example in Fig. 5.1. The entire structure is divided into the superstructure, two isolators, and the damper. The superstructure, which is a conventional steel moment frame, is analyzed numerically in the host. The two isolators and the damper, whose restoring force behavior is complicated, are tested in three stations. The host and the three stations are geographically distributed, but they do the test collaboratively by carefully exchanging data. The data exchange is implemented through the data exchange interfaces, a standard platform for communication between the host and all the stations. Details about the data exchange interface are given below.

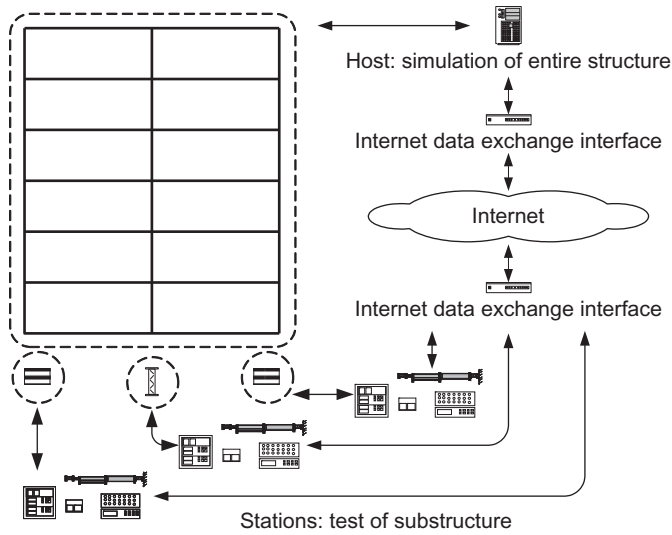

FIGURE 5.1 System framework.

The equations of motion for the entire structure are formulated in the host. A general finite element program adopting an implicit integration scheme is used for the analysis of the computed part. This is different from many previous applications, in which the program that solved the associated equations of motions was developed by researchers themselves and adopted an explicit integration scheme to conform to the principle of the online test. To accommodate an implicit scheme with the online test, this study adopted a method in which the tangent stiffnesses of the tested substructures are estimated after each loading step. Details of the method to estimate the tangent stiffness will be explicated in Section 5.3. The procedure to implement the system is shown schematically in Fig. 5.2. The initial stiffness matrix $[K_m]$ is established, and the initial force vector $\{F_m\}$ is assigned for the substructure located in each station. The stiffness matrices and the force vectors of all stations are sent to the host over the Internet and transformed from the respective local coordinates to the global coordinate set for the analysis in the host. The initial global stiffness matrix $[K_G]$ (commonly equals the elastic stiffness matrix) and force vector $\{F_G\}$ (commonly

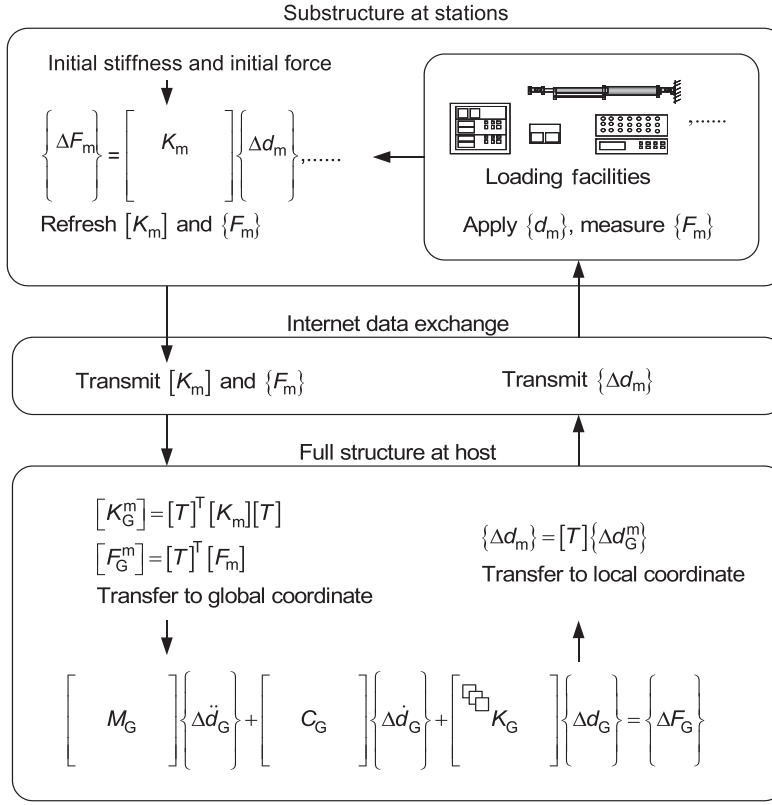

FIGURE 5.2 Implementation of substructure technique.

equal to a null vector) of the entire structure are constructed in the host, and initialization is completed. The global incremental displacement vector is calculated by solving the equations of motion of the entire system. The corresponding incremental displacement vectors assigned for the substructures are sent to all stations after the transformation from the global to local coordinates. Physical tests are to start in the stations, and the test specimens are loaded to the respective target displacements. Upon completion of loading, the reactional forces are measured, and the incremental stiffness is predicted for each substructure. The estimated substructure stiffness matrix $[K_m]$ and the measured substructure force vector $\{F_m\}$ are sent to the host over the Internet again, and the global stiffness matrix and force vector are refreshed. The procedure is repeated up to the end of the online test.

5.2.2 Internet Data Exchange Interface

The Internet online test system with the tests conducted in geographically distributed stations requires data exchange over the Internet. Although the data exchange interface could be in any form as long as it is communicable between the host and all stations, some characteristics are preferred. First is stability: unlike numerical analyses, in which everything can be restarted from the beginning if something does not function properly, a return to the initial stage is not practical when physical tests are involved. Hence, the data exchange interface should be stable enough to guarantee the tests without interruption. Second is security: if the data exchange interface is not secure, the Internet online test is susceptible to malfunctions. Third is convenience: researchers involved in the Internet online test are mostly structural engineers rather than software engineers. The interface has to be user-friendly enough to be mastered by these researchers without their spending too much time to learn about special techniques of the interface. A simple data exchange solution has been proposed by Tada and Kuwahara [13], and it was adopted for the Internet online test presented in this chapter.

Data Exchange Solution

In the proposed solution, a technique of sharing files and folders implemented by operating systems is utilized. The exchanged data are packed as temporary files, and the host and stations exchange data through the temporary files stored in the sharing directories. In principle, any protocol, i.e., smb, afp, ftp, and http, is acceptable for the Internet connection, but an appropriate protocol has to be selected according to the computer system and network environment. Figure 5.3a shows an example with one host and three stations. One host directory and three station directories are created in a server computer on the Internet. The host has "read and write" (RW) permissions in its own host directory, and has "read only" (RO) permission in all other station directories. Each station has

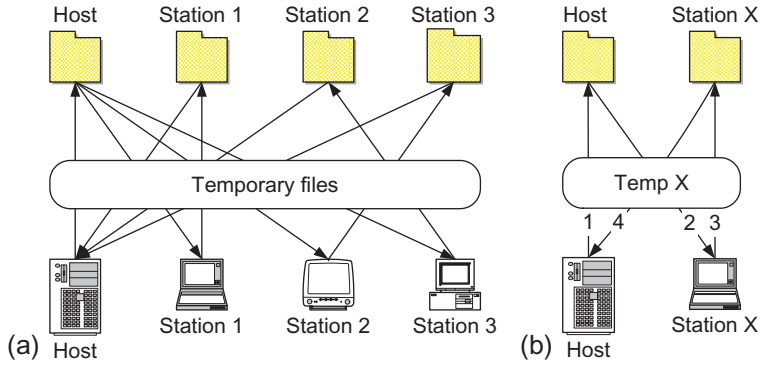

FIGURE 5.3 Data exchange interface: (a) one host and three stations, (b) one host and one station.

RW permission in its own station directory, RO permission in the host directory, and no permission to the other station directories. With reference to Fig. 5.3a, the host can RW files in the directory of "Host," and read files in the directories of "Stations 1, 2, and 3"; Station 1 (2 or 3) can RW files in the directory of "Station 1 (2 or 3)" and read files in the directory of "Host." Three sets of temporary files are created corresponding to the three pairs of communication between the host and the stations. Each set of temporary files includes a file created by the host in the directory of "Host," and a file created by a station in the directory of that station. Different temporary file names are adopted to avoid conflict in the directory of "Host."

Figure 5.3b describes details of communication between the host and one station. Suppose the host is named "Host," the station chosen is "Station X," and the temporary file name is designated as "Temp X." The procedure for one round of communication is as follows:

Host deletes "Temp X" and creates "Temp X" in the directory of "Host"
"Station X" reads "Temp X" in the directory of "Host"
"Station X" deletes "Temp X," and creates "Temp X" in the directory of "Station X"
"Host" reads "Temp X" in the directory of "Station X."

One round of data exchange is accomplished through the four steps above. It is notable that the procedure above follows a basic rule: "who creates and who deletes," which ensures Internet security.

To return to the Internet online test, the host creates a file to specify the commands (i.e., the next target displacements). All the stations keep monitoring the state of the host directory, and read the commands as soon as they become available. Physical tests are then conducted at the stations, and the files that include the results are created in the corresponding station directories. The host keeps querying the state of all the station directories, and reads the data from the station directories as soon as they become available.

Generic Data Format

The information to be exchanged varies with the type of tests. In order to standardize the Internet data exchange interface, a generic data format is adopted. The data formats are given in Tables 5.1 and 5.2 for "from host to station" and "from station to host," respectively, although they are rather similar in structure. The first line gives the type of communication, number of integer data, number of real data, and data exchange counter. The type of communication defines the content of the data package, i.e., "0" means that the data package is for initialization. The number of integer and the number of real data specify how many integer and real data should be read from this package. The data exchange counter is used to check whether the data package is updated. Let us suppose that the system has completed 800 steps and is waiting for the 801st step. If the data transferring counter remains at 800, the system recognizes that the data are not updated yet, and the system has to wait. Specific information, such as the load case, load step, stiffness, force, and so forth, are placed in the second and third lines.

Validation of Interface

In 2003, Tada et al. conducted an Internet analysis in Japan [13]. Ten organizations participated, 12 personal computers and 1 server computer were used, and a braced steel moment frame was analyzed. The 13 computers owned by the 10 organizations implemented the analysis collaboratively. The entire structure

TABLE 5.1 Generic Exchanged Data Format for Internet Online Test (Host to Station)

Row	Content	Interpretation
1st	Type of communication	0: Initialization 1: Loading 3: Checking 9: Completion
	Number of integer	Integer type data in the 2nd row
	Number of real	Real type data in the 3rd row
	Transferring counter	For checking whether the content is updated
2nd	Load case index	Load case
	Load step index	Load step
3rd	Time	For dynamic response analysis
	Incremental displacement	Incremental displacements corresponding to the boundary DOFs of substructures

TABLE 5.2 Generic Exchanged Data Format for Internet Online Test (Station to Host)

Row	Content	Interpretation
1st	Type of communication	100: Initialization 101: READY 103: UNREADY
	Number of integer	Integer type data in the 2nd row
	Number of real	Real type data in the 3rd row
	Transferring counter	For checking whether the content is updated
2nd	Null	No integer needed to be transferred
	Stiffness	Stiffness matrix of substructures after static condensation
3rd	Reactional force	Reactional forces corresponding to boundary DOFs of substructures
	Strain energy	Strain energies of substructures used to check energy balance

was divided into 13 substructures. Twelve substructures (beams and braces) were analyzed by the 12 personal computers. The server computer was in charge of the global analysis control. The data exchange interface adopted in this study was used in the analysis for Internet communication between the 12 personal computers and the server computer. The success of the analysis demonstrated that the proposed Internet data exchange interface is capable of exchanging data in a stable and robust manner between more than 10 computers across the Internet.

Data Exchange Algorithm

Multiple rounds of data exchange in the single load step were executed for the Internet online test. This cautious approach was adopted to ensure the secure transfer of data between the host and stations. In the numerical analysis domain, a single round of data exchange is commonly sufficient, and if unloading is detected in the analysis, the analysis only needs to return to the previous step and recalculate using the unloading stiffness. In the online test, such a return is not practical, because the test is conducted physically. Although multiple rounds of data exchange are more time-consuming, it is deemed worthwhile because a physically tested specimen is never able to return to the previous state once it sustains plastic deformations.

Figure 5.4 shows a flowchart of the proposed data exchange algorithm. In each load step, the host refreshes the global stiffness matrix and solves the

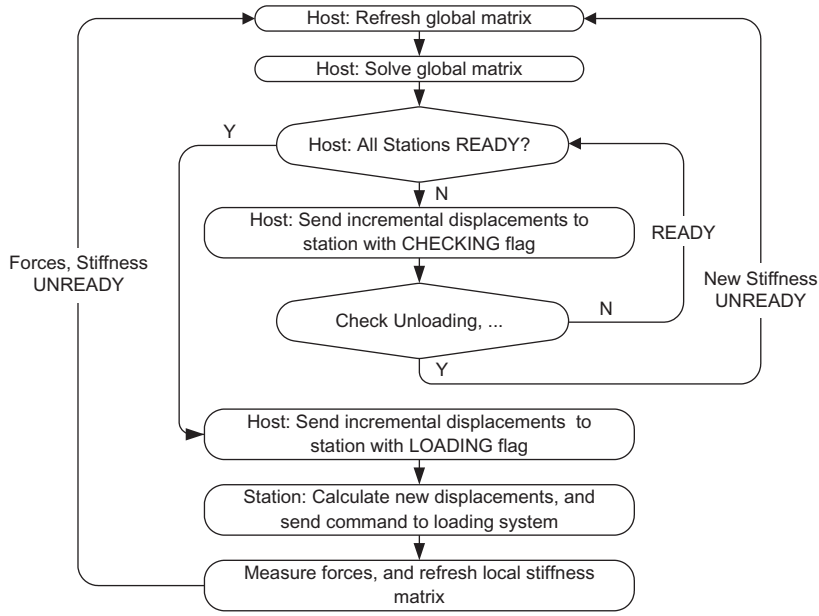

FIGURE 5.4 Flowchart of data exchange algorithm.

incremental displacements for the next step of the entire structure. Then the displacements specified to each substructure with a "CHECKING" flag are sent to the corresponding station. After receiving the command, the station checks the status of loading or unloading. If unloading occurs, a new stiffness with an "UNREADY" flag is returned to the host; otherwise a "READY" flag is returned to the host. The host checks the information from all the stations. If the station status is still "UNREADY," new incremental displacements are calculated and sent to all the stations once again with a "CHECKING" flag. The host repeats the procedure and sends the final incremental displacements to all the stations with a "LOADING" flag after all the stations return a "READY" flag to the host. The stations start to load only after receiving the command with a "LOADING" flag. After loading is completed, the measured forces and predicted stiffnesses are sent back to the host, and the stations are set at "UNREADY."

Practical Environment Using Interface

The practical Internet online environment shown in Fig. 5.5 was constructed between Osaka University and Kyoto University of Japan.

One host and one station were designated in Osaka University and Kyoto University, respectively. The tested structure was divided into a computed part and a tested part. The computed part is simulated numerically by the program

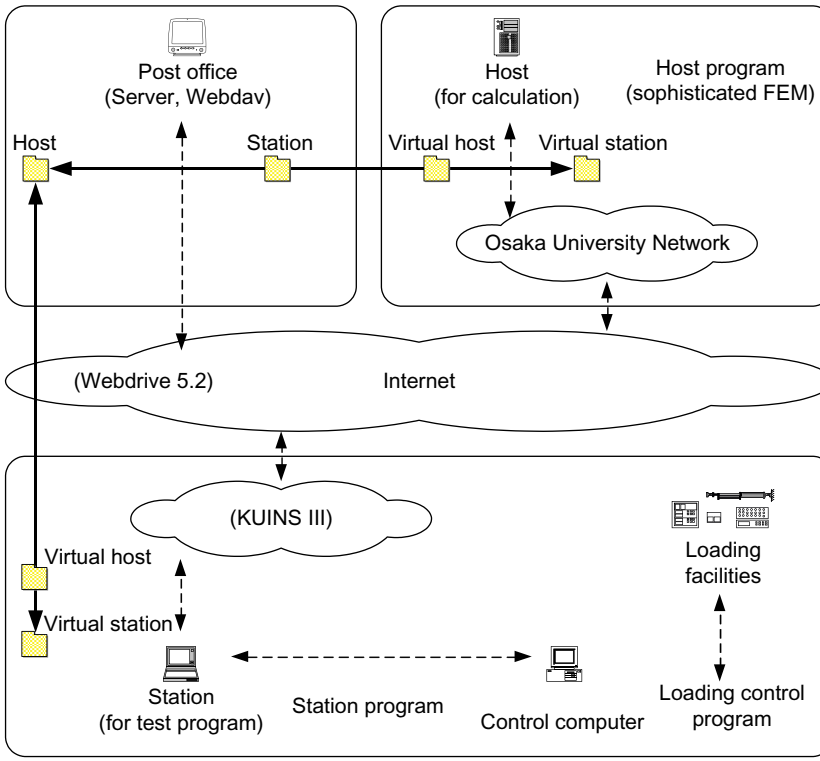

FIGURE 5.5 Proposed Internet online test system.

installed at the host station at Osaka University, which was connected to the Osaka University Network (ODINS). The physical test was carried out in Kyoto University. An Internet test program was developed for the control algorithm. The test program was run in the station computer connected to the Kyoto University Network (KUINS III). The station computer was also connected to a control computer that supervised and controlled the loading facilities such as jacks and controllers. In the test, the station computer sends commands to the control computer, and the control computer supervises the action of loading facilities. The loading system was used successfully for several online tests [14]. ODINS and KUINS III were connected to the Internet through LAN cables. Strict firewalls are set up in KUINS III, and direct "Point to Point" connections are prohibited between the computers within a local network and those outside, but some services like http, ftp, and socks are available through the proxy. In this study, the http protocol was used to connect the station computer and the server computer. The data exchange was implemented by a dynamic link library (DLL), which was used for all the computers that participated in the Internet online test. In order to simplify the implementation, a program

named "WebDrive" [15] was used in this study. "WebDrive" is able to map remote directories and files on the Internet to local directories and files. The function of passing across the firewalls through the proxy was also provided in the "WebDrive." Although only one host and one station were used in this study, the proposed interface is capable of performing the Internet online test with multiple stations.

5.3 ACCOMMODATION WITH IMPLICIT FINITE ELEMENT PROGRAM

5.3.1 Importance of Stiffness Prediction

Most finite element programs use implicit procedures for the time history analysis of structures. Material nonlinearities are commonly handled by iterations and/or incremental formulations. However, iterations are prohibitive in the online test, because it is impractical to make the test structure return to the previous position once loaded. Traditionally, the online test adopts an explicit integration with the equations of motion being formulated with respect to the overall (not incremental) quantities. If the substructure online test is combined with an existing finite element program, problems of "implicit versus explicit" and "overall versus incremental" shall be resolved. The approach adopted in this study was to estimate the tangent stiffness based on the experimental information acquired in the previous steps, compute the incremental displacements for the next step using an implicit algorithm, lead the test structure to the target displacements, and measure the corresponding reactional forces. An imbalance restoring force, arising as a result of the difference between the predicted and actual stiffnesses, was compensated in the next step as a pseudoexternal force.

5.3.2 Proposed Prediction Method

In this study, the physical substructure test was conducted for 1-DOF; hence the tangent stiffness to be estimated is a scalar. The stiffness cannot be estimated accurately by a simple division of the incremental force by the incremental displacement in the last two steps, because control and measurement errors exist in practical experiments. The proposed method employs linear fitting to smear the control and measurement errors. Details of the prediction procedure are as follows:

Using the least squares method, find the slope and intercept values of a linear function, $f(u)$, shown in Equation (5.1) that best represents the linear fit of n sets of the previous test data points $S_i(u_i, f_i)$. Here, u_i and f_i are the displacement and force in the ith step:

$$f(u) = \text{Slope} \times u + \text{Intercept} \tag{5.1}$$

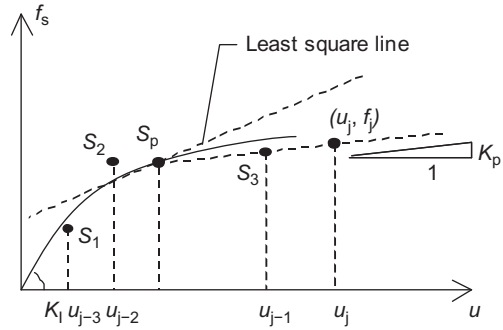

FIGURE 5.6 Proposed procedure of stiffness prediction using three sample data.

1. Find a new set of data (u_p, f_p) on the linear function shown in Equation (5.1):

$$u_p = \frac{\sum_{i=j-n}^{j-1} u_i}{n} \tag{5.2}$$

$$f_p = f(u_p) = \text{Slope} \times u_p + \text{Intercept} \tag{5.3}$$

2. Predict the force at u_j using a linear extrapolation based on two sets of data: (u_p, f_p) and (u_{j-1}, f_{j-1}):

$$f_j = f(u_j) = f_p \frac{u_j - u_p}{u_p - u_{j-1}} + f_{j-1} \frac{u_j - u_{j-1}}{u_{j-1} - u_p} \tag{5.4}$$

3. Calculate the predicted stiffness by:

$$K_P = \frac{f_P - f_{j-1}}{u_P - u_{j-1}} \tag{5.5}$$

An example is given in Fig. 5.6. S_1, S_2, and S_3 are the data of the previous three steps. A linear function was constructed using the least squares method based on S_1, S_2, and S_3, and the predictor data point S_p is constructed using Equations (5.2) and (5.3). The predictor stiffness is calculated based on the predictor data point S_p and the last sample data point S_3 using Equations (5.4) and (5.5).

5.4 INTERNET ONLINE TEST OF BASE-ISOLATED STRUCTURE

Online tests were carried out to examine the effectiveness of the proposed Internet online test system. Primary targets for verification included: (1) applicability of the system; (2) robustness of the Internet data exchange interface; and (3) efficiency of the stiffness prediction method.

5.4.1 Base-Isolated Structure Model

A base-isolated structure shown in Fig. 5.7a was adopted as the example structure. It was an eight-story, two-span steel moment frame isolated by rubber bearings and treated as a planar structure. As shown in Fig. 5.7b, the substructuring technique was employed in the test. The superstructure was modeled numerically, and the base-isolation layer was tested physically.

The superstructure was modeled by lumped masses, beam elements, and column elements. In the model, each beam was divided into six beam elements, and an associated lumped mass was assigned in each node. This discretization was adopted to trace the beam deflection more accurately. A finite element program code developed by Tada [13] was used as the host program for numerical simulation of the superstructure. A concentric plastic hinge was assigned at each end of the beam and column elements to allow for member plastification, and interaction between the axial force and moment was taken into account for yielding of the plastic hinges. Both the material and geometric nonlinearities were also taken into account. This model, having 315-DOFs, was deemed significantly more accurate than stick models (by story-to-story representation) conventionally adopted in many previous online tests. In this study, the base-isolation layer was taken to move only horizontally, with the assumption that the base-isolators were infinitely stiff in the vertical direction. Then, the DOF shared by the superstructure and the base-isolation layer was reduced to 1 (designated as Node *I* in Fig. 5.7b), i.e., the horizontal displacement and force of the base-isolation layer.

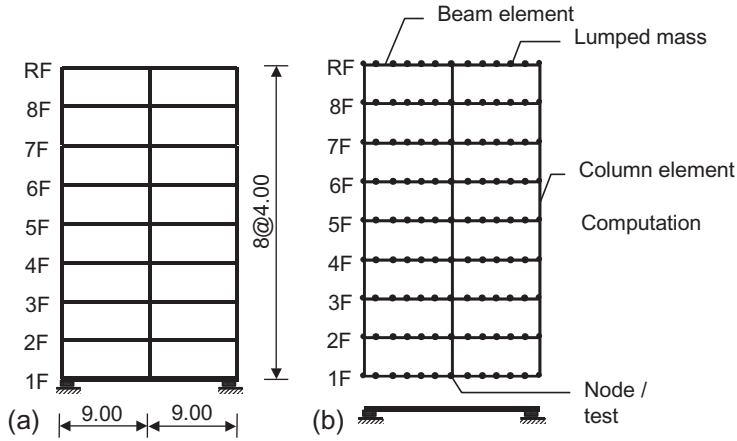

FIGURE 5.7 Structure adopted for demonstration test: (a) base-isolated structure, (b) model.

5.4.2 Test Setup and Test Specimen

The test setup, shown in Fig. 5.8a and b, includes the loading frame, two jacks (one for horizontal loading and the other for vertical loading), and the test specimen. The test specimen featured two identical high damping rubber bearings (HDRBs) securely fastened by high-tension bolts to the base steel beam at the bottom and to an inverted T-shaped loading frame at the top. The base steel beam was tied down to the loading frame, and the two jacks were attached at the top of the inverted T-shaped loading frame. Both the base steel beam and the T-shaped loading frame were designed to be rigid enough relative to the rubber bearings. The two rubber bearings were placed 1.0 m apart in the center-to-center length, and the jacks were attached at a height of 1.5 m, measured from the bottom of the HDRBs to the top of the T-shaped loading frame (Fig. 5.9a).

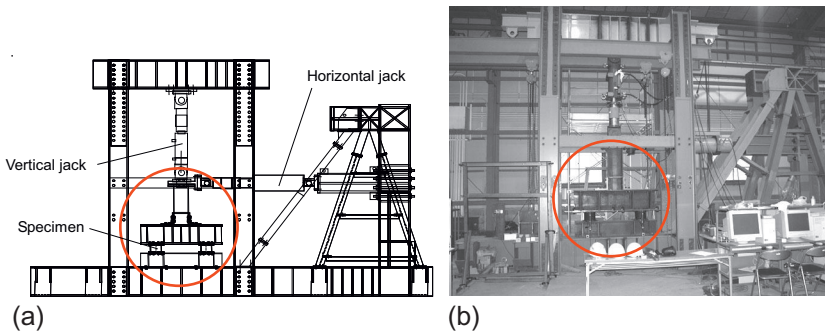

FIGURE 5.8 Test setup: (a) test specimen and loading frame, (b) view of test setup.

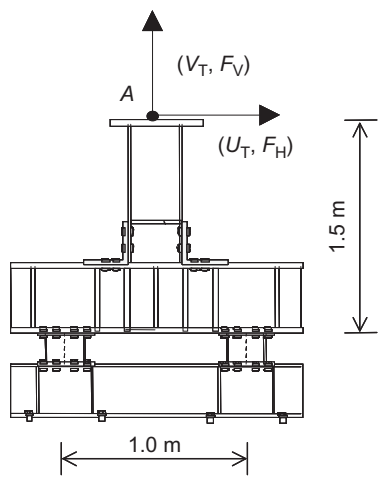

FIGURE 5.9 Measurement of diplacement and force.

The vertical jack applied to the rubber bearings was a constant vertical force equal to the gravity, and the horizontal jack was displacement-controlled in accordance with the displacement commanded by the online test.

Figure 5.9 shows measurement details. The digital displacement transducers and load cells of the two jacks, both attached at Point A, measured the horizontal displacement U_T, the horizontal reaction force F_H, the vertical displacement V_T, and the vertical reaction force F_V. The horizontal jack's displacement was taken to be the horizontal displacement of the test specimen. It was justified because the T-shaped loading frame was designed to be rigid enough as compared to the rubber bearings, and the test specimen did not rotate due to the very large compressive stiffness of the test HDRBs.

Although only the horizontal interaction between the superstructure and base-isolation layer was considered explicitly in the model, the effects of overturning moment on the base-isolation layer were partially included in the physical test. This is because, in the loading system used in the test, the horizontal jack through the inverted T-shaped loading frame applied overturning moment automatically in addition to horizontal force. This corresponded to the situation that the location of the center of horizontal forces applied to the superstructure was taken to remain unchanged.

The HDRBs of the test specimen had the dimensions with a diameter of 200 mm and a total rubber thickness of 85 mm. From comparison in the cross-sectional area, the total rubber thickness, the shape factors, rubber's shear modulus between the prototype HDRBs and the tested HDRBs, the scale-ratios of 1:4 and 1:20 were adopted for the horizontal displacement and horizontal force, respectively. In other words, one-fourth of the displacement predicted by solving the equations of motion of the base-isolated structure was applied into the test specimen, and the force measured by the test specimen was increased by 20 times when inserted into the solution of the equations of motion.

5.4.3 Test Results

Three Internet online tests, Tests, 1, 2, and 3, were carried out in this study. In all three tests, the fault-normal component of the JMA Kobe record [16] was used. Tests 1 and 2 did not adopt the proposed stiffness prediction method; instead, the initial stiffness was used for the predicted stiffness throughout the test. The difference between Tests 1 and 2 was the integration time interval, i.e., 0.02 s for Test 1 and 0.01 s for Test 2. Test 3 adopted the proposed stiffness prediction method, with the integration time interval of 0.02 s.

All three tests were carried out without any trouble in loading, computation, and data exchange. Statistics on time consumption are shown in Table 5.3, indicating that the time consumed for the Internet data exchange comprised about 20-30% of the total time. It looks relatively slow but worked stably. A total of 6000 rounds of data exchange were executed during the three tests, and not a single trouble was encountered. The system proved to be robust, because it

TABLE 5.3 Three Type of Internet Online Test

		Time consumed (min)			
	Step	Total	Loading	Connection	Computation
Test 1	750	160	120	40	<1
Test 2	1500	250	170	80	<2
Test 3	750	170	120	50	<1

was able to resume even in an Internet transmission jam. This was validated by intentionally unplugging the LAN cable; the system kept waiting until the cable was connected again. As described earlier, the Internet data exchange in this study adopted a file transmission procedure. File transmission is available directly or by proxy in most networks. Although it is not necessarily the most efficient solution, this type of transmission does not require special permissions for transferring data across firewalls and other security restrictions. The strategy of "who creates and who deletes" adopted in the data exchange interface was believed to prevented users' misoperation and other malicious entrance.

The experimental hysteresis curves for Tests 1, 2, and 3 are shown as solid lines in Fig. 5.10a, c, and e, respectively. The corresponding predicted hysteresis curves are also plotted as broken lines in these figures. The following procedure was adopted for plotting the predicted hysteresis curves. The assumed elastic stiffness was used for the first three steps, and the tangent stiffness was estimated using the corresponding prediction method from the fourth step and after. At each step, the incremental force was estimated as the product of the predicted stiffness and incremental displacement, and the overall force was taken to be the current force added by the incremental force. The overall force and displacement are plotted in Fig. 5.10. As indicated in the figures, the tested and predicted hysteresis curves are somewhat different in Tests 1 and 2. This is because the initial stiffness was significantly different from the actual stiffness once the specimen yielded. The tested and predicted hysteresis curves agree well in Test 3, because the specimen stiffness was predicted accurately in this test. The energy time histories are obtained for Tests 1, 2, and 3, shown in Fig. 5.10b, d, and f. Two energy time histories are plotted in these figures. One is the external work calculated in reference to the nodal forces and displacements, and the other is the internal energy calculated from the stresses and strains of the individual elements. The two energies are to be identical to satisfy the dynamic equilibrium. In Test 1, significant imbalance energy occurred, because the stiffness evaluation was not accurate. The imbalanced energy decreased in Test 2, because a smaller time interval was adopted, but it was still notable. This suggests that use of the initial stiffness as the predicted

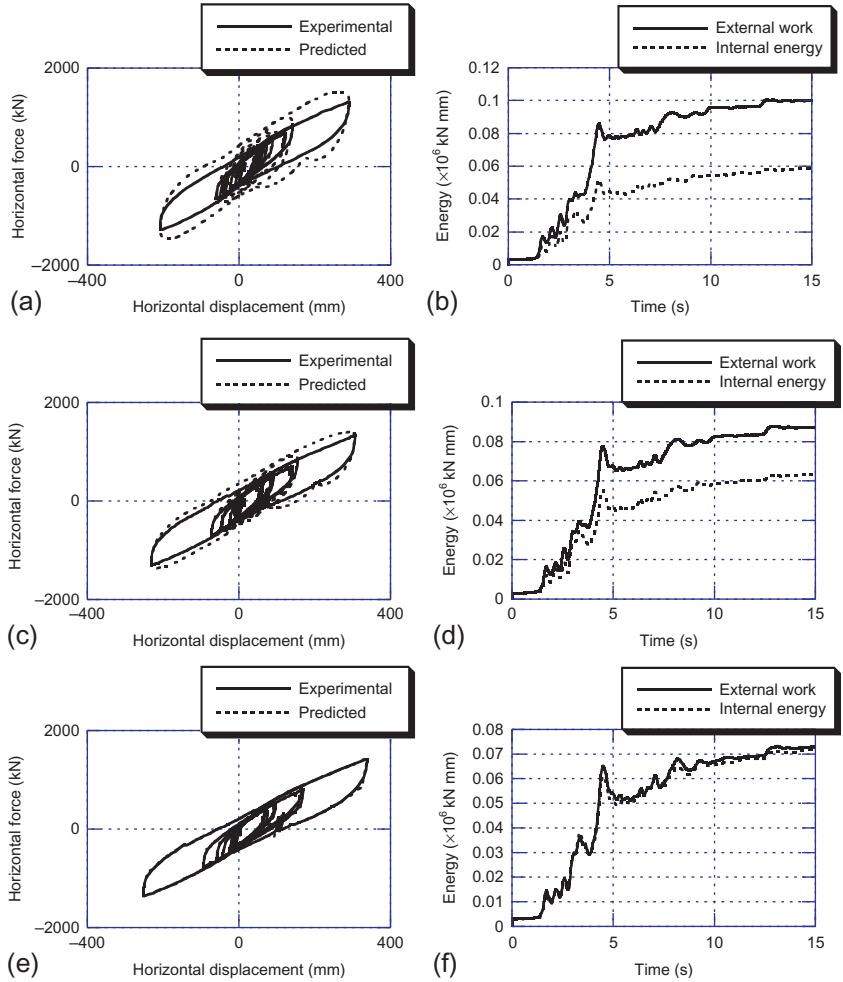

FIGURE 5.10 Test results: (a) hysteresis curves of Test 1, (b) energy time history of Test 1, (c) hysteresis curves of Test 2, (d) energy time history of Test 2, (e) hysteresis curves of Test 3, (f) energy time history of Test 3.

stiffness is not effective. The stiffness was predicted with a sufficient accuracy in Test 3, and the imbalanced energy was negligible. This observation proves that the proposed stiffness prediction method is effective.

Two more alternatives were investigated for the tangent stiffness prediction. To this end, the response time history obtained from Test 3 was used. Figure 5.11a shows the case when using a linear extrapolation. In this case, the stiffness was simply estimated by dividing the incremental force by the incremental displacement in the immediate previous step. As expected, the predicted stiffness is unstable, and it occurs when the incremental displacement is

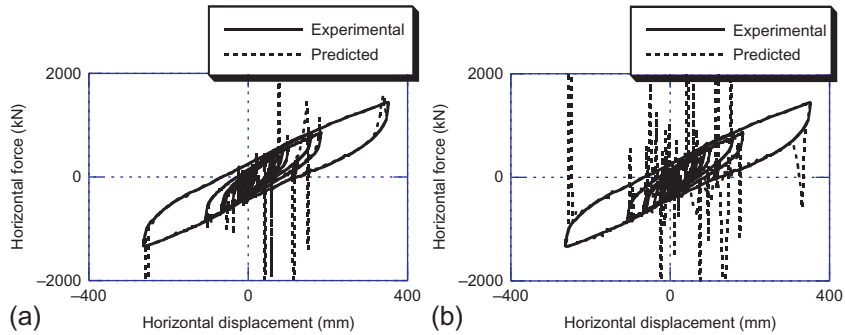

FIGURE 5.11 Validation of stiffness prediction: (a) linear extrapolation, (b) third-order polynomial.

very small. This is because the force errors generated in the physical test are amplified by dividing a small incremental displacement, and become significant. Figure 5.11b shows the case when using a polynomial extrapolation. In this case, a third-order polynomial function was constructed based on the data in the previous three steps, and the tangent stiffness was predicted as the slope at the last step. The experimental and predicted curves are significantly different. Many other alternatives were also considered for the stiffness prediction, and the one proposed in this study was found to be the best, although it was rather serendipitous.

The displacement and reactional force time histories of the three tests are compared in Fig. 5.12a and b. It is observed that Test 3 responded larger than Test 2, and Test 2 responded larger than Test 1. The reason is that the imbalanced energy is the largest in Test 1, smaller in Test 2, and negligible in Test 3. The imbalanced energy acted as additional dissipated energy in the tests. The difference is most significant at the 5th second, at which a large pulse of the ground motion occurred, causing large displacements and intensive plasticities at the base-isolation layer. The imbalance energy was the largest for Tests 1 and 2 at that moment.

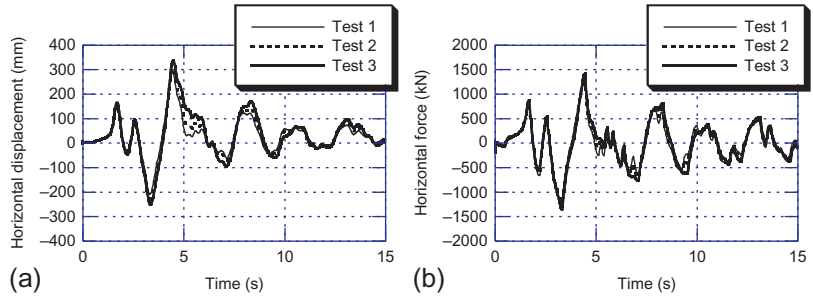

FIGURE 5.12 Comparison among Tests 1, 2, and 3: (a) displacement history, (b) force history.

5.5 CONCLUSIONS

This chapter presented an Internet online test system developed for the simulation of earthquake responses of structures. The system consists of the host, stations, and data exchange interfaces. In the system, the substructure online test was considered, and the test was combined with a FEM type of program that adopted incremental formulation and implicit integration algorithms. The test and analysis were conducted at separate locations, and the data necessary to exchange between them were transmitted over the Internet. A procedure of sharing files and folders implemented by standard operating systems was adopted for the data exchange. The procedure did not require special permission for transmitting data across firewalls and other security restrictions; hence the data exchange was available and easily implemented. The stability and security of the data exchange procedure was verified through 6000 rounds of data transmission; no single trouble was encountered. The host analyzes the computed parts, collects information from the stations, and simulates the response of the entire structure. A tangent stiffness prediction method was proposed by which the information obtained from the physical online test can be incorporated into a numerical analysis program that utilizes incremental formulation and implicit integration algorithms. The proposed stiffness prediction method made use of the force and displacement data of the previous three steps. The method was compared with various alternatives for the stiffness prediction, and its effectiveness was demonstrated by a series of physical tests applied to a base-isolated building model.

REFERENCES

[1] Shing PB, Nakashima M, Bursi OS. Application of pseudo dynamic test method to structural research. Earthq Spectra 1996;12:29–56.

[2] Nakashima M. Development, potential, and limitations of real-time online (pseudo-dynamic) testing. Philos Trans R Soc Lond A 2001;359:1851–67.

[3] Okada T, Okada K, Seki M. Response test of RC space frame under biaxial input motion (part 1: test method). In: Proceedings of the annual meeting of the architectural institution of Japan, Tokyo, Japan; 1981. p. 1279–80 [in Japanese].

[4] Tagami J, Ishii K, Iizuka M, Ishida M. Application of substructure pseudodynamic test to base-isolated structure. In: Proceedings of the 4th US national conference on earthquake engineering II. El Cerrito, CA: Earthquake Engineering Research Institute; 1990. p. 599–608.

[5] Tsutumi H, et al. Substructure pseudo dynamic test with rotation control. In: Proceedings of the 4th US national conference on earthquake engineering II. El Cerrito, CA: Earthquake Engineering Research Institute; 1990. p. 525–34.

[6] National Science Foundation. Network for earthquake engineering simulation (NEES): earthquake engineering research equipment, program solicitation. Report NSC00-6, USA: National Science Foundation; 2000.

[7] National Science Foundation. Network for earthquake engineering simulation (NEES): system integration, program solicitation. Report NSC00-7, USA: National Science Foundation; 2000.

[8] National Science Foundation. Network for earthquake engineering simulation (NEES): consortium development, program solicitation. Report NSC 01-56, USA: National Science Foundation; 2001.
[9] Tsai K, et al. Network platform for structural experiment and analysis (I). Report NCREE-03-021, Taiwan: National Center for Research on Earthquake Engineering; 2003.
[10] Sugiura K, Nagata N, Suzuka Y, Watanabe E. Internet related structural testing. In: Proceedings of the eighth KKNN seminar on civil engineering, Singapore; 1998. p. 219–24.
[11] Watanabe E, Yun C, Sugiura K, Park D, Nagata K. Online interactive testing between KAIST and Kyoto University. In: Proceedings of the fourteenth KKNN symposium on civil engineering, Kyoto, Japan; 2001. p. 369–74.
[12] Wang K, Tsai K, Wang S, Cheng W, Yang Y. Networked hybrid test frameworks and examples. In: The fifth seminar on earthquake engineering for building structures (SEEBUS), Kyoto, Japan; 2003. p. 81–90.
[13] Tada M, Kuwahara S. Basic study on the system of structural analysis by unifying various programs through Internet. J Struct Constr Eng Trans AIJ 2004;580(6):113–20.
[14] Nakashima M, Akazawa T, Igarashi H. Pseudo dynamic testing using conventional testing devices. J Earthq Eng Struct Dyn 1995;24(10):409–1422.
[15] WebDrive online manual. South River Technologies, LLC; 2003.
[16] Nakashima M, Matsumiya T, Asano K. Comparison in earthquake responses of steel moment frames subjected to near-fault strong motions recorded in Japan, Taiwan, and the U.S. In: International workshop on annual commemoration of Chi-Chi earthquake, Taipei, Taiwan, September 18-20; 2000. p. 112–23.

Chapter 6

Internet Online Hybrid Test Using Separated-Model Framework

Chapter Outline

6.1 INTRODUCTION

In most previous applications of the substructure online hybrid test, the adopted numerical models used relatively crude assumptions and a limited number of degrees of freedom (DOF), a typical one of which was a stick model with lumped masses. Subsequent improvements to numerical analyses have been very positive

Development of Online Hybrid Testing. http://dx.doi.org/10.1016/B978-0-12-803378-4.00006-6

for earthquake response simulation, and many finite element (FEM) software applications have been made available for general purpose. In such circumstances, it would seem to be very effective to use a FEM software application for the computation of the numerical substructures [1–3] (see Chapter 5).

The reality, however, is rather different: such applications have been found to be limited. Before incorporating a FEM application into the substructure online hybrid test, the code has to be modified such that it pauses its execution after every time step, sends the data (commonly the reactional force data) to another program that supervises the operation, receives a new set of data (commonly the displacement data) for the next time step, and then resumes the execution for the step. For example, the online hybrid test system used in European laboratory for structural assessment [1] employed a FEM program named CastEM for the FEM modeling of analytical substructures. In their procedure, a condensed effective mass matrix should be transported to the online hybrid test program from CastEM, which involves modification of the source code. In each step, the accelerations at the common DOF should be transferred from online hybrid test program to CastEM, and symmetrically, the pseudo-force should be sent from CastEM to the online hybrid test program. The operations required modification of the source code of CastEM. A framework developed by Takahashi and Fenves [3], in which OpenSees was incorporated into the system of numerical simulation, a special element, named the "experimental element," was added into the source code of OpenSees. As may readily be speculated, such modifications are, however, not easy, partially because of the rigid input and output rules adopted in most of the general-purpose FEM codes. Furthermore, ordinary users are not able to touch the source codes, or are not allowed to revise the codes due to legal restrictions. Presented in this chapter is a method in which a general-purpose FEM application is combined in the substructure online hybrid test. In the proposed method, the dilemma described above is resolved with repeated use of the restart procedure commonly featured by general-purpose FEM applications.

This chapter consists of three sections. The first presents the constituent parts of the proposed method, which include two different models, one used to solve equations of motion and the other to obtain restoring forces, the procedure that repeatedly applies the restarting procedure, and the high-speed data exchange scheme through Internet. The second gives two numerical example applications of the proposed method to demonstrate its effectiveness. In that section, all substructures are treated locally and numerically by a general-purpose FEM program, ABAQUS [4]. Presented in the final section is the demonstration test, which simulates the response of an eight-story base-isolated building structure subjected to an extremely large ground motion and collision with the surrounding retaining walls. In this example, the superstructure is modeled numerically, and its restoring forces are solved by ABAQUS, while the base-isolation layer and surrounding retaining walls are modeled experimentally and the associated restoring forces are obtained by a physical test.

6.2 DEVELOPMENT OF SEPARATED-MODEL FRAMEWORK

6.2.1 Design of Separated-Model Framework

The proposed online hybrid test system adopts the substructuring technique, in which part of the structure is modeled numerically and the rest is tested physically. Two special features are notable in the system: (1) two separate models are adopted for the analysis, one for the simulation of structural dynamics and the other for the acquisition of the restoring forces; and (2) it makes use of a FEM analysis code, readily available on the market, without any modification of the source code [5].

The framework is shown in Fig. 6.1. A base-isolated building is chosen as an example to describe the proposed system. The structure is divided into two parts: the superstructure and the base-isolation layer. The superstructure is modeled numerically, while the base-isolation layer is tested physically. Furthermore, the numerical model is represented by a sophisticated FEM model to obtain the superstructure's restoring forces accurately. The test of the base-isolation layer is to acquire accurate information about its restoring force. The entire structure is modeled as a relatively simple 9-DOF system, in which one floor is represented by one mass and one story is represented by one horizontal spring. Disparity in the model sophistication becomes reasonable in a situation like; a sophisticated static model is needed for accurate evaluation of member internal forces and deformations; all the while, the dynamics of the structure are well represented by the first several vibration modes, which may be determined from a model with much fewer DOF. This disparity is justified in this example, in which the restoring force behavior is very complex but the dynamics are relatively straightforward.

In the proposed system, the time integration scheme should be chosen according to the complexity of the dynamic model. If the dynamic model

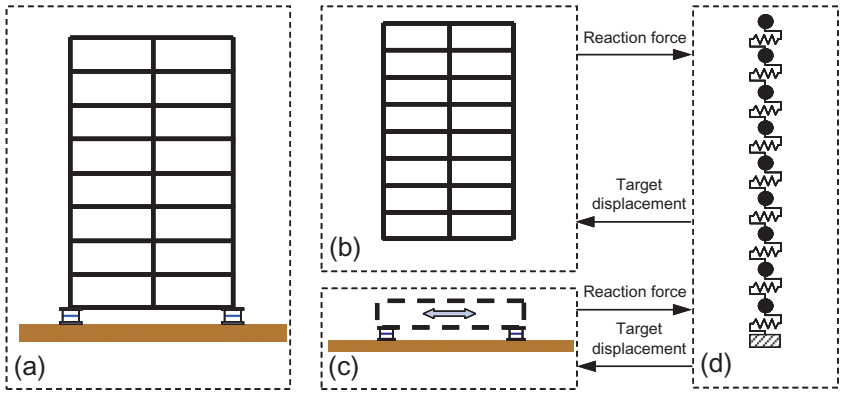

FIGURE 6.1 Outline of proposed system framework. (a) Entire base-isolated structure, (b) numerical superstructure, (c) experimental base-isolation layer, and (d) dynamic model.

contains many DOF, a time integration scheme that ensures stability with respect to the time should be selected. In this particular study, the dynamics of the structure was assumed to be relatively simple. Therefore, the explicit Newmark-β scheme [6] was adopted because of its simplicity, which is shown in the following equations:

$$\mathbf{d}_{n+1} = \mathbf{d}_n + \Delta t \mathbf{v}_n + 0.5\Delta t^2 \mathbf{a}_n \tag{6.1}$$

$$\mathbf{M}\mathbf{a}_{n+1} + \mathbf{C}\mathbf{v}_n + \mathbf{R}^{\mathrm{F}}_{n+1} + \mathbf{R}^{\mathrm{B}}_{n+1} = \mathbf{f}_{n+1} \tag{6.2}$$

$$\mathbf{v}_{n+1} = \mathbf{v}_n + \Delta t(1-\gamma)\mathbf{a}_n + \Delta t\gamma \mathbf{a}_{n+1} \tag{6.3}$$

where $\mathbf{d}$, $\mathbf{v}$, and $\mathbf{a}$ are the displacement, velocity, and acceleration vectors, respectively; Δt is the time interval; subscripts n and $n+1$ represent the time integration steps n and $n+1$; and γ is the parameter of the explicit Newmark-β scheme, adopted as 0.5 in this study. The adopted time integration scheme is explicit, meaning that stability and accuracy conditions should be checked carefully. The stability condition of the explicit Newmark-β scheme is given as [7]:

$$\omega \Delta t \leq 2 \tag{6.4}$$

Due to the explicitness of the time integration scheme, the target displacements for the next step can be computed by Equation (6.1) with only the information known at the current step. This explicitness makes iteration for loading of a physically tested nonlinear system unnecessary. The computed displacements are transferred to the numerical substructure and the experimental substructure. The restoring forces of the entire structure are calculated as the vectorial combination of the reaction force vectors obtained from the numerical substructure and the experimental substructure, denoted in Equation (6.2) as $\mathbf{R}^{\mathrm{F}}_{n+1}$ and $\mathbf{R}^{\mathrm{B}}_{n+1}$, respectively. Note that the governing equations of motion do not have to be formulated in an incremental manner owing to the direct use of reaction forces. Using these restoring forces, the equations of motion are solved by Equations (6.2) and (6.3).

6.2.2 System Implementation

In accordance with the framework of the proposed online hybrid test system, a main control program and an FEM control program were developed to supervise the entire process. The right-hand side in Fig. 6.2 shows the flowchart of the main control program. The program handles the discretized dynamic model having 9-DOF as indicated in Fig. 6.1, and also supervises the experimental substructure, i.e., the base-isolation layer shown in Fig. 6.1. The left-hand side of Fig. 6.2 is the flowchart of the FEM control program that handles the numerical substructure, i.e., the superstructure in Fig. 6.1.

Since the interfaces to the loading device and data collecting system are given as *Visual Basic* modules, *Visual Basic* was chosen for the main control programming language. The major functions of the main control program are

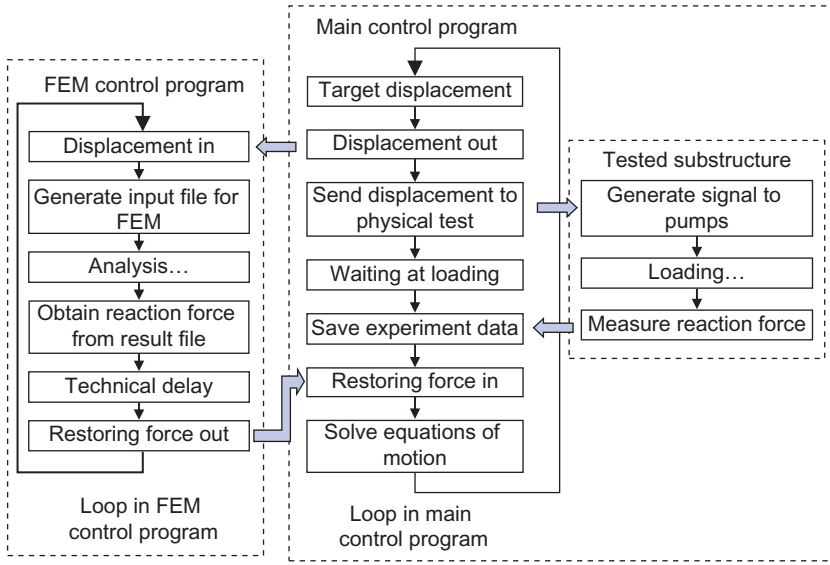

FIGURE 6.2 Two programs used for system control.

(1) to solve the equations of motion of the discretized dynamic model; (2) to send the target displacements to the numerical substructure and receive the restoring forces from the analysis; and (3) to supervise the physical test and obtain the restoring forces from the test. The FEM control program can be developed using any modern programming language. In this study, *FORTRAN* 90 is adopted. The tasks of this program are (1) to generate the input files for each step of FEM analysis; (2) to prompt the FEM analysis; and (3) to interpret the analysis results and obtain the reaction forces.

The two programs, i.e., the main control program and the FEM control program, work simultaneously but on different computers and communicate with each other over the Internet. Figure 6.2 also shows the flow of Internet communication. In each step, the main control program computes the target displacements for the associated DOF of the discretized dynamic model and sends them to the numerical substructure, which is analyzed by the FEM control program. The main control program also transfers the target displacements of the experimental substructure to the computer for controlling the test. The main control program then waits and checks the loading status of the physical test continuously. Once the loading is finished, the restoring forces measured in the experimental substructure are fed back to the main control program and saved on its hard disk. The main control program also collects the restoring forces of the numerical substructure. In reference to the restoring forces collected from the substructures, the entire restoring force vector is calculated. Finally, the equations of motion are computed using Equations (6.2) and (6.3), and all of the necessary data for the next step become ready.

The FEM control program stays at the starting point until the new target displacements are received. Upon receipt of the target displacements, an input file that includes the target displacements and other information such as structural configuration needed for the FEM analysis is generated. This file is a standard input file that can be read by the FEM preprocessor. The FEM control program evokes the FEM software for the current step analysis. While the FEM software runs, the FEM control program awaits. Once the analysis is completed, the FEM control program awakes to interpret the result file transferred from the FEM software. This result file is written in text format. Once the reaction forces are sent back to the main control program, does the FEM control program return to the starting point, making itself ready for the next step analysis. In practical implementation of the FEM control program, the result file is written in the hard disk at completion of the current step analysis, but with a certain lag. If the FEM control program attempts to interpret the result file before the result file is saved in the hard disk, a fatal error would occur and the FEM control program would be terminated. To avoid this potential problem, a "technical delay" (Fig. 6.2) of 1.0 s is introduced before the start of the feedback process.

When the experimental substructure is loaded in each step, the numerical substructure is being analyzed simultaneously. This parallelism improves the time efficiency significantly, as will be discussed later.

6.2.3 High-Speed Data Exchange Scheme Using a Socket Mechanism

Two solutions were considered for exchanging data across the Internet. One is to utilize a standard protocol usually implemented by the operating system for sharing files and folders, such as the one used in Chapter 5. The feasibility of this solution has been proven, but the speed of data transmission is not necessarily fast enough [8]. The other is to utilize a standard message-passing interface (MPI) [9]. MPI is a standard library specification for message passing. It was designed to run on distributed-memory multiprocessors, networks of workstations, and combinations of both, achieving a standard in parallel computing. However, this approach was found to be unsuitable, because most of current implementations, e.g., MPICH, LAM/MPI, and MPI-G2 [9], have the following limitations. (1) Among the various processes connected by MPI, only the main process, defined commonly as Process 0, is designed to accept interruption by users. This is acceptable for parallel computing, but does not meet the demands of the online hybrid test system, because all stations in the online hybrid test system, especially those involving physical tests, require interruption by users. (2) MPI can be run on various types of operating system, e.g., Windows and Linux. However, implementations to date support only a single type of operating system in one application. This limitation significantly restricts the capacity of distributed task sharing over the Internet. (3) Original implementations of MPI were applicable only on local LANs. Recent implementations are being

extended to the Internet, i.e., MPI-G2. They still face many difficulties associated with strict firewalls. To this end, a socket mechanism [10] based on the TCP/IP protocol was adopted to provide flexible and high-speed data exchange over the Internet.

The procedure [11] of data exchange using the socket mechanism is as follows: (1) the Server establishes a listening socket and waits for connections from clients; (2) the Client creates a client socket and attempts to connect to the Server; (3) the Server accepts the Client connection attempt; (4) the Server and Client start to send and receive data using the socket being established; (5) the Server and Client close the connection after the completion of data exchange. As shown in Fig. 6.3a and b, two types of data exchange are

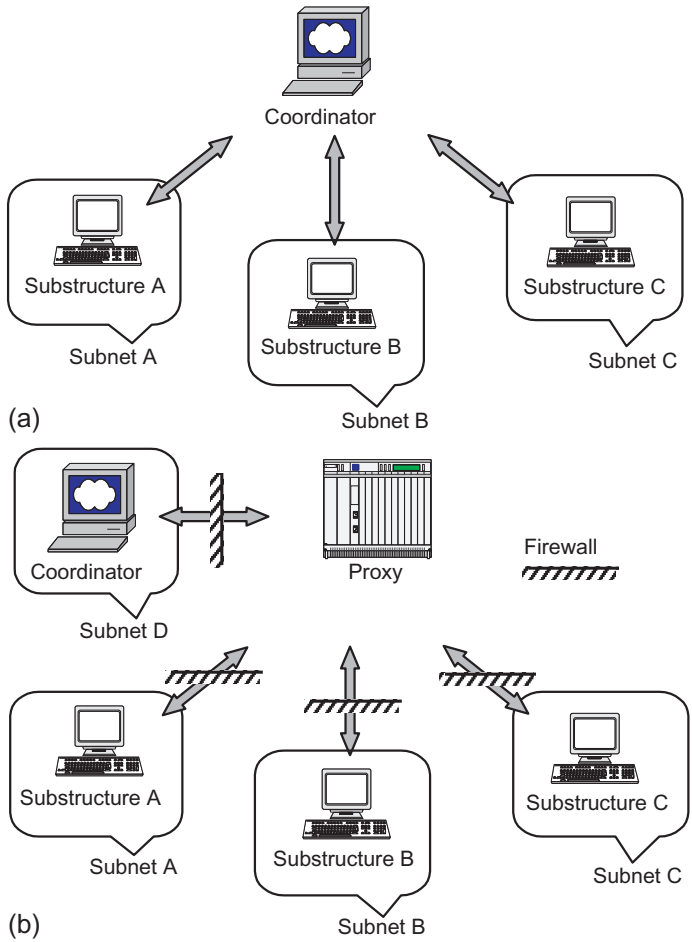

FIGURE 6.3 Data exchange: (a) direct data exchange and (b) data exchange through a proxy program.

considered, i.e., direct data exchange and data exchange through proxy. In the direct data exchange, Coordinator and Substructures are set as Server and Clients, respectively. In the data exchange through proxy, Coordinator and substructures are set as Clients, and the proxy is set as Server. Here, proxy is a program developed for forwarding data between Server and Clients. The data exchange through proxy is particularly useful specifically in the situations when strict firewalls are present. To simplify the application of the socket mechanism, the raw socket application programming interfaces, commonly provided by the operating systems, are encapsulated into a library. Data exchange over the Internet is realized using a few interface functions, i.e., "SOCKETI" and "SOCKETO" for the direct data exchange, and "SOCKETIP" and "SOCKETOP" for the data exchange through proxy.

In order to increase the efficiency and security of data transmission, an encode-decode procedure was adopted for data transmission. In the procedure: (1) all data to be transmitted are encoded into a byte stream, e.g., 4 bytes for an integer and 8 bytes for a double precision float; (2) the byte stream is transmitted over the Internet using the socket mechanism; (3) the transmitted byte stream is decoded to the original data upon reaching the destination. Data are arranged in a network byte order when encoded, and then rearranged in a machine byte order when it is decoded. Such treatment is particularly useful to solve potential problems associated with the exchange of data between different computer systems, i.e., some computer systems using "Big Endian" byte order, while others using "Little Endian" byte order. This data exchange solution was validated for Windows, Linux, and Macintosh systems, and it has proven to be portable and efficient.

6.2.4 Incorporation of FEM Programs Using Restart Capability

In this study, a general-purpose FEM software application, ABAQUS, was adopted for the numerical analysis. The restarting capability of ABAQUS is the decisive component for using a general-purpose software application with the proposed system. ABAQUS can write the model definition and all information to the current state in a set of restart files. This allows an analysis to pause at a certain step and to resume the analysis at a later time. With repeated use of this capability, ABAQUS can keep pace with the step-by-step time integration. In the proposed system, the restarting analysis is executed as many times as the integration time steps. When a restart analysis is completed for the current step, all information up to the present state is restored by ABAQUS, and the reaction forces are saved into a text file, which can readily be interpreted by the FEM control program. For the next step of restart analysis, the state at the end of the previous step is recovered first, and then the analysis is processed with a new input file, in which the next target displacements are written as the loading set. Note that with the progression of the analysis, the restored information for restart increases gradually, which will be discussed later.

An I/O interface is devised for communication with ABAQUS. Two functions are implemented in the interface, i.e., for generation of input files for the ABAQUS analysis and for interpretation of the analysis results obtained by ABAQUS. In the implementation, only standard input and output procedures provided by ABAQUS are employed; thus we do not need any change to the ABAQUS source code.

Running ABAQUS with an input file is the most common way to conduct ABAQUS analyses. The input file is interpreted by ABAQUS, the analysis model is constructed, and consistency is checked before execution. ABAQUS accepts an input file in the text format, which can be created by any text editor. As stated in last section, two types of analysis are employed in this study, i.e., normal analysis and restarting analysis. For respective analyses, different sets of input files are created. One is the normal input file for the normal analysis, and the other is the restarting input file for the restarting analysis. Both files are composed of a series of text lines of ABAQUS command, parameters, and detailed data. Although similar in most contents, the two types of input files are different in some specifications.

The normal input file begins with a "*HEADING" section, which is used to define the title of the analysis. Following the "*HEADING" section, the normal input file usually contains a model definition section, in which nodes, elements, materials, and boundaries of the analyzed structural model are defined. At the end of the normal input file, a "*STEP" section is defined. This section includes the definition of analysis type, loading pattern, and output requirements. It is the most critical portion in the proposed system since the ABAQUS analysis is affected by the definitions in this section. The section accepts multiple steps, and several types of analyses, i.e., "static analysis," "modal analysis," and "dynamic analysis," are possible to run in accordance with the corresponding ABAQUS commands and parameters. In this section, some specially required output, for example, "reactional forces," "displacements," and "modal shapes," can be requested by such output commands as "*OUTPUT HISTORY", "*OUTPUT FIELD", and "*NODE FILE". Particularly in this study, one of the most important commands is "*RESTART, WRITE". This command is to have ABAQUS save the current status of the analyzed model, including the coordinates of each node, stress and strain of each element, and loading path, to a hard disk for succeeding restarting analyses.

Similar to the normal input file, the restarting input file also begins with a "*HEADING" section. Different from the normal input file, a command "*RESTART, READ" is used instead of the model definition section following the "*HEADING" section. The command "*RESTART, READ" is the counterpart of the command "*RESTART, WRITE." It asks ABAQUS to load the existing analysis model from the hard disk instead of creating a new structural model. The structural status (coordinates of each node, stress and strain of each element, and loading path) being saved by "*RESTART, WRITE" is taken as the initial status in the restarting analysis. The "*STEP" section is also the

essence of the restarting input file. Analysis type, loading pattern, and output requirements are also defined in this section. Note that "*RESTART, WRITE" also needs to be included in the "*STEP" section for succeeding restarting analyses.

In this study, the control program creates the input file automatically by calling a function "WRITE" provided in *FORTRAN* 90 instead of using a text editor.

ABAQUS outputs several types of result files for each analysis. In this study, the ".fil" file is adopted because of its handiness. Related information is obtained by interpreting the .fil file, and details are as follows:

ABAQUS supports two formats for the .fil file, i.e., binary and text. In this study, a command, "*FILE FORMAT, ASCII", is used to control the output file with a text format. The contents of the .fil file consist of many data blocks, such as structural information data block including nodal coordinates, element definition, and output data block requested by users. Restart analysis rewrites the structural information appending to the existing structural information data blocks by adding the output data of the current analysis to the end of the file as a new data block. Thus the .fil file contains a structural information data block and many output data blocks including all of the previous analyses up to the current analysis.

The contents of the .fil file, particularly the analysis results, are determined by specifications in "*STEP" section of the input file. For instance, a command "*NODE FILE" with parameters "RF" and "U" asks ABAQUS to output nodal reactional forces and displacements to the .fil file, respectively. Following the requests specified in the "*STEP" section of the input file, ABAQUS outputs the results in special sequenced records. Each record has the following format: record length, record type identifier, and specific attributes. An example record, which represents the nodal reactional force, is given in Fig. 6.4a.

Each record starts with an asterisk (*) and contains some attributes. As shown in Fig. 6.4b, separated into several parts by commas, each part starts with a character and is followed by detailed data. The first attribute specifies the length of the record. In this part, "I" represents the integer type of data. "1" means this integer has one digit, and "6" is the value of the integer. Therefore, "I 16" specifies that the record includes six attributes in total. The second part

```
*I 16I 3104I 13D-3.146528846903050D+05D 1.461770741
164485D+05D-4.615186066685873D+08
```

(a)

```
'I 16', 'I 3104', 'I 13', 'D-3.146528846903050D+05',
'D 1.461770741164485D+05', 'D-4.615186066685873D+08'
```

(b)

FIGURE 6.4 Example record of nodal reactional force.

specifies the record identifier, which gives the physical meaning of this record, i.e., "displacement" and "reactional force." It is also an integer number given by "I 3104." Following the same rule, "I" represents the integer type of data, and "3" means this integer has three digits; "104" is value of the integer, which gives the ID of the identifier; "104" represents "reaction forces." Assignment of identifiers is specified in ABAQUS documentation [1]. The next part "I 13" specifies this record is for node number "3." What follows are the three attributes, which give three components of reactional forces (two translations and one rotation). In each attribute, Character "D" represents double type of data, and a specific double value is given after Character "D."

In this study, the control program reads the output records one by one using a function "READ" provided in *FORTRAN* 90. According to the format of the records, the related information is obtained through a series of functions on string operation, i.e., "TRIM" and "LENGTH" provided also in *FORTRAN* 90. Since the control program reads and interprets records one by one from the beginning, it becomes time-consuming when the .fil file is made huge. This occurs because ABAQUS outputs all results in the entire loading history, and each analysis result is treated as a separate data block and storied successively. To save time for interpretation of the outputs, a special technique designated as "jump to bottom" is adopted. The essence of the technique is to scan the .fil file without interpreting any records, and locate the last data block directly, and only the records in the last data block are interpreted. The technique saves time, and it satisfies our requirement since the interested information is only in the last data block. A preliminary investigation was carried out, and it was found that for a .fil file with a size of 600 kb, it took 8 s when interpreting all of the information, whereas the time used was nearly null when using the "jump to bottom" technique.

6.3 PRELIMINARY INVESTIGATIONS OF SEPARATED-MODEL FRAMEWORK

6.3.1 Seismic Simulation of a One-Story Braced Frame

A one-story steel braced frame [12] treated as a planar structure was analyzed in this study. As shown in Fig. 6.5, the one-story frame has a pair of identical braces in the middle bays. The cross-sections of the beams, columns, and braces are listed in Table 6.1. The braces have a slenderness of 125 with respect to the weak axis, and they buckle in large compressive axial load. The tops of the five columns were assumed to sustain identical horizontal displacements, thus the dynamic model was simplified to a single degree-of-freedom (SDOF) system. A concentrated mass of 157×10^3 kg was assigned to the floor, and the first period of the frame was given as 0.5 s.

The substructuring technique was employed, and the braced frame was divided into two parts, i.e., the bare frame and the pair of braces (Fig. 6.6).

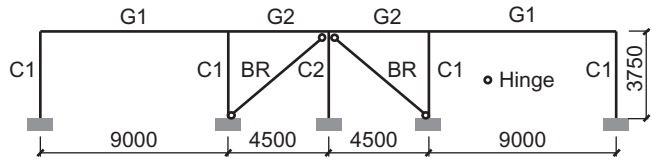

FIGURE 6.5 Dimensions of one-story braced frame (unit: mm).

TABLE 6.1 Cross-sections of Beams, Columns, and Braces (Unit: mm)

Type	Height	Width	Web	Flange
C1	475	332.5	11.71	20.78
C2	175	175	4.139	10.94
G1	350	200	6.34	13.33
G2	550	220	10.21	14.67
BR	175	175	4.139	10.94

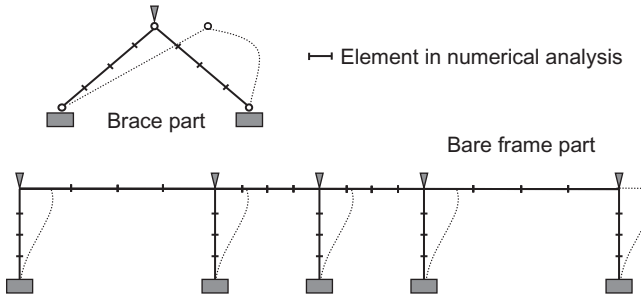

FIGURE 6.6 Substructures of the one-story steel frame.

The bare frame that consists of steel beams and columns and beams was taken as the computed part and analyzed by ABAQUS. The pair of braces was taken as the tested part since the cyclic behavior of the braces is deemed much more complex than the behavior of the bare frame. In this particular study, this part was also treated numerically and analyzed by ABAQUS instead of a physical test.

In the detailed ABAQUS analysis, each of beam, column, and brace members was represented by four Euler-Bernoulli beam elements. The bilinear model considering kinematic hardening (Fig. 6.7) was adopted for the material. In order to simulate the buckling behavior of the braces in ABAQUS, initial imperfection was supplied to the braces by the imposition of a small constant

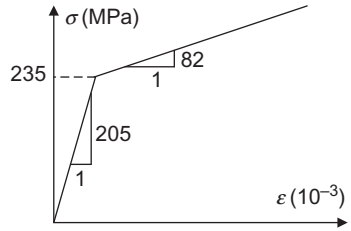

FIGURE 6.7 Stress-strain relationship of bilinear model.

moment couple at both ends of the braces. The moment couple was very small, giving a lateral deflection of 1/750 of the total brace length at the mid-length.

Elastic free vibration analysis was conducted for the one-story braced frame. An initial velocity of 1.0 m/s was assigned to the floor, and 2 s of responses were simulated. In this analysis, the braces were assumed to remain unbuckled, stiffness-proportional damping with the damping ratio of 0.05 was assigned, and the integration time interval of 0.01 s was adopted. The displacement time history is shown in Fig. 6.8. As shown in the figure, the frame vibrates in a period of 0.5 s, and the vibration magnitude decays with time, with the rate of decay corresponding to that to be achieved for the damping ratio of 0.05. This was the first analysis using the proposed method, and the result promised the effectiveness of the method.

Nonlinear time history analysis was carried out for the one-story steel braced frame. The NS component of 1940 El Centro ground motion was adopted again.

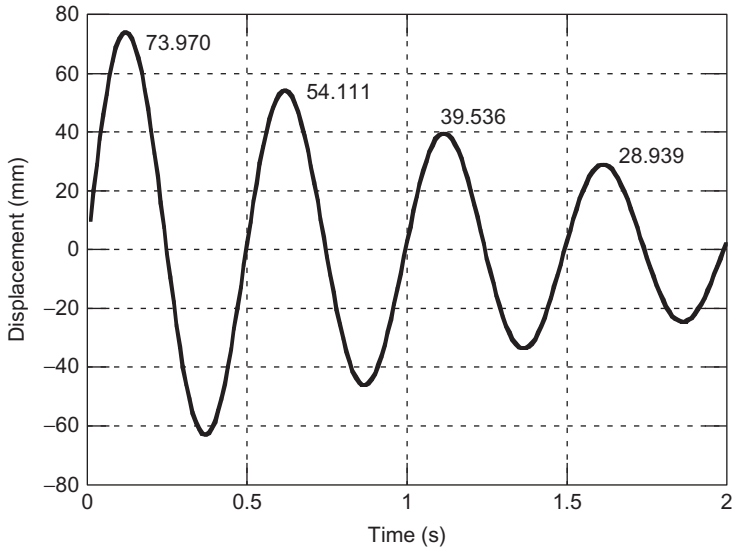

FIGURE 6.8 Displacement response of free vibration analysis.

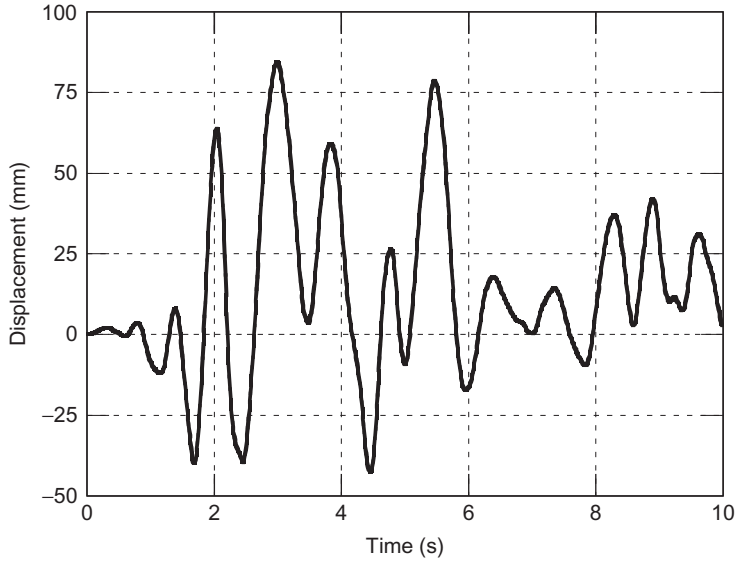

FIGURE 6.9 Response of one-story braced frame.

Stiffness-proportional damping was adopted and the damping ratio of 0.05 was assigned for the one-story braced frame. Both the material and geometric nonlinearities were taken into account by the detailed ABAQUS analysis. The analysis was completed successfully without any malfunction, and the story displacement time history is shown in Fig. 6.9. The hysteresis curve is also plotted in Fig. 6.10. Complex buckling behavior of the steel braced frame is notable.

6.3.2 Seismic Simulation of a Three-Story Braced Frame

A three-story braced frame [12] treated as a planar structure is given in Fig. 6.11. It has three pairs of braces, each of which is installed in one story. The cross-sections of the beams, columns, and braces are listed in Table 6.2. The slenderness of the braces about the weak axis is 96, 110, and 125 for the first, second, and third stories, respectively. In the analysis, the tops of the five columns at each floor were assumed to sustain identical horizontal displacements, thus the dynamic model was simplified to a 3-DOF system. Three concentrated masses of 600×10^3 kg, 400×10^3 kg, and 400×10^3 kg were assigned for the first, second, and third floors, respectively, and the first to third periods of the frame were estimated to be 0.469 s, 0.206 s, and 0.133 s, respectively.

The three-story steel braced frame was divided into four parts, i.e., three pairs of braces and one bare frame (Fig. 6.12). The bare frame was taken as the computed part and analyzed by ABAQUS. The three pairs of braces were

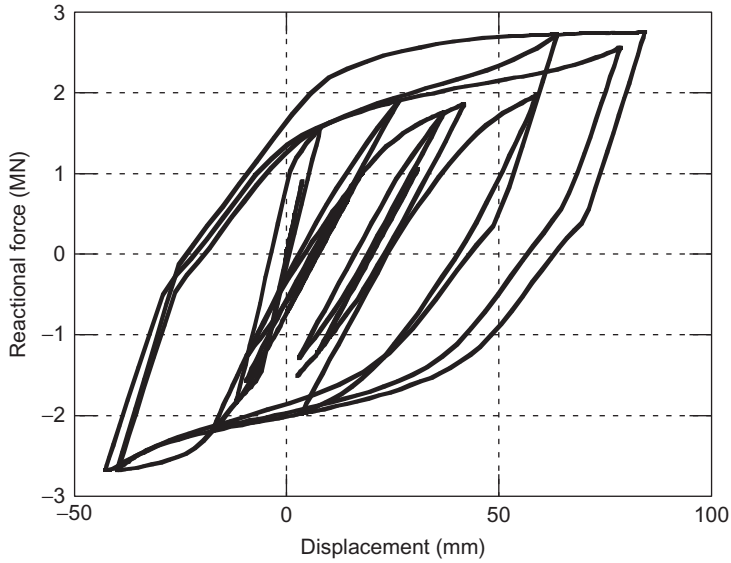

FIGURE 6.10 Hysteresis behavior of one-story braced frame.

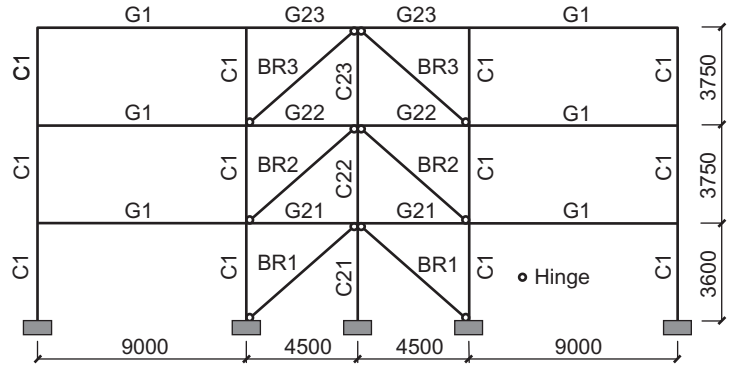

FIGURE 6.11 Dimensions of three-story steel frame (unit: mm).

taken as the tested parts. In this study, they were also simulated numerically by three separate ABAQUS analyses.

First, linear elastic time history analysis was conducted for the three-story braced frame. The brace were assumed to remain unbuckled in the analysis. The NS component of 1940 El Centro record was adopted for a duration of primary motion of 10 s. The displacement time history is shown in Fig. 6.13a-c. For the purpose of comparison, the displacement time history obtained from another 3-DOF model subjected to the identical ground motion is also plotted in Fig. 6.13a-c. In the 3-DOF model, the stiffness of each story was estimated from static pushover analyses of the entire structure by means of ABAQUS. As

TABLE 6.2 Cross-sections of Beams, Columns, and Braces (Unit: mm)

Type	Height	Width	Web	Flange
C1	475	332.5	11.71	20.78
G1	350	200	6.34	13.33
C21	300	300	7.095	18.75
C22	250	250	5.912	15.63
C23	175	175	4.139	10.94
G21	600	240	11.14	16
G22	300	200	5.359	13.33
G23	300	200	5.359	13.33
BR1	225	225	5.321	14.06
BR2	200	200	4.37	12.5
BR3	175	175	4.139	10.94

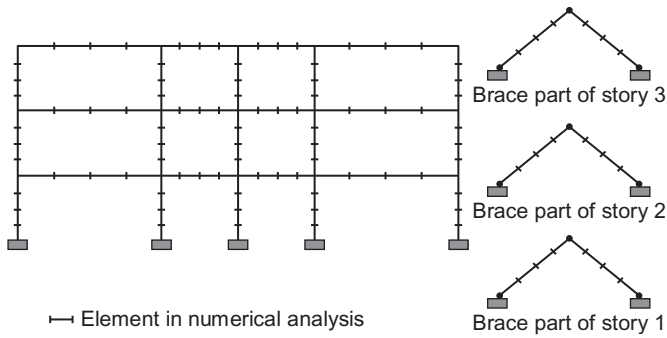

FIGURE 6.12 Substructures of three-story braced steel frame.

shown in the figure, the responses are identical between the proposed analysis and the analysis for the 3-DOF model. This observation further proves the effectiveness of the proposed method.

Nonlinear time history analysis was then carried out for the three-story steel braced frame. The NS component of 1940 El Centro ground motion was adopted again. Stiffness-proportional damping was adopted and the damping ratio of 0.05 was assigned for the first mode in the three-story braced frame. Both the material and geometric nonlinearities were taken into account by the detailed ABAQUS analysis. The story displacement time histories are shown in Fig. 6.14, and the hysteresis curves of each story are plotted in Fig. 6.15a-c.

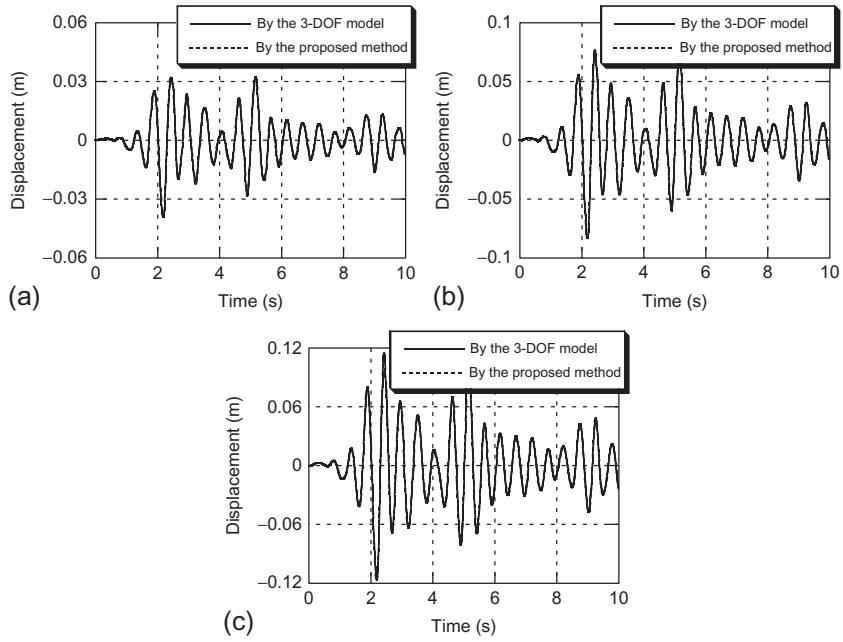

FIGURE 6.13 Displacement response of elastic model. (a) Response of the first story, (b) response of the second story, and (c) response of the third story.

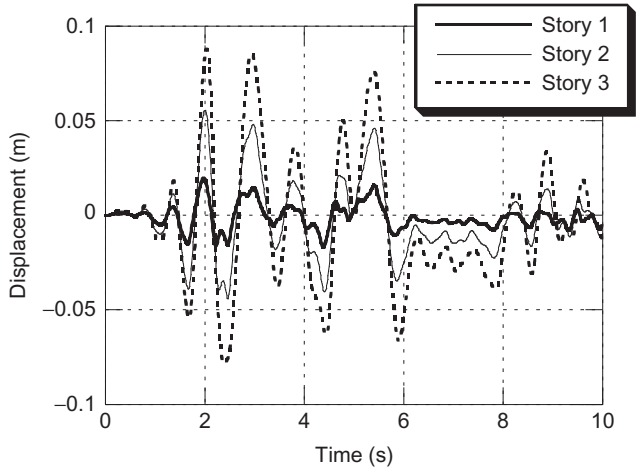

FIGURE 6.14 Nonlinear displacement responses of three-story steel braced frame.

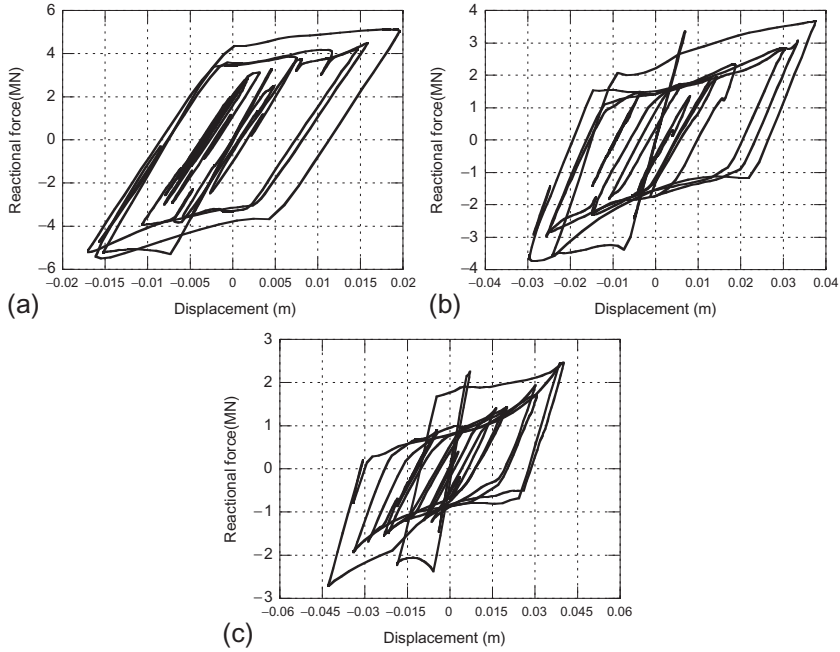

FIGURE 6.15 Hysteresis curve of stories of the two structures. (a) Hysteresis of first story, (b) hysteresis of second story, and (c) hysteresis of third story.

6.4 DISTRIBUTED ONLINE HYBRID TEST ON A BASE-ISOLATED BUILDING

The proposed system was used to simulate the earthquake responses of an eight-story base-isolated structure. The entire structure, including the superstructure and the base-isolation layer, responds like a SDOF system, because the superstructure is much stiffer than the base-isolation layer. In a very severe earthquake event, however, the base-isolation layer may undergo an extremely large displacement, causing it to collide against the surrounding retaining walls. Should this happen, the superstructure would sustain yielding and subsequent damage. Such a response was chosen for the object of simulation.

6.4.1 Prototype Structure

This eight-story base-isolated structure chosen for this study was one actually built in downtown Tokyo. One bay, shown in Fig. 6.16, including a planar superstructure, a base-isolation layer with two isolators, and two pieces of retaining walls, was taken as a model to be examined. The dynamics of this structure is fairly simple and modeled as a 9-DOF system (including the base-isolation layer).

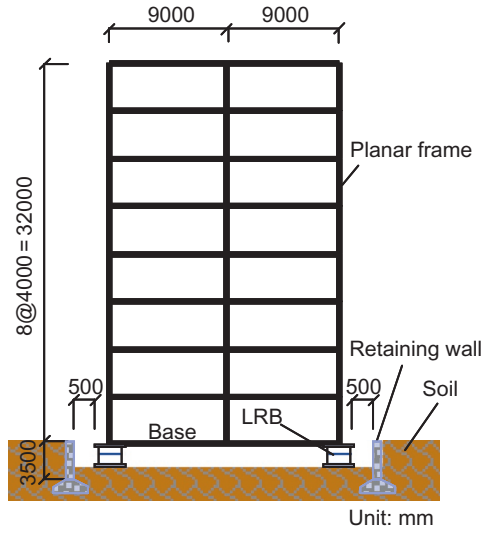

FIGURE 6.16 Dimensions of eight-story base-isolated structure.

The superstructure is an eight-story, two-span steel moment frame, which includes the foundation beams. Each story is 4 m high, and each bay is 9 m wide. Dimensions of the cross-sections used for beams and columns of the superstructure are listed in Table 6.3. The elastic modulus of the steel material was 205.8 GPa; the yielding stress was 259 MPa. The superstructure was modeled and numerically processed using ABAQUS. The base-isolation layer consists of two high damping rubber bearings (HDRBs), the tops of which are fastened at the bottom of the superstructure and the bottoms of which are fixed on the ground, as shown in Fig. 6.16. The diameter of HDRB is 1000 mm and the height is 600 mm. The total thickness of the rubber is 300 mm. The nominal horizontal stiffness of HDRB is 1.05 kN/mm, and the nominal vertical stiffness is 3350 kN/mm. Two retaining walls, one on each side of the base-isolation layer, are present. The tops of the retaining walls were aligned to the upper surface of the foundation beams. The wall height is 3.5 m. The retaining wall has a thickness of 300 mm. The clearance between the base-isolation layer and the retaining wall is 500 mm. Not only the concrete wall but also the soil behind it should be taken into account for the estimation of the reaction provided by the wall when the base-isolation layer collided with the retaining wall. In reference to [13], in which a nonlinear FEM analysis was conducted for the reinforced concrete wall with the soil, the initial stiffness was set at 93.3 kN/mm and the yielding strength was 2250 kN.

The hysteretic behavior of HDRBs was considered difficult to model numerically. The restoring force behavior of the retaining walls when they collided against the base-isolation layer was also considered to be complex. For these reasons, the base-isolation layer and retaining walls were taken to be tested.

TABLE 6.3 Cross-sections of Beams, Columns, and Mass (Unit: mm, kg)

Story	Side columns	Middle column	Beams	Mass
8	□-800 × 600 × 33	H-600 × 300 × 16 × 22	H-750 × 400 × 19 × 36	180,000
7	□-800 × 600 × 33	H-600 × 300 × 16 × 22	H-750 × 350 × 16 × 36	108,000
6	□-800 × 600 × 36	H-600 × 300 × 16 × 25	H-750 × 350 × 16 × 36	108,000
5	□-800 × 600 × 36	H-600 × 300 × 16 × 25	H-750 × 400 × 16 × 36	108,000
4	□-800 × 600 × 36	H-600 × 300 × 16 × 25	H-750 × 400 × 16 × 36	108,000
3	□-800 × 600 × 39	H-600 × 300 × 16 × 28	H-750 × 400 × 19 × 40	108,000
2	□-900 × 700 × 42	H-600 × 300 × 16 × 25	H-750 × 400 × 19 × 40	108,000
1	□-900 × 700 × 42	H-600 × 300 × 16 × 25	H-800 × 400 × 19 × 40	108,000
Base			H-1000 × 400 × 19 × 40	108,000

'□' refers to a tube section.

6.4.2 Numerical Simulation of Superstructure

The superstructure was modeled in ABAQUS using the Euler-Bernoulli beam elements. The columns and beams were divided into four and eight elements, respectively, as shown in Fig. 6.17. The model had a total of 675 DOF, which was believed to ensure more accurate responses than a story-by-story stick model commonly used in many previous substructure online hybrid tests, particularly when the superstructure would sustain inelastic action. Both the material and geometrical nonlinearities were considered. The steel material was taken to be bilinear following the kinematic hardening rule, with the parameters defined in Section 6.4.1. The superstructure was initially gravity-loaded, and the final state of the gravity analysis was taken to be the initial state of the earthquake response analysis. The target displacement assigned for each story (given by the analysis of the dynamic model) was imposed as the forced displacement at all nodes belonging to the story.

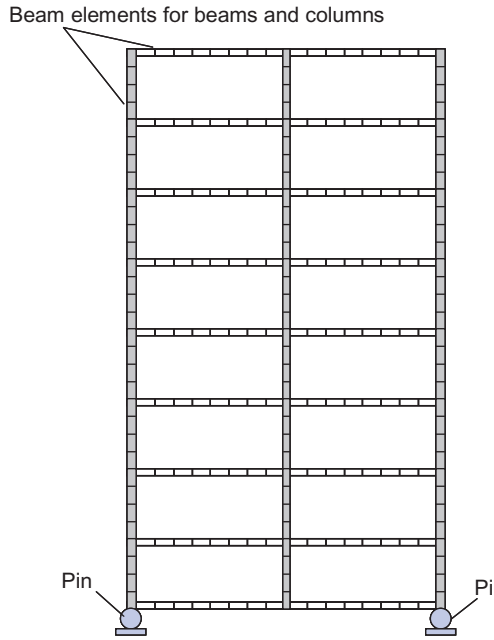

FIGURE 6.17 Numerical model of superstructure by ABAQUS.

6.4.3 Specimen for Base-Isolation Layer

Because of limitations of space and capacity of the loading devices, the diameters of the prototype base isolators were scaled down to one-fifth its size. The tested HDRBs had a diameter of 200 mm, a height of 165 mm, and a total rubber thickness of 85 mm. In reference to the displacement scale ratio of 1:5, a force scale ratio of 1:25 should be adopted. The overall hysteresis looked very similar. Discrepancy of the force, however, was notable between the prototype and tested bearings because of the difference in the aspect ratio and material stiffness between the prototype and specimen. In consideration of this difference, a force scale ratio of 1:50 instead of 1:25 was adopted. This means that the displacement imposed on the specimen was one-fifth of that calculated by the dynamic model, and the force obtained from the specimen was enlarged by 50 times for the dynamic model.

The test setup and its overview are shown in Fig. 6.18. The two-scaled HDRBs were securely fastened by high-tension bolts to the base beam at the bottom and to an inverted "T-shaped" frame on the top. Two hydraulic jacks, one horizontal and one vertical, were placed on the top of the loading frame. The horizontal jack, controlled by the displacement, was used to push or pull the specimen horizontally to the target displacement. The vertical jack was used to supply a constant vertical force that represented gravity. Detailed measurements (Fig. 6.18b) are given in Ref. [14] (see Chapter 4).

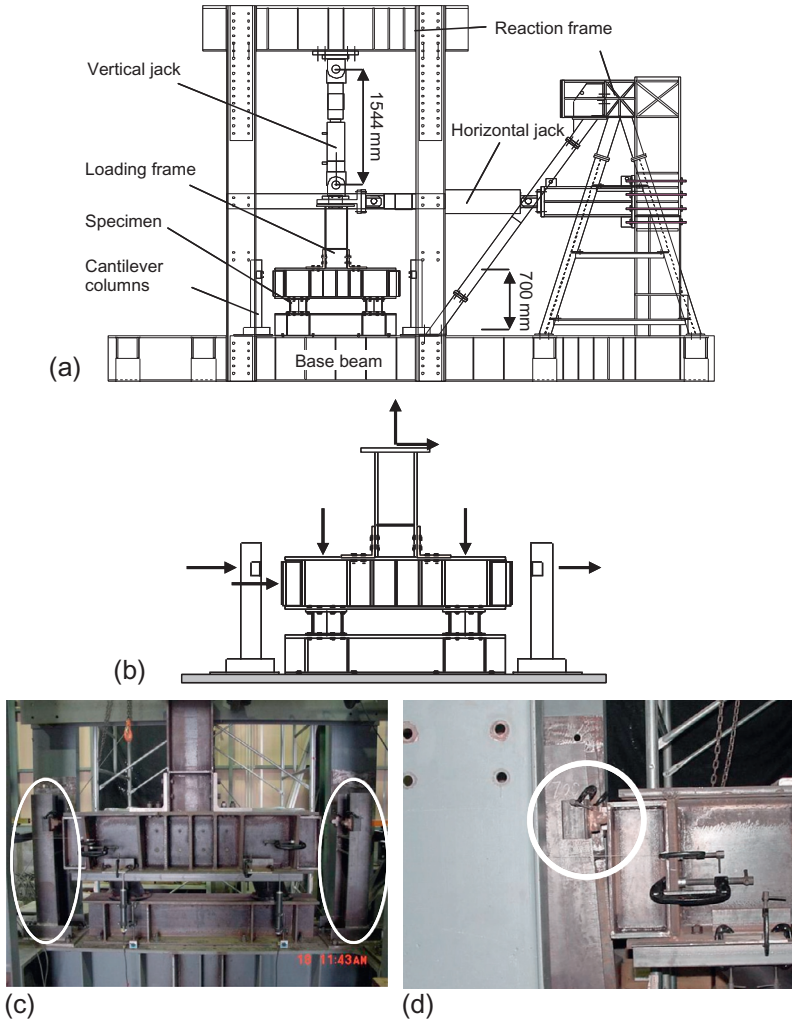

FIGURE 6.18 Overview and details of specimen. (a) Loading system, (b) measurement of specimen, (c) cantilever columns, and (d) contact with wall.

6.4.4 Specimen for Retaining Walls

The retaining walls were scaled following the scale ratio adopted for the base-isolation layer. The material properties of the concrete and soil were hard to reproduce in a scaled model. In this study, the retaining wall was mimicked by a cantilever steel column that had elastic stiffness and yield strength approximately equal to 1/10 and 1/50 those of the original retaining wall and soil [13], respectively. The cantilever steel column had a stiffness of 9.33 kN/mm, and a yielding force of 45 kN. To match these values, a steel column with a wide-

flange cross-section (H300 × 150 × 9 × 6.5) and a height of 700 mm was chosen and set to resist about the weak axis.

Two cantilever steel columns (Fig. 6.18c) were placed on each side of the loading frame. The gap between the cantilever column and the loading frame was set at 100 mm, following the adopted scale ratio of 1:5 (500 mm for the prototype building). At the height of 700 mm on each cantilever column, two pairs of special components, whose details are shown in Fig. 6.18d, were attached to ensure a point-surface contact between the base-isolation layer (the loading frame) and the retaining wall (the cantilever column).

6.4.5 Test Environment Design

The test system is shown in Fig. 6.19. This system consists of two domains: i.e., the office domain and the laboratory domain, which correspond to the numerical substructure and the experimental substructure, respectively. Two computers are placed in the office domain: one is used for the ABAQUS analysis, on which the FEM control program runs, and the other is used for data exchange, on which Proxy runs. The laboratory domain included the specimen, the loading frame, two jacks (one for horizontal loading and the other for vertical loading), two pumps, two pump controllers, two computers (one for loading control and the other for computation), one switch box, and one data logger. The computer for computation ran the main control program. The computer for control was used to transfer the target displacement or force and send it to the pump controllers. It also received feedback data from the pump controllers. Two pumps, controlled by the two pump controllers, were employed to supply oil to the two jacks. The measured displacements and reaction forces from the two jacks were fed back to both the pump controllers and the switch box.

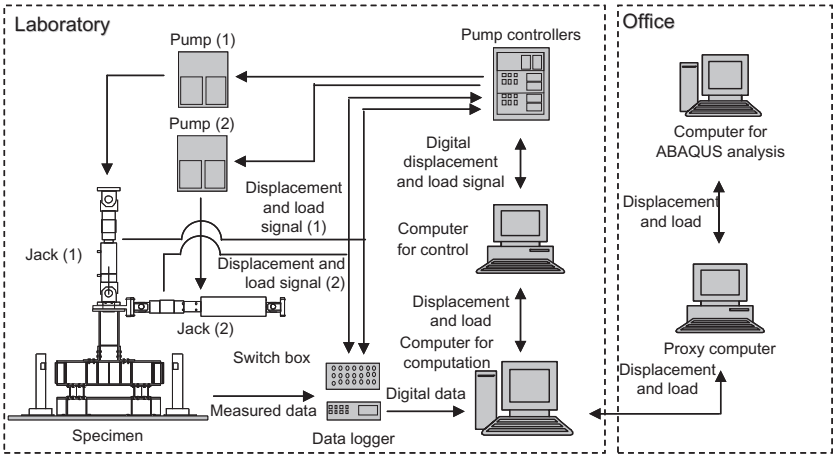

FIGURE 6.19 Distributed environment for test and analysis.

Through the switch box and data logger, the data were sent to the computer for computation. Details can be found elsewhere [15].

6.4.6 Elastic Properties of Structure

The natural periods of the overall structure and the superstructure, 9-DOF and 8-DOF dynamic models, respectively, were examined. For the overall structure, the post-yield stiffness of the base-isolation layer, 2.1 kN/mm, was adopted. When collision of the base-isolation layer with the retaining wall was considered, the stiffness of the base-isolation layer was the sum of the post-yield stiffness of the base-isolation layer and the initial stiffness of the retaining wall. The first and the highest periods of the overall structure with and without collision and of the superstructure when the base-isolation layer was assumed to be fixed are listed below. For the superstructure, the first period was 1.215 s, and the period of the eighth mode was 0.049 s. The first and the highest periods of the entire structure without collision were 4.639 s and 0.050 s, respectively. When the base-isolation layer collided with the retaining wall, the stiffness of the layer increased significantly. The first and the highest periods were 1.404 s and 0.049 s, respectively. For a given time interval, 0.01 s, the adopted explicit Newmark-β method was found to ensure stable responses in accordance with Equation (6.4).

6.4.7 Pushover Analysis

Pushover analysis was carried out for the base-fixed superstructure to examine the yield displacements and succeeding inelastic behavior. The FEM model specified in Section 6.4.2 was used and analyzed by ABAQUS. A horizontal force pattern prescribed in the Japanese seismic code for building structures [16] was adopted. Figure 6.20 shows the results of pushover analysis. The

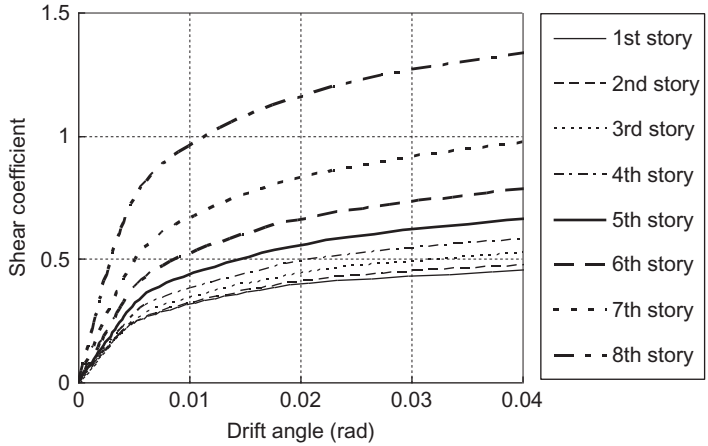

FIGURE 6.20 Pushover results of superstructure.

results were used to capture the overall damage with respect to the story drift. Each story starts yielding at a story drift angle of about 0.005 rad, and develops significant plasticity by the time the story drift angle reaches 0.01 rad.

6.4.8 Quasi-Static Test

To check the behavior of the specimen, especially at and after the contact with the surrounding retaining walls, a static loading test on the base-isolation layer was carried out prior to the online hybrid test. A cyclic loading history as shown in Fig. 6.21 was adopted for the horizontal displacement. The obtained hysteresis curve is shown in Fig. 6.22. Since the gaps between the contact surfaces

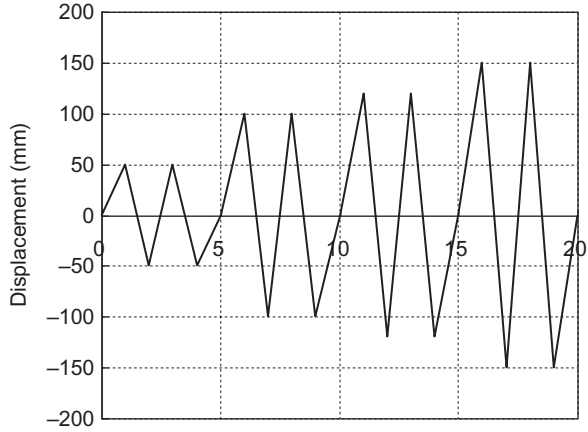

FIGURE 6.21 Loading history in quasi-static test.

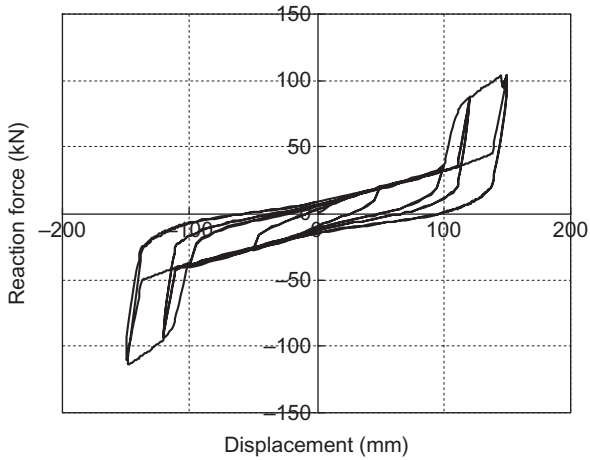

FIGURE 6.22 Hysteresis behavior of base-isolation layer obtained from quasi-static test.

were 100 mm, collision did not take place until the horizontal loading reached the fifth cycle, in which the displacement amplitude reached 125 mm. During contact, the cantilever columns were pushed 25 mm from their original upright position, but no significant plasticization occurred in the cantilever columns (Fig. 6.22). Another two rounds of loading with an amplitude of 150 mm were imposed on the specimen, and the cantilever columns exhibited significant nonlinearity. The curve shows a notable increase in the stiffness of the base isolation after collision. The yielding stiffness of the HDRBs measured from the curves was 0.114 kN/mm, and the initial stiffness of the cantilever column was 8.8 kN/mm. The corresponding design values were 0.105 and 9.33 kN/mm (the values after reduction in scale). Correlation between the test and design values was found to be reasonable.

6.4.9 Earthquake Response Simulation

An earthquake response of the eight-story base-isolated structure was simulated for 15 s of the fault-normal component of the Takatori record obtained in the 1995 Hyogoka-Nanbu (Kobe) earthquake. The input motion was doubled to ensure that the deformations of the base-isolation layer would be large enough that collision would take place. Rayleigh damping was adopted for the superstructure with damping ratios of 0.02 and 0.03 for the first and second modes, respectively.

The proposed system performed well during the entire period, without any malfunction. The maximum story drift angles of the superstructure are shown in Fig. 6.23. The figure also shows the maximum story drift angles in the absence of a collision. The collisionless response was obtained numerically by ABAQUS, in which the base-isolation layer was assumed to be bilinear.

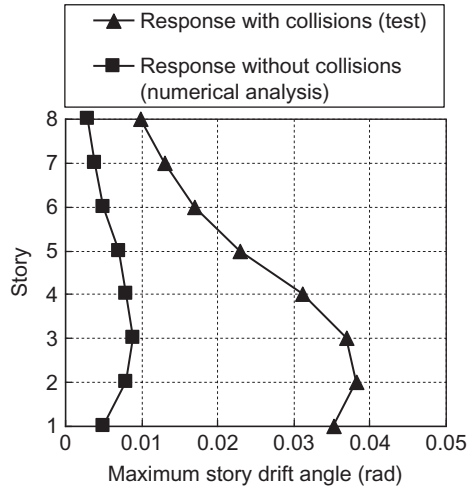

FIGURE 6.23 Maximum story drift angle in superstructure.

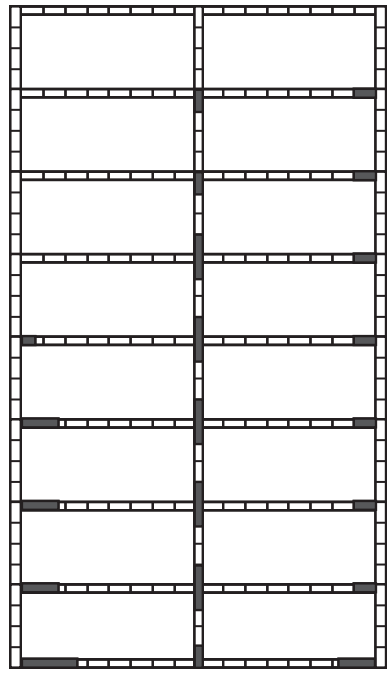

FIGURE 6.24 Yielding behavior of superstructure.

The story drift angles did not exceed 0.01 rad if no collision occurred, even for a ground motion twice as large as the original. When collision occurs, the story drift angles become significantly larger than 0.01 rad. In reference to Fig. 6.20, the beams sustained about two to four times the yield drift angle. Figure 6.24 shows the distribution of plastified ranges of beams at 6.37 s, at which the largest deformation was obtained.

The displacement response of the base-isolation layer is shown in Fig. 6.25. Collision took place three times, at 6.2 s in the positive direction and at 5.6 and 7.6 s in the negative direction. The corresponding hysteresis curves of the base-isolation layer are plotted in Fig. 6.26. It reveals that at each collision, resistance increases significantly. The cantilever column during collision in the positive direction entered a plastic range and experienced a residual displacement of 10 mm after unloading, which enlarged the gap between the specimen and the cantilever column. Because of this enlargement, further collision did not take place in the positive direction. Collision occurred twice in the negative direction, but the cantilever column behaved almost elastically.

6.4.10 Time Efficiency of Experiment

The time consumed in the test was examined. It took 7.8 h to simulate 15 s of the earthquake response, with an integration interval of 0.01 s. The times exhausted

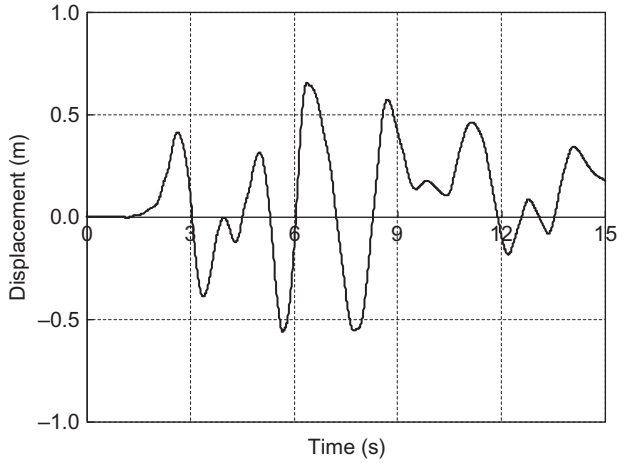

FIGURE 6.25 Response of base-isolation layer.

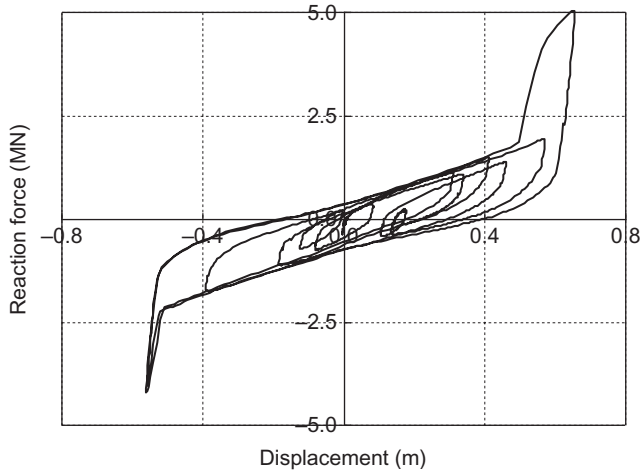

FIGURE 6.26 Hysteresis behavior of base-isolation layer.

by the experimental and numerical parts are shown in Fig. 6.27. The time used by the physical test consists of the loading time (15,135 s) and time waiting for ABAQUS analysis (12,928 s). The time consumed by the numerical analysis included the time for the ABAQUS analysis module (24,274 s), the time for feedback process module (0 s), the time for the technical delay (1500 s), and the time waiting for the test (2286 s). Since the physical test and the numerical analysis ran simultaneously, the times used by the two parts were the same. The time consumed by dynamic analysis was negligible (0 s as shown in Fig. 6.27) since the equations of motion for small DOFs were solved. The time used for the

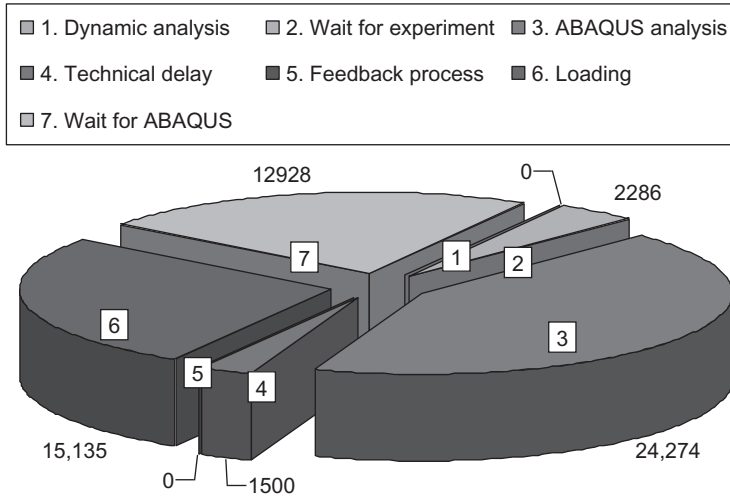

FIGURE 6.27 Time consumption of test and numerical analysis.

technical delay was set to take 1 s for each step, and therefore 1500 s were consumed in total. This was 5% of the time used in the entire simulation.

The time consumed by the ABAQUS analysis with respect to the time step is plotted in Fig. 6.28. The time used by ABAQUS analysis increases over time, because the restart analysis required more time to read the data from all of the previous steps up to the current step. The loading time was rather irregular, because it depended on the displacement increment in each step. In reference to Fig. 6.28, it took about 10 s on average for one loading step.

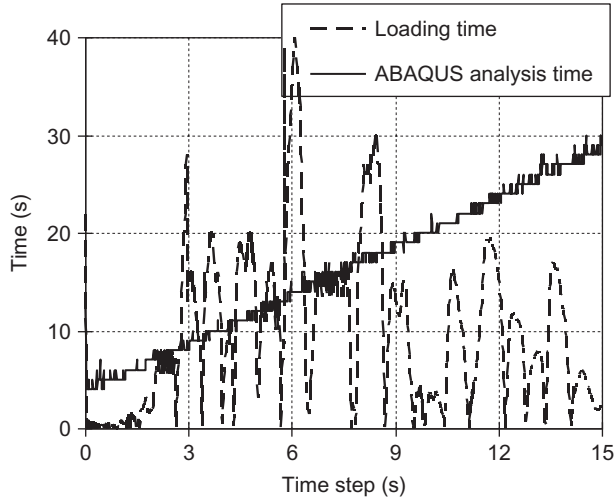

FIGURE 6.28 Time consumption for loading and ABAQUS analysis with respect to time step.

6.5 CONCLUSIONS

This chapter presented a substructure online hybrid test into which a general-purpose FEM program is incorporated. This test uses the separated-model framework, in which two models are setup for the dynamics and the static behavior of one structure, respectively. Such a program is powerful and versatile in increasing the modeling accuracy for the numerical portion, thus enhancing the applicability of the substructure online hybrid test. The decisive challenge in this new development is how to combine the test with a FEM program in which modifications of the source code are strictly prohibited. The proposed framework was demonstrated by an eight-story base-isolated structure considering the collision effect with the surrounding retaining walls. The following conclusions can be found from the studies for the proposed distributed online hybrid test system:

(1) In many structures, the structural dynamics can be represented by a fewer DOF than the structural static hysteresis. The static behavior of the structure is simulated by sophisticated FEM models and test specimens. Therefore, the models with different sophistication can be adopted for dynamics and static behavior, respectively. This separation makes the substructure online hybrid test system more versatile.

(2) The explicit Newmark method is not necessarily the only time integration algorithm that can be used for this system. Any time integration algorithm can be adopted. Implementation for the other time integration algorithm, such as implicit algorithms, may have hardware requirement. In this study, the explicit Newmark method is adopted only because of its simplicity.

(3) The high-speed data exchange scheme using a socket mechanism based on TCP/IP protocol is demonstrated to be stable and fast. In this study, transfer of data requires almost no time.

(4) The standard I/O scheme is employed for the incorporation of general-purpose FEM programs. There is no need to modify the source code of these programs, thus the system can be easily implanted for structural laboratories having different analytical tools. The key component in the use of the standard I/O only is the repeated adoption of the restart capacity offered as a standard procedure by many FEM programs.

(5) The time required for each step of the FEM analysis increased almost linearly over time, because of the longer overhead time needed for restarting with an increasing number of previous steps. A total of 7.8 h were needed to complete the test. Out of the total hours, the time needed was 4.2 h for the physical test (i.e., loading), and 6.7 h for the numerical analysis (including I/O). The loading and numerical analyses ran in parallel. The test was made quasi-statically; hence the overhead time associated with restarting was not a serious drawback in terms of the time efficiency.

(6) The response of the superstructure would increase greatly after collision takes place.

(7) The plastification is limited mainly in lower several stories, and amplification of the displacement responses decrease with the height.

(8) The collision effect would lessen in subsequent collisions, because the gap between the base-isolation layer and surrounding retaining wall would increase by previous collisions.

(9) Although the ground motion was enlarged by two times a very large motion recorded in the 1995 Kobe earthquake, collision occurred only for three times, meaning that the gap commonly adopted in Japanese design law of 500-600 mm, is generally sufficient.

REFERENCES

[1] Pinto AV, Pegon P, Magonette G, Tsionis G. Pseudo-dynamic testing of bridges using non-linear substructuring. Earthq Eng Struct Dyn 2004;33:1125–46.

[2] Pan P, Tada M, Nakashima M. Online hybrid test by internet linkage of distributed test and analysis domains. Earthq Eng Struct Dyn 2005;34:1407–25.

[3] Takahashi Y, Fenves GL. Software framework for distributed experimental-computational simulation of structural systems. Earthq Eng Struct Dyn 2006;35:267–91.

[4] ABAQUS version 6.4 documentation. USA: ABAQUS, Inc.; 2003.

[5] Wang T, Pan P, Nakashima M. Online hybrid test combining with general-purpose finite element software. J Earthq Eng Struct Dyn 2006;35:1471–88.

[6] Newmark NM. A method of computation for structural dynamics. J Am Soc Civ Eng ASCE 1959;85:67–94.

[7] Nakashima M. Part 1: Relationship between integration time interval and response stability in pseudo dynamic testing. J Struct Constr Eng 1985;353:29–36.

[8] National Science Foundation. Network for earthquake engineering simulation (NEES): consortium development, program solicitation. Report NSC01-56, USA: National Science Foundation; 2001.

[9] Snir M, Otto S, Huss-Lederman S, Walker D, Dongarra J. 2nd ed. MPI: the complete reference, vol. 1. Cambridge, MA: The MIT Press; 1998.

[10] Kernighan BW, Pike R. The UNIX programming environment. Englewood Cliffs, NJ: Prentice-Hall; 1984.

[11] Pan P, Tomofuji H, Wang T, Nakashima M, Ohsaki M, Mosalam KM. Development of peer-to-peer (P2P) internet online hybrid test system. J Earthq Eng Struct Dyn 2006;35(7):867–90.

[12] Kanao I, Nakashima M, Takehara S. Braced frame model considering buckling and fracture and its responses under near-fault strong motions. J Struct Constr Eng 2004;577:117–22 [in Japanese].

[13] Kashiwa H, Nakayasu N, Nakashima M. Response and damage of base-isolated buildings subjected to very large earthquakes. J Struct Eng 2005;51B:237–46 [in Japanese].

[14] Pan P, Nakashima M, Tomofuji H. Online hybrid test using displacement-force mixed control. Earthq Eng Struct Dyn 2005;34:869–88.

[15] Nakashima M, Akazawa T, Igarashi H. Pseudo-dynamic testing using conventional testing devices. Earthq Eng Struct Dyn 1995;24:1409–22.

[16] The Building Center of Japan. The building standard law of Japan. Tokyo, Japan, 2000.

Chapter 7

An Internet Online Hybrid Test Using Peer-to-Peer Framework

Chapter Outline

7.1 INTRODUCTION

The concept of the substructural online hybrid test has been applied by many researchers, with notable developments and applications [1–13]. Despite wide variation of details, most of those substructural online hybrid tests formulate

Development of Online Hybrid Testing. http://dx.doi.org/10.1016/B978-0-12-803378-4.00007-8

and solve the equations of motion for the entire structure and conduct the analysis and tests at the same location.

It is appealing to conduct tests in multiple locations, exchange necessary data over the Internet, and simulate the earthquake response of a very large structural system so that such a test environment will significantly increase the capacity of the substructural online hybrid test. The concept of an "Internet online hybrid test" (see Chapter 5) has been addressed over recent years [14–16], and a few real applications have been reported [17–21]. To fully take the advantage of "Internet testing" or "distributed testing," it is important to standardize and simplify the interfaces of diverse subsystems so that they can be effectively incorporated into an integrated Internet test system. Such standardization and simplification also require the subsystems to be highly encapsulated.

It is appealing to incorporate an existing finite element (FEM) program that has been developed for numerical analyses into the online hybrid test system to increase the versatility of online hybrid tests, particularly the accuracy of the behavior of the computed part (see Chapter 6). One of the solutions is to modify the source code to adjust it to the online test system [22,23] (see Chapter 5). However, this is difficult, because the program is commonly so complex that modification of the source code involves huge efforts and needs special expertise. Furthermore, most commercial FEM programs are copyright-protected, and modifications to the source code have to resolve legal issues. It would be much more effective if a highly encapsulated FEM program could be incorporated into the online test system as a black box, accessible only through standard input and output (I/O).

It is also appealing for the equations of motion to be formulated independently for each substructure and solved in parallel. Parallel computing is known to increase capacity and efficiency significantly for computation of large systems.

To this end, a new Internet online hybrid test system, a "peer-to-peer (P2P) Internet online hybrid test system," is proposed. In the system, the simulated structure is divided into multiple substructures, all substructures are equally treated, and each substructure is analyzed or tested in a subsystem. The equations of motion are not formulated for the entire structure but for each substructure separately. Substructures are treated as highly encapsulated and independent systems, and only a standard I/O is used to exchange data on the displacements and forces at the boundaries. This enables the handy incorporation of existing FEM programs. A program called "Coordinator," equipped with an iterative algorithm based on quasi-Newton iterations, is developed to achieve compatibility and equilibrium at the boundaries, and a test procedure featuring two rounds of quasi-Newton iterations is adopted to avoid iteration for the substructure being tested physically. A fast and stable solution using a socket mechanism is developed for data exchange over the Internet (see Chapter 6), and an Internet hybrid test environment is constructed.

This chapter consists of three portions. The first describes the details about the design and implementation of the system. Then, the applicability and effectiveness of the proposed system are validated by an earthquake response simulation of a base-isolated structure. In conclusion, the convergence of the P2P Internet online hybrid test system involving structural nonlinearities is investigated.

7.2 DEVELOPMENT OF P2P FRAMEWORK

7.2.1 Design of P2P Framework

As shown in Fig. 7.1, the simulated structure is divided into several substructures. Unlike the conventional online hybrid test system, the P2P Internet online hybrid test system treats all substructures equally as independent subsystems, regardless of their being tested or analyzed. The equations of motion are not formulated for the entire structure but for each substructure separately. Interactions among substructures are considered so that compatibility and equilibrium are satisfied at the boundaries. The details of the procedure are given below.

Figure 7.2 shows a case in which the simulated structure is divided into two substructures. One substructure called the "Analysis Substructure" is analyzed numerically, and the other named "Test Substructure" is tested physically. A program called "Coordinator" is developed to satisfy equilibrium and compatibility at the boundaries between the two substructures. First, Coordinator determines the displacements at the boundary and sends the displacements to the two substructures. The boundary displacements are taken to be identical in the two substructures so that comparability is satisfied all the time. For the analysis substructure, the boundary displacements are taken as the external load, and the reaction forces at the boundary are calculated by solving the

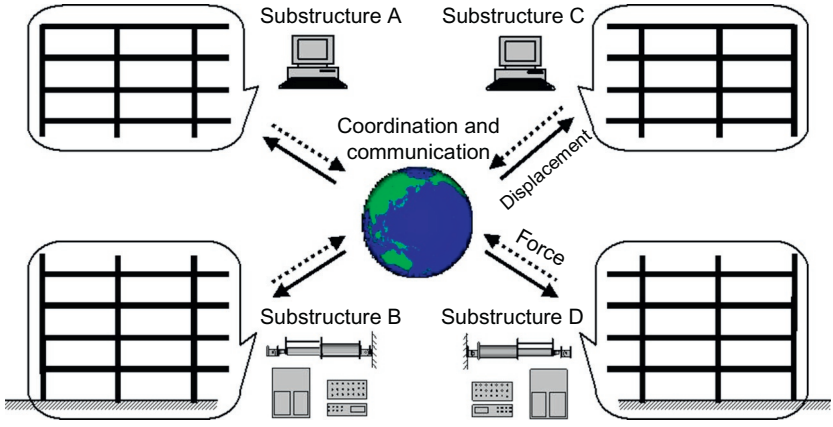

FIGURE 7.1 Concept of substructuring technique.

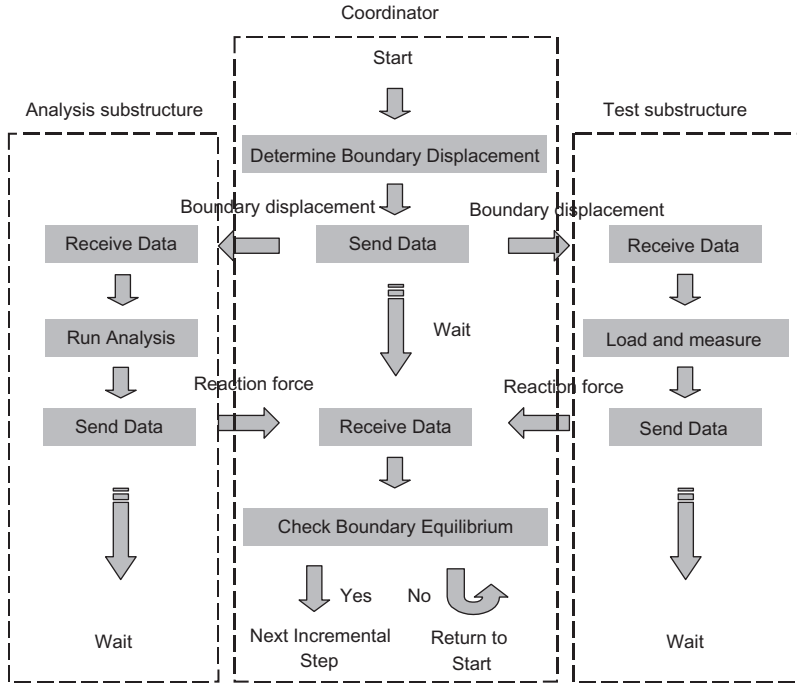

FIGURE 7.2 System design.

equations of motion. For the tested substructure, the boundary displacements are imposed on the test specimen, and the reaction forces are measured directly. These reaction forces at the boundary are sent to Coordinator, and Coordinator checks the equilibrium at the boundary. If the equilibrium is satisfied, simulation of the current step is completed. Otherwise, Coordinator specifies new boundary displacements in reference to the unbalanced forces and repeats the above procedure until the boundary equilibrium is satisfied.

In the above procedure, the equations of motion are not formulated for the entire structure but for respective substructures separately. This ensures the independence of respective substructures. In each substructure, only the boundary displacements and corresponding reaction forces are treated as I/O interfaces, while the rest is encapsulated within the substructure. Such encapsulation makes it feasible to take the substructure as a black box and use existing analysis tools [24]. Two issues have to be resolved to realize the system: (1) Coordinator should be able to determine and modify the boundary displacements. This involves trials and errors, and an effective iterative procedure has to be employed; (2) trial and error is acceptable for numerical simulation but prohibitive in physical tests. A way to overcome this dilemma should be devised. Solutions for the two issues are described below.

7.2.2 Iteration by Quasi-Newton Method

Suppose that the simulated structure is divided into two substructures as shown in Fig. 7.3. In each substructure, the nodal displacements and forces are divided into the interior (within the substructure) and exterior (at boundaries) parts, represented by subscript "in" and "ex." Symbols, "d," "F," and "R," represent displacements, forces, and reaction forces, respectively, and "1" and "2" represent Substructures 1 and 2. The equilibrium equations for each substructure are as follows:

$$\begin{bmatrix} [k_i^{\mathrm{II}}] & [k_i^{\mathrm{IE}}] \\ [k_i^{\mathrm{EI}}] & [k_i^{\mathrm{EE}}] \end{bmatrix} \begin{Bmatrix} \{d_i^{\mathrm{in}}\} \\ \{d_i^{\mathrm{ex}}\} \end{Bmatrix} = \begin{Bmatrix} \{F_i^{\mathrm{in}}\} \\ \{R_i\} \end{Bmatrix} \tag{7.1}$$

Equation (7.1) yields:

$$\{R_i\} = [k_i^{\mathrm{EI}}][k_i^{\mathrm{II}}]^{-1}\{F_i^{\mathrm{in}}\} + \left([k_i^{\mathrm{EE}}] - [k_i^{\mathrm{EI}}][k_i^{\mathrm{II}}]^{-1}[k_i^{\mathrm{IE}}]\right)\{d_i^{\mathrm{ex}}\} \tag{7.2}$$

where $i = 1$ and 2 are for Substructures 1 and 2, respectively. To satisfy the compatibility and equilibrium:

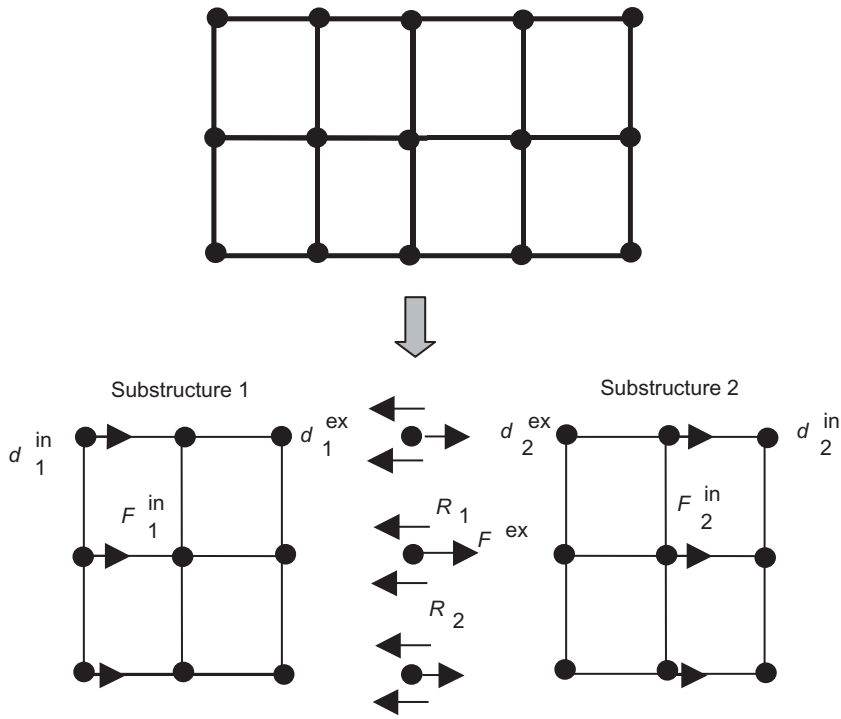

FIGURE 7.3 Outline of substructuring.

$$\left\{d_1^{\text{ex}}\right\} = \left\{d_2^{\text{ex}}\right\} = \left\{d^{\text{ex}}\right\} \tag{7.3}$$

$$\{R_1\} + \{R_2\} = \{F^{\text{ex}}\} \tag{7.4}$$

Equations (7.2)–(7.4) yield:

$$\left(\left[k_1^{\text{EE}}\right] + \left[k_2^{\text{EE}}\right] - \left[k_1^{\text{EI}}\right]\left[k_1^{\text{II}}\right]^{-1}\left[k_1^{\text{IE}}\right] - \left[k_2^{\text{EI}}\right]\left[k_2^{\text{II}}\right]^{-1}\left[k_2^{\text{IE}}\right]\right)\{d^{\text{ex}}\}$$
$$= \{F^{\text{ex}}\} - \left[k_1^{\text{EI}}\right]\left[k_1^{\text{II}}\right]^{-1}\left\{F_1^{\text{in}}\right\} - \left[k_2^{\text{EI}}\right]\left[k_2^{\text{II}}\right]^{-1}\left\{F_2^{\text{in}}\right\} \tag{7.5}$$

According to Equation (7.5), d^{ex} can be solved directly if all stiffness matrices are known. However, the P2P Internet online hybrid test system does not require the formulation of the stiffness matrices but only accepts the standard I/O, i.e., the displacement and forces at the boundaries. The following procedure was devised to overcome it.

A family of quasi-Newton methods has been developed for optimization and also for iteration in the solution of nonlinear systems [25,26]. These methods involve updating the coefficient matrix (or rather its inverse) to provide a secant approximation of the matrix. Among the family of quasi-Newton methods available, four updates are commonly used because of their advantages of global and superlinear convergence for linear problems and local and superlinear convergence for nonlinear problems. The four updates are Boryden's 1965 update for nonlinear equations, Powell's symmetric form of Broyden's update, the Davidon-Fletcher-Powell update, and the Broyden-Fletcher-Goldfarb-Shanno (BFGS) update [27]. BFGS update [28] is adopted in this study as the most popular among them. The BFGS method adopts the following procedure (Fig. 7.4):

Suppose that the equilibrium equations are given as

$$[K]\{d\} - \{P\} = 0 \tag{7.6}$$

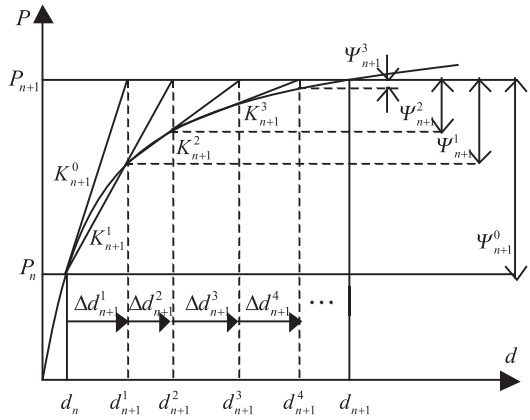

FIGURE 7.4 Quasi-Newton method.

where $[K]$ is the stiffness matrix and $\{d\}$ is the displacement vector. Define the unbalanced force vector $\{\Psi\}$ as

$$\{\Psi\} = \{P\} - [K]\{d\} \tag{7.7}$$

In each step of simulation (from step $n+1$ in this example), the equilibrium equations are solved in an incremental form:

$$\left\{\Delta\Psi^i_{n+1}\right\} = \left\{\Psi^i_{n+1}\right\} - \left\{\Psi^{i-1}_{n+1}\right\} \tag{7.8}$$

$$\left\{\Delta d^i_{n+1}\right\} = \left\{d^i_{n+1}\right\} - \left\{d^{i-1}_{n+1}\right\} \tag{7.9}$$

The stiffness matrix is formulated only in the first step. To simplify the formulation, the inverse stiffness matrix is used. In the iteration $(i-1)$ to (i), the BFGS method updates its inverse stiffness matrix $\left[K^{i-1}_{n+1}\right]^{-1}$ to $\left[K^i_{n+1}\right]^{-1}$ as

$$\left[K^i_{n+1}\right]^{-1} = \left([I] - \frac{\left\{\Delta d^i_{n+1}\right\}\left\{\Delta\Psi^i_{n+1}\right\}^T}{\left\{\Delta d^i_{n+1}\right\}^T\left\{\Delta\Psi^i_{n+1}\right\}}\right)\left[K^{i-1}_{n+1}\right]^{-1}\left([I] - \frac{\left\{\Delta\Psi^i_{n+1}\right\}\left\{\Delta d^i_{n+1}\right\}^T}{\left\{\Delta d^i_{n+1}\right\}^T\left\{\Delta\Psi^i_{n+1}\right\}}\right) + \frac{\left\{\Delta d^i_{n+1}\right\}\left\{\Delta d^i_{n+1}\right\}^T}{\left\{\Delta d^i_{n+1}\right\}^T\left\{\Delta\Psi^i_{n+1}\right\}} \tag{7.10}$$

and update the displacement vector $\left\{d^i_{n+1}\right\}$ to $\left\{d^{i+1}_{n+1}\right\}$ as

$$\left\{\Delta d^{i+1}_{n+1}\right\} = \left[K^i_{n+1}\right]^{-1}\left\{\Psi^i_{n+1}\right\} \tag{7.11}$$

$$\left\{d^{i+1}_{n+1}\right\} = \left\{d^i_{n+1}\right\} + \left\{\Delta d^{i+1}_{n+1}\right\} \tag{7.12}$$

Iteration terminates when the convergence condition is satisfied. The convergence condition is specified with TOL (a small number such as 0.001) as a convergence tolerance:

$$\left\{\Delta d^{i+1}_{n+1}\right\}^T\left\{\Psi^i_{n+1}\right\} \le \mathrm{TOL}\left\{\Delta d^i_{n+1}\right\}^T\left\{\Psi^{i-1}_{n+1}\right\} \tag{7.13}$$

The quasi-Newton method gradually builds up an approximate secant stiffness matrix using the gradient information supplied by previous iterations, so that it is able to find the point of equilibrium without the knowledge of tangential stiffness matrix at any single point. This advantage makes it very suitable for this study.

Back to the P2P Internet online hybrid test system and focusing on Equation (7.5):

$$K = \left[k^{\mathrm{EE}}_1\right] + \left[k^{\mathrm{EE}}_2\right] - \left[k^{\mathrm{EI}}_1\right]\left[k^{\mathrm{II}}_1\right]^{-1}\left[k^{\mathrm{IE}}_1\right] - \left[k^{\mathrm{EI}}_2\right]\left[k^{\mathrm{II}}_2\right]^{-1}\left[k^{\mathrm{IE}}_2\right] \tag{7.14}$$

$$P = \left\{F^{\mathrm{ex}}\right\} - \left[k^{\mathrm{EI}}_1\right]\left[k^{\mathrm{II}}_1\right]^{-1}\left\{F^{\mathrm{in}}_1\right\} - \left[k^{\mathrm{EI}}_2\right]\left[k^{\mathrm{II}}_2\right]^{-1}\left\{F^{\mathrm{in}}_2\right\} \tag{7.15}$$

the equilibrium equations at the boundaries are given as

$$[K]\{d^{\text{ex}}\} - \{P\} = 0 \tag{7.16}$$

the unbalanced force $\{\Psi\}$ is

$$\{\Psi\} = \{P\} - [K]\{d^{\text{ex}}\} = \{F^{\text{ex}}\} - (\{R_1\} + \{R_2\}) \tag{7.17}$$

Comparing Equations (7.16) and (7.17) with Equations (7.6) and (7.7), we find that the quasi-Newton iterative procedure is applicable to the iterative solution for the boundary equilibrium in the P2P Internet online hybrid test system. Note that the above formulation is for a static equilibrium. It is equally applicable to a dynamic equilibrium if the associated equations of motion are described in the form of effective static equations.

7.2.3 P2P Internet Online Hybrid Test Scheme

The quasi-Newton method involves iterations, whereas physical loading does not accept iteration because of the path-dependence [16]. To solve this dilemma, the following treatment is adopted in the P2P online hybrid test system. In each step of simulation, only a single physical loading is conducted. During the iterations within a single step of analysis, the test substructure is assumed to respond elastically, and the incremental force is taken to be the elastic stiffness, which is estimated prior to the test, multiplied by the incremental displacement (Fig. 7.5). In the single step of simulation, two rounds of quasi-Newton iteration are employed for the overall structure. The first round is to find the correct boundary displacements with respect to the assumed elastic

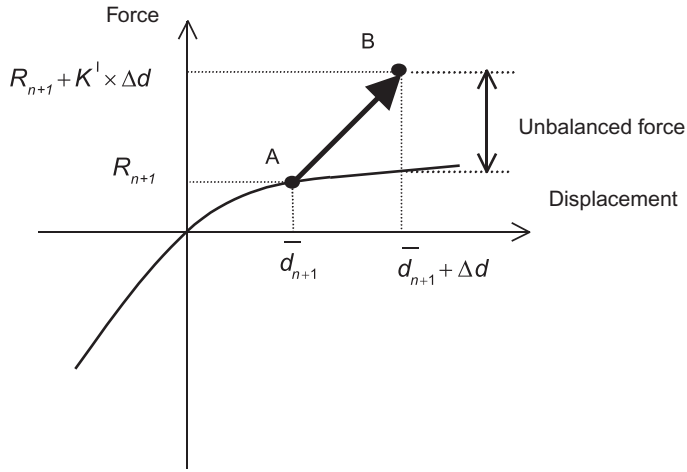

FIGURE 7.5 Compensation scheme for physically tested part.

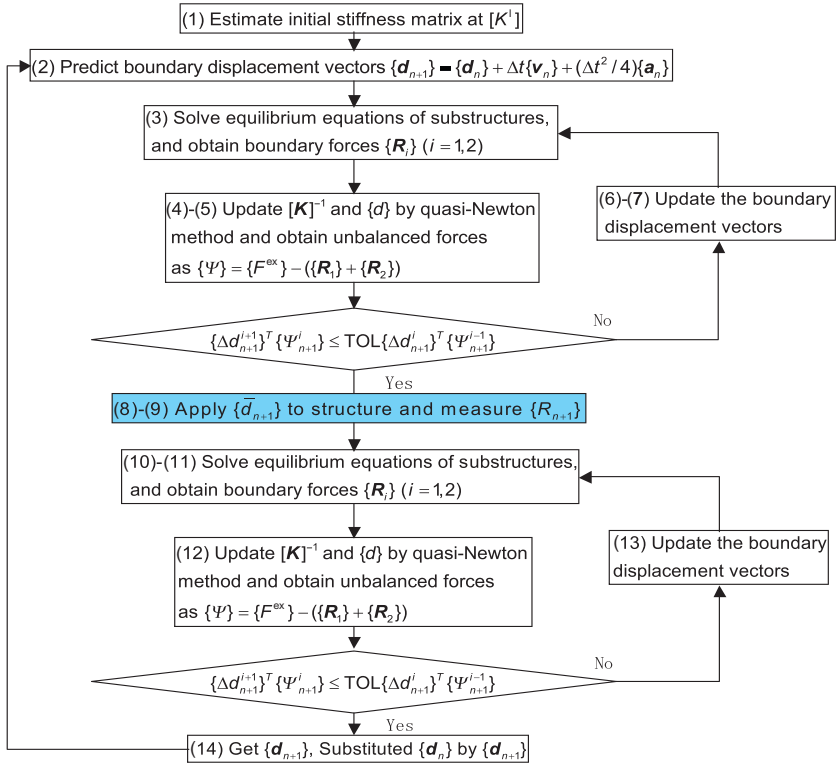

FIGURE 7.6 P2P Internet online hybrid test algorithm.

stiffness of the tested substructure. The second round is to compensate the unbalanced forces at the boundary between the tested and numerically analyzed substructure, given as a result of the elastic assumption. The procedure consists of the following steps (Fig. 7.6):

(1) Estimate the initial stiffness matrix $[K^I]$, associated with the degrees of freedom (DOFs) at the boundaries. This is defined as

$$\left[K^{\mathrm{I}}\right] = \left[k_1^{\mathrm{EE}}\right] + \left[k_2^{\mathrm{EE}}\right] - \left[k_1^{\mathrm{EI}}\right]\left[k_1^{\mathrm{II}}\right]^{-1}\left[k_1^{\mathrm{IE}}\right] - \left[k_2^{\mathrm{EI}}\right]\left[k_2^{\mathrm{II}}\right]^{-1}\left[k_2^{\mathrm{IE}}\right] \tag{7.18}$$

The initial stiffness matrix is needed particularly for starting the quasi-Newton iteration, but it does not have to be completely precise. The method for estimation adopted in this study is first to construct a matrix having the dimension equal to the number of DOFs at the boundaries, second to estimate the diagonal terms of the matrix by applying a unit displacement for each DOF, and third to assign zeros to the rest of the terms of the matrix. This step is conducted only in the very beginning of the simulation.

(2) Predict the displacement vector at the boundaries.

$$\left\{\widetilde{d}_{n+1}\right\} = \{d_n\} + \Delta t\{v_n\} + \frac{\Delta t^2}{4}\{a_n\} \tag{7.19}$$

At the beginning of the iteration, a set of trial boundary displacements needs to be determined. One way is to use the displacements obtained from the previous step. In this study, a set of displacements expressed by Equation (7.19) is used. These are the predictor displacements used in prediction-correction methods, and they are expected to be closer to the true displacements in the next steps, hence reducing the number of iterations.

(3) Apply the predicted boundary displacements to the associated substructures as externally applied forced displacements, and obtain the corresponding reaction forces at the boundaries $\left\{\widetilde{R}_{n+1}\right\}$.

(4) Calculate the unbalanced force vector $\left\{\widetilde{\Psi}^i_{n+1}\right\}$ at the boundaries from the reaction forces and external forces. Here i indicates ith iteration.

(5) Update the stiffness matrix using the BFGS procedure:

$$\left[K^i_{n+1}\right]^{-1} = \left([I] - \frac{\left\{\Delta\widetilde{d}^i_{n+1}\right\}\left\{\Delta\widetilde{\Psi}^i_{n+1}\right\}^T}{\left\{\Delta\widetilde{d}^i_{n+1}\right\}^T\left\{\Delta\widetilde{\Psi}^i_{n+1}\right\}}\right)\left[K^{i-1}_{n+1}\right]^{-1}\left([I] - \frac{\left\{\Delta\widetilde{\Psi}^i_{n+1}\right\}\left\{\Delta\widetilde{d}^i_{n+1}\right\}^T}{\left\{\Delta\widetilde{d}^i_{n+1}\right\}^T\left\{\Delta\widetilde{\Psi}^i_{n+1}\right\}}\right) + \frac{\left\{\Delta\widetilde{d}^i_{n+1}\right\}\left\{\Delta\widetilde{d}^i_{n+1}\right\}^T}{\left\{\Delta\widetilde{d}^i_{n+1}\right\}^T\left\{\Delta\widetilde{\Psi}^i_{n+1}\right\}} \tag{7.20}$$

(6) Update the boundary displacement vector:

$$\left\{\Delta\widetilde{d}^{i+1}_{n+1}\right\} = \left[K^i_{n+1}\right]^{-1}\left\{\widetilde{\Psi}^i_{n+1}\right\} \tag{7.21}$$

(7) Repeat Steps (3)-(6) with the new predictor displacement vector until the convergence is attained:

$$\{\bar{d}_{n+1}\} = \left\{\widetilde{d}_{n+1}\right\} + \sum_i \left\{\Delta\widetilde{d}^{i+1}_{n+1}\right\} \tag{7.22}$$

(8) Calculate the total predicator displacement vector, load the tested substructure to the associated predictor displacements, measure the reaction forces, and update the reaction force vector from $\left\{\widetilde{R}_{n+1}\right\}$ to $\{\bar{R}_{n+1}\}$.

(9) Refresh the unbalanced force vector $\left\{\overline{\Psi}^k_{n+1}\right\}$ based on the new reaction forces and external forces at the boundaries. Here k indicates that iterations in Steps (3)-(6) are carried out k times. At Step (7), the unbalanced

forces disappear once following the execution of quasi-Newton iterations, but $\left\{\overline{\Psi}_{n+1}^{k}\right\}$ become nonzero again because of the nonlinearity of the tested substructure (Fig. 7.5). This generates new unbalanced forces. The unbalanced forces are corrected in Steps (10)-(12).

(10) Refresh the boundary displacement vector based on the new unbalanced forces and update the stiffness matrix $\left[K_{n+1}^{k}\right]$ obtained at Step (7):

$$\left\{\Delta\bar{d}_{n+1}^{j+1}\right\}=\left[K_{n+1}^{j}\right]^{-1}\left\{\overline{\Psi}^{j}{}_{n+1}\right\} \tag{7.23}$$

(11) Apply the boundary displacements to the corresponding substructures as externally applied forced displacements, and calculate the corresponding reaction forces. For the tested substructure, the reaction forces are calculated again using the elastic stiffness:

$$\bar{R}_{n+1}=\bar{R}_{n+1}+\left[K^{\mathrm{I}}\right]\Delta\bar{d}_{n+1}^{j+1} \tag{7.24}$$

(12) Update the stiffness matrix again using the BFGS procedure:

$$\begin{aligned}\left[K_{n+1}^{j+1}\right]^{-1}=&\left([I]-\frac{\left\{\Delta\bar{d}_{n+1}^{j+1}\right\}\left\{\Delta\overline{\Psi}^{j+1}{}_{n+1}\right\}^{T}}{\left\{\Delta\bar{d}_{n+1}^{j+1}\right\}^{T}\left\{\Delta\overline{\Psi}^{j+1}{}_{n+1}\right\}}\right)\left[K_{n+1}^{j}\right]^{-1}\left([I]-\frac{\left\{\Delta\overline{\Psi}^{j+1}{}_{n+1}\right\}\left\{\Delta\bar{d}_{n+1}^{j+1}\right\}^{T}}{\left\{\Delta\bar{d}_{n+1}^{j+1}\right\}^{T}\left\{\Delta\overline{\Psi}^{j+1}{}_{n+1}\right\}}\right)\\&+\frac{\left\{\Delta\bar{d}_{n+1}^{j+1}\right\}\left\{\Delta\bar{d}_{n+1}^{j+1}\right\}^{T}}{\left\{\Delta\bar{d}_{n+1}^{j+1}\right\}^{T}\left\{\Delta\overline{\Psi}^{j+1}{}_{n+1}\right\}}\end{aligned} \tag{7.25}$$

(13) Repeat Steps (10)-(12) until the convergence condition is satisfied, and obtain the final displacement vector:

$$\{d_{n+1}\}=\left\{\bar{d}_{n+1}\right\}+\sum_{j}\left\{\Delta\bar{d}_{n+1}^{j+1}\right\} \tag{7.26}$$

(14) Continue to the next step of simulation.

7.2.4 Incorporation of General-Purpose FEM Program

In this system, encapsulation of numerical substructures makes it feasible to take each substructure as a black box and use an existing FEM code. The key for this application is the restart capability [29,30]. Suppose the equilibrium state of the $(n-1)$th step analysis has already been achieved. In the nth step analysis, each numerical substructure first accepts one trial displacement set (d_n^1) from Coordinator and take the displacements as the boundary. Then, the analysis of this substructure restarts from the final state of the previous step, and the corresponding reactional force is calculated. This restart is called

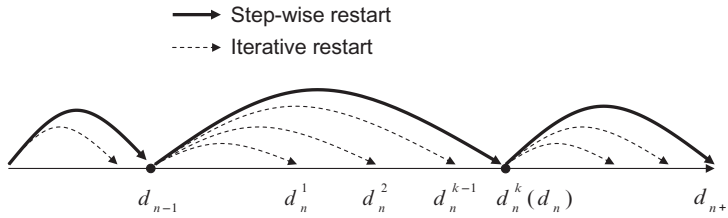

FIGURE 7.7 Restart capability of general-purpose finite element program.

"iterative restart," as shown by dashed lines in Fig. 7.7. The reactional force is then sent back to Coordinator, but may not satisfy equilibrium. Coordinator generates the next trial displacement set (d_n^2). The "iterative restart" is carried out for each substructure correspondingly, until the equilibrium at the boundaries is satisfied, and the final state of the current step is achieved. The last "iterative restart" with trial displacement set d_n^k calculates the final state of each substructure and provides information (d_n, v_n, a_n) for the next step analysis. Therefore, it is a successive procedure and called the "step-wise restart," as shown by solid lines in Fig. 7.7.

7.3 VERIFICATION TEST OF BASE-ISOLATED STRUCTURE

7.3.1 Structure Model and Substructuring

The earthquake responses of a base-isolated structure subjected to ground motions were simulated using the proposed P2P online hybrid test system. The example structure, which resembles a base-isolated structure constructed in downtown Tokyo, is shown in Fig. 7.8a. It is an eight-story and two-span by six-span steel moment frame isolated by high damping rubber bearings

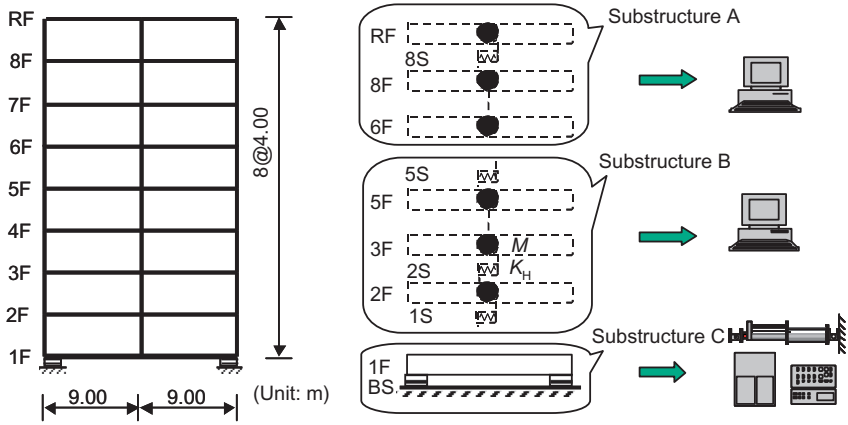

FIGURE 7.8 Base-isolated structure model: (a) basic dimensions; (b) division into substructures.

(HDRBs). In the simulation, it was treated as a planar structure. As shown in Fig. 7.8b, the substructuring technique is employed, and the entire structure is divided into three substructures, i.e., Substructures A, B, and C. Substructures A and B, which formed the superstructure (the steel moment frame), were assigned as the computed parts, and Substructure C, which was the base-isolation layer (consisting of two HDRBs), was assigned as the tested part. Here the superstructure was intentionally divided into two substructures to demonstrate the capacity of the P2P online hybrid test system to handle multiple computed substructures in a parallel mode, which is expected to increase the speed of the system particularly when the computed substructures are complicated. The superstructure was modeled as a linear spring-mass system, with one mass per floor and one spring per story, and analyzed as Substructures A and B. The base-isolation layer was modeled as a single degree of freedom (SDOF) system with a mass and a spring, and tested as Substructure C. The fundamental periods of the entire structure in the base-fixed condition and base-isolated condition (with respect to the stiffness of the base-isolation layer that corresponded to a 150% strain in the rubber) were 1.26 s and 3.76 s, respectively. Details on the mass and stiffness properties assigned to the structure and the properties of the base-isolation layer are given elsewhere [31] (see Chapter 4).

The equations of motion were not formulated for the overall base-isolated structure but formulated and solved for each substructure. Substructures A and B were analyzed and Substructure C was tested. The Newmark-β method with $\beta = 1/4$ and $\gamma = 1/2$ was adopted for solving the equations of motion of each substructure as shown in Equations (7.27)–(7.30). Equation (7.27) indicates the basic equations of motion. This equation is further rewritten as Equation (7.28) using equivalent stiffness $[\bar{K}]$ and forces $[\bar{f}]$, which are given in Equations (7.29) and (7.30), respectively. In the equations, $[K]$, $[M]$, and $[C]$ are the stiffness matrix, mass matrix, and damping matrix, and $\{d\}$, $\{v\}$, $\{a\}$ are the displacement, velocity, acceleration vector, with all quantities defined for each substructure.

$$[M]\{a\}_{n+1} + [C]\{v\}_{n+1} + [K]\{d\}_{n+1} = -[M]\{1\}\ddot{u}_g \tag{7.27}$$

$$[\bar{K}]\{d\}_{n+1} = \{\bar{f}\}_{n+1} \tag{7.28}$$

$$[\bar{K}] = [K] + \frac{\gamma}{\beta\Delta t}[C] + \frac{1}{\beta\Delta t^2}[M] \tag{7.29}$$

$$\{\bar{f}\}_{n+1} = -[M]\{1\}\ddot{u}_g + [C]\left\{\frac{\gamma}{\beta\Delta t}\{d\}_n + \left(\frac{\gamma}{\beta} - 1\right)\{v\}_n + \Delta t\left(\frac{\gamma}{2\beta} - 1\right)\{a\}_n\right\} + [M]\left\{\frac{1}{\beta\Delta t^2}\{d\}_n + \frac{1}{\beta\Delta t}\{v\}_n + \left(\frac{1}{2\beta} - 1\right)\{a\}_n\right\} \tag{7.30}$$

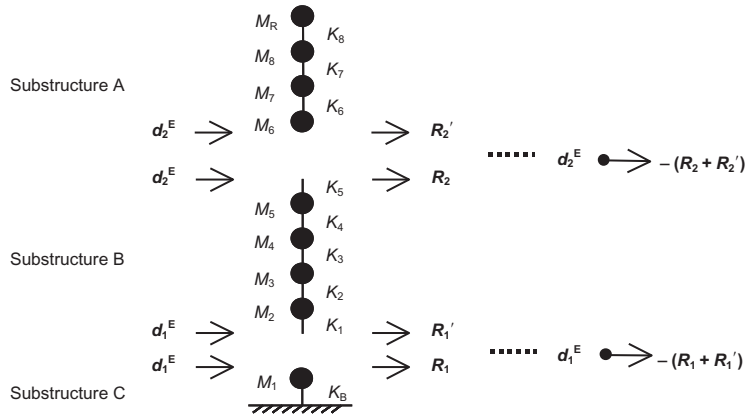

FIGURE 7.9 Scheme of substructuring.

In reference to Fig. 7.9, Substructure A (consisting of masses M_6 to M_R and springs of K_6 to K_8), Substructure B (consisting of masses M_2 to M_5 and springs of K_1 to K_5), and Substructure C (consisting of a mass M_1 and a spring of K_B) were analyzed or tested separately. In this study, the superstructure including Substructures A and B were assumed to respond elastically, and viscous damping was neglected in all substructures.

Substructure A is a 4-DOF system, Substructure B is a 6-DOF system, and Substructure C, which represents the base-isolation layer, is a SDOF system. The equations of motion are solved in a static form using the equivalent stiffness and forces (refer to Equations 7.29 and 7.30). Equation (7.31) has to be satisfied to guarantee the compatibility at boundaries:

$$\begin{Bmatrix} d_1^{\mathrm{E}} \\ d_2^{\mathrm{E}} \end{Bmatrix} = \begin{Bmatrix} d_1 \\ d_6 \end{Bmatrix} \tag{7.31}$$

Equation (7.32) is to satisfy the equilibrium at the boundaries:

$$K_{\mathrm{E}} \Delta d_{\mathrm{E}} = \Psi = \begin{Bmatrix} -\left(R_1 + R_1'\right) \\ -\left(R_2 + R_2'\right) \end{Bmatrix} = 0 \tag{7.32}$$

Note that the external force is zero in this particular example. Displacements d_1^{E} and d_2^{E} were applied to the corresponding substructures in reference to Equation (7.31), the reaction forces $R_1, R_2, R_1{}'$, and $R_2{}'$ were computed or measured from the corresponding substructures, and Equation (7.32) was used to check the equilibrium at the boundaries. The Coordinator program was in charge of these tasks. In this particular application of the P2P Internet online hybrid test system, the Coordinator program was implemented in the subsystem that operated the physical test of Substructure C. Accordingly, data exchange over the Internet between the Coordinator program and Substructure C was not needed.

7.3.2 Internet Online Hybrid Test Environment

Figure 7.10 shows the P2P Internet online hybrid test environment developed at Kyoto University in Japan. Substructures A and B were numerically simulated by two separate PCs placed in a students' office. The Internet connection of the students' office belongs to a network in the Kyoto University Network named KUINS III. KUINS III features high speed and high security, with a strict firewall directly managed by the University. Substructure C was tested physically by an online testing system in a test laboratory. The Coordinator program was also run in the laboratory. The Internet connection of the laboratory also belongs to KUINS III. The Internet connection of the students' office and that of the laboratory, however, belong to different subnets. Direct connection is strictly prohibited between subnets within KUINS III. Because of the firewall, data exchange through proxy, as described before, was adopted. A proxy program was installed in a computer placed in another office, whose Internet connection belongs to another type of Kyoto University Network named KUINS II. KUINS II is not administered by the university but by individual researchers. The computer connected to KUINS II was configured to accept TCP/IP connections from KUINS III subnets through specific ports. The proxy program set up TCP/IP connections with the analysis programs of substructures A and B, and the program that operates Coordinator and the physical test of Substructure C. The proxy program forwards the boundary displacements from Coordinator to Substructures B and C, and passes the forces from Substructure B and C to Coordinator. Information about displacements and forces is an encoded byte stream when passing the proxy program, and the proxy program does not decode the byte stream,

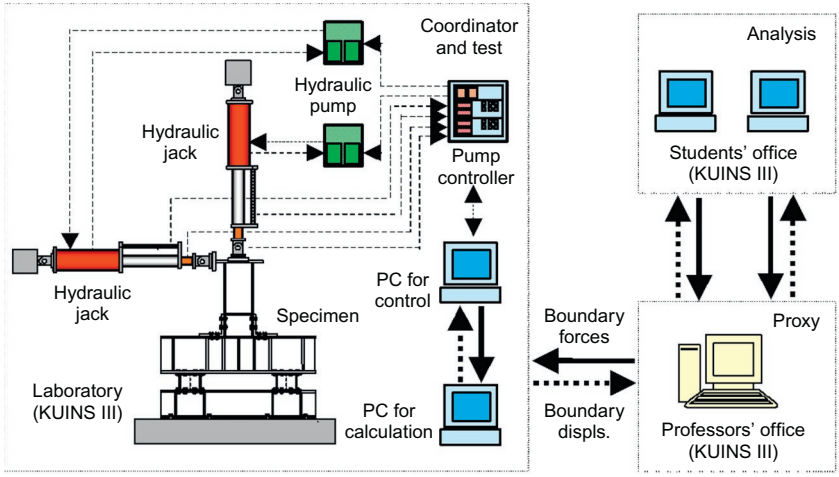

FIGURE 7.10 Internet online hybrid test environment.

for time efficiency. Note that data exchange between Coordinator and Substructure C was not needed since they were run in the same computer.

The online loading system includes two quasi-static loading jacks, two hydraulic pump systems, two pump controllers, and two PCs, i.e., "PC for control" and "PC for operation." "Coordinator" and test control programs were installed in "PC for operation." "PC for operation" was connected to "PC for control," which supervised and controlled the loading facilities such as jacks and controllers. The online loading system was used successfully for several online hybrid tests [31–33].

7.3.3 Test Setup and Test Specimen

The test setup, shown in Fig. 7.11a and b, includes the loading frame, two jacks (one for horizontal loading and the other for vertical loading), and the test specimen. The test specimen featured two identical HDRBs securely fastened by high-tension bolts to the base steel beam at the bottom and to an inverted T-shaped loading frame at the top. The base steel beam was tied down to the loading frame, and the two jacks were attached at the top of the inverted T-shaped loading frame. Both the base steel beam and the T-shaped loading frame were designed to be rigid enough relative to the rubber bearings. Dimension and measurement details are given by Pan et al. [31]. The vertical jack applied to the rubber bearings was a constant vertical force equal to the gravity, and the horizontal jack was displacement-controlled in accordance with the displacement demanded by the online test.

Although only the horizontal interaction between the superstructure and base-isolation layer was considered explicitly in the model, the effects of overturning moment on the base-isolation layer were partially included in the physical test. This is because, in the loading system used in the test, the horizontal jack through the inverted T-shaped loading frame applied overturning moment automatically in addition to the horizontal force. This corresponded to the

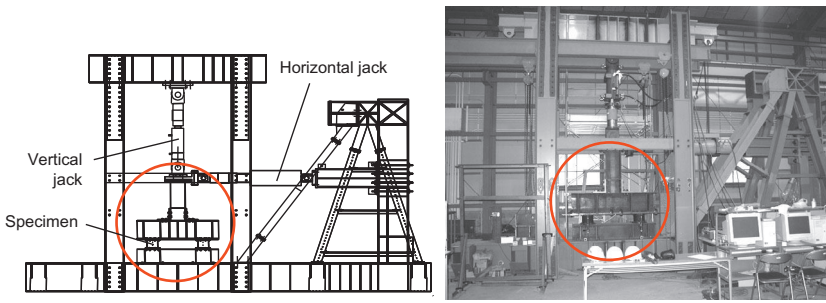

FIGURE 7.11 Test setup: (a) test specimen and loading frame, (b) view of test setup.

assumption that the location of the center of horizontal forces applied to the superstructure remained unchanged.

Scale ratios of 1:4 and 1:40 were adopted for the horizontal displacement and horizontal force, respectively, based on comparison of the cross-sectional area, the total rubber thickness, the shape factors, and the rubber's shear modulus between the prototype HDRBs and the tested HDRBs. In other words, one-fourth of the displacement predicted by solving the equations of motion of the base-isolated structure was applied to the test specimen, and the force measured by the test specimen was increased by 40 times when inserted into the solution of the equations of motion.

7.3.4 Test Results

A physical Internet online hybrid test was carried out to demonstrate the effectiveness of the P2P Internet online hybrid test system. To calibrate the accuracy of the test results, a physical online hybrid test using the conventional substructuring technique was also conducted. In the conventional online hybrid test, the elastic superstructure was simulated numerically, the base-isolation layer was tested physically, and the equations of motion were formulated and solved for the entire structure by a single program having an operator splitting integration method [34,35]. The initial stiffness of the specimen is 5.25 kN/mm, which was measured prior to the test. The fault-normal component of the JMA Kobe record [36] was used for both tests, and the integration time interval was taken to be 0.01 s. Both tests were conducted successfully, and the test results are shown in Fig. 7.12.

The horizontal force versus displacement curves and displacement time histories of the base-isolation layer are plotted in Fig. 7.12a and b. The solid lines represent the results obtained from the online hybrid test using the conventional substructuring technique, and the dashed lines are the results obtained from the P2P Internet online hybrid test. The two tests produced very similar results with a difference of the maximum displacement not $>5\%$. The same HDRBs were used for both tests on different days, and the discrepancy shown in Fig. 7.12 was attributed to a slight difference in hysteretic behavior of the HDRBs tested on different days. To demonstrate the validity of this attribution, two numerical analyses were conducted. In the numerical simulation, all the conditions were identical with the corresponding P2P Internet online hybrid tests except that the base-isolation layer was also numerically modeled instead of being physically tested. The base-isolation layer was modeled as bilinear. Figure 7.13a and b shows the horizontal force versus displacement and displacement time histories of the base-isolation layer. The solid and dashed lines represent the results obtained from the conventional online hybrid test method and P2P Internet online hybrid test system. The results obtained from the two numerical analyses are identical, indicating that the P2P Internet online hybrid test system is accurate.

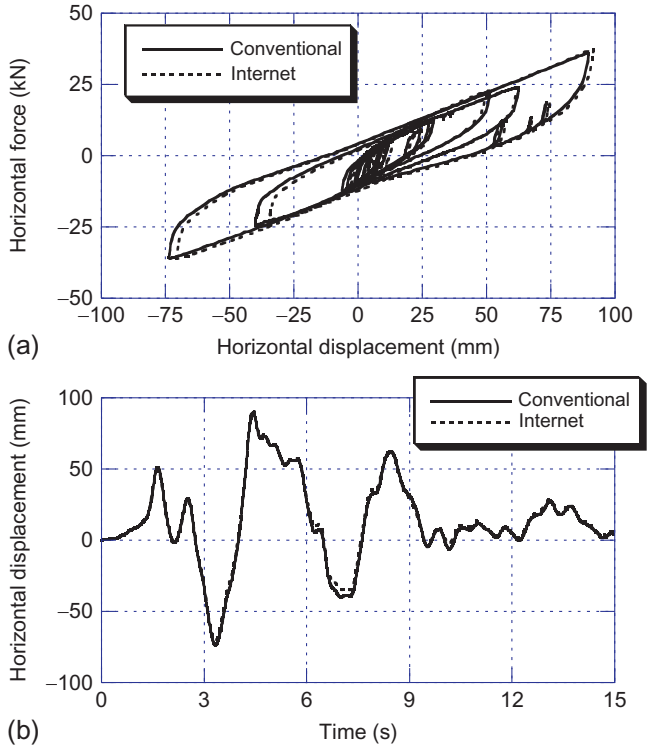

FIGURE 7.12 Responses of two online tests: (a) hysteresis curves, (b) displacement histories.

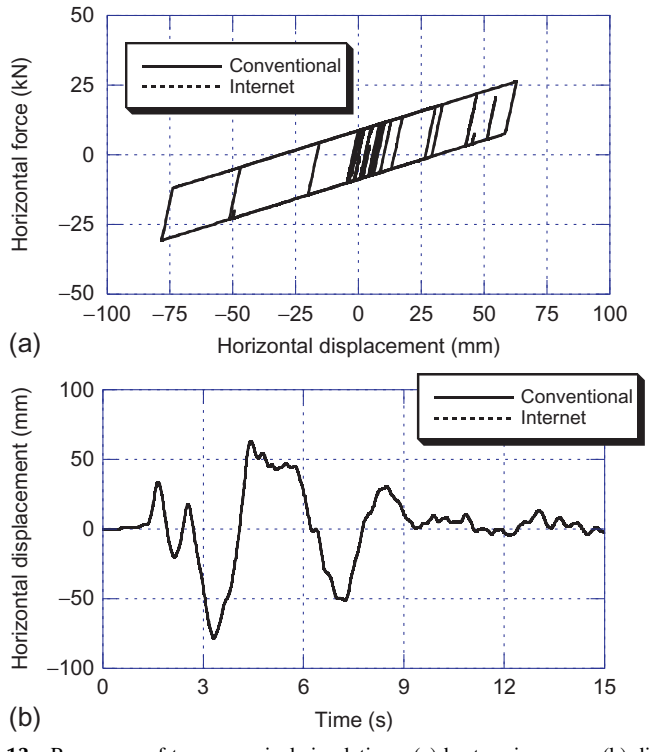

FIGURE 7.13 Responses of two numerical simulations: (a) hysteresis curves, (b) displacement histories.

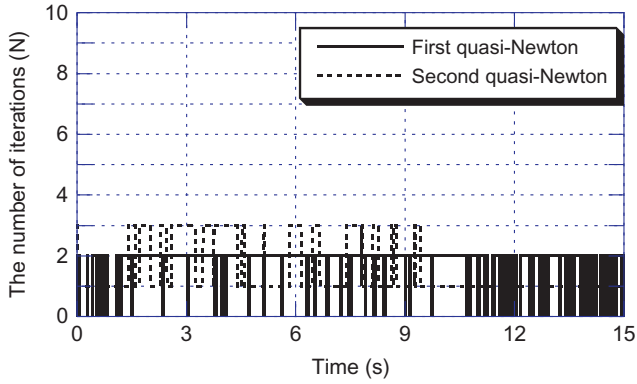

FIGURE 7.14 Number of iterations.

The number of iterations needed to achieve the equilibrium at the boundaries was evaluated. As indicated in the previous section, two rounds of quasi-Newton iterations were executed. The first round of quasi-Newton iteration was to find the correct boundary displacements, with the tested substructure taken to be linear and having the assumed elastic stiffness, and the second round was to compensate for the unbalanced forces generated as a result of the elastic assumption. As shown in Fig. 7.14, the numbers of the first round of quasi-Newton iterations (solid lines) are not >2. Zero iteration means that the predictor displacements were so correct that they satisfied the equilibrium without any modification. The numbers of the second round of quasi-Newton iterations (dashed lines) are about 1 in the first 2 s, about 3 in 3-9 s, and about 1 in the last few seconds. These numbers occurred primarily because the displacement responses were rather small in the first and last few seconds, and were relatively large between 3 and 9 s. Large responses corresponded to significant plasticity, and thus generated relatively large unbalanced forces, which were to be compensated for in the second round of quasi-Newton iteration.

The time consumed for the test was also evaluated. Figure 7.15a and b shows the time histories of the times consumed in loading and Internet communication, respectively. Figure 7.15c compares the time histories of cumulative times consumed for loading, communication, and total. The time consumed by calculation was negligible because the model was very small, so it was discounted. The time consumed for loading was a function of the command displacement. It was longer when the response was large. On average, the loading time was about 8.9 s for one step. The time consumed for Internet communication was not >0.1 s except for a few pulses. According to Fig. 7.15c, the time consumed for loading constituted more than 95% of the time consumed for the total test. This is obviously because of fast Internet communication and relatively slow quasi-static loading.

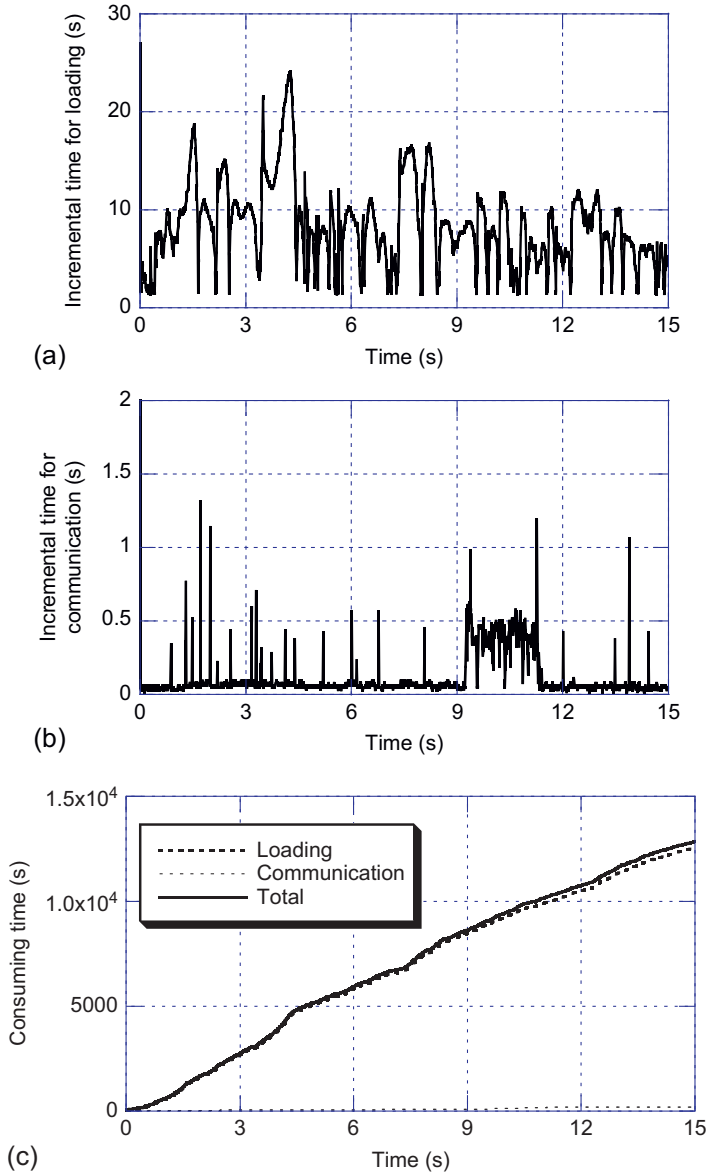

FIGURE 7.15 Time consumed in test: (a) time history of time consumed for loading, (b) time history of time consumed for Internet communication, (c) comparison between time consumed for loading, Internet communication, and total test.

Figure 7.16 shows the accuracy of the test control. Figure 7.16a compares the time histories of the target and measured displacements, and Fig. 7.16b plots the difference between the two displacements. The tolerance of the displacement control error was set at ± 0.06 mm. According to the figure, the control

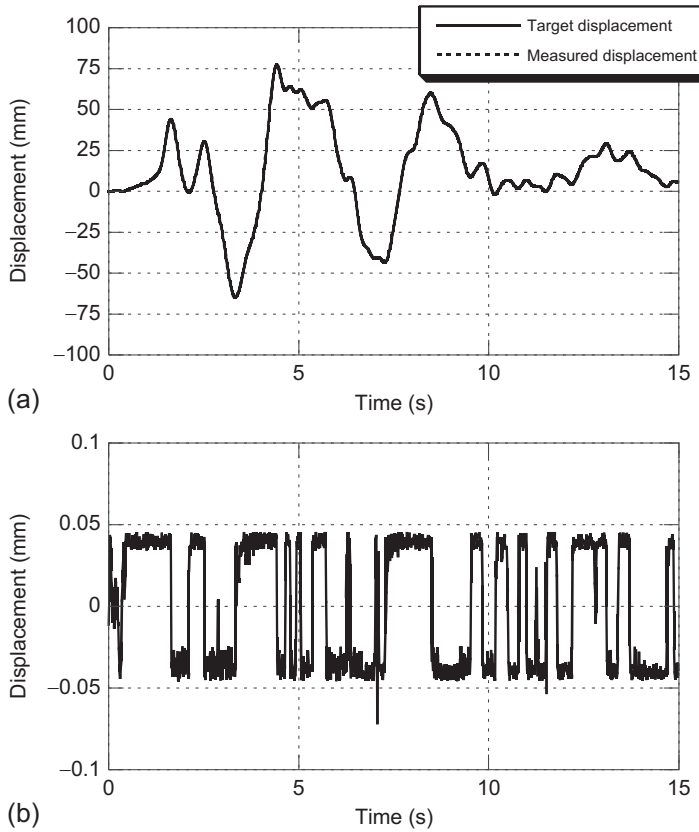

FIGURE 7.16 Accuracy of test control: (a) time histories of target and measured displacements, (b) time history of the difference between target displacement and measured displacement.

errors are always smaller than ± 0.05 mm, demonstrating that the test was controlled accurately.

7.4 CONVERGENCE CRITERIA ON P2P INTERNET ONLINE HYBRID TEST SYSTEM INVOLVING STRUCTURAL NONLINEARITIES

7.4.1 Introduction

In Section 7.3, the P2P online hybrid test system was applied for the seismic simulation of a base-isolated structure where only the tested base isolation-layer involved great nonlinearity, while the numerical substructures stayed within elastic range. The convergence is relatively easy because the nonlinearity to be handled by the quasi-Newton procedure is significantly reduced

by the linear implementation of the numerical substructures. The P2P online hybrid test system, however, is more general than this application since the linear assumption is not mandatory in the system formulation. The convergence of the system should be investigated especially when nonlinearity is considered for all substructures. In the P2P Internet online hybrid test system, the convergence is dominated by the quasi-Newton procedure. Therefore, the convergence is guaranteed unless the effective static stiffness matrix becomes negative definite, which is not considered here. The convergence speed is the main concern to be examined, because nonlinearity may result in a large number of iterations and the system becomes inefficient. Note that it is the convergence of the quasi-Newton procedure to be investigated, not the two-round predicting-correcting test procedure.

Considering the procedure used for the P2P Internet online hybrid test system, the following factors may affect the convergence speed greatly: (1) the convergence criteria and tolerance adopted; (2) type of divisions into substructures; (3) number of DOF on the boundaries; and (4) initial stiffness prescribed for the first quasi-Newton procedure. The effects of the four factors are examined and summarized in the following sections. A mass-spring model with 9-DOF is employed for these examinations. The Ramburg-Osgood (RO) function, which employs two parameters, i.e., α and γ, to define the shape of the function, is adopted to mimic the nonlinearity of each story. The story mass and stiffness definition are listed in Table 7.1.

TABLE 7.1 Materials Considered for Convergence Speed Examination

Story	Mass (ton)	Initial stiffness (kN/mm)	Yielding strength (kN)	α	γ
T9	180	65.4	654	0.25	5
T8	108	72.0	720	0.25	5
T7	108	75.6	756	0.25	5
T6	108	77.8	778	0.25	5
T5	108	80.7	807	0.25	5
T4	108	86.8	868	0.25	5
T3	108	102	1020	0.25	5
T2	108	148	1480	0.25	5
T1	108	200	2000	0.25	5

7.4.2 Investigation of Convergence Criteria and Tolerance

Convergence criteria need to be established to judge whether the iterative quasi-Newton procedure converges within a preset tolerance or not. In this study, the unbalanced force is the most straightforward criterion, but numerical difficulties may arise for stiff structures. To control the trial displacements is a candidate, which, however, may require different tolerances for the translations and rotations. Considering these difficulties, the unbalanced energy is an appealing alternative. The unbalanced energy can be defined as the product of the unbalanced force and the displacement increment. It is noted that this convergence criterion is not sensitive to the types of displacements and the structural strength. To further mitigate the effect of external excitations, the relative unbalanced energy can be used, which may be most suitable for the iterative quasi-Newton procedure.

In this section, six kinds of convergence criteria, i.e., displacement, relative displacement, unbalanced force, relative unbalanced force, unbalanced energy, and relative unbalanced energy, are examined. Listed below are the formulations of the six convergence criteria, where $\| \ \|$ is the norm of a vector; $| \ |$ is the absolute value of a scalar; and STOL. is the tolerance.

(1) Displacement criterion

$$\left\| d_{n+1}^{i+1} - d_{n+1}^{i} \right\| < \text{STOL.} \tag{7.33}$$

where d_{n+1}^{i+1} is the displacement of the current iteration of the $(n+1)$th step and d_{n+1}^{i} is the displacement of the previous iteration of the $(n+1)$th step.

(2) Relative displacement criterion

$$\frac{\left\| d_{n+1}^{i+1} - d_{n+1}^{i} \right\|}{\left\| d_{n+1}^{i+1} - d_{n} \right\|} < \text{STOL.} \tag{7.34}$$

where d_{n+1}^{i+1} is the displacement of the current iteration of the $(n+1)$th step, d_{n+1}^{i} is the displacement of the previous iteration of the $(n+1)$th step, and d_{n} is the displacement of the (n)th step.

(3) Unbalanced force criterion

$$\left\| {}^{\text{unb}}F_{n+1}^{i} \right\| < \text{STOL.} \tag{7.35}$$

where ${}^{\text{unb}}F_{n+1}^{i}$ is the unbalanced force of the previous iteration of the $(n+1)$th step.

(4) Relative unbalanced force criterion

$$\frac{\left\| {}^{\text{unb}}F_{n+1}^{i} \right\|}{\left\| {}^{\text{unb}}F_{n+1}^{0} \right\|} < \text{STOL.} \tag{7.36}$$

where ${}^{\text{unb}}F_{n+1}^{i}$ is the unbalanced force of the current iteration of the $(n+1)$th step, and ${}^{\text{unb}}F_{n+1}^{0}$ is the unbalanced force of the first iteration of the $(n+1)$th step.

(5) Unbalanced energy criterion

$$\left|{}^{\text{unb}}F_{n+1}^{i}\cdot\left(d_{n+1}^{i+1}-d_{n+1}^{i}\right)\right|<\text{STOL}. \tag{7.37}$$

where ${}^{\text{unb}}F_{n+1}^{i}$ is the unbalanced force of the current iteration of the $(n+1)$ th step, d_{n+1}^{i+1} is the displacement of the current iteration of the $(n+1)$th step, and d_{n+1}^{i} is the displacement of the previous iteration of the $(n+1)$th step.

(6) Relative unbalanced energy criterion

$$\frac{\left|{}^{\text{unb}}F_{n+1}^{i}\cdot\left(d_{n+1}^{i+1}-d_{n+1}^{i}\right)\right|}{\left|{}^{\text{unb}}F_{n+1}^{0}\cdot\left(d_{n+1}^{i+1}-d_{n}\right)\right|}<\text{STOL}. \tag{7.38}$$

where ${}^{\text{unb}}F_{n+1}^{i}$ is the unbalanced force of the current iteration of the $(n+1)$ th step, d_{n+1}^{i+1} is the displacement of the current iteration of the $(n+1)$th step, d_{n+1}^{i} is the displacement of the previous iteration of the $(n+1)$th step, ${}^{\text{unb}}F_{n+1}^{0}$ is the unbalanced force of the first iteration of $(n+1)$th step, and d_n is the displacement of the (n)th step.

Physical meanings of the six convergence criteria are illustrated by Fig. 7.17, which shows the iterative quasi-Newton procedure employed by the Coordinator. At the beginning of the $(n+1)$th step, the displacements in the previous step are applied to all substructures. The restoring forces obtained from the substructures are combined to form the unbalanced force at the boundaries, shown as ${}^{\text{unb}}F_{n+1}^{0}$ in Fig. 7.17. Then the iterative quasi-Newton procedure is conducted to eliminate the unbalanced force and generate a new trial displacement. Each iteration includes one unbalanced force ${}^{\text{unb}}F_{n+1}^{i}$ and the corresponding new trial displacement d_{n+1}^{i+1}. These variables are evaluated using the displacement and force type convergence criteria. The unbalanced energy represented by the

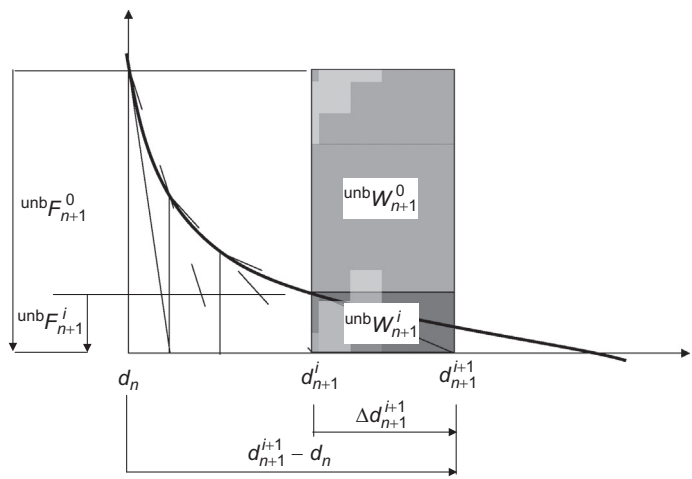

FIGURE 7.17 Illustrative presentation of convergence criteria.

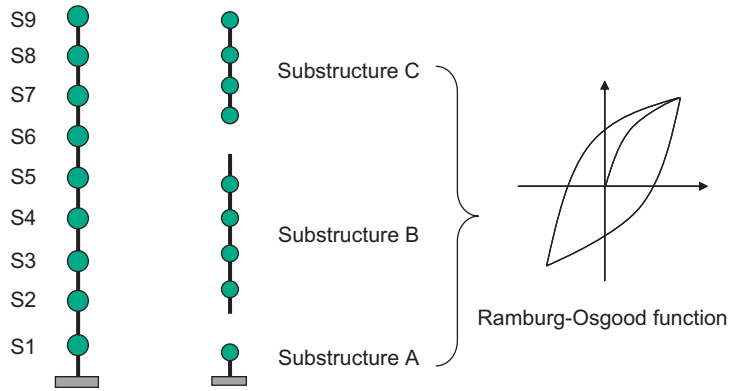

FIGURE 7.18 Nine-degrees-of-freedom (DOF) mass-spring model used for convergence criteria examination.

net-meshed area, ${}^{\text{unb}}W^{i}_{n+1}$, is the product of the displacement increment and the unbalanced force of the current iteration, and is taken as the numerator of the relative unbalanced energy criterion. The area with slashed lines, ${}^{\text{unb}}W^{0}_{n+1}$, is the product of the original unbalanced force and the displacement increment, which is taken as the denominator of the relative unbalanced energy criterion.

The six criteria are examined for a mass-spring model with 9-DOF. The 9-DOF are divided into three groups, as shown in Fig. 7.18. The bottom DOF is taken as Substructure A; the 2nd to 5th DOF are taken as Substructure B; and the left are taken as Substructure C. To compare these convergence criteria, other parameters, such as the convergence tolerance, material model, and initial stiffness, are kept identical for all six cases. Here, the convergence tolerance is set to be 10^{-9}. Note that the largest displacement of one story is about 0.1 m, the largest force is about 3,000,000 N, and the maximum energy dissipated by one story is about 4000 J. Therefore, 10^{-9} is small enough to obtain accurate responses. The initial stiffness of both boundaries is set to 10^{3} kN/mm. The RO function is adopted to simulate the hysteretic loop of each story. In these examinations, an upper bound of the number of iterations is adopted to prevent endless iteration. Here it is set to be 20 times.

The responses of the 1st and 9th DOF using different convergence criteria are compared with the response obtained for the entire model in Fig. 7.19. The hysteretic loops of the first and seventh stories are also compared in Fig. 7.20 for all convergence criteria. The responses and hysteretic loops match almost perfectly, demonstrating the validity of the quasi-Newton procedure when considering nonlinearity for all substructures. The number of iterations in each step is plotted in Fig. 7.21 for the six cases with different convergence criteria.

Major findings from the numerical examinations are summarized as follows:

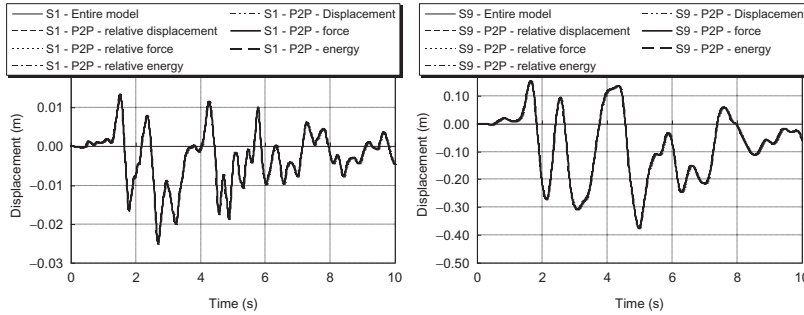

FIGURE 7.19 Response comparison of S1 and S9 for six convergence criteria.

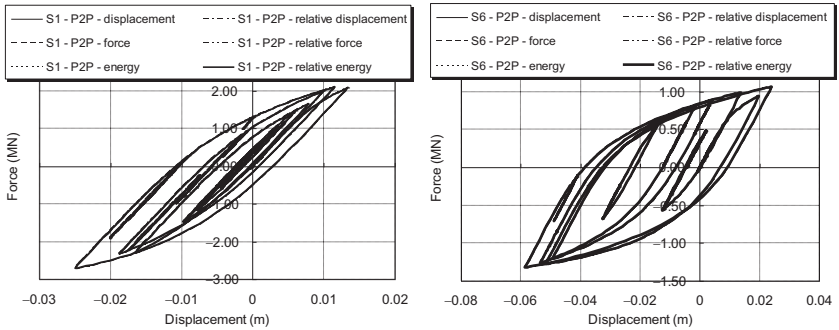

FIGURE 7.20 Hysteresis comparison of S1 and S6 for six convergence criteria.

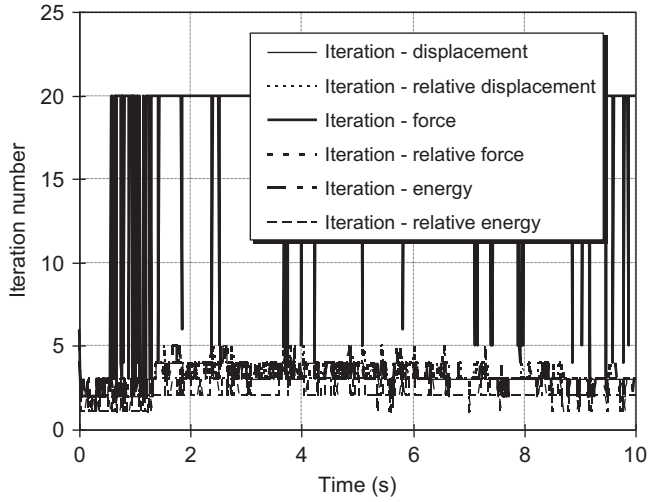

FIGURE 7.21 Number of iterations in each step for six convergence criteria.

(1) Accurate responses can be obtained by the quasi-Newton procedure with any kind of convergence criterion. When the unbalanced force is used as the convergence criterion, some steps reach the upper limit of the number of iterations, but a good result is still obtained. The reason is explained in the third conclusion.

(2) If only considering the first step, it uses 4, 5, 6, 5, 4, and 4 iterations for the convergence criterion: displacement, relative displacement, unbalanced force, relative unbalanced force, unbalanced energy, and relative unbalanced energy, respectively. And averagely, it needs 3.172, 3.139, 18.063, 3.139, 3.299, and 2.045 iterations, respectively. Therefore, the relative unbalanced energy is the most efficient criterion. Others are basically the same.

(3) When the unbalanced force is used for the convergence criterion, the number of iterations reaches 20 times in some steps, but good response is still obtained. This difficulty arises because of a limited numerical precision of the double-precision data type used in the program. In this study, the stiffness of the model is in a range of 10^9. The displacement increment calculated as the product of the inversion of stiffness and the tolerance of the unbalanced force is about 10^{-18}, which exceeds the numerical precision of the double-precision data type, and results in no change in displacement. Thus, the quasi-Newton procedure never converges. When the tolerance is changed to 10^{-6}, this difficulty is removed and the quasi-Newton procedure converges after a certain number of iterations.

(4) The relative unbalanced energy is preferable not only because it is easier to be achieved, but also because it is not affected by structural properties and external forces, thus more general. In the following study, the relative unbalanced energy is selected as the criterion.

In what follows, the magnitude of tolerance is examined using the relative unbalanced energy criterion. A suitable tolerance is important for the quasi-Newton procedure since too strict a tolerance would induce unnecessary iterations and eventual difficulty in convergence. Too loose a tolerance will result in responses with lack of accuracy. This examination is based on the previous analysis for checking the relative unbalanced energy criterion. Four levels of tolerances are examined, i.e., 0.1, 10^{-3}, 10^{-6}, and 10^{-9}, which are designated as T1, T3, T6, and T9, respectively. Note that the maximum energy dissipated by one story is about 4000 J, T6 and T9 may be sufficient for accurate responses, while T1 and T3 may not. The responses of the 1st and 9th DOF are plotted in Fig. 7.22 for the four cases. The number of iterations of each step is also shown in Fig. 7.23.

From these examinations, the following observations are made:

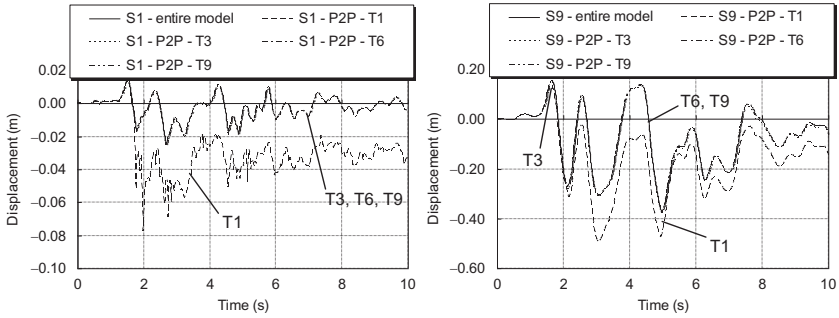

FIGURE 7.22 Response comparison of S1 and S9 for four tolerances.

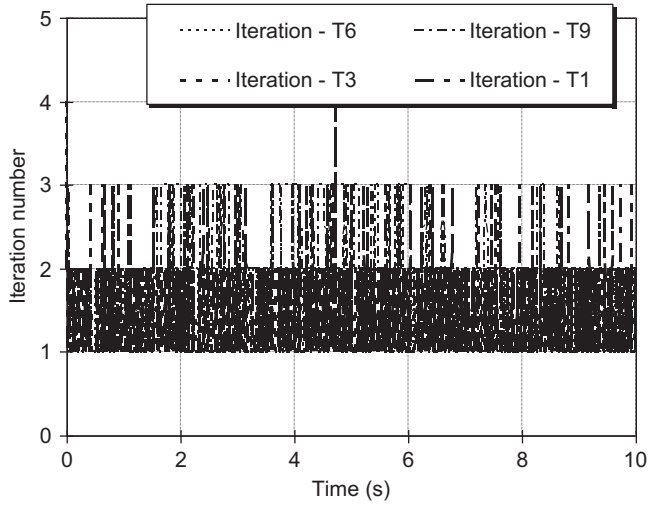

FIGURE 7.23 Iteration number comparison for four tolerances.

(1) A loose tolerance would bring inaccurate results. When using 0.1 for the tolerance, the responses deviate greatly from the responses to be. If the tolerance becomes smaller, the responses also become closer to the exact responses. When 10^{-6} is adopted as the tolerance, the responses are almost identical with the exact responses. In the following study, 10^{-9} is adopted as the base line.

(2) No great difference is observed for the number of iterations of each step among the four cases. The average numbers are 1.289, 1.163, 1.537, and 2.045, respectively, for T1, T3, T6, and T9. This naturally shows that a stricter tolerance requires a larger number of iteration.

7.4.3 Examination on Type of Divisions into Substructures

Examined in this section is the effect of the type of division on the convergence speed. A mass-spring model with 9-DOF is used here. The relative unbalanced energy criterion is adopted, and the convergence tolerance is set at 10^{-9}. The initial stiffness of any boundary is set to 10^3 kN/mm. Four types of divisions shown in Fig. 7.24 are examined. The entire model is divided into three substructures. For Case 1 and Case 3, the dividing positions are located at the mass nodes (called the mass boundary); while for Case 2 and Case 4, at least one boundary is located at the middle point between the adjacent 2-DOF, which is called the massless boundary. The stiffness associated to the massless boundary is two times the stiffness before dividing. The responses of the 1st and 9th DOF are shown in Fig. 7.25, which are compared with the exact responses. The number of iterations of each step is compared in Fig. 7.26 for the four cases.

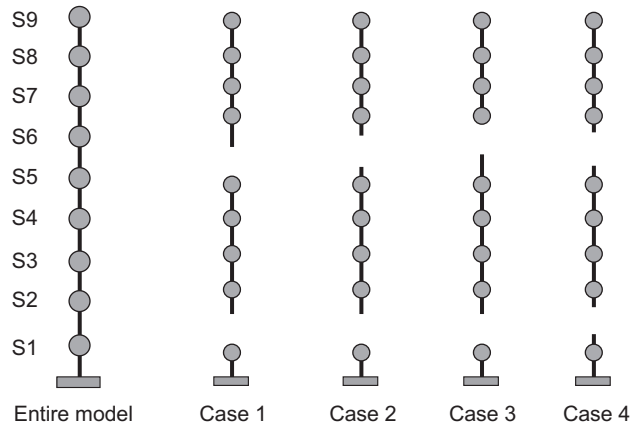

FIGURE 7.24 Four types of divisions into substructures.

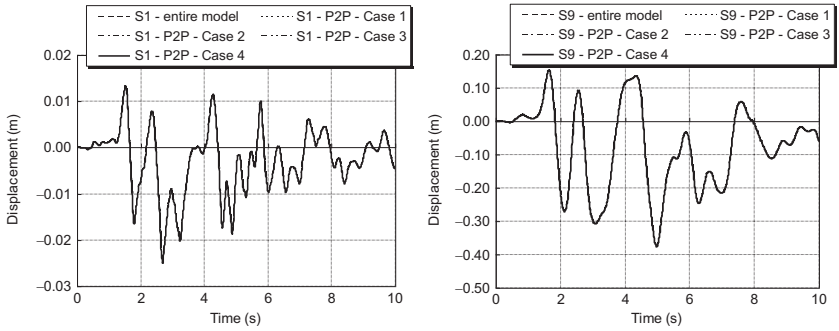

FIGURE 7.25 Comparison of responses of S1 and S9 for four cases of division.

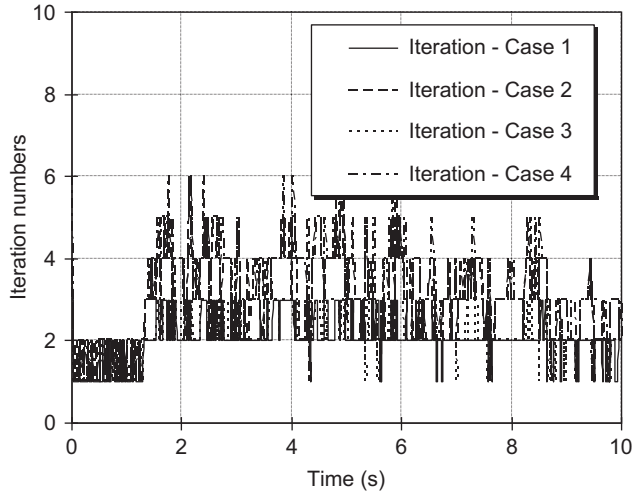

FIGURE 7.26 Comparison of number of iterations for four cases of division.

Major findings are as follows:

(1) Correlation between the responses obtained from the quasi-Newton procedure and the exact responses is shown in Fig. 7.25, which demonstrates that the quasi-Newton procedure converges no matter where the structure is divided into substructures.

(2) Case 2 and Case 4 need more iterations than Case 1 and Case 3. On the average, Case 2 and Case 4 need 2.946 and 3.103 times of iteration, respectively; while Case 1 and Case 3 need 2.018 and 2.045 times, respectively. In Case 2 and Case 4, the stiffness of some elements of the substructures is larger than that in Case 1 and Case 3. Therefore, the same displacement increment would result in a larger unbalanced force in Case 2 and Case 4 than that in Case 1 and Case 3. That is why Case 2 and Case 4 need more iterations than Case 1 and Case 3.

7.4.4 Number of DOF on Boundaries

In order to investigate the effect of the number of boundary DOF on the convergence speed, eight analysis cases are chosen for the mass-spring model with 9-DOF, as shown in Fig. 7.27. The eight analysis cases have 1-8 boundary DOF. The relative unbalanced energy criterion is adopted, and the convergence tolerance is set to be 10^{-9} for all analysis cases. The initial stiffness of any boundary is set to 10^3 kN/mm. The responses of the 1st and 9th DOF are plotted in Fig. 7.28 and compared with the exact responses. The number of iterations of each step is also compared in Fig. 7.29 for each case.

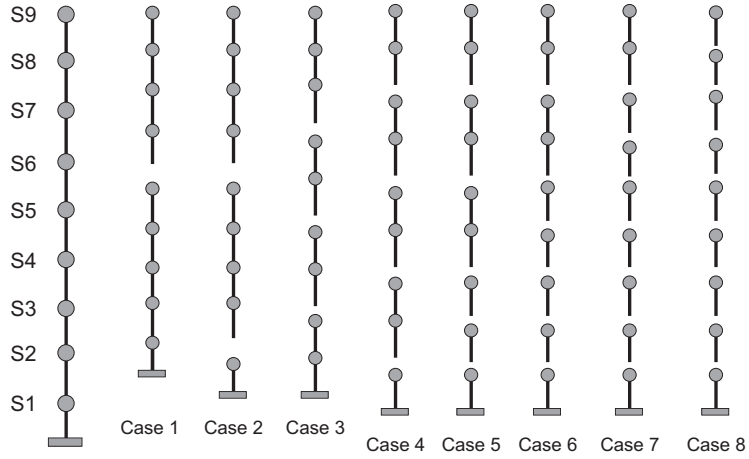

FIGURE 7.27 Eight cases of division with different boundary DOF.

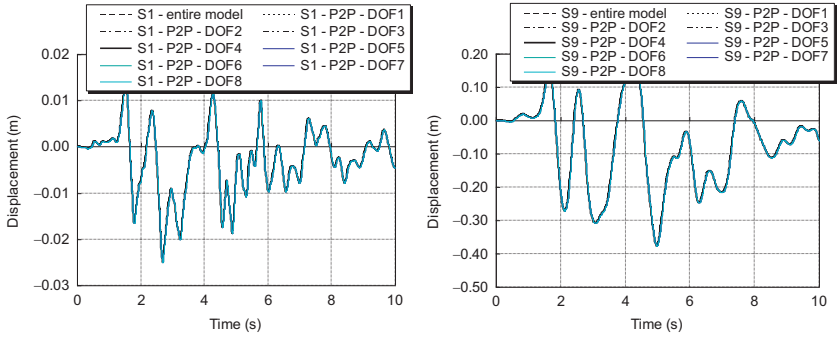

FIGURE 7.28 Comparison of responses of S1 and S9 for eight cases.

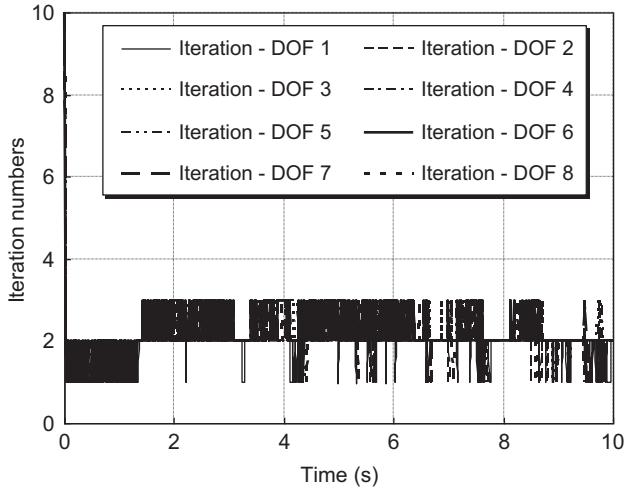

FIGURE 7.29 Comparison of number of iterations for eight cases.

Major findings are as follows:

(1) The quasi-Newton procedure converges no matter how many DOF are associated with the boundaries.

(2) It is observed from Fig. 7.29 that the number of boundary DOF affect only the convergence speed of the first several steps, but have little influence on the following steps. The reason is that the stiffness matrix after the first several steps is close enough to the tangential stiffness matrix, while the nonlinearity simulated by the RO function changes mildly such that it always converges in a limited number of iterations no matter how many DOF do exist on the boundaries.

(3) For the first several steps (the first step of Case 1-Case 5; the first two steps of Case 6-Case 8), 2, 4, 6, 8, 10, 13, 15, 17 iterations are needed to obtain a stiffness matrix close enough to the tangential stiffness matrix. The stiffness matrix of the mass-spring model is in a tri-diagonal form. That is the reason why the number of iterations increases almost linearly with the number of boundary DOF.

7.4.5 Investigation on Initial Stiffness

Examined in this section is the effect of the initial stiffness prescribed for the first step of the quasi-Newton iteration. In this study, the mass-spring model with 9-DOF is divided into three substructures, as shown in Fig. 7.18. The relative unbalanced energy is taken for the convergence criterion, and the tolerance is set to be 10^{-9}. Five analysis cases using different initial stiffness matrices are considered. The matrices are listed in Table 7.2. The number of iterations of each step is compared in Fig. 7.30 for the five analysis cases.

TABLE 7.2 Matrices Employed by Five Analysis Cases

Analysis case	Initial matrix at boundaries
Case 1 (large soft)	$\begin{bmatrix} 10^6 & 0 \\ 0 & 10^6 \end{bmatrix}$
Case 2 (small soft)	$\begin{bmatrix} 10^9 & 0 \\ 0 & 10^9 \end{bmatrix}$
Case 3 (exact)	$\begin{bmatrix} 4.887\times10^9 & 2.030\times10^4 \\ 2.030\times10^4 & 4.570\times10^9 \end{bmatrix}$
Case 4 (small hard)	$\begin{bmatrix} 10^{10} & 0 \\ 0 & 10^{10} \end{bmatrix}$
Case 5 (large hard)	$\begin{bmatrix} 10^{13} & 0 \\ 0 & 10^{13} \end{bmatrix}$

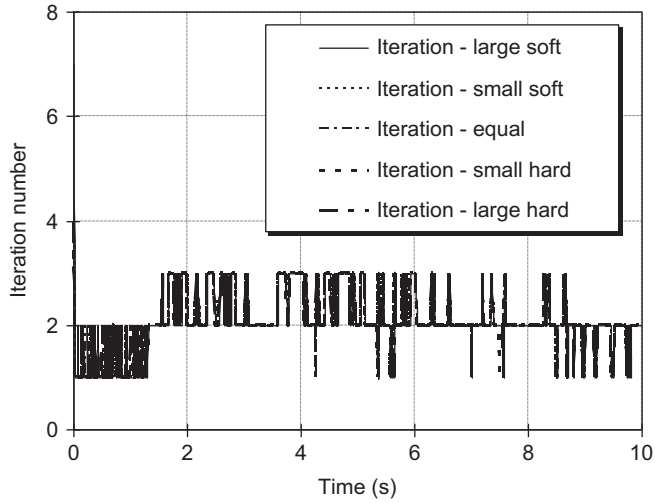

FIGURE 7.30 Comparison of number of iterations for five initial stiffness matrices.

The initial stiffness affects only the first step of quasi-Newton procedure, while the rest are almost identical. Numbers of iterations of the first step are 7, 4, 1, 4, and 4 times for the five analysis cases, respectively. It means a good estimation of initial stiffness can speed up the convergence in the first step. In the two-round predicting-correcting test procedure, the initial stiffness is always used for the prediction and correction of the experimental substructures. The convergence speed is greatly improved if a good approximation of the stiffness is used in each step of analysis.

7.4.6 Summary

In this part, the convergence speed of the iterative quasi-Newton procedure is explored in terms of the convergence criteria, tolerance, type of divisions of the structure, number of boundary DOF, and the approximation of the initial stiffness. Major findings are summarized as follows:

(1) The relative unbalanced energy is the most suitable convergence criterion for the iterative quasi-Newton procedure, because it is not sensitive to the variety of boundaries, structures, and external excitations.
(2) If the relative unbalanced energy criterion is adopted, the tolerance of 10^{-6} is strict enough to obtain accurate responses without losing the efficiency for the system whose maximum energy of one story dissipated in one step is about 4000 J.
(3) The quasi-Newton procedure converges no matter how the structure is divided and how many boundary DOF.
(4) It is slower to converge for a stiffer structure, because a larger unbalanced energy would occur for the same displacement increment.

(5) More DOF are associated with the boundaries, and a larger number of iterations is needed.
(6) A good approximation of the initial stiffness matrix associated with the boundaries may reduce the number of iterations greatly. This gives a clue for the improvement of efficiency of the P2P framework.

These are the preliminary examinations for incorporating numerical nonlinear substructures in the P2P Internet online hybrid test system. It has been demonstrated that the convergence of the quasi-Newton procedure is guaranteed, and the efficiency of the system will not be affected greatly if a limited number of DOF is associated with the boundaries.

7.5 NUMERICAL CHARACTERISTICS OF P2P PREDICTOR-CORRECTOR PROCEDURE

7.5.1 Introduction

The predictor-corrector procedure employs linear stiffness assumption on tested substructures to avoid iteration. This would introduce error into the dynamic system, which probably leads stability and accuracy issues. In this section, the numerical characteristics of the predictor-corrector procedure, particularly those associated with the linear stiffness assumption, are examined by means of the spectral method. The two-round quasi-Newton test scheme is recast into a recursive matrix form for an equivalent linear SDOF undamped model, and the stability and accuracy conditions are obtained by examining the spectral radius of the matrix.

During the predicting and correcting procedures, the restoring force of the tested substructure is always obtained numerically. Physical loading is conducted only once between the predicting and correcting procedures. For the numerical substructures, the actual stiffness can be used, but for the tested substructures use of the actual stiffness is not practical, because of the limited resolutions in the measurement. Therefore, an assumed stiffness, k_I, is adopted instead. The initial stiffness is commonly adopted as the assumed stiffness. This treatment introduces a force error. This will be explained for a linear tested substructure having a stiffness of k_0. The dynamics of the tested substructure is recast into an effective static form [37] and illustrated as in Fig. 7.31. Suppose all previous n steps are exactly simulated. In the beginning of the $(n+1)$th step, k_I is used to calculate the predicting displacement $\widetilde{d}_{n+1}$. This predicting path is plotted as the thick solid arrow in Fig. 7.31. The tested substructure is then loaded from $\widetilde{d}_n$ to $\widetilde{d}_{n+1}$ with respect to the actual effective stiffness k_0 (the dashed arrow as shown in Fig. 7.31). At the displacement of $\widetilde{d}_{n+1}$, a force imbalance is present. To compensate for the imbalanced force, the correcting procedure, indicated by the dotted arrow, is implemented. Note that the corrected displacement, d_{n+1}, may not be the same as the exact displacement, d^*_{n+1}. The error is introduced due to the difference between k_I and k_0. This infers that

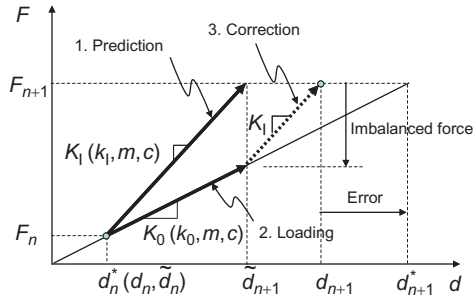

FIGURE 7.31 Error introduced by test scheme featuring two-round quasi-Newton procedure.

the assumed stiffness, k_I, had better not be too different from the actual stiffness, k_0. Quantification of this error is explored in the following sections.

7.5.2 Recursive Matrix of Two-Round Quasi-Newton Test Scheme

Stability and accuracy characteristics of the proposed P2P test scheme are examined in terms of the error introduced by the linear assumption adopted for the tested substructures. All other errors such as the controlling and measuring errors and other noises are ignored. To focus on this error, the model with a single tested substructure is adopted. The tested substructure contains only 1-DOF and this DOF is treated as the boundary, with the absence of the adjacent numerical substructures. Viscous damping is not considered. With this treatment, the error characteristics associated with the linear assumption can be singled out. In the following derivation, the ratio of the initial stiffness k_I to the actual stiffness k_0 is denoted as θ, i.e., $\theta = k_I/k_0$. Note that $\theta > 1$ corresponds to the case when the structure exhibits hysteresis of a softening-type.

Suppose that the equilibrium at the end of the nth step has already been achieved at point C_n, as shown in Fig. 7.32. In the $(n+1)$th step, the predicted displacement $\tilde{d}_{n+1}$ is calculated by solving the equation of motion using the

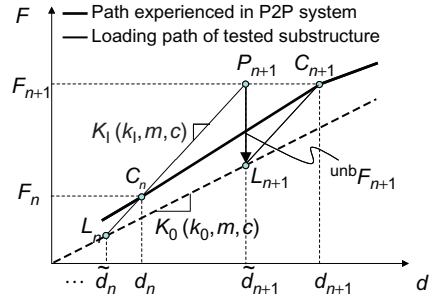

FIGURE 7.32 Restoring force versus displacement in two-round quasi-Newton test scheme.

initial stiffness k_{I}, and the balanced point is denoted as P_{n+1}. The predicting procedure adopts the averaged acceleration algorithm [37] and is expressed as

$$m\widetilde{a}_{n+1}+r_n+k_{\mathrm{I}}\left(\widetilde{d}_{n+1}-d_n\right)=f_{n+1} \tag{7.39}$$

$$\widetilde{d}_{n+1}=d_n+\Delta t v_n+\frac{1}{4}(a_n+\widetilde{a}_{n+1})\Delta t^2 \tag{7.40}$$

$$\widetilde{v}_{n+1}=v_n+\frac{1}{2}(a_n+\widetilde{a}_{n+1})\Delta t \tag{7.41}$$

$$r_n=k_0\widetilde{d}_n+k_{\mathrm{I}}\left(d_n-\widetilde{d}_n\right) \tag{7.42}$$

where the displacement $\widetilde{d}_n$ represents the predicted displacement in the nth step.

Then the system is loaded from the previous predicted displacement $\widetilde{d}_n$ to the current predicted displacement $\widetilde{d}_{n+1}$, correspondingly from point L_n to point L_{n+1}, shown in Fig. 7.32, which results in an imbalanced force of ${}^{\mathrm{unb}}F_{n+1}$, represented by the vertical arrow from point P_{n+1} to point L_{n+1}. Then the correcting procedure is implemented using the initial stiffness k_{I} once again, and the balanced point C_{n+1} is achieved. The equation of motion is solved again by the averaged acceleration algorithm, as expressed as

$$ma_{n+1}+r_{n+1}=f_{n+1} \tag{7.43}$$

$$d_{n+1}=d_n+\Delta t v_n+\frac{1}{4}(a_n+a_{n+1})\Delta t^2 \tag{7.44}$$

$$v_{n+1}=v_n+\frac{1}{2}(a_n+a_{n+1})\Delta t \tag{7.45}$$

$$r_{n+1}=k_0\widetilde{d}_{n+1}+k_{\mathrm{I}}\left(d_{n+1}-\widetilde{d}_{n+1}\right) \tag{7.46}$$

Equations (7.39)–(7.46) can be recast into the following recursive matrix form:

$$\mathbf{X}_{n+1}=\mathbf{A}\mathbf{X}_n+\mathbf{L}_{n+1} \tag{7.47}$$

$$\mathbf{A}=\begin{bmatrix}
\dfrac{4\left(4+(2\theta-1)\Omega^2\right)}{\left(4+\theta\Omega^2\right)^2} & \dfrac{4\Delta t\left(4+(2\theta-1)\Omega^2\right)}{\left(4+\theta\Omega^2\right)^2} & \dfrac{\Delta t^2\left(4+(2\theta-1)\Omega^2\right)}{\left(4+\theta\Omega^2\right)^2} & \dfrac{(\theta-1)^2\Omega^4}{\left(4+\theta\Omega^2\right)^2} \\
-\dfrac{2\Omega^2\left(4+\theta^2\Omega^2\right)}{\Delta t\left(4+\theta\Omega^2\right)^2} & 1-\dfrac{2\Omega^2\left(4+\theta^2\Omega^2\right)}{\left(4+\theta\Omega^2\right)^2} & \dfrac{\Delta t}{2}-\dfrac{\Delta t\Omega^2\left(4+\theta^2\Omega^2\right)}{2\left(4+\theta\Omega^2\right)^2} & \dfrac{2(\theta-1)^2\Omega^4}{\Delta t\left(4+\theta\Omega^2\right)^2} \\
-\dfrac{4\Omega^2\left(4+\theta^2\Omega^2\right)}{\Delta t^2\left(4+\theta\Omega^2\right)^2} & -\dfrac{4\Omega^2\left(4+\theta^2\Omega^2\right)}{\Delta t\left(4+\theta\Omega^2\right)^2} & -\dfrac{\Omega^2\left(4+\theta^2\Omega^2\right)}{\left(4+\theta\Omega^2\right)^2} & \dfrac{4(\theta-1)^2\Omega^4}{\Delta t^2\left(4+\theta\Omega^2\right)^2} \\
\dfrac{4}{4+\theta\Omega^2} & \dfrac{4\Delta t}{4+\theta\Omega^2} & \dfrac{4\Delta t^2}{4+\theta\Omega^2} & \dfrac{(\theta-1)\Omega^2}{4+\theta\Omega^2}
\end{bmatrix} \tag{7.48}$$

$$\mathbf{X}_n = \begin{Bmatrix} d_n \\ v_n \\ a_n \\ \widetilde{d}_n \end{Bmatrix},\ \mathbf{L}_{n+1} = \begin{Bmatrix} \dfrac{\left(4+(2\theta-1)\Omega^2\right)\Delta t^2}{\left(4+\theta\Omega^2\right)^2} \\ \dfrac{2\left(4+(2\theta-1)\Omega^2\right)\Delta t}{\left(4+\theta\Omega^2\right)^2} \\ \dfrac{4\left(4+(2\theta-1)\Omega^2\right)\Delta t}{\left(4+\theta\Omega^2\right)^2} \\ \dfrac{\Delta t^2}{4+\theta\Omega^2} \end{Bmatrix} \frac{f_{n+1}}{m},\ \Omega = \omega\Delta t,\ \omega = \sqrt{\frac{k_0}{m}} \tag{7.49}$$

where Ω and ω are the sampling and circular frequency of the SDOF system, respectively.

7.5.3 Stability Characteristics

The stability of a time integration algorithm is characterized by whether or not the error introduced by the previous steps remains uniformly bounded during the following steps, which can be represented by the spectral radius $\rho(\mathbf{A})$ of the amplification matrix $\mathbf{A}$. This is also called the spectral stability criteria [37], described such that "the error is bounded for $n \to \infty$ if and only if $\rho(\mathbf{A}) \leq 1$." In this study, $\mathbf{A}$ has four eigenvalues and is determined by the following characteristic equation, with λ as an eigenvalue:

$$\lambda\left\{\left(\theta\Omega^2+4\right)\lambda^3+\left[\theta(1+\theta)\Omega^4-20(\theta-1)\Omega^2-32\right]\lambda^2+\right.$$

$$\left.\left[\theta(2-\theta)\Omega^4+8(2\theta-1)\Omega^2+16\right]\lambda+\left[\theta(1-\theta)\Omega^2-4(\theta-1)\right]\right\}=0 \tag{7.50}$$

Figure 7.33 shows the spectral radii obtained from the above equation. In Fig. 7.33a, the stiffness ratio θ ranges from 1 to 100, and the spectral radius does not exceed unity, suggesting that the stability of the test scheme is ensured when $\theta \geq 1$. That is, the test scheme is unconditionally stable for structures having a force-displacement relationship of a softening type. When θ ranges from 0 to 1, it may exceed unity if Ω is larger than $1.42\mathrm{e}^{12.714\theta^{4.486}}$, as shown in Fig. 7.33b. This implies a conditional stability in this range.

7.5.4 Accuracy Characteristics

According to Belytschko and Hughes [37], the displacement in one step can be written as a linear combination of the eigenvalues of the amplification matrix $\mathbf{A}$. Among the four eigenvalues of Equation (7.47), two are real values, with one of them equal to zero, and the other two are a pair of complex conjugates. Then d_n can be expressed as

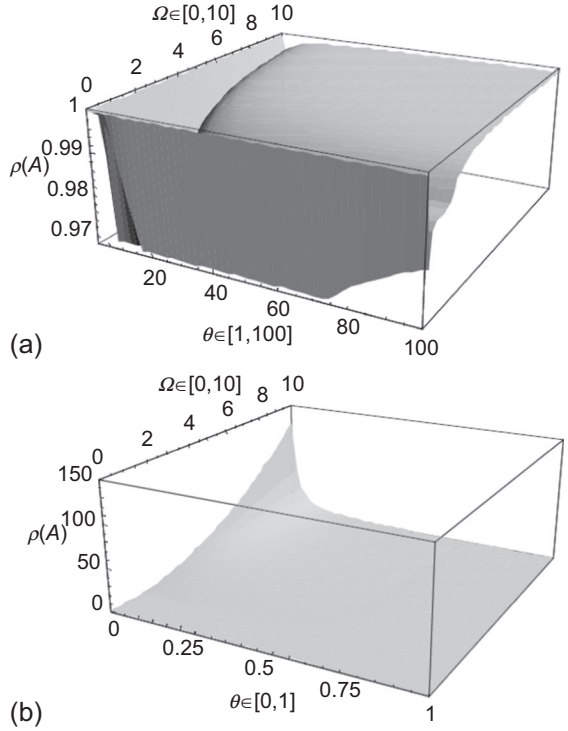

FIGURE 7.33 Spectral radii of two-round quasi-Newton test scheme: (a) spectral radius for $\theta \geq 1$, (b) spectral radius for $0 \leq \theta < 1$.

$$
\begin{aligned}
& d_n = \exp\left(-\overline{\xi}\,\overline{\omega} t_n\right)\left(c_1 \cos \overline{\omega} t_n + c_2 \sin\, \overline{\omega} t_n\right) + c_3 \lambda_3^n \\
& \text{where} \quad \lambda_{1,2} = A \pm Bi = \exp\left[\overline{\Omega}\left(-\overline{\xi} \pm i\right)\right] \\
& \qquad \lambda_3 \text{ is a real value, and } \lambda_4 = 0 \\
& \qquad \overline{\omega} = \overline{\Omega}/\Delta t \\
& \qquad \overline{\xi} = -\ln\left(A^2 + B^2\right)/\left(2\overline{\Omega}\right) \\
& \qquad \overline{\Omega} = \arctan\left(B/A\right) \\
& \qquad \chi = \frac{\overline{T} - T}{T} = \frac{\omega - \overline{\omega}}{\overline{\omega}} = \frac{\Omega - \overline{\Omega}}{\overline{\Omega}}
\end{aligned}
\tag{7.51}
$$

$\overline{\xi}$ is defined as the numerical dissipation, χ is the period distortion, $\overline{\omega}$ is the numerical circular frequency, and $\overline{\Omega}$ is the numerical sampling frequency.

Three numerical cases, Cases 1-3 with $\theta = 1$, 16, and 100, respectively, are taken as examples. Unconditional stability is ensured for all cases. The numerical characteristics of Case 1 with $\theta = 1$ are actually identical to those of the averaged acceleration algorithm. To show the acceptable accuracy of the

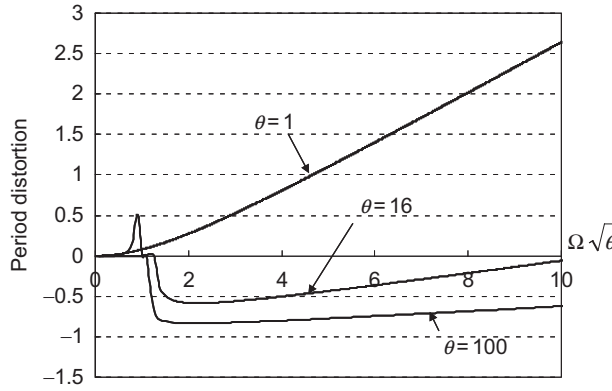

FIGURE 7.34 Comparison of period distortion for three cases.

proposed P2P system, the period distortions of the three Cases are compared and plotted in Fig. 7.34. It is observed from Fig. 7.34 that the P2P system is accurate at small sampling frequencies (when $\overline{\Omega}\sqrt{\theta} = 0.6$, the period distortion $\chi = 3\%$, -0.3%, and 2% for $\theta = 1$, 16, and 100, respectively), and still commensurate in accuracy with the averaged acceleration algorithm for larger sampling frequencies (for example, when $\overline{\Omega}\sqrt{\theta} = 4$, the period distortion $\chi = 80\%$, -50%, and -80% for $\theta = 1$, 16, and 100, respectively).

7.6 CONCLUSIONS

The P2P Internet online hybrid test system proposed in this study is a distributed online hybrid test system using substructuring technique [38]. In this system, the simulated structure is divided into multiple substructures. All substructures are equally treated and geographically distributed to various laboratories, which enables the system to integrate the resources of these laboratories for seismic simulation of large-scale structures. A center part called "Coordinator" is devised to achieve the compatibility and equilibrium on the boundaries between the substructures. Each substructure is implemented as a highly encapsulated and independent "Partner" with limited data on the boundary, such as displacements and reactional forces, exchanged with the "Coordinator." Each "Partner" can be treated as the experimental part or analytical part according to the user's concerns. The system is characterized with the following features:

(1) The equations of motion are formulated for each substructure separately, but not for the entire structure as did in the conventional substructural online hybrid test. The size of the equations of motion is reduced. Therefore, a faster computation may be achieved. The separated formulation also enables the parallel computation of substructures which is known to increase capacity and efficiency significantly for computation of large systems.

(2) An iterative quasi-Newton procedure is employed by the "Coordinator" to satisfy the boundary conditions between all substructures. The implementation in the "Coordinator" in fact is an equation solution procedure for the boundaries. Any type of Newton's method can be chosen for this solution. The exact amplification matrix, i.e., the stiffness matrix that is only related to the boundaries, however, is unavailable because of the involvement of experimental substructures. The quasi-Newton procedure hereby is the best choice because it does not need any exact stiffness, and the convergence rate is super-linear.

(3) A testing scheme featuring a two-round quasi-Newton procedure is devised to avoid iteration for the substructures being tested physically. This is a typical predicting and correcting scheme, each corresponding to one round quasi-Newton procedure. In one step of analysis, the experimental substructures are always assumed to be linear elastic, and the nonlinearities are taken into consideration only by the onetime loading between the predicting and correcting quasi-Newton procedures. This linear assumption may introduce numerical damping into the system [29], which is deemed helpful for suppressing higher mode responses generated by the experimental errors.

(4) The incorporation of existing FEM programs into the online hybrid test system is believed to be able to increase the versatility of online hybrid tests, particularly the accuracy of the behavior of the computed part [30]. It would be much more effective if a highly encapsulated FEM program could be incorporated into the online test system as a black box, accessible only through standard I/O. Restart capability is the key to realize this application [39]. Two kinds of restart are employed by this system, i.e., "iterative restart" and "step-wise restart." "Iterative restart" is a trying procedure used to find the true state of the current step, which always restarts from the true state of the previous step. "Step-wise restart" is the last step of the "Iterative restart." It records the true state of each step.

(5) The reactional force acquired from each substructure is a dynamic reactional force which includes the effect of the inertia force and the viscous damping force on the boundary.

(6) It is unnecessary for the substructures to have the same damping. This is very appealing when the characteristics of substructures are significantly different.

(7) A fast and stable solution using a socket mechanism is developed for data exchange over the Internet, and an Internet hybrid test environment is constructed. The interfaces of diverse "Partners" are standardized and simplified so that they can be incorporated effectively into the integrated Internet test system. Such standardization and simplification also require the substructures to be highly encapsulated.

(8) The relative unbalanced energy is the most suitable convergence criterion for the iterative quasi-Newton procedure, which converges no matter how

the structure is divided and how many boundary DOF. Furthermore, more DOF are associated with the boundaries, and a larger number of iterations is needed. Besides, a good approximation of the initial stiffness matrix associated with the boundaries may reduce the number of iterations greatly. This gives a clue for the improvement of efficiency of the P2P framework.

(9) The convergence of the two-round quasi-Newton test scheme is guaranteed if the referenced stiffness (normally the initial stiffness) is not smaller than the actual stiffness. The P2P system is accurate when the integration time interval is small, and commensurate in accuracy with the averaged acceleration algorithm for larger sampling frequencies.

REFERENCES

[1] Takanashi K, Udagawa K, Seki M, Okada T, Tanaka H. Nonlinear earthquake response analysis of structures by a computer actuator online system (part 1: details of the system). Trans Archit Inst Jpn 1975;229:77–83 [in Japanese].

[2] Takanashi K, Nakashima M. Japanese activities on online testing. J Eng Mech 1987;113:1014–32.

[3] Mahin SA, Shing PB, Thewalt CR, Hanson RD. Online test method: current status and future directions. J Struct Eng 1989;115:2113–28.

[4] Shing PB, Nakashima M, Bursi OS. Application of pseudo dynamic test method to structural research. Earthq Spectra 1996;12:29–56.

[5] Nakashima M. Development, potential, and limitations of real-time online (pseudo-dynamic) testing. Philos Trans R Soc Lond A 2001;359:1851–67.

[6] Pegon P, Pinto AV. Pseudo-dynamic testing with substructuring at the ELSA laboratory. J Earthq Eng Struct Dyn 2000;29:905–25.

[7] Ohi K, Lin X, Takanashi K. Sub-structure pseudo-dynamic test scheme suitable for bending-shear type flexible steel frames. J Struct Const Eng Trans Archit Inst Jpn 2001;540:49–56 [in Japanese].

[8] Molina FJ, Verzeletti G, Magonette G, Buchet PH, Renda V, Geradin M, et al. Pseudodynamic tests on rubber base isolators with numerical substructuring of the superstructure and strain-rate effect compensation. J Earthq Eng Struct Dyn 2002;31:1563–82.

[9] Pinto AV, Pegon P, Magonette G, Tsionis G. Pseudo-dynamic testing of bridges using non-linear substructuring. J Earthq Eng Struct Dyn 2004;33:1125–46.

[10] Yang W, Nakano Y, Sanada Y. Substructure on-line test technique using non-linear hysteresis modeling with neural network. J Struct Constr Eng Trans Archit Inst Jpn 2004;582:73–80 [in Japanese].

[11] Wu B, Xu G, Wang Q, Williams SM. Operator-splitting method for real-time substructure testing. J Earthq Eng Struct Dyn 2006;35:293–314.

[12] Wallace MI, Sieber J, Neild SA, Wagg DJ, Krauskopf B. Stability analysis of real-time dynamic substructuring using delay differential equation models. J Earthq Eng Struct Dyn 2005;34:1817–32.

[13] Neild SA, Stoten DP, Drury D, Wagg DJ. Control issues relating to real-time substructuring experiments using a shaking table. J Earthq Eng Struct Dyn 2005;34:1171–92.

[14] National Science Foundation. Network for earthquake engineering simulation (NEES): earthquake engineering research equipment, program solicitation. Report NSC00-6, USA: National Science Foundation; 2000.

[15] National Science Foundation. Network for earthquake engineering simulation (NEES): system integration, program solicitation. Report NSC00-7, USA: National Science Foundation; 2000.
[16] Tsai K, Hsieh S, Yang Y, Wang K, Wang S, Yeh C, et al. Network platform for structural experiment and analysis (I). Report NCREE-03-021, Taiwan: National Center for Research on Earthquake Engineering; 2003.
[17] Sugiura K, Nagata N, Suzuka Y, Watanabe E. Internet related structural testing. In: Proceedings of the eighth KKNN seminar on civil engineering, Singapore; 1998. p. 219–24.
[18] Watanabe E, Yun C, Sugiura K, Park D, Nagata K. Online interactive testing between KAIST and Kyoto University. In: Proceedings of the fourteenth KKNN symposium on civil engineering, Kyoto, Japan; 2001. p. 369–74.
[19] Wang K, Tsai K, Wang S, Cheng W, Yang Y. Networked hybrid test frameworks and examples, In: The fifth seminar on earthquake engineering for building structures (SEEBUS), Kyoto, Japan; 2003. p. 81–90.
[20] Takahashi Y, Fenves GL. Software framework for distributed experimental-computational simulation of structural systems. J Earthq Eng Struct Dyn 2006;35:267–91.
[21] Wang T, Pan P, Tomofuji H, Nakashima M, Ohsaki M. Online hybrid test combined with general-purpose finite element program. J Struct Eng Archit Inst Jpn 2005;51B(3):261–8.
[22] Pan P, Tada M, Nakashima M. Online hybrid test by Internet linkage of distributed test and analysis domains. J Earthq Eng Struct Dyn 2005;11:1407–25.
[23] ABAQUS version 6.4 documentation. USA: ABAQUS, Inc.; 2003.
[24] Broyden CG. A class of method for solving nonlinear simultaneous equation. Math Comput 1965;19:577–93.
[25] Broyden CG. Quasi-Newton methods and their application to function minimization. Math Comput 1967;21:368–81.
[26] Dennis JE, More JJ. Quasi-Newton method, motivation and theory. SIAM Rev 1977;19 (1):46–89.
[27] Bathe KJ. Finite element procedures. Englewood Cliffs, NJ: Prentice hall; 1996. pp. 759–761.
[28] National Science Foundation. Network for earthquake engineering simulation (NEES): consortium development, program solicitation. Report NSC01-56, USA: National Science Foundation; 2001.
[29] Yoshitake N, Wang T, Pan P, Nakashima M. A distributed online hybrid test using commercial finite element program, part 1: accuracy characteristic of proposed system. In: Proceedings of technical papers of Kinki branch; 2006, pp. 297–300.
[30] Wang T, Pan P, Nakashima M. On-line hybrid test combining with general-purpose finite element software. J Earthq Eng Struct Dyn 2006;35:1471–88.
[31] Pan P, Nakashima M, Tomofuji H. Online test using displacement-force mixed control. J Earthq Eng Struct Dyn 2005;34:869–88.
[32] Nakashima M, Kanao I, Liu D. Lateral instability and lateral bracing of steel beams subjected to cyclic loading. J Struct Eng ASCE 2002;128(10):1308–16.
[33] Nakashima M, Akazawa T, Igarashi H. Pseudo dynamic testing using conventional testing devices. J Earthq Eng Struct Dyn 1995;24(10):1409–22.
[34] Hughes TJR, Pister KS, Taylor RL. Implicit-explicit finite elements in nonlinear transient analysis. Comput Methods Appl Mech Eng 1979;17–18:159–82.
[35] Nakashima M, Kaminosono T, Ishida M, Ando K. Integration techniques for substructure pseudo dynamic test. In: 4th US national conference on earthquake engineering, Palm Springs, CA; 1990.
[36] Nakashima M, Matsumiya T, Asano K. Comparison in earthquake responses of steel moment frames subjected to near-fault strong motions recorded in Japan, Taiwan, and the U.S. In: International workshop on annual commemoration of Chi-Chi earthquake, Taipei, Taiwan, September 18-20; 2000. p. 112–23.

[37] Belytschko T, Hughes TJR. Computational methods for transient analysis. Computational methods in mechanics, vol. 1. Amsterdam, The Netherlands: Elsevier Science B.V.; 2001.
[38] Pan P, Tomofuji H, Wang T, Nakashima M, Ohsaki M, Mosalam KM. Development of peer-to-peer (P2P) internet online hybrid test system. J Earthq Eng Struct Dyn 2006;35(7):867–90.
[39] Wang T, Pan P, Yoshitake N, Nakashima M. A distributed online hybrid test using commercial finite element program, part 2: application using multiple nonlinear finite element codes. In: Proceedings of technical papers of Kinki branch; 2006.

Chapter 8

Application of an Online Hybrid Test in Engineering Practice

Chapter Outline

8.1 INTRODUCTION

Only real applications in engineering practice can promote the development of the online hybrid test. However, there are few real applications, particularly because the engineers are not necessarily familiar with the loading equipments and the online hybrid techniques. In this chapter, two typical applications will be presented, one of a conventional online hybrid test and one of a peer-to-peer (P2P) Internet online hybrid test, in order to demonstrate the utility and efficiency of this method.

Development of Online Hybrid Testing. http://dx.doi.org/10.1016/B978-0-12-803378-4.00008-X

8.2 APPLICATION EXAMPLE OF A CONVENTIONAL ONLINE HYBRID TEST

8.2.1 Project Brief

In this section, the seismic performance of a retrofitted reinforced concrete (RC) shear wall building is evaluated through substructure online hybrid tests. These old buildings were constructed in 1970s in Beijing, China, featured with a fishbone-type RC shear wall structural system and prefabricated RC claddings as nonstructural enclosing. When being designed, very limited seismic specifications were considered. Recent field investigation reveals that the concrete strength is quite low, and the longitudinal reinforcement ratio is much smaller than that stipulated by the current seismic design code. More seriously, earthquake vibration of the fishbone-type structure is dominated by torsional vibration mode, a very poor seismic performance judged by engineering experience. To improve the seismic performance, a new seismic retrofitting technology is developed using prefabricated RC panels with sufficient steel rebars. The RC claddings are first replaced by these RC panels, which are securely attached to the existing structure by post-cast concrete. These RC panels thus constitute two longitudinal shear walls parallel to the existing one. Further, each piece of transverse wall is extended at both sides by the RC panels, which serve as enhanced boundary elements. These transverse RC panels would be connected tightly to the longitudinal RC panels to form a space structure with very large stiffness in the plane and sufficient stability out of the plane. The performance of this new type of structure, however, needs thorough examination with regards to both construction techniques and seismic behavior.

8.2.2 Prototype and Substructures

To examine the performance of this new type of structure, a 14-story structure is taken as an example. The seismic performance of the retrofitted structure is investigated by substructure online hybrid tests. Due to the limited space of the laboratory, a 1/2 scaled model only including the bottom eight stories were tested. As shown in Fig. 8.1a, the specimen contains three bays in X direction (longitudinal) and four bays in Y direction (transversal). The members within B-C and C-D bays represent old buildings, while those align to D and B axes represent the longitudinal RC panels, and the elements at the D-E and A-B bays are transversal RC panels. These RC panels were poured *in situ*, but after the part representing the old building completed. The total height of the tested structure model is 12.74 m, including a 0.5 m high foundation and a 0.7 m high load beam above the roof of the specimen, as shown in Fig. 8.1b. The story heights are all 1.45 m. The thickness of the shear walls is 80 mm for the part representing the old building, while 100 mm for the retrofitting RC panels. The gravity of the upper stories is exerted to the tested structure model by using prestressed

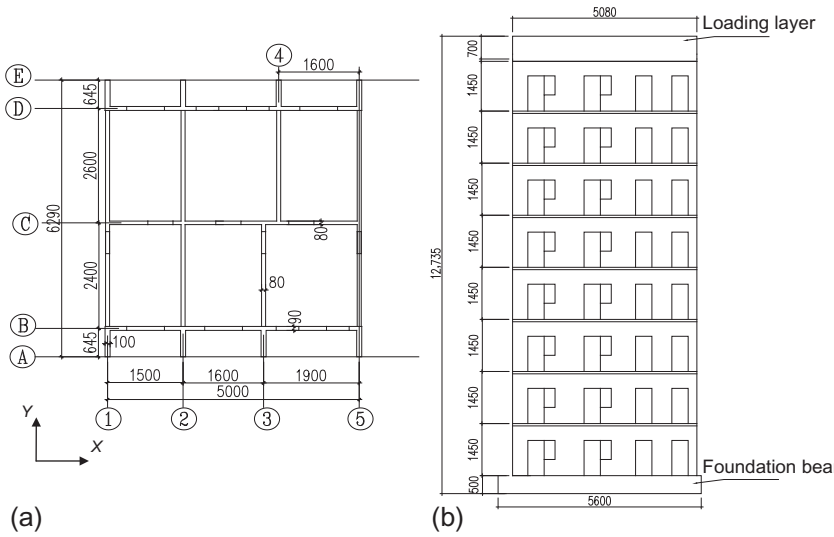

FIGURE 8.1 Illustration of test structure model: (a) plan view and (b) elevation view.

bars, and the axial force ratio of each wall of the specimen is maintained identical to the prototype. Considering that the structure is relatively weak in the longitudinal direction, particularly due to many openings for windows and doors, the pseudodynamic tests were carried out along the longitudinal direction.

8.2.3 Dynamics of the Retrofitted Structure

Considering the limitation of laboratory facilities, the dynamics of the retrofitted structure was simplified as a 4-degree-of-freedom (DOF) mass-spring system. The bottom eight stories, designated as the experimental substructure, were simplified to be a 2-DOF system, and the upper six stories were simplified to be another 2-DOF system, implemented as the simulated substructure. As shown in Fig. 8.2, the floor masses were lumped to the closest DOF when determining the mass matrix. The initial stiffness matrix can be obtained through numerical simulation or physical tests. In this example, it is obtained through physical tests. The procedure is as follows: (1) K_1 and K_2, which represent the equivalent stiffnesses of the bottom four stories and stories 5-8, respectively, were obtained through initial quasi-static tests. It is found that K_1 and K_2 are rather close. (2) The thickness of the shear wall of upper six stories is identical to that of the bottom eight stories. Considering that K_3 and K_4 represent the equivalent stiffnesses of the stories 9-11 and stories 12-14, respectively, K_3 and K_4 are taken to be 1.33 times of K_1 and K_2. (3) The stiffness of the entire structure can be assembled using K_1 to K_4. The equations of motion are then established for the prototype. The displacements obtained in the numerical

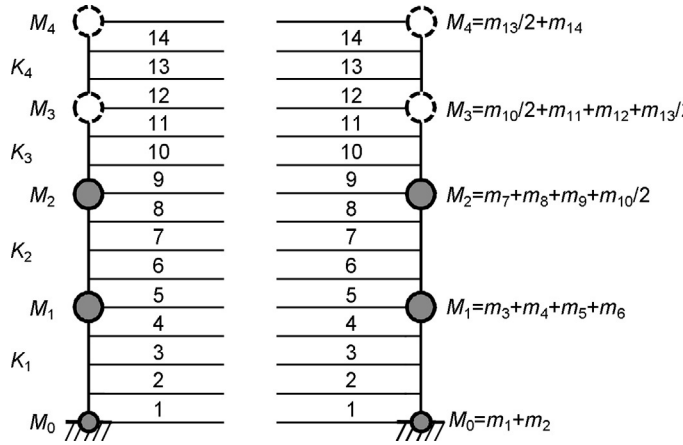

FIGURE 8.2 DOFs of the structure.

TABLE 8.1 Masses and Initial Stiffnesses of Structure Model

DOF	1	2	3	4
Mass ($\times 10^3$ kg)	632	553	474	237
Stiffness (kN/mm)	300	300	400	400

model are multiplied by a factor of 0.5 before loading to the tested structure, the forces obtained from the tested structure are multiplied by a factor of 4 before returning to the numerical model, and the stiffnesses obtained from the physical tests are multiplied by a factor of 2 before assembling the stiffness matrix of the dynamic model. The stiffnesses and masses of the dynamic model are given in Table 8.1. Stiffness proportional damping is adopted, and the damping ratio is taken to be 5% for the fundamental mode. The operator-splitting algorithm was employed and the time interval was taken as 0.01 s.

8.2.4 Configuration of the Hybrid Test System

The configuration of the hybrid test system is shown in Fig. 8.3, where three computers were employed, namely the dynamic solver, the experimental substructure, and the controller. The experimental substructure communicates with the dynamic solver through the Internet. A similar technique as that developed in Chapter 6 is adopted for the networked-based data exchange. The computer named "experimental substructure" is needed to coordinate transformation between the local actuator coordinate and the global coordinate system. It is also responsible of generating command signals for the external control of the

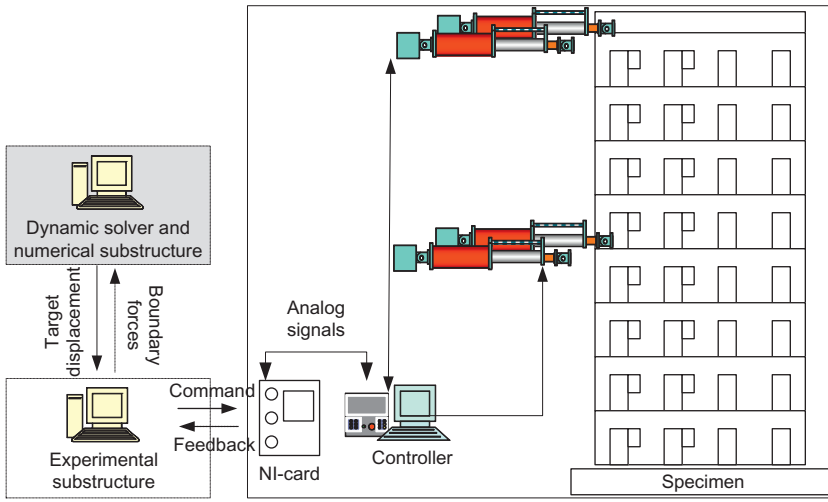

FIGURE 8.3 Configuration of the hybrid test system.

controller, and acquiring the feedback forces from the data acquisition channels of the controller. Note that the equipped servo controller, named SC6000© and manufactured by Shore Western®, is an analog type. An AD/DA conversion is thus necessary. The signal distribution and collection, as well as the AD/DA conversion, are accomplished by a signal input and output device, NI-6259 USB© produced by National Instrument®. The voltage corresponding to the target displacement is output to the analog controller, which further drives the servo valve attached to the actuator. Once the specimen is loaded to the expected position, a voltage corresponding to the restoring force is measured through a load cell inserted between the actuator piston and the specimen. The NI-card then converts the analog voltage to a series of digital numbers. A sampling rate of 100 Hz is adopted for both command generating and signal acquisition processes.

8.2.5 Loading Scheme

According to the simplification of structural dynamics, the loading points were arranged at the fourth and the eighth floors with two loading points for each floor, because of the loading capacity of employed facilities, i.e., 1000 kN for each. To avoid the local tensile failure at the loading points, compression shall be always guaranteed. For this purpose, at the eighth floor, post-tensioned strands were employed to put pre-compression on concrete beams. At the fourth floor, an external steel loading beam was attached to the structure, as shown in Fig. 8.4a. The gap between the steel beam and the specimen was eliminated by post-cast high-strength cement. Loading facilities at the fourth floor were

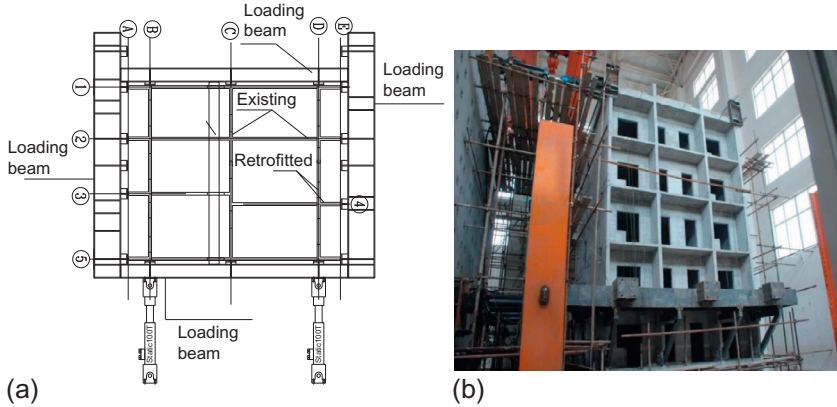

FIGURE 8.4 Arrangement of loading points: (a) loading frame at fourth floor and (b) tested structure.

connected to the steel beam. When pushing, the force passed directly to the specimen. When pulling, the force was exerted as pushing on the specimen from the opposite side of the loading facilities. Figure 8.4b shows the view of the specimen with loading frames at the roof and the fourth floor, respectively.

8.2.6 Input Ground Motions and Intensity

A ground motion recorded at El-Centro during the 1940 Imperial Valley earthquake was selected as the input excitation. Figure 8.5 gives the time history of the original ground motion. It was scaled in this study to 400 Gal corresponding to the rare earthquake of Beijing with the exceedance probability of 2-3% in 50 years.

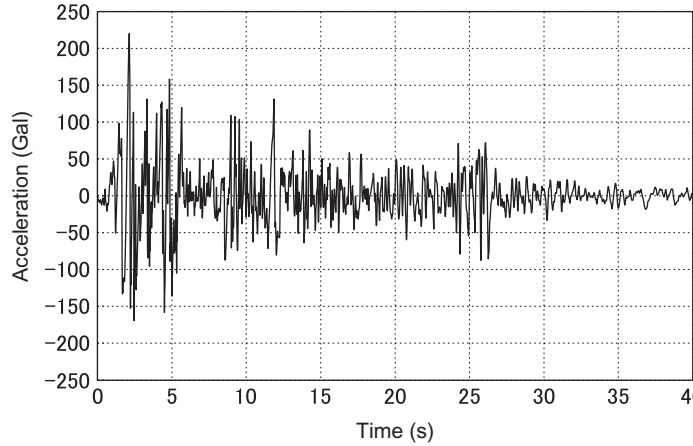

FIGURE 8.5 Acceleration time history of input ground motion.

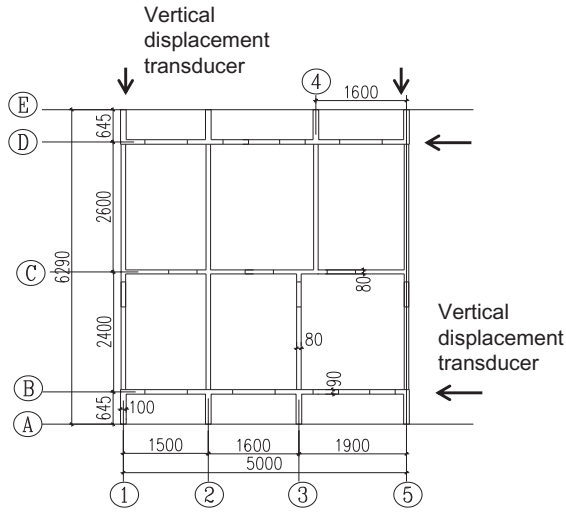

FIGURE 8.6 Arrangement of displacement transducers.

8.2.7 Measurement Scheme

Displacement transducers were arranged at floor level to measure the interstory drift. As shown in Fig. 8.6, 32 displacement transducers were used in total with four at each floor. Among the four transducers for each floor, two were in the *X* direction and two in the *Y* direction. All the displacement transducers were arranged close to the edge of the structure model to check the possible torsion effects.

8.2.8 Test Results

Figure 8.7a shows the displacement response of each floor under the input ground motion. It can be observed that the structure mainly vibrates in the first vibration mode. The peak displacement at the top floor is 90 mm, which corresponds to an overall structure displacement angle of 1/200, and the maximum interstory drift angle is 1/190, not exceeding the interstory drift limit given in the Chinese seismic design code, i.e., 1/120.

Figure 8.7b shows the hysteresis curve of base shear versus top displacement. It can be observed that the structure suffers notable plasticity. As shown in Fig. 8.7c and d, the coupling beam has been seriously damaged, and the bottom of the shear walls has been crushed due to large compression forces.

8.3 APPLICATION EXAMPLE OF P2P INTERNET ONLINE HYBRID TEST

8.3.1 Project Brief

In order to calibrate the safety margin of a steel structure designed in accordance with Japanese seismic design code, the collapse of a one-bay, four-story steel

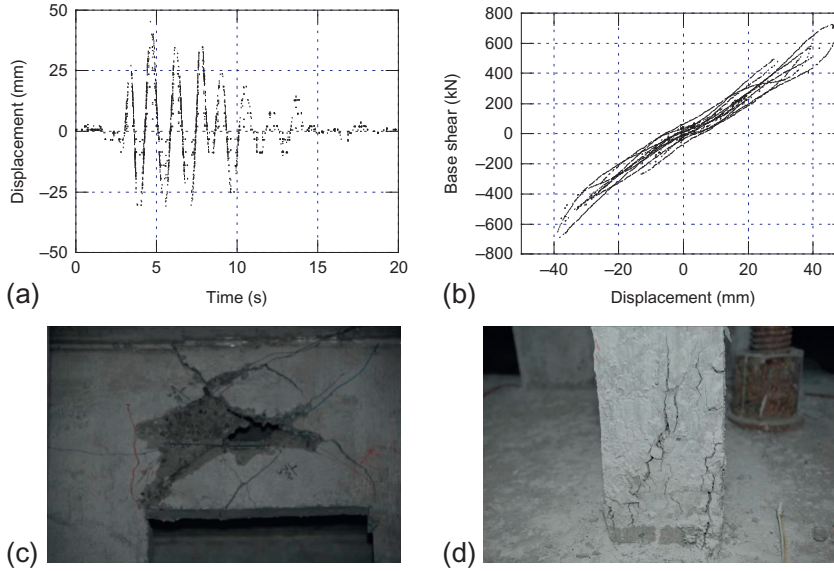

FIGURE 8.7 Response of structure model: (a) displacement history, (b) hysteresis curve, (c) damage of coupling beam, and (d) damage of shear wall.

moment frame is simulated by the proposed P2P Internet online hybrid test system (see Chapter 7). The typical beam hinging mechanism, which is ensured by a strong-column, weak-beam design, is reproduced. The plastic hinges at the two column bases are taken as the experimental portions, while the superstructure is analyzed numerically by a general-purpose finite element program. The implicit plastic rotations of the two column bases are treated as boundary displacements. The three substructures are distributed to different locations. A large ground motion is repeatedly imposed until the column bases lose their capacity to sustain the gravity load. As a result, significant deterioration is observed at both column bases.

8.3.2 Target Structure

The target structure, as shown in Fig. 8.8a, is a four-story moment frame with two spans in the long direction and one span in the short direction. This structure was designed using the current seismic design methods, and satisfies the Building Standard Law of Japan and all related design and construction codes. The structure is studied in the short direction because it is relatively softer with a natural period in this direction of 0.97 s. The floors are made of reinforced concrete slabs. The three pieces of planer frames running in the short direction are identical in terms of the member sizes and steel grade, which are listed in Table 8.2. Only the middle frame, as shown in Fig. 8.8b, is used as the

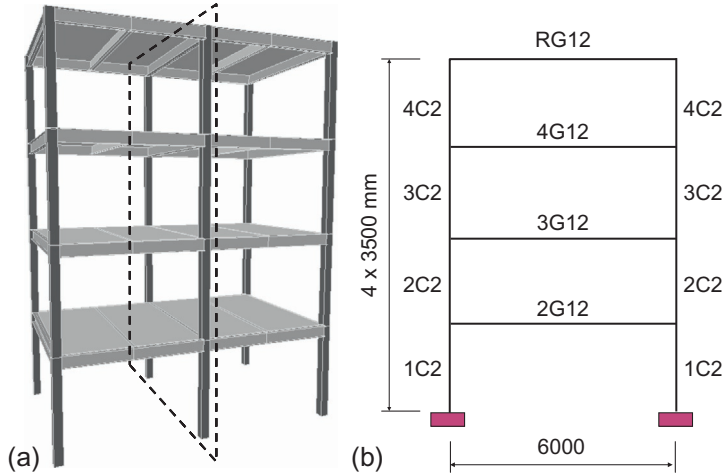

FIGURE 8.8 Four-story steel moment frame (unit: mm): (a) global view and (b) dimensions of middle planar frame.

TABLE 8.2 Sections and Materials of Columns and Beams (Unit: mm)

Columns			Beams		
No.	*Section*	*Material*	*No.*	*Section*	*Material*
4C2	□-300 × 9	BCR295[a]	RG12	H-346 × 174 × 6 × 9	SN400[a]
3C2	□-300 × 9	BCR295	4G12	H-354 × 176 × 8 × 13	SN400
2C2	□-300 × 9	BCR295	3G12	H-400 × 200 × 8 × 13	SN400
1C2	□-300 × 9	BCR295	2G12	H-404 × 201 × 9 × 15	SN400

'□' refers to a tube section.
[a]*Steel grade Japanese Industrial Standards.*

simulation prototype because it sustains the largest gravity loads based on typical load distribution.

The two-dimensional frame is examined by pushover analysis, using ABAQUS to construct a finite element method (FEM) model for the middle frame. Each column and beam is modeled as a line element with concentrated plasticity at both ends to simulate the beam hinging mechanism, as shown in Fig. 8.9a. The moment-rotation relationship of the inserted plastic hinge is treated as perfectly plastic. Although this model is somewhat simple for simulating the behavior at large deformation levels, it does provide a general understanding of the collapse behavior, in light of the fact that there are limited models which

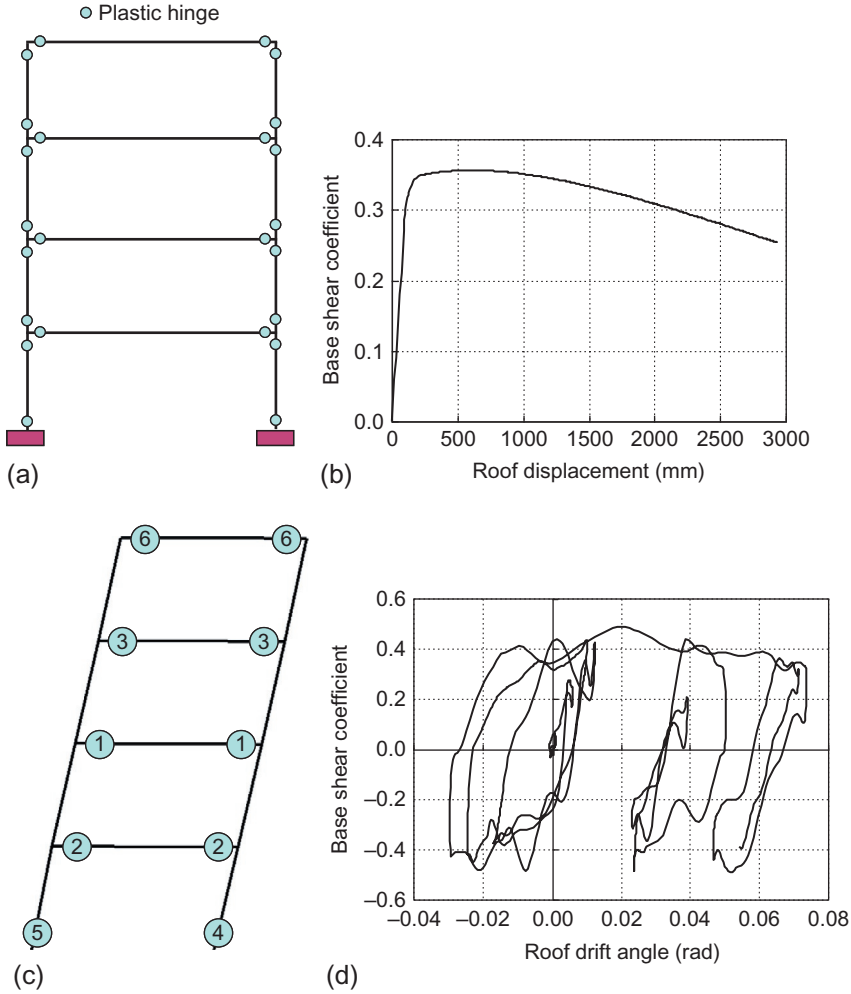

FIGURE 8.9 Results of pushover analysis: (a) FEM model, (b) base shear coefficient versus roof displacement relationship, (c) sequence of plastic hinges, and (d) dynamic behavior of first story using ground motion recorded at JR Takatori, at Hyogoken-Nanbu earthquake, 1995.

accurately predict the beam and column hinge behavior to large deformation levels. The interaction between axial force and moment is considered for the column hinges, but not for the beams, due to the small axial force experienced by the beams. The effect of the concrete slab is not considered in this model. The gravity load is evenly distributed at the top of each column for each floor level, and structure level geometric nonlinearity, P-Δ effect, is considered for the collapse simulation. The horizontal seismic force pattern follows the A_i distribution commonly used in Japanese seismic design. The analysis proceeded until the

structure lost its capacity to sustain the gravity loads, indicating collapse, as shown in Fig. 8.9b where the base shear coefficient is plotted against the roof displacement. The final deformation state is shown in Fig. 8.9c with the plastification sequence. One round of time history analysis using the ground motion recorded at JR Takatori during the 1995 Hyogoken-Nanbu earthquake was also conducted. The relationship between the base shear coefficient and the roof drift angle is shown in Fig. 8.9d. In both analyses, plastic hinges occur only at the beam ends and column bases, while the columns remain in the elastic range as expected from the "strong column, weak-beam design."

8.3.3 Substructures

Significant strength deterioration will occur at the column bases, along with local buckling and fracture when undergoing large deformation. This complex behavior cannot be accurately represented by the plastic hinges employed in the FEM model for the pushover analysis. Therefore, the two plastic hinges at the column bases are tested physically, while the superstructure is treated numerically, as shown in Fig. 8.10. The superstructure is to be simulated by ABAQUS. The details of the FEM model are identical to the FEM model used for the pushover analysis excluding the column bases. However, to treat the plastic hinges experimentally is not straightforward, primarily because the plastic hinge does not form until yielding occurs. To overcome this difficulty, a very large stiffness is assigned to the experimental substructure to approximate its infinite initial

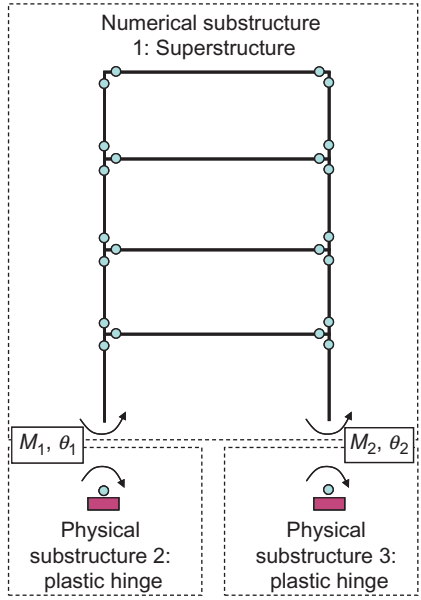

FIGURE 8.10 Division to substructures.

stiffness, so that a continuous performance is achieved. In doing so, it is assumed that the plastic hinge and the rest of the column can be treated as two springs in series with stiffness (k_p) to be assigned to the plastic hinge. This stiffness should be ideally infinite, but for practical purposes significantly larger than the elastic stiffness of the column (k_{col}). Thus, the stiffness assigned to the plastic hinge is taken as 10 times the column stiffness, $k_p = 10\, k_{col}$.

8.3.4 Improved Test Scheme of P2P Framework

The linear assumption for the tested substructures in the quasi-Newton procedure may introduce some errors into the system (see Chapter 7). It is concluded that a larger difference between the assumed stiffness and the actual stiffness introduces a larger error. In this study, the large approximate stiffness adopted for the plastic hinges will be taken as the assumed stiffness within the P2P framework. A value of 10 times the stiffness of the column is selected to maintain the overall stiffness of the first story. However, the use of this fixed stiffness value may introduce large excess energy during the post-yielding stage because of the difference between it and the actual stiffness at this point, as shown in Fig. 8.4. To reduce this excess energy, the secant stiffness is adopted to calculate the restoring force of the tested substructure during the two round quasi-Newton procedures. In the first round of the quasi-Newton procedure, the secant stiffness obtained from the previous step is used. After physical loading, the secant stiffness is updated using the measured moment and rotation for the second round of the quasi-Newton procedure. Whenever unloading occurs, the secant stiffness is updated by the initial stiffness. The excess energy introduced by the secant stiffness is much smaller than that associated with the initial stiffness, providing a more accurate response (Fig. 8.11).

8.3.5 Numerical Analyses by P2P Framework

In order to demonstrate the effectiveness of the improved test scheme using the secant stiffness, two sets of numerical analyses are conducted using the P2P

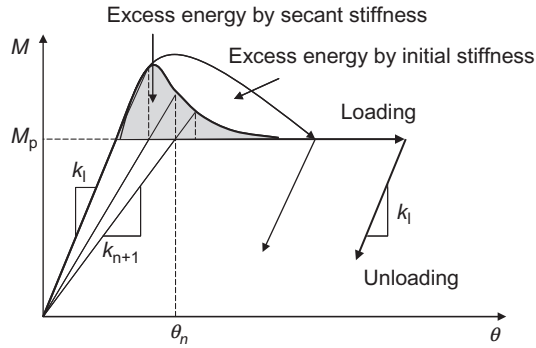

FIGURE 8.11 Improved test scheme using secant stiffness in linear assumption.

framework. The first uses the original initial stiffness scheme and the second uses the improved secant stiffness scheme. The superstructure is simulated using ABAQUS, and the two plastic hinges at the column bases are also simulated numerically adopting an elastic-perfect plastic model. For comparison, a complete numerical analysis using the same FEM model used for the pushover analysis is also performed. The fault-normal component of the 1995 JMA Kobe ground motion is adopted for these analyses. A 28% difference in the displacement response of the first story can be observed in Fig. 8.12a between the initial stiffness scheme and the overall analysis, while the difference is rather limited, 3%, when comparing the secant stiffness with the overall analysis. It is also observed in Fig. 8.12b that the initial stiffness scheme introduces more excess

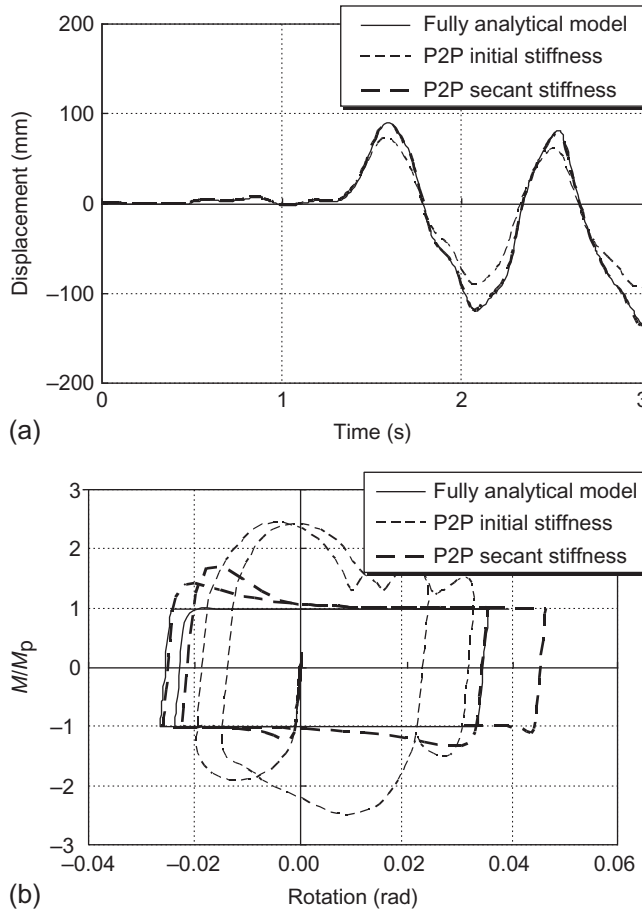

FIGURE 8.12 Comparison between initial-stiffness prediction, secant-stiffness prediction, and full numerical analysis: (a) displacement histories of first story and (b) hysteretic behavior of one of the column base.

energy, 62%, than the secant stiffness scheme, 5%, when compared with the overall numerical analysis. These comparisons demonstrate the effectiveness of the improved test scheme.

8.3.6 Distributed Test Environment

For this online hybrid test, three substructures are included, namely the left column base, the right column base, and the superstructure. These substructures are each distributed to different locations: the structures laboratory on the Katsura campus of Kyoto University, the structures laboratory on the Uji campus of Kyoto University, and an office on the Katsura campus of Kyoto University, respectively. The configuration of the distributed system is shown in Fig. 8.13. In each of the tested domains, there are two similar sets of loading facilities. In the office on the Katsura campus, a computer is used to run the ABAQUS analysis. The "Coordinator" program runs on a computer at an office on the Uji campus. Communication between all domains requires a proxy program due to the presence of a firewall in each network. Details of this data exchange scheme are similar to those described in Chapter 6.

8.3.7 Implementation of Tested Substructures

The plastic rotations of the two column bases are implemented as the boundary displacements. Such a treatment is unique, in that only the plastic hinge is considered as the experimental substructure, thus avoiding difficulties in assuming a finite length of the plastic hinges. However, the plastic rotations cannot be imposed directly to the tested substructures. For this reason, a cantilever column

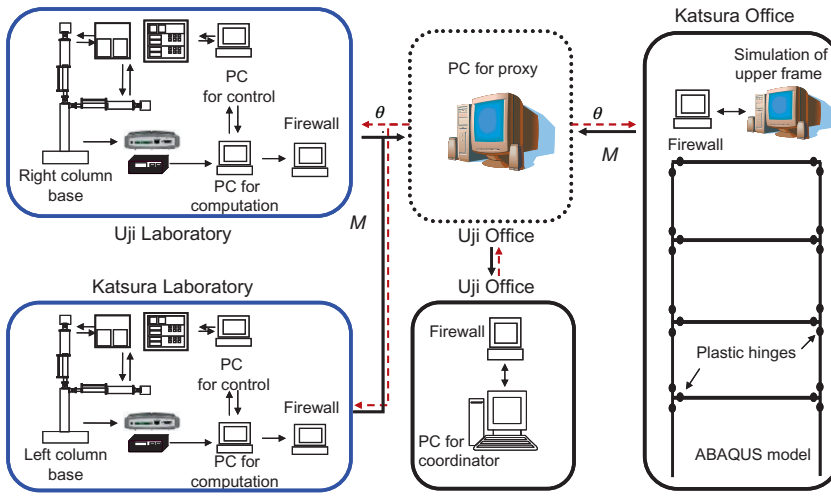

FIGURE 8.13 Distributed online hybrid test system.

is designed so that the plastic rotation can be imposed as a translational displacement. The plastic hinge forms at the fixed end of the cantilever column, and the plastic rotation is controlled by the horizontal displacement at the free end. The target horizontal displacement equals the sum of the displacement induced by the plastic rotation at the column base and the elastic deformation of the cantilever column, as Equation (8.1). The elastic stiffness of the specimen is obtained from preliminary quasi-static tests. To achieve the exact solution from Equation (8.1), the moment value should be the one measured from the specimen. However, this moment cannot be obtained unless the physical loading is conducted. To avoid such an impasse, the value obtained from the first round quasi-Newton procedure is used instead.

$$\delta_{n+1} = L\theta_{c,n+1} + \frac{M^*_{n+1}}{K_c} \tag{8.1}$$

δ_{n+1} is the target loading displacement; L is the distance from the center of the top connector to the base plate; $\theta_{c,n+1}$ is the predicted plastic rotation from the first round of the quasi-Newton procedure; K_c is the elastic stiffness of specimen; M^*_{n+1} is the predicted moment from the first round of the quasi-Newton procedure.

The cantilever column for each substructure is a cold-formed, box section, steel tube with a width-thickness ratio of 33. The column section is scaled to 2/3 of the prototype. The plastic rotation of the specimen is identical to that of the prototype, while the corresponding moment is scaled to 8/27 [$=(2/3)^3$] of that of the prototype. The height of the specimen is chosen according to the facility setup in each laboratory, 1186 mm for the specimen located in the Katsura laboratory, and 1265 mm for the specimen located in the Uji laboratory. The cantilever column is welded to a base plate, which is securely fastened on the foundation beams using high-tension bolts. The tension in the bolts is enough to prevent the base plate from rotating, so that it can be treated as a fixed end. The top end of the cantilever column is connected to the two jacks, one horizontal and one vertical, as shown in Fig. 8.14. The horizontal jack is controlled by displacement to achieve the corresponding plastic rotation, while the vertical jack is controlled by force and provides the varying axial force obtained based on the previous analysis step of the numerical substructure.

8.3.8 Distributed Test

The P2P framework using the improved test scheme is employed to conduct the online hybrid simulation of the target structure. A time interval of 0.01 s is adopted. The fault-normal ground motion recorded at the JR Takatori station during the 1995 Hyogoken-Nanbu earthquake is used. The ground motion is enlarged by 1.5 times to ensure severe damage to the column base and eventual collapse. The enlarged ground motion has a peak pseudovelocity of approximately 9.8 m/s. Only the first 10 s of the ground motion, which contains the

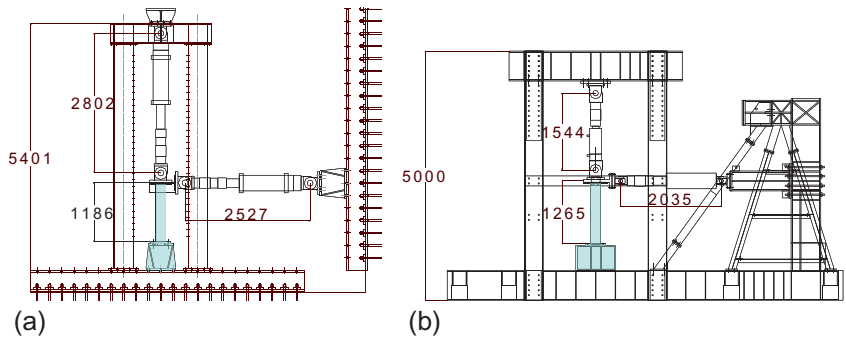

FIGURE 8.14 Test specimen (Unit: mm): (a) specimen for left column base (Katsura Laboratory) and (b) specimen for right column base (Uji Laboratory).

largest components of the acceleration, are considered and repeated twice to achieve a full collapse of this structure. After the first application of the ground motion, the structure is allowed to undergo free vibration for one-second before the second application of the ground motion until collapse. The entire input ground motion adopted for this study is shown in Fig. 8.15.

8.3.9 Verification of P2P Framework

The roof displacement response obtained using the P2P framework is plotted in Fig. 8.16a and compared with the results when the structure is only analyzed numerically. The same FEM model as that used for the pushover analysis is

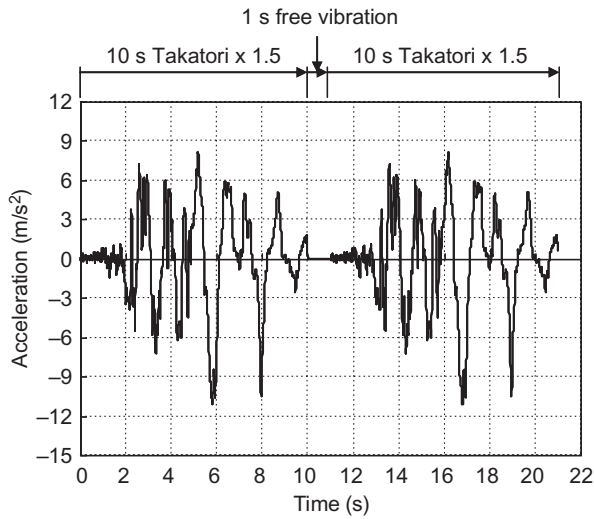

FIGURE 8.15 Input ground motion.

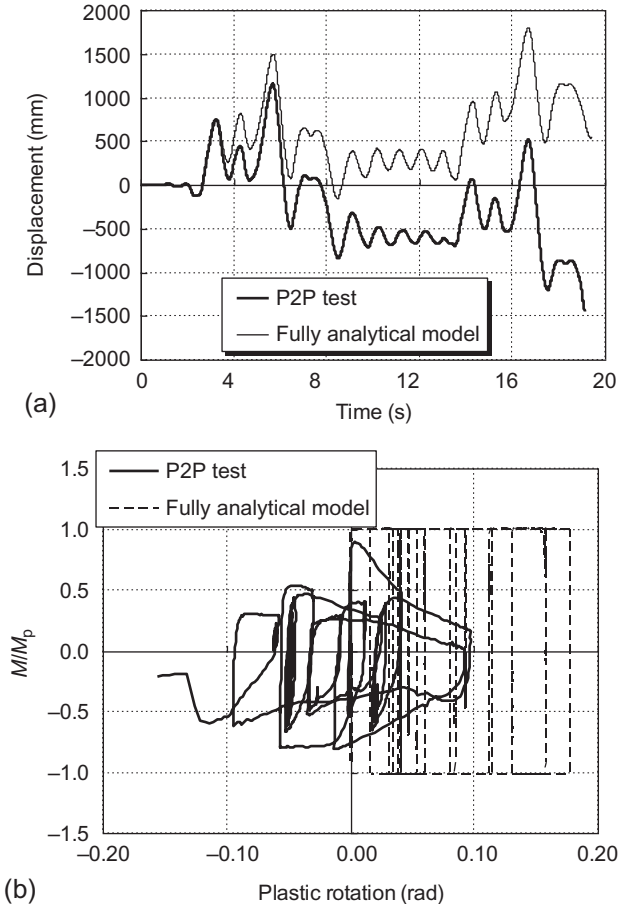

FIGURE 8.16 Comparison between P2P test and fully numerical analysis: (a) roof displacement time history and (b) hysteretic comparison of left column base between test and analysis.

used for the numerical analysis of the entire frame. The responses for the first 3 s are similar to each other with a maximum difference of only 4%, which demonstrates the validity of the P2P framework. After the first 3 s, significant differences can be observed. For the P2P test, local buckling occurs at the column bases and a degradation of the strength is observed. For the FEM analysis, the perfectly plastic model adopted for the plastic hinges cannot simulate such degradation, as shown in Fig. 8.16b. Furthermore, it is observed from the P2P test results that the maximum moment relative to the plastic moment of the column bases is smaller than one because of the interaction between the moment and axial force. The perfectly plastic model, however, does not consider the axial force-moment interaction. The benefits of physically testing the two column bases are evident. It also should be noted that, although the behavior of each

tested substructure appears to be unstable, the P2P framework works smoothly and convergence is guaranteed. These observations demonstrate that the P2P framework is capable of handling multiple tested substructures with significant unstable behavior.

8.3.10 Efficiency of P2P Framework

The numbers of iterations during the first and second rounds of the quasi-Newton procedure are plotted in Fig. 8.17a with respect to the time step. The first round of the quasi-Newton procedure required 1-2 iterations to reach convergence for all steps, while the second round of the quasi-Newton procedure needed 1-4 iterations for small responses and 4-6 iterations for larger responses.

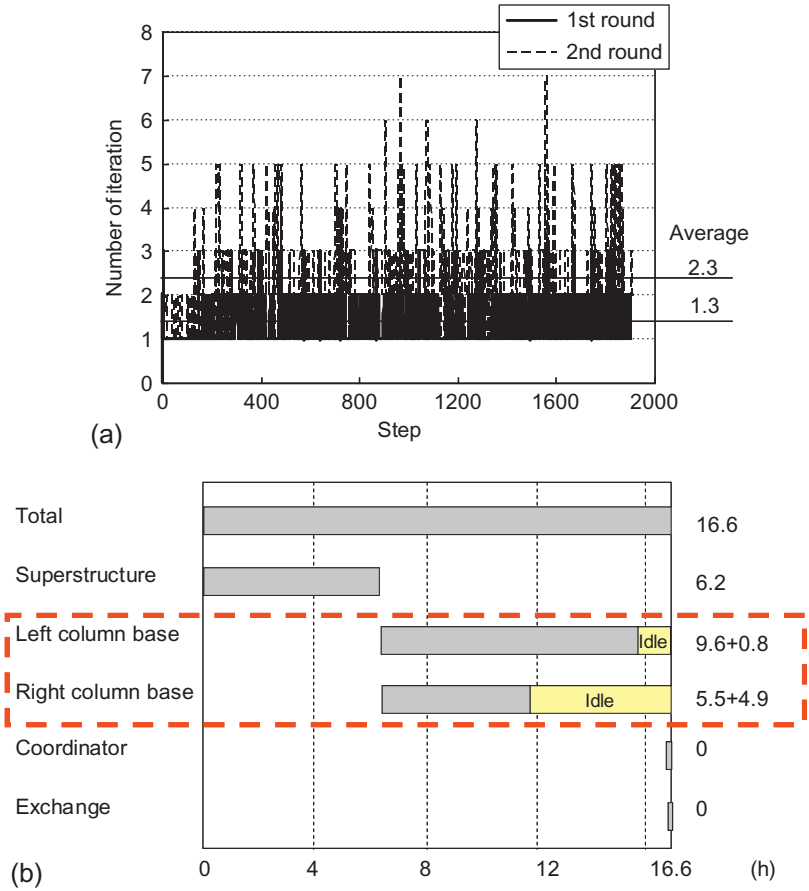

FIGURE 8.17 Time efficiency: (a) number of iterations per time step and (b) time consumed by each substructure.

On average, the first and second rounds of the quasi-Newton procedure required 1.3 and 2.3 iterations, respectively.

The simulation continues until collapse occurs 19.12 s into the input motion, meaning, 1912 steps of simulation in total were conducted. The entire simulation required approximately 16.6 h. Figure 8.17b shows the time consumed by each substructure. The ABAQUS simulation for the superstructure required 6.2 h. A total of 9.6 and 5.5 h were needed for the left and right experimental column base substructures on the Katsura campus and Uji campus, respectively. The computation time consumed by the "Coordinator" program and the communication time are approximately zero. The difference between the two tested substructures can be attributed to the differences in the loading facilities used for each substructure. Note that the implementation of the tested substructures in the P2P framework is in parallel. Thus, if the loading of one specimen finishes, the procedure must wait for the later to finish, as well, before continuing. This waiting time exists for both tested substructures, 0.8 and 4.9 h for the left and right column bases, respectively. However, the parallel nature of the P2P system improves the efficiency by 22% [=(6.2+9.6+5.5 − 16.6)/21.3].

8.3.11 Practical Evaluation of Collapse Limit of the Frame

In the FEM model of the superstructure, the concrete slab is not simulated and it is observed that the plastic hinges first occur at the beam ends during the simulation, followed by the formation of hinges at the column bases. Therefore, once the column bases lost their ability to sustain the loads, the structure starts to collapse due to P-Δ effects. Thus, a redistribution of the large moment to the top ends of the columns at the first story does not occur. In this study, the collapse is defined as the monotonic increase of the horizontal displacement of the superstructure. The rotation time histories of the two column bases are plotted in Fig. 8.18a. The column bases survived after several cycles of large deformation up to 0.1 rad, which is significantly larger than that considered in the seismic design code. After 18.71 s of the input motion, the rotations in the left and right column bases increased monotonically from −0.062 to −0.068 rad until exceeding −0.15 rad at 19.11 and 19.05 s, respectively. The vertical displacement is also examined for the right column base located on the Uji campus. At 18.71 s, the ability of the specimen to sustain axial load diminished resulting in a sharp increase in the vertical displacement, as shown in Fig. 8.18b. The simulation is terminated at 19.12 s when the stroke capacity of the loading facility at the Uji laboratory is reached.

8.3.12 Complex Behavior of Column Bases

The relationship between the moment and plastic rotation for the two column bases is plotted in Fig. 8.19, with the moment normalized by the full-plastic moment. The shape of the sections at various instances is also shown, together

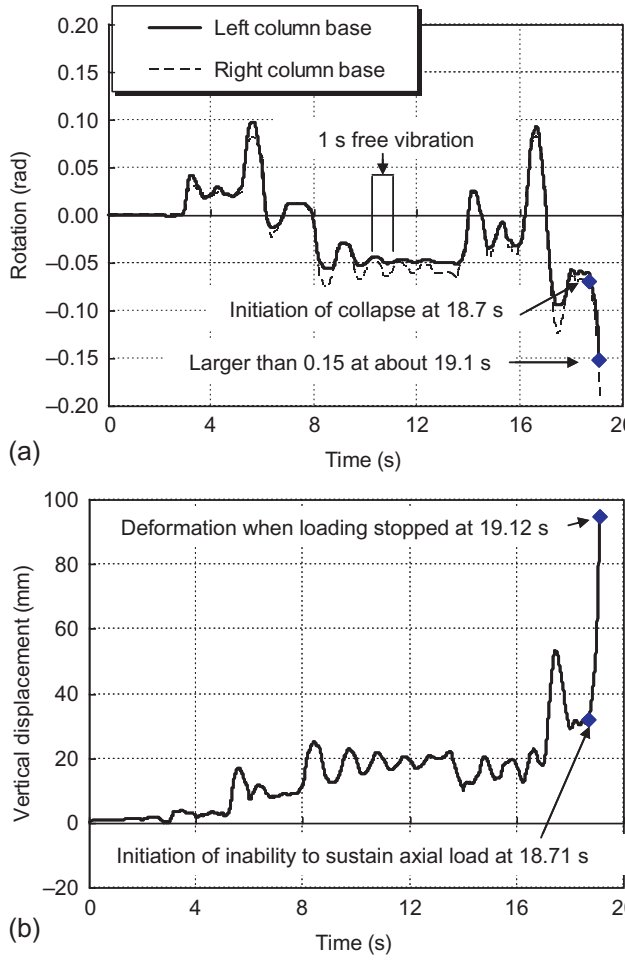

FIGURE 8.18 Responses at column bases: (a) rotation histories to collapse and (b) axial deformation history of right column base (Uji).

with the loading direction at that time. Significant differences in the hysteretic behavior can be observed from these figures, which is primarily attributed to the varying axial force imposed on the two column bases. Figure 8.20 shows the axial force time histories for the two column bases, which are given as the axial force ratio, i.e., the axial force normalized by the plastic axial force. The axial force ratio imposed on each specimen varies between −0.02 and 0.32, where compression is defined as positive. Given that the moment capacity of the column bases varies with axial load, these ranges of axial force can have a significant effect on the behavior of the individual column bases. At the maximum axial force ratio of 0.32, which occurs in the left column base at 2.96 s, the

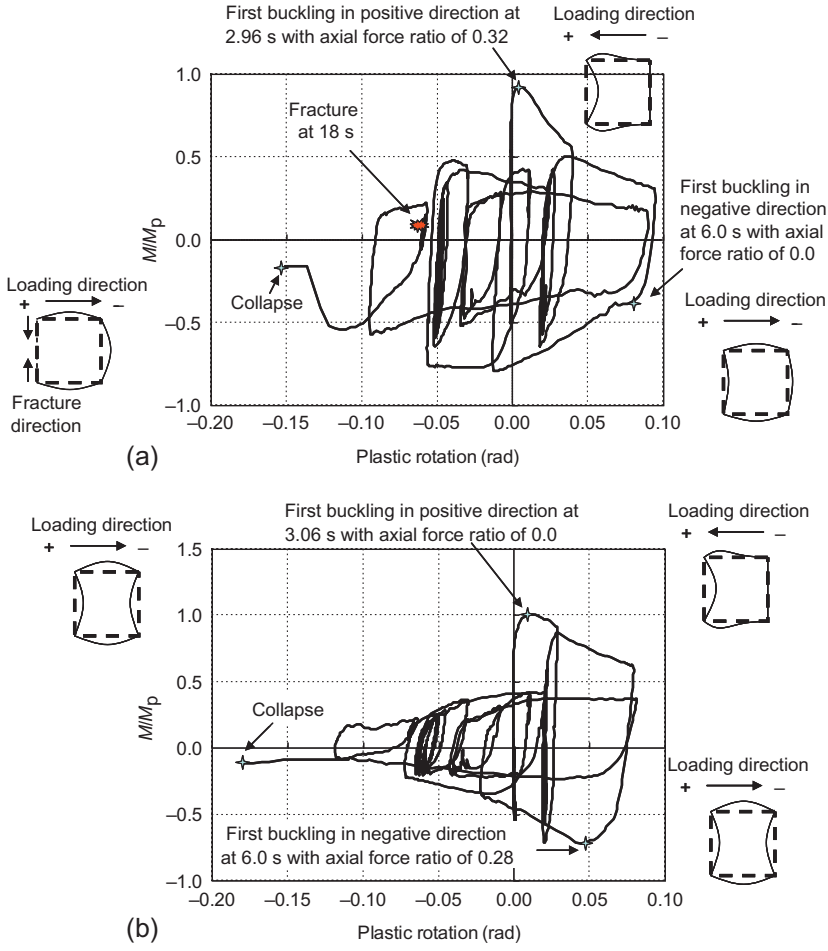

FIGURE 8.19 Hysteretic behavior of column bases: (a) left column base (Katsura) and (b) right column base (Uji).

full-plastic moment capacity cannot be achieved. Only 88% of the plastic moment capacity is obtained before first buckling occurred in the positive direction. For the right column base, the full-plastic moment can be achieved at first buckling, because the axial force ratio is approximately zero.

As a result of the varying axial load, the left column base experiences buckling in the positive direction at an earlier point, 2.96 s, than the right column base, 3.06 s. Comparing the axial force ratios at these times shows that the left column has a much larger compression force, 0.32, compared with the right column base, 0.0. The larger axial force ratio causes the left column to first undergo buckling at a much smaller plastic rotation of 0.004 rad compared with the right column base which first underwent buckling at a plastic rotation of 0.011 rad.

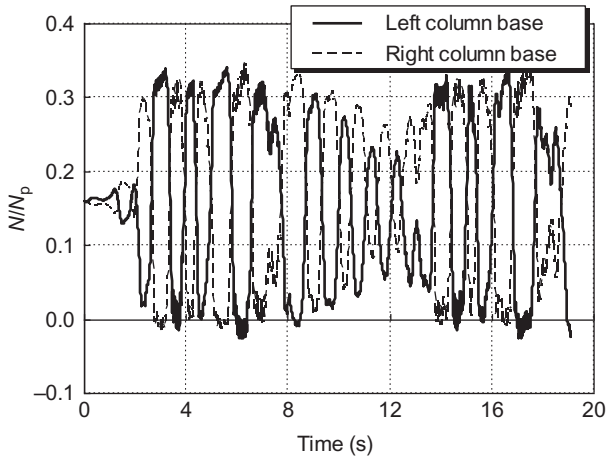

FIGURE 8.20 Time histories of axial forces imposed on column bases.

The resulting strength degradation at this point is more significant for the left column base with a decrease from 0.88 to 0.5 as compared with the right column base, which decreased from approximately 1.0-0.9, as a result of there being almost no axial force on the right column base at the onset of first buckling. However, the degradation rate does switch for the two column bases when they buckle in the negative direction due to a decrease in the axial force ratio of the left column base (0.07) and an increase in the axial force ratio of the right column base (0.28). The results show the complexity of moment rotation behavior associated with the formation and deterioration of plastic hinges at the column base, particularly due to the varying axial load.

The behavior of the two column bases after buckling in the negative direction is of interest. The strength of the left column base degrades from -0.42 to -0.38, but then increases to -0.8. The reason for this increase is that the axial force ratio, -0.02, is small, resulting in limited buckling deformation allowing for moment capacity to increase after initial buckling. This behavior is not observed in the right column base due to the large axial force ratios when deformation occurs in the negative direction. The right column base shows continuous strength degradation from -0.82 to -0.27.

Consequently, the different axial load histories result in different failure states, as shown in Fig. 8.21. For the left column base, fracture occurs on the surface in the positive loading direction due to the significant accumulation of plastic deformation at this surface. The fracture starts from the rounded corners of the steel tube and moves toward the middle. Eventually, the initial fracture penetrates the entire surface. Local buckling on the opposite surface of the left column base is limited. For the specimen located at the Uji campus, significant local buckling on both loading direction surfaces is observed, but fracture did not initiate.

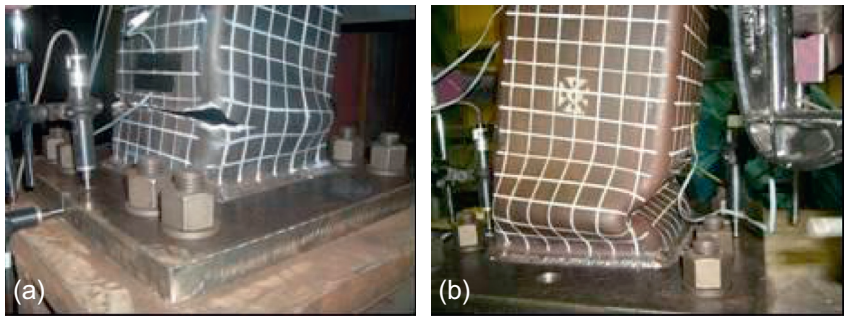

FIGURE 8.21 Local buckling and fracture of column bases: (a) left column base (Katsura) and (b) right column base (Uji).

8.4 SUMMARY AND CONCLUSIONS

This chapter gives two applications of an online hybrid test in engineering practice to demonstrate its utility and efficiency. An online hybrid test successfully applied to a retrofitted structure to investigate its seismic behavior is first introduced. Although simple, the online hybrid test framework works effective and performs stably. The simplifications adopted in this study could be an option when testing complex structures but with simple dynamics. The results obtained from the experiment demonstrate that the proposed retrofitting technology is one of the feasible approaches to enhance the seismic performance of high-rise shear wall buildings with limited seismic detailing.

Then, the seismic simulation of a four-story steel moment frame using an improved P2P online hybrid test system is presented. The entire structure is divided into three substructures. The superstructure is treated numerically using ABAQUS, while the two plastic hinges at the column bases are the experimental substructures, which are physically tested in different locations. A strong ground motion is employed and imposed on the structure twice to ensure collapse after significant strength deterioration of the column bases. The P2P online hybrid test system encountered no significant problems in dealing with this highly unstable behavior and the experimental substructures in multiple locations. The major findings are summarized as follows:

(1) In order to improve the accuracy of the P2P framework when applied to tested substructures with distinct initial and post-yielding stiffness, the linear assumption is updated by using the secant stiffness based on the previous loading force and displacement.

(2) The improved P2P framework is able to handle multiple tested substructures. The obtained results are deemed more accurate than those obtained from the fully analytical FEM model. By testing the column bases, the strength deterioration due to the local buckling and fracture can be accurately obtained, while it is rather difficult to simulate this behavior

numerically. The improved P2P framework is demonstrated to be stable even though the tested substructures have significant unstable behavior.

(3) Collapse behavior of a steel moment frame is simulated reasonably using the P2P system. Significant deterioration at column bases is observed. The column bases sustained a varying axial force and survived after several cycles of large deformation up to 0.1 rad, which is much larger than that considered in the current seismic design codes. It is also observed that the varying axial force affects the behavior of column bases significantly.

Chapter 9

Summary and Conclusions

Chapter Outline

The online hybrid test has a history of more than 30 years, and it has been demonstrated as an effective approach for the earthquake response simulation of structures. The test, when combined with substructuring techniques, is called a "substructure online hybrid test," and is particularly appealing for the earthquake response simulation of large-scale structures. Recently, some major improvements of the substructure online hybrid test are concentrated on the displacement-force mixed control, the incorporation of finite element source codes for numerical substructures, and the distribution of substructures to different locations geographically. Most previous applications of the substructure online hybrid test combined with finite element programs, however, require modification of the source code to interact with the experimental substructures, which makes the online hybrid test system too rigid to be implanted from one structural test environment to another. The concept of the geographical distribution of substructures was proposed several years ago, and a few real applications were carried out. To fully take advantage of "distributed testing," it is important to standardize and simplify the interfaces of diverse subsystems so that they can be effectively incorporated into an integrated Internet test system. For these two reasons, it is beneficial if each substructure is highly encapsulated with standard interfaces for interaction with other substructures. In this study, most effort focuses on the development and application of four online hybrid test systems.

Development of Online Hybrid Testing. http://dx.doi.org/10.1016/B978-0-12-803378-4.00009-1

The first system is the *online hybrid test using displacement-force mixed control*. Two types of mixed control are devised: the displacement-force "combined control" and "switching control." In the first type, one jack is operated in displacement-control, while the other jack is operated in force-control. In the second type, one actuator is controlled by displacements sometimes and by force otherwise, depending on the state of the layer.

The second system is the *Internet online hybrid test system using a host-station framework*. This system consists of the host, stations, and data exchange interfaces. The test and analyses are conducted at separate locations, and the data necessary to exchange between them are transmitted over the Internet. In the system, the substructure online test is considered, and the test is combined with a finite element method (FEM) type of program that adopts incremental formulation and implicit integration algorithms.

The third system is the *Internet online hybrid test system using a separated-model framework* into which a general-purpose FEM program is incorporated. Two separated models are adopted in this system; one for the dynamics and the other for the hysteretic behavior of the structure to be analyzed. The equations of motion are formulated for the entire structure, while the hysteretic behavior is obtained from sophisticated FEM models or from experiments directly. In this framework, all substructures are treated equally, which makes the system more versatile, since various FEM programs or experiment facilities can be selected for different substructures according to their individual characteristics. The system utilizes a high-speed data exchange procedure using a socket mechanism.

The fourth system is the *Internet online hybrid test system using a peer-to-peer framework*. A "Coordinator" equipped with an iterative algorithm based on the quasi-Newton iteration is developed to achieve compatibility and equilibrium between substructures. A test procedure, featuring two rounds of quasi-Newton iterations and using the assumed elastic stiffness, is adopted to avoid iteration for the substructure being tested physically. In this system, the equations of motion are formulated not for the entire structure, but for each substructure, treating all substructures equally and independently. Each substructure is encapsulated, and only standard input and output (I/O), i.e., displacements and forces at the boundaries, are used as interfaces. Multiple general-purpose finite element (FEM) programs can be incorporated into this system in accordance with the characteristics of respective numerical substructures.

This book consists of nine chapters. Chapter 1 is the background of this study, and this chapter gives the summary and conclusions. Chapters 2–8 constitute the main part of the book: (1) basics of time integration algorithms; (2) typical time integration algorithms; (3) online hybrid test using mixed control; (4) Internet online hybrid test using host-station framework; (5) separated-model framework and its demonstration examples; (6) peer-to-peer (P2P) framework, its preliminary demonstration test, and its convergence speed investigation; (7) application in engineering practice. The major findings of each chapter are summarized below.

9.1 TIME INTEGRATION ALGORITHMS

In Chapter 2, the basics of time integration algorithms, which are important to solve the equations of motion of online hybrid tests, are introduced. The existing time integration algorithms are grouped into such families as: (1) linear multistep methods; (2) Newmark's family; (3) collocation methods; (4) α-family; (5) ρ-family; and (6) mixed implicit-explicit methods. The superiority of one family over the others is summarized in terms of the following rules: (a) self-restart procedure; (b) second-order accuracy; (c) unconditional stability; and (d) optimal and controllable numerical dissipation.

(1) Most linear multistep methods require information of several previous steps and thus are not self-started. By carefully selecting the difference equations for the acceleration and velocity terms, the other three rules can be satisfied.
(2) Newmarks' family methods are self-started. If the parameters are carefully selected, the second-order accuracy and unconditional stability can be achieved. The numerical dissipation, however, exists only when the method is first-order accurate. Furthermore, numerical dissipation of the methods is not necessarily desirable, since it may affect the lower modes significantly.
(3) Collocation methods, α-family methods, and ρ-family methods can satisfy all of four rules.
(4) The numerical properties of mixed implicit-explicit methods are different for the implicit and explicit domains. They are quite dependent on the algorithm adopted for each domain.

Summarized in Chapter 3 are implementations of some notable time integration algorithms for the online hybrid test. They are categorized into: (1) application of explicit algorithms and (2) applications of implicit algorithms.

(1) Explicit algorithms are most convenient and easier to be incorporated into the online hybrid test system but most of them have time interval limitations.
(2) Implicit algorithms are always appealing in terms of unconditional stability and numerical dissipation. Difficulties are encountered, however, when applied to online hybrid tests. The main concern is that the iterative procedures required in implicit algorithms may introduce undesirable loading and unloading in tested structures whose hystereses are path-dependent.

9.2 ONLINE HYBRID TEST USING MIXED CONTROL

In Chapter 4, an online test technique that employs mixed control of displacement and force is presented. Indeed, displacement-control is not practicable when the structure is too stiff to accurately control the loading actuator's displacement. Two types of mixed control are considered. One is called "combined

control," in which one jack is force-controlled and the other is displacement-controlled, with fine tuning of motion of the two jacks; and the other is called "switching control," in which one jack is operated by displacement-control but switched to force-control upon request. The proposed mixed control technique was used to simulate earthquake responses of an eight-story base-isolated structure. The superstructure and base-isolation layer were assigned as the computed part and tested part, respectively. The superstructure was treated as a mass-spring system, with one mass per floor and one horizontal and one vertical spring per story.

"Combined control" was applied to simulate the earthquake responses of the base-isolated structure when subjected to both horizontal and vertical ground motions. A horizontal jack was used to impose lateral displacement of the base-isolation layer (displacement-controlled), and a vertical jack was used to impose axial forces on the layer (force-controlled). The force applied was given as the product of the assumed stiffness and the vertical displacement (estimated by the direct integration of the associated equations of motion). In consideration of rather strong dependency of the horizontal stiffness of the base-isolation layer on the vertical stresses imposed on the layer, application of varying axial forces in tune with the horizontal deformations is justified. The online test with the proposed mixed control was successful, with accurate displacement- and force-control achieved for both jacks.

"Switching control" was applied to simulate the earthquake responses of the base-isolated structure when subjected to large vertical motions and hence involving tension in base-isolation layer. To consider significant differences in stiffness when the layer takes compression and tension, force-control (similar to the one used in combined mixed control) was adopted when taking compression and switched to displacement-control once taking tension. Switching from force to displacement or vice versa was satisfactory, particularly when adopting time-varying integration to specify the precise switching point.

9.3 INTERNET ONLINE HYBRID TEST USING HOST-STATION FRAMEWORK

Chapter 5 presents an Internet online test system developed for the simulation of earthquake responses of structures. The system consists of the host, stations, and data exchange interfaces. In the system, the substructure online test is considered, and the test is combined with a FEM type of program that adopted incremental formulation and implicit integration algorithms. The test and analysis are conducted at separate locations, and the data necessary to exchange between them are transmitted over the Internet. A procedure of sharing files and folders implemented by standard operating systems is adopted for the data exchange. The procedure does not require special permission for transmitting data across firewalls and other security restrictions; hence the data exchange is accessible and easily implemented. The stability and security of the data exchange

procedure was verified through 6000 rounds of data transmission; not a single problem was encountered. The host analyzes the computed parts, collects information from the stations, and simulates the response of the entire structure. A tangent stiffness prediction method is proposed by which the information obtained from the physical online test can be incorporated into a numerical analysis program that utilizes incremental formulation and implicit integration algorithms. The proposed stiffness prediction method makes use of the force and displacement data of the previous three steps. The method was compared with various alternatives for the stiffness prediction, and its effectiveness was demonstrated by a series of physical tests applied to a base-isolated building model.

9.4 SEPARATED-MODEL FRAMEWORK AND ITS DEMONSTRATION EXAMPLES

Chapter 6 presents a substructure online hybrid test into which a general-purpose FEM program is incorporated. This test uses the separated-model framework, in which two models are set up for the dynamics and the static behavior of one structure, respectively. Such a program is powerful and versatile in increasing the modeling accuracy for the numerical portion, thus enhancing the applicability of the substructure online hybrid test. The decisive challenge in this new development is how to combine the test with a FEM program in which modifications of the source code are strictly prohibited. The proposed framework was demonstrated by an eight-story base-isolated structure considering the collision effect with the surrounding retaining walls. The following conclusions were found from the studies for the proposed distributed online hybrid test system:

(1) In many structures, the structural dynamics can be represented by a fewer degrees of freedom than the structural static hysteresis. The static behavior of the structure is simulated by sophisticated FEM models and test specimens. Therefore, the models with different sophistication can be adopted for dynamics and static behavior, respectively. This separation makes the substructure online hybrid test system more versatile.

(2) The explicit Newmark method is not necessarily the only time integration algorithm that can be used for this system. Any time integration algorithm can be adopted. Implementation for the other time integration algorithms, such as implicit algorithms, may have hardware requirement. In this study, the explicit Newmark method is adopted only because of its simplicity.

(3) The high-speed data exchange scheme using a socket mechanism based on TCP/IP protocol is demonstrated to be stable and fast. In this study, transfer of data requires almost no time.

(4) The standard I/O scheme is employed for the incorporation of general-purpose FEM programs. There is no need to modify the source code of these programs, thus the system can be easily implanted for structural

laboratories having different analytical tools. The key component in the use of the standard I/O only is the repeated adoption of the restart capacity offered as a standard procedure by many FEM programs.

(5) The time required for each step of the FEM analysis increased almost linearly over time, because of the longer overhead time needed for restarting with an increasing number of previous steps. A total of 7.8 h were needed to complete the test. Out of the total hours, the time needed was 4.2 h for the physical test (i.e., loading) and 6.7 h for the numerical analysis (including I/O). The loading and numerical analyses ran in parallel. The test was made quasi-statically; hence the overhead time associated with restarting was not a serious drawback in terms of the time efficiency.

(6) The response of the superstructure would increase greatly after collision takes place.

(7) The plastification is limited mainly in lower several stories, and amplification of the displacement responses decrease with the height.

(8) The collision effect would lessen in subsequent collisions, because the gap between the base-isolation layer and surrounding retaining wall would increase by previous collisions.

(9) Although the ground motion was enlarged by two times a very large motion recorded in the 1995 Kobe earthquake, collision occurred only three times, meaning that the gap commonly adopted in Japanese design law of 500-600 mm is generally sufficient.

9.5 P2P FRAMEWORK AND ITS PRELIMINARY DEMONSTRATION TEST

The P2P Internet online hybrid test system proposed in Chapter 7 is a distributed online hybrid test system using the substructuring technique. In this system, the simulated structure is divided into multiple substructures. All substructures are equally treated and geographically distributed to various laboratories, which enables the system to integrate the resources of various laboratories for seismic simulation of large-scale structures. A central part called "Coordinator" is devised to achieve the compatibility and equilibrium on the boundaries between the substructures. Each substructure is implemented as a highly encapsulated and independent "Partner" with limited data on the boundary, such as displacements and reactional forces, exchanged with the "Coordinator." Each "Partner" can be treated as the experimental part or analytical part according to the user's option. The system is characterized with the following features:

(1) The equations of motion are formulated for each substructure separately, but not for the entire structure as did in the conventional substructural online hybrid test. The size of the equations of motion is reduced. Therefore, a faster computation may be achieved. The separated formulation also enables the

parallel computation of substructures which is known to increase the capacity and efficiency significantly for computation of large systems.

(2) An iterative quasi-Newton procedure is employed by the "Coordinator" to satisfy the boundary conditions between all substructures. The implementation in the "Coordinator" in fact is an equation solution procedure for the boundaries. Any type of Newton's method can be chosen for this solution. The exact amplification matrix, i.e., the stiffness matrix that is only related to the boundaries, however, is unavailable because of the involvement of experimental substructures. The quasi-Newton procedure devised in this study is the best choice, because it does not need any exact stiffness, and the convergence rate is super-linear.

(3) A testing scheme featuring a two-round quasi-Newton procedure is devised to avoid iteration for the substructures being tested physically. This is a typical predicting and correcting scheme, each corresponding to one round quasi-Newton procedure. In one step of analysis, the experimental substructures are always assumed to be linear elastic, and the nonlinearities are taken into consideration only by the one-time loading between the predicting and correcting quasi-Newton procedures. This linear assumption may introduce numerical damping into the system, which is deemed helpful for suppressing higher mode responses that may be generated by the experimental errors.

(4) The incorporation of existing finite element programs into the online hybrid test system is believed to be able to increase the versatility of online hybrid tests, particularly the accuracy of the behavior of the computed part. It would be much more effective if a highly encapsulated finite element program could be incorporated into the online test system as a black box, accessible only through standard I/O. Restart capability is the key to realize this application. Two kinds of restart are employed by this system, i.e., "iterative restart" and "step-wise restart." "Iterative restart" is a procedure used to find the true state of the current step, which always restarts from the true state of the previous step. "Step-wise restart" is the last step of the "iterative restart." It records the true state of each step.

(5) The reactional force acquired from each substructure is a dynamic reactional force, which includes the effect of the inertia force and the viscous damping force on the boundary.

(6) It is unnecessary for the substructures to have the same damping. This is very appealing when the characteristics of substructures are significantly different.

(7) A fast and stable solution using a socket mechanism is developed for data exchange over the Internet, and an Internet hybrid test environment is constructed. The interfaces of diverse "Partners" are standardized and simplified, so that they can be incorporated effectively into the integrated Internet test system. Such standardization and simplification also require the substructures to be highly encapsulated.

(8) The relative unbalanced energy is the most suitable convergence criterion for the iterative quasi-Newton procedure, which converges no matter how the structure is divided and how many boundary degrees of freedom. Furthermore, more degrees of freedom are associated with the boundaries and a larger number of iterations is needed. Also, a good approximation of the initial stiffness matrix associated with the boundaries may reduce the number of iterations greatly. This helps with the improvement of efficiency of the P2P framework.

(9) The convergence of the two-round quasi-Newton test scheme is guaranteed if the referenced stiffness (normally the initial stiffness) is not smaller than the actual stiffness. The P2P system is accurate when the integration time interval is small, and commensurate in accuracy with the averaged acceleration algorithm for larger sampling frequencies.

9.6 THE APPLICATION OF ONLINE HYBRID TEST IN ENGINEERING PRACTICE

Chapter 8 gives two applications of the online hybrid test in engineering practice to demonstrate its utility and efficiency. An online hybrid test successfully applied to a retrofitted structure to investigate its seismic behavior is first introduced. Although simple, the online hybrid test framework works effectively and performs stably. The simplifications adopted in this study could be an option when testing complex structures but with simple dynamics. The results obtained from the experiment demonstrate that the proposed retrofitting technology is one of the feasible approaches to enhance the seismic performance of high-rise shear wall buildings with limited seismic detailing.

Then, the seismic simulation of a four-story steel moment frame using an improved P2P online hybrid test system is presented. The entire structure is divided into three substructures. The superstructure is treated numerically using ABAQUS, while the two plastic hinges at the column bases are the experimental substructures, which are physically tested in different locations. A strong ground motion is employed and imposed on the structure twice to ensure collapse after significant strength deterioration of the column bases. The P2P online hybrid test system encountered no significant problems in dealing with this highly unstable behavior and the experimental substructures in multiple locations. The major findings are summarized as follows:

(1) In order to improve the accuracy of the P2P framework when applied to tested substructures with distinct initial and post-yielding stiffness, the linear assumption is updated by using the secant stiffness based on the previous loading force and displacement.

(2) The improved P2P framework is able to handle multiple tested substructures. The obtained results are deemed more accurate than those obtained from the fully analytical FEM model. By testing the column bases, the

strength deterioration due to the local buckling and fracture can be accurately obtained, while it is rather difficult to simulate this behavior numerically. The improved P2P framework is demonstrated to be stable even though the tested substructures have significant unstable behavior.

(3) Collapse behavior of a steel moment frame is simulated reasonably using the P2P system. Significant deterioration at column bases is observed. The column bases sustained a varying axial force and survived after several cycles of large deformation up to 0.1 rad, which is much larger than that considered in the current seismic design codes. It is also observed that the varying axial force affects the behavior of column bases significantly.

Appendix A

List of Exiting Time Integration Algorithms

Method	Formulation	Stability condition	Accuracy
Central difference method (CDM)	$ma_n + cv_n + kd_n = f_n$ $a_n = (d_{n+1} - 2d_n + d_{n-1})/\Delta t^2$ $v_n = (d_{n+1} - d_{n-1})/2\Delta t$	$\Omega < 2\sqrt{1-\xi^2}$	Second order
Trapezoidal rule	$ma_{n+1} + cv_{n+1} + kd_{n+1} = f_{n+1}$ $v_{n+1} = 2(d_{n+1} - d_n)/\Delta t - v_n$ (Note that the equation of motion is first cast into a set of first-order ordinary differential equations and then using the difference equation.)	Unconditionally stable	Second order
Gear's two-step method	$ma_{n+1} + cv_{n+1} + kd_{n+1} = f_{n+1}$ $v_{n+1} = (3d_{n+1} - 4d_n + d_{n-1})/2\Delta t$	Unconditionally stable	Second order
Houbolt's method	$ma_{n+1} + cv_{n+1} + kd_{n+1} = f_{n+1}$ $a_{n+1} = (2d_{n+1} - 5d_n + 4d_{n-1} - d_{n-2})/\Delta t^2$ $v_{n+1} = (11d_{n+1} - 18d_n + 9d_{n-1} - 2d_{n-2})/6\Delta t$	Unconditionally stable	Second order
Park's method	$ma_{n+1} + cv_{n+1} + kd_{n+1} = f_{n+1}$ $v_{n+1} = (10d_{n+1} - 15d_n + 6d_{n-1} - d_{n-2})/6\Delta t$	Unconditionally stable	Second order
Average acceleration method	$ma_{n+1} + cv_{n+1} + kd_{n+1} = f_{n+1}$ $d_{n+1} = d_n + \Delta t v_n + 0.25\Delta t^2(a_n + a_{n+1})$ $v_{n+1} = v_n + 0.5\Delta t(a_n + a_{n+1})$	Unconditionally stable	Second order
Linear acceleration method	$ma_{n+1} + cv_{n+1} + kd_{n+1} = f_{n+1}$ $d_{n+1} = d_n + \Delta t v_n + \Delta t^2 a_n/3 + \Delta t^2 a_{n+1}/6$ $v_{n+1} = v_n + 0.5\Delta t(a_n + a_{n+1})$	$\omega\Delta t < 2\sqrt{3}$	Second order

Continued

Method	Formulation	Stability condition	Accuracy
Fox–Goodwin method	$ma_{n+1} + cv_{n+1} + kd_{n+1} = f_{n+1}$ $d_{n+1} = d_n + \Delta t v_n + 5\Delta t^2 a_n/12 + \Delta t^2 a_{n+1}/12$ $v_{n+1} = v_n + 0.5\Delta t(a_n + a_{n+1})$	$\omega \Delta t < \sqrt{6}$	Fourth order
Explicit Newmark-β method	$ma_{n+1} + cv_{n+1} + kd_{n+1} = f_{n+1}$ $d_{n+1} = d_n + \Delta t v_n + 0.5\Delta t^2 a_n$ $v_{n+1} = v_n + 0.5\Delta t(a_n + a_{n+1})$	$\Omega < 2\sqrt{1-\xi^2}$	Second order
Modified Newmark-β method	$ma_{n+1} + cv_{n+1} + [(1+\alpha)k + \rho m/\Delta t^2]d_{n+1}$ $-(\alpha k + \rho m/\Delta t^2)d_n = f_{n+1}$ ($\alpha \geq 0$ and $\rho < 0$) $d_{n+1} = d_n + \Delta t v_n + 0.5\Delta t^2 a_n$ $v_{n+1} = v_n + 0.5\Delta t(a_n + a_{n+1})$		
γ-Function explicit method	$ma_{n+1} + cv_{n+1} + kd_{n+1} = f_{n+1}$ $d_{n+1} = d_n + \Delta t v_n + 0.5\Delta t^2 a_n$ $v_{n+1} = v_n + \Delta t(1-\gamma)a_n + \Delta t \gamma a_{n+1}$ $\gamma = 0.5 + \sum_{i=1}^{\infty}(-1)^{i+1} c_i \left(\Delta t^2 k/m\right)^{2i-1}$, c_i is a constant.	$\gamma \geq 0.5$ $\Omega < 2/(\gamma - 0.5)$	Second order
Chung explicit method	$ma_{n+1} + cv_{n+1} + kd_{n+1} = f_{n+1}$ $d_{n+1} = d_n + \Delta t v_n + (0.5-\beta)\Delta t^2 a_n + \beta \Delta t^2 a_{n+1}$ $v_{n+1} = v_n + \Delta t(1.5a_{n+1} - 0.5a_n)$	$1 \leq \beta \leq \frac{28}{27}$ $\Omega \leq 2/\sqrt{4\beta - 3}$	Second order

Continued

Method	Formulation	Stability condition	Accuracy
Chang explicit method	$ma_{n+1} + cv_{n+1} + kd_{n+1} = f_{n+1}$ $d_{n+1} = d_n + \beta_1 \Delta t v_n + \beta_2 \Delta t^2 a_n$ $v_{n+1} = v_n + 0.5\Delta t(a_n + a_{n+1})$ $\beta_1 = \dfrac{1 + 0.5\Delta tc/m}{1 + 0.5\Delta tc/m + 0.25\Delta t^2 k^1/m}$ $\beta_2 = \dfrac{0.5}{1 + 0.5\Delta tc/m + 0.25\Delta t^2 k^1/m}$	Unconditionally stable	Second order
Wilson-θ method	$ma_{n+\theta} + cv_{n+\theta} + kd_{n+\theta} = f_{n+\theta}$ $a_{n+\tau} = a_n + (a_{n+1} - a_n)\tau/\Delta t^2$ $v_{n+\tau} = v_n + a_n\tau + (a_{n+1} - a_n)\tau^2/2\Delta t$ $d_{n+\tau} = d_n + v_n\tau + \dfrac{1}{2}a_n\tau^2 + (a_{n+1} - a_n)\tau^3/6\Delta t, \quad (0 \le \tau \le \theta)$	$\theta \ge 1.37$ Unconditionally stable	Second order
Collocation method	$ma_{n+\theta} + cv_{n+\theta} + kd_{n+\theta} = f_{n+\theta}$ $a_{n+\theta} = (1-\theta)a_n + \theta a_{n+1}$ $f_{n+\theta} = (1-\theta)f_n + \theta f_{n+1}$ $v_{n+\theta} = v_n + \theta\Delta t[(1-\gamma)a_n + \gamma a_{n+\theta}]$ $d_{n+\theta} = d_n + \theta\Delta t v_n + (\theta\Delta t)^2[(1-2\beta)a_n + 2\beta a_{n+\theta}]/2$	$\gamma = 0.5$, $\theta \ge 1$, and $\dfrac{\theta}{2(1+\theta)} \ge \beta \ge \dfrac{2\theta^2 - 1}{4(2\theta^3 - 1)}$ Unconditionally stable	Second order
Hilber-Hughes-Taylor-α method (HHT-α method)	$ma_{n+1} + (1+\alpha)cv_{n+1} - \alpha cv_n + (1+\alpha)kd_{n+1} - \alpha kd_n$ $= (1+\alpha)f_{n+1} - \alpha f_n$ $d_{n+1} = d_n + \Delta t v_n + (0.5-\beta)\Delta t^2 a_n + \beta\Delta t^2 a_{n+1}$ $v_{n+1} = v_n + \Delta t(1-\gamma)a_n + \Delta t\gamma a_{n+1}$	$\beta = \dfrac{1}{4}(1-\alpha)^2$, $\gamma = \dfrac{1}{2} - \alpha - \dfrac{1}{3} \le \alpha \le 0$ Unconditionally stable	Second order
Wood-Bossak-Zienkiewicz-α method (WBZ-α method)	$(1-\alpha)ma_{n+1} + \alpha ma_n + cv_{n+1} + kd_{n+1} = f_{n+1}$ $d_{n+1} = d_n + \Delta t v_n + (0.5-\beta)\Delta t^2 a_n + \beta\Delta t^2 a_{n+1}$ $v_{n+1} = v_n + \Delta t(1-\gamma)a_n + \Delta t\gamma a_{n+1}$	$\beta \ge \dfrac{\gamma}{2} \ge \dfrac{1}{4}$, $\alpha + \gamma = \dfrac{1}{2}$ Unconditionally stable	Second order

Continued

Method	Formulation	Stability condition	Accuracy
Generalized-α method	$ma_{n+1-\alpha_m} + cv_{n+1-\alpha_f} + kd_{n+1-\alpha_f} = f_{n+1-\alpha_f}$ $d_{n+1} = d_n + \Delta t v_n + (0.5-\beta)\Delta t^2 a_n + \beta \Delta t^2 a_{n+1}$ $v_{n+1} = v_n + \Delta t(1-\gamma)a_n + \Delta t \gamma a_{n+1}$ $d_{n+1-\alpha_f} = (1-\alpha_f)d_{n+1} + \alpha_f d_n, v_{n+1-\alpha_f} = (1-\alpha_f)v_{n+1} + \alpha_f v_n$ $a_{n+1-\alpha_m} = (1-\alpha_m)a_{n+1} + \alpha_m a_n, f_{n+1-\alpha_f} = (1-\alpha_f)f_{n+1} + \alpha_f f_n$	$\alpha_m \le \alpha_f \le \frac{1}{2}\beta \ge \frac{1}{4} + \frac{1}{2}(\alpha_f - \alpha_m)$ Unconditionally stable	$\gamma = \frac{1}{2} - \alpha_m + \alpha_f$ Second order
Explicit generalized-α method	$ma_{n+1-\alpha_m} = f_{n+1-\alpha_f} - r(d_n)$ $d_{n+1} = d_n + \Delta t v_n + (0.5-\beta)\Delta t^2 a_n + \beta \Delta t^2 a_{n+1}$ $v_{n+1} = v_n + \Delta t(1-\gamma)a_n + \Delta t \gamma a_{n+1}$ $a_{n+1-\alpha_m} = (1-\alpha_m)a_{n+1} + \alpha_m a_n$	$\Omega_b < (1+\rho_b)\sqrt{2-\rho_b}$	$\gamma = \frac{3}{2} - \alpha_m$ Second order
ρ-Method	$d_{n+1} = d_n + \Delta d$ $v_{n+1} = \frac{2}{\Delta t}\Delta d - v_n + \frac{1-\rho}{1+\rho}\Delta t a_n$ $a_{n+1} = \frac{(1+\rho)(1+\rho^2)}{\Delta t^2}(\Delta d - \Delta t v_n) + (1-\rho-\rho^3)a_n$ $\left(m + \frac{\Delta t}{2}c + \frac{\Delta t^2}{2(1+\rho)}k^1\right)\Delta d = \Delta t m v_n + \frac{\rho-1}{2(1+\rho)}\Delta t^2 m a_n$ $+ \frac{\Delta t^2}{2}(f_n^* - q_n - b^* q'_{n+1})$ $f_n^* = \frac{1}{\Delta t}\int_{t_n}^{t_{n+1}} f(t)\mathrm{d}t,\ b^* = \frac{1}{\Delta t}\int_{t_n}^{t_{n+1}} b(t)\mathrm{d}t$	$\rho \le 1$ Unconditionally stable	Second order
Implicit-explicit method	$\mathbf{M}\mathbf{a}_{n+1} + \mathbf{C}^{\mathrm{I}}\mathbf{v}_{n+1} + \mathbf{C}^{\mathrm{E}}\tilde{\mathbf{v}}_{n+1} + \mathbf{K}^{\mathrm{I}}\mathbf{d}_{n+1} + \mathbf{K}^{\mathrm{E}}\tilde{\mathbf{d}}_{n+1} = \mathbf{F}_{n+1}$ $\tilde{\mathbf{d}}_{n+1} = \mathbf{d}_n + \Delta t \mathbf{v}_n + (0.5-\beta)\Delta t^2 \mathbf{a}_n$ $\tilde{\mathbf{v}}_{n+1} = \mathbf{v}_n + \Delta t(1-\gamma)\mathbf{a}_n$ $\mathbf{d}_{n+1} = \tilde{\mathbf{d}}_{n+1} + \beta \Delta t^2 \mathbf{a}_{n+1}$ $\mathbf{v}_{n+1} = \tilde{\mathbf{v}}_{n+1} + \Delta t \gamma \mathbf{a}_{n+1}$ $\mathbf{M} = \mathbf{M}^{\mathrm{I}} + \mathbf{M}^{\mathrm{E}},\ \mathbf{C} = \mathbf{C}^{\mathrm{I}} + \mathbf{C}^{\mathrm{E}},\ \mathbf{K} = \mathbf{K}^{\mathrm{I}} + \mathbf{K}^{\mathrm{E}},\ \mathbf{F} = \mathbf{F}^{\mathrm{I}} + \mathbf{F}^{\mathrm{E}},$ Superscripts I and E refer to the implicit and explicit groups, respectively.	If $\gamma \ge 0.5$, $\mathbf{B}^{\mathrm{I}} + \bar{\mathbf{B}}^{\mathrm{E}}$ is positive definite, and $\mathbf{K}^{-1}$ exists, it is unconditionally stable. $\mathbf{B}^{\mathrm{I}} = \mathbf{M}^{\mathrm{I}} + \Delta t(\gamma - 0.5)\mathbf{C}^{\mathrm{I}}$ $+ \Delta t^2(\beta - 0.5\gamma)\mathbf{K}^{\mathrm{I}}$ $\bar{\mathbf{B}}^{\mathrm{E}} = \mathbf{M}^{\mathrm{E}} + \Delta t(\gamma - 0.5)\mathbf{C}^{\mathrm{E}}$ $+ \Delta t^2(\beta - 0.5\gamma)\mathbf{K}^{\mathrm{E}}$ $-\Delta t \gamma \mathbf{C} - \Delta t^2 \beta \mathbf{K}$	$\gamma = 0.5$ Second order

Appendix B

Implementation of the OS Method

In this section, implementation of the OS method is illustrated by using a program language called "Visual Basic." Note that essentially any language will be acceptable.

```
'// Global variables for Dynamic analysis
Global g_dblGroundMotion(1 to NSTEP) As Double    ' Record the ground motions
Global g_lngCurStep As Long
Global g_lngPreStep As Long
Global g_dblPreTime As Double
Global g_dblCurTime As Double
Global g_VecPreDisp(1 to NDOF) As Double          ' Displacement of
                                                    previous step
Global g_VecPrePredictDisp(1 to NDOF) As Double  ' Predict displacement of previous step
Global g_VecPreVelo(1 to NDOF) As Double          ' Velocity of previous step
Global g_VecPreAcce(1 to NDOF) As Double          ' Acceleration of previous step
Global g_VecCurDisp(1 To NDOF) As Double          ' Displacement of current step
Global g_VecCurPredictDisp(1 To NDOF) As Double   ' Predict displacement of current step
Global g_VecCurVelo(1 To NDOF) As Double          ' Velocity of current
                                                    step
Global g_VecCurAcce(1 To NDOF) As Double          ' Acceleration of current step
Global g_VecPreResForce(1 To NDOF) As Double      ' Previous total restoring force to predicted displacement
Global g_VecCurResForce(1 To NDOF) As Double      ' Current total restoring force to predicted displacement
Global g_VecPreForce(1 To NDOF) As Double         ' Previous total corrected restoring force
Global g_VecCurForce(1 To NDOF) As Double         ' Current total corrected restoring force
Global g_VecStoryDrift(1 To NDOF) As Double       ' Story drift angle
Global g_VecStoryShear(1 To NDOF) As Double       ' Story shear force
Global g_MatStiff(1 To NDOF, 1 To NDOF) As Double ' Stiffness matrix
Global g_MatStiffNum(1 To NDOF,1 To NDOF) As Double ' Stiffness matrix for numerical substructure
Global g_MatMass(1 To NDOF,1 To NDOF) As Double   ' Mass matrix
Global g_MatDamping(1 To NDOF,1 To NDOF) As Double ' Damping matrix
```

```
′// Global variables for physical test
Global g_intTested(1 To NDOF) As Integer    ′ If physical tested DOF

′// This subroutine is used to solve the equations of motion using the OS algorithm
Public Sub OS()
    On Error GoTo PROC_ERR

    ′// Local variables used for iteration.
    Dim lngLoopI, lngLoopJ, lngLoopK As Long

    ′// Local variable used for calculation
    Dim dbTempForce As Double
    Dim VecCal1() As Double
    Dim VecCal2() As Double
    Dim VecCal3() As Double
    Dim VecCal4() As Double
    Dim VecUnit() As Double
    ReDim VecCal1(1 To NDOF)
    ReDim VecCal2(1 To NDOF)
    ReDim VecCal3(1 To NDOF)
    ReDim VecCal4(1 To NDOF)
    ReDim VecUnit(1 To NDOF)
    Dim MatCal1() As Double
    Dim MatCal2() As Double
    ReDim MatCal1(1 To NDOF, 1 To NDOF)
    ReDim MatCal2(1 To NDOF, 1 To NDOF)
```

```
′// Start solving equations of motion
For lngLoopI = 1 To g_lngTotalStep
    g_lngCurStep = lngLoopI
    g_dblCurTime = g_lngCurStep * g_dblInterval

    ′// Calculate the displacement of the current step
    ′// d'=dn + dt Vn + (0.5 - beta) dt*dt an
    Call VectorSuperposition(g_VecPreDisp, g_VecPreVelo, 1.0#, g_dblInterval, VecCal1, CInt(NDOF))
    Call VectorSuperposition(VecCal1, g_VecPreAcce, 1.0#, (0.5 - g_dblParameters(1)) * g_dblInterval ^2, g_VecCurPredictDisp,
    CInt(NDOF))
    Call MatrixVectorMultiply(g_MatStiffNum, g_VecCurPredictDisp, _
                                    g_VecCurResForceNum, CInt(NDOF), CInt(NDOF))

    ′// get restoring forces for the tested dofs
    For lngLoopK = 1 To NDOF
        If g_intTested(lngLoopK) = 1 Then
            ′ convert to mm, then to test model scale, and conduct physical loading
            g_mode1(lngLoopK).SetSetptToValue(g_VecCurPredictDisp(lngLoopK) * 1000 * g_dblForceScale(lngLoopK),
            g_dbLoadTime(lngLoopK))
        End If
        End If
    Next lngLoopK

    For lngLoopK = 1 To NDOF
        g_VecCurResForceExp(lngLoopK) = 0.0#
        If g_intTested(lngLoopK) = 1 Then
```

```
            If g_intActNum(lngLoopK) = 1 Then
                g_signals(lngLoopK) = gStation.FloatSignals.Find(g_strForceSignal1(lngLoopK))
                g_VecCurResForceExp(lngLoopK) = g_signals(lngLoopK).Value * 1000 / g_dblForceScale(lngLoopK)
                ' convert to N, then to fully model scale
            ElseIf g_intActNum(lngLoopK) = 2 Then
                dbTempForce = 0.0#
                g_signals(lngLoopK) = gStation.FloatSignals.Find(g_strForceSignal1(lngLoopK))
                dbTempForce = g_signals(lngLoopK).Value
                g_signals(lngLoopK) = gStation.FloatSignals.Find(g_strForceSignal2(lngLoopK))
                g_VecCurResForceExp(lngLoopK) = dbTempForce + g_signals(lngLoopK).Value
                g_VecCurResForceExp(lngLoopK) = g_VecCurResForceExp(lngLoopK) * 1000 / g_dblForceScale
                (lngLoopK)
                ' convert to N, then to fully model scale
            End If
        End If
Next lngLoopK

Call VectorSuperposition(g_VecCurResForceExp, g_VecCurResForce Num, _
                                1.0#, 1.0#, g_VecCurResForce, CInt(NDOF))
'// end of getting restoring forces

'// Caculate effective stiffness matrix: D = M + C dt Gamma + K dt^2 Beta
Call MatrixSuperposition(g_MatDamping, g_MatStiff, g_dblInterval * g_dblParameters(2), g_dblInterval ^ 2 *
g_dblParameters(1), _
                                MatCal1, CInt(NDOF), CInt(NDOF))
Call MatrixSuperposition(g_MatMass, MatCal1, 1.0#, 1.0#, MatCal2, CInt(NDOF), CInt(NDOF))
```

```
′// Calculate effective external force: F = -M I ag - C (Vn + dt (1 - Gamma) An) - R
For lngLoopJ = 1 To NDOF
    VecUnit(lngLoopJ) = 1.0#
Next lngLoopJ

Call MatrixVectorMultiply(g_MatMass, VecUnit, VecCal1, CInt(NDOF), CInt(NDOF))

Call VectorSuperposition(g_VecPreVelo, g_VecPreAcce, 1.0#, (1.0# - g_dblParameters(2)) * g_dblInterval, VecCal2,
CInt(NDOF)) ′ Never change VecCal2
Call MatrixVectorMultiply(g_MatDamping, VecCal2, VecCal3, CInt(NDOF), CInt(NDOF))

Call VectorSuperposition(VecCal1, VecCal3, -1.0# * g_dblGroundMotion(lngLoopI) * g_dblMotionScale, -1.0#, Vec-
Cal4, CInt(NDOF))
Call VectorSuperposition(VecCal4, g_VecCurResForce, 1.0#, -1.0#, VecCal1, CInt(NDOF))

′// Find the inverse of D
Call MatrixInverse(MatCal2, MatCal1, CInt(NDOF))

′// Find the acceleration, velocity and displacement of the current step
Call MatrixVectorMultiply(MatCal1, VecCal1, g_VecCurAcce, CInt(NDOF), CInt(NDOF))
Call VectorSuperposition(g_VecCurPredictDisp, g_VecCurAcce, 1.0#, g_dblInterval ^2 * g_dblParameters(1), g_VecCurDisp,
CInt(NDOF))
Call VectorSuperposition(VecCal2, g_VecCurAcce, 1.0#, g_dblParameters(2) * g_dblInterval, g_VecCurVelo, CInt
(NDOF))

′// Find the corrected restoring force
```

```
Call VectorSuperposition(g_VecCurDisp, g_VecCurPredictDisp, 1.0#, -1.0#, VecCal1, CInt(NDOF))
Call MatrixVectorMultiply(g_MatStiff, VecCal1, VecCal2, CInt(NDOF), CInt(NDOF))
Call VectorSuperposition(g_VecCurResForce, VecCal2, 1.0#, 1.0#, g_VecCurForce, CInt(NDOF))

'// Update story drift and story shear force
For lngLoopJ = 1 To NDOF
    If lngLoopJ = 1 Then
        g_VecStoryDrift(lngLoopJ) = g_VecCurDisp(lngLoopJ)
    Else
        g_VecStoryDrift(lngLoopJ) = g_VecCurDisp(lngLoopJ) - g_VecCurDisp(lngLoopJ - 1)
    End If
Next lngLoopJ

For lngLoopJ = NDOF To 1 Step -1
    If lngLoopJ = NDOF Then
        g_VecStoryShear(lngLoopJ) = g_VecCurResForce(lngLoopJ)
    Else
        g_VecStoryShear(lngLoopJ) = g_VecCurResForce(lngLoopJ) + g_VecStoryShear(lngLoopJ + 1)
    End If
Next lngLoopJ

'// Saving the results
Call SaveData(1)

'// Monitoring the loading for each story
Call frmMain.Monitoring()
```

```
            '// Update the responses
            g_lngPreStep = g_lngCurStep
            g_dblPreTime = g_dblCurTime
            For lngLoopJ = 1 To NDOF
                g_VecPreDisp(lngLoopJ) = g_VecCurDisp(lngLoopJ)
                g_VecPrePredictDisp(lngLoopJ) = g_VecCurPredictDisp(lngLoopJ)
                g_VecPreVelo(lngLoopJ) = g_VecCurVelo(lngLoopJ)
                g_VecPreAcce(lngLoopJ) = g_VecCurAcce(lngLoopJ)
                g_VecPreResForce(lngLoopJ) = g_VecCurResForce(lngLoopJ)
                g_VecPreForce(lngLoopJ) = g_VecCurForce(lngLoopJ)
            Next lngLoopJ
        Next lngLoopI

PROC_EXIT:
    MsgBox("Simulation using OS method completed sucessfully!", vbOKOnly)
    Exit Sub

PROC_ERR:
    MsgBox("Error occurs!" & vbCrLf & Err.Description, vbOKOnly, "Error occurs when executing OS method!")
    GoTo PROC_EXIT

End Sub
```

Index

Note: Page numbers followed by *f* indicate figures and *t* indicate tables.

I

L

M

N

O

P

Q

R

S

T

V

W